NTNU – Trondheim
Norwegian University of
Science and Technology

Antenna Systems for NUTS

Sigvald Marholm

Master of Science in Electronics
Submission date: July 2012
Supervisor: Egil Eide, IET
Co-supervisor: Irene Jensen, SINTEF
Roger Birkeland, IET

Norwegian University of Science and Technology
Department of Electronics and Telecommunications

Problem Statement

The task is to build antennas, including necessary feeding networks, for VHF and UHF for the NTNU Test Satellite (NUTS). The antennas should be made such that the received signal strength on ground is as high as practically possible, taking into account that the satellite will orbit the Earth. The mechanical construction of the antennas is to be emphasized. They should be made compatible with each other, with other modules on-board the satellite, and with the environment in space. The radiation patterns should also be measured on a mock-up of the satellite.

Preface

This thesis is the result of work done during spring 2012, contributing to the NTNU Test Satellite (NUTS) project. Being part of team such as NUTS has been both rewarding and challenging. Building a satellite is a difficult task, and writing a thesis for such a project means that you will be faced with very realistic problems whose answers are not printed in a text book. It is therefore necessary to search for solutions, learning theory, applying theory, and learning to use tools as problems arise. This is very instructive and motivating, but it is also often synonymously with more work. Unfortunately, realistic problems also means that there will be problems, some of which are not solvable within the time and scope of a masters thesis.

NUTS is also a highly interdiciplinary project, and it is necessary to cooperate with students from other departments. At the time being, the NUTS team consists of students and staff from six NTNU departments: IET, ITK, ITEM, IDI, IMP and PHYS. It is important to understand their problems, and how your work is related to theirs in a dynamical way. The Norwegian Center for Space-related Education (NAROM) is also involved in the project.

Finally, taking part of the NUTS project must also be seen partly as volunteer work. The students involved with NUTS is involved in marketing, public relations, as well as other tasks that needs to be done. The author, for instance, has been involved in the development of a LaTeX Beamer template for NUTS presentation slides. He has also accepted helping NUTS with creating a new link budget in the future.

Acknowledgements

There has been a lot to do this semester, and I believe much of it would not have been possible without the help and support from others. First, I would like to thank my supervisors Egil Eide and Irene Jensen for meeting with me on a regular basis. They have always pointed me in the right direction, and are a valuable resource of expertise. They should also be thanked for helping me with measurements and lending me equipment.

I would also like to thank Roger Birkeland, the project manager for NUTS, for making this interesting master project available, for leading the NUTS team in a good way, and proof-reading my report. I would also like to thank the whole NUTS team for both social and professional gatherings as well as many fruitful discussions. I will in particular thank Marianne Bakken (working with signal processing for the NUTS payload) for proof-reading my thesis, and for her cooperation with the downlink capacity analysis, and Kai Inge Midtgård Rokstad (working with the mechanical structure) for answering numerous questions regarding mechanical design.

Terje Mathiesen should be thanked for advices regarding RF-design, for granting me access to the microwave laboratory, and for lending me equipment. Andreas Østensen has helped me with production of the PCBs by the use of a milling-machine. Tore Landsem has made the teflon blocks used in the antennas and provided me with bolts and nuts and access to certain facilities at his mechanical workshop. Ingulf Helland has also shown his interest in my project, and helped me with soldering equipment, as well as contributing with his advices regarding electronics design.

The Experts in Team group who chose to build and test a model of the deployment mechanism should also be thanked for choosing that task, which proved the concept of the deployment mechanism, and brought further knowledge about its properties into the NUTS team. Finally, I would also like to thank other students at my office, “Fragleberg”, and at the neighbour office “Gjøkeredet”, for coffee-breaks with fruitful discussions.

Sigvald Marholm
Trondheim, 03.07.12

Abstract

NTNU is aiming to build and launch a small student satellite compliant with the double CubeSat standard, by 2014. The NTNU Test Satellite (NUTS) will carry two radio tranceivers and a beacon transmitter, all located in the VHF and UHF amateur bands. The goal of this thesis was to build the whole antenna systems for the spacecraft.

Turnstile antennas were chosen both for UHF and VHF, since they yield the highest received signal strength on ground throughout the whole pass of the satellite. In order to reach this conclusion, a study of how the choice of spacecraft antennas dynamically influence the link margin was carried out. Furthermore, the antennas was made by measuring tape, and is to be wrapped around the satellite until deployment. This is for the satellite to be within the size constraints of a double CubeSat during launch. The measuring tape will be tightened to the satellites body by nylon thread, which will be burnt off by Nichrome-wire to release the measuring tape when the satellite is in-orbit. The measuring tape is mounted in between two circuit boards constituting the internal part of the antenna module. The feeding network is encapsulated by these two circuit boards. The module is made such that the antenna complies with the CubeSat standard, and such that it can be integrated with other modules on-board the satellite, such as the camera.

Feeding the antennas turned out more difficult than first anticipated. Whereas conventional feeding networks for turnstile antennas typically comprises baluns and arrangements of coaxial cable comparable to the wavelength, such solutions are not feasible within the satellite due to size constraints. As a result a lumped feeding network was designed, that could be mounted on one of the circuit boards.

Because of the many reactive components in the feeding network, it became necessary to determine how deviations in component values affect the performance of the circuit. Statistical simulations was performed, and the deviations may cause an unbalance between the amplitudes and phases of the outputs. But this results in less than half a dB additional losses in the link budget.

A refinement of electromagnetic antenna simulations from previous work was also carried out. With this, the performance of the antennas was verified, and their lengths were optimized to yield the best possible match. The VHF antenna is near-ideal both in terms of pattern and matching. The pattern of the UHF antenna is somewhat distorted, but it is still considered to be the best suited antenna of those considered. The matching of the UHF antenna could have been better, but is considered acceptable. Moreover, the mutual coupling between the VHF and UHF antennas were studied, with the conclusion that the antennas may very well co-exist on-board the satellite.

Finally, both the feeding network and the VHF antenna were successfully built and tested. The feeding network had an insertion loss of less than 2 dB, whereas the pattern of the antenna was measured to be near-ideal. Unfortunately, a fault has occurred on the UHF feeding network, which also prohibits the pattern for the UHF antenna to be measured. Nonetheless, all the parts constituting it has been built, and all the necessary simulations are done. Previous and future troubleshooting of the feeding network is also discussed.

Samandrag (Abstract in Norwegian)

NTNU planlegger å byggje og lansere ein liten studentsatellitt i samsvar med CubeSat standarden, innan utgongen av 2014. NTNU Testsatellitt (NUTS) vil innhalde to radioar samt ein radiofyr. VHF og UHF radioamatørbanda vil bli brukt til dette. Målet med denne avhandlinga var å byggje heile antennesystemet til satelliten.

Kryssa dipolantenner blei valgt, både for UHF og VHF, ettersom dei gir den høgaste mottekne signalstyrkjen på bakken gjennom heile passet. For å finne ut dette, blei det undersøkt korleis val av antenner dynamisk påverkar linkmarginen. I tillegg har dei nemnde antenne blitt mekanisk bygd av måleband og vil bli bretta rundt satellitten før utløysing. Dette er for å oppføglje CubeSat standarden med tanke på plass. Målebanda vil bli festa til satellitten med nylontråd som vil bli brent av ved Nichrome-tråd for å utløyse antennene når satellitten er i bane. Målebanda er festa mellom to kretskort som utgjer den indre delen av antennemodulen. Matenettverket ligger mellom desse kretskorta. Modulen er laga slik at antennene er kompatible med CubeSat standarden og dei andre modulane ombord i satellitten. Til dømes er det tilgjengeleggjort plass for kameralinse, naudsynte kontakter og festeanordningar.

Å mate antenne viste seg å være vanskelegare enn først trudd. Typisk er matenettverk til kryssa dipolantenner laga av balunar og koaksialkablar av lengder samanliknbare med bølgjelengda. Slike løysingar er ikkje praktiske på satellitten grunna plassmangel. Difor blei eit diskret matenettverk laga. Grunna dei mange reaktive komponentane i matenettverket, var det naudsynt undersøkje korleis avvik i komponentverdiar påverkar ytelsen til kretsen. Statistiske simuleringar blei gjort, og det viser seg at avvika kan skape ubalanse mellom amplitude og fase på utgongane. Men dette fører til under ein halv dB tap i linkbudsjettet.

Ei utbetra antennesimulering blei også utført. Dette bekrefta at antennnene fungerte som dei skulle. Lengdene blei optimert slik at impedanstilpassinga blei så bra som mogleg. VHF antenna er omtrent som ei teoretisk kryssa dipolantenne både når det kjem til stårlingsdiagram og impedanstilpassing. Strålingsdiagrammet til UHF antenna er ikkje like ideelt, men kryssa dipolantenna er framleis holdt for å være den mest passande antenna. Impedanstilpassinga til UHF antenna kunne ha vore betre men er akseptabel. Vidare er den gjensidige koplinga mellom VHF og UHF antennene studert, med den konklusjonen at antennene godt kan brukast på satellitten samstundes.

Til slutt blei matenettverket og VHF antenna bygd og testa. Matenettverket har eit innskotstap på mindre enn 2 dB og diagrammet til antenna blei målt til å være nær det ideelle. Diverre oppstod det ein feil på matenettverket til UHF som også forhindra målingar av UHF antenna. Uansett har alle delane blitt laga og alle naudsynte simuleringar har også blitt gjort. Tidlegare og framtidig feilsøkjing av matenettverket er også diskutert.

Contents

List of Figures

List of Tables

List of Abbreviations

ADCS Attitude Determination and Control System

ADS Agilent Advanced Design System

AUT Antenna Under Test

BeCu Beryllium Copper

BER Bit Error Rate

bps bits-per-second

CMRR Common-Mode Rejection Ratio

COTS Commercially available Off-The-Shelf

CST Computer Simulation Technology Microwave Studio

CW Continuous Wave

DUT Device Under Test

EiT Experts in Team

EPS Electrical Power System

FR4 Flame Retardant 4

FSK Frequency-Shift Keying

FSPL Free-Space Path Loss

GPIB General Purpose Interface Bus

IARU International Amateur Radio Union

IC Integrated Circuit

IET Institute for Electronics and Telecommunication (a department at NTNU)

IR Infrared

PCB Printed Circuit Board

LEO Low Earth Orbit

LH Left Handed

LHCP Left Hand Circular Polarized

LHEP Left Hand Elliptical Polarized

LHM Left Handed Material

LNA Low Noise Amplifier

LQPS Lumped Quadrature Power Splitter

LWPS Lumped Wilkinson Power Splitter

MCU Microcontroller Unit

MM Metamaterial

MMIC Monolithic Microwave Integrated Circuit

NAROM Norwegian Center for Space-related Education

Nichrome Nickel-Chromium alloy

NTNU Norwegian University of Technology and Science

NUTS NTNU Test Satellite

P-POD Poly-Picosatellite Orbital Deployer

PDF Probability Density Function

PEC Perfect Electric Conductor

PLF Polarization Loss Factor

P&TT The Norwegian Post and Telecommunications Authority

QPS Quadrature Power Splitter

QWT Quarter Wave(length) Transformer

RAAN Right Ascension of the Ascending Node

RF Radio Frequency

RH Right Handed

RHCP Right Hand Circular Polarized

RHEP Right Hand Elliptical Polarized

RHM Right Handed Material

SEU Single Event Upset

SMA SubMiniature version A

SNR Signal-to-Noise Ratio

SRF Self-Resonant Frequency

STK Analytical Graphics, Inc. Satellite Toolkit

TEM Transverse Electromagnetic

TCC Temperature Coefficient of Capacitance (C)

TCL Temperature Coefficient of Inductance (L)

TCR Temperature Coefficient of Resistance (R)

TL Transmission Line

TRL Through-Reflect-Line

TT&C Telemetry, Tracking and Command

UHF Ultra High Frequencies

VHF Very High Frequencies

VSWR Voltage Standing Wave Ratio

WPS Wilkinson Power Splitter

1 Introduction

The *Norwegian University of Technology and Science* (NTNU) is aiming to launch a $10 \times 10 \times 20$ cm nanosatellite[1] during the year 2014 [2]. The satellite is named *NTNU Test Satellite* (NUTS) and it will comply with the CubeSat standard [3]. NUTS will mainly be built by students and its primary goal is to educate students. In that sense the satellite is guaranteed to be a success, as there is no way a satellite can be launched without the people building it learning from it.

The primary *technical* goal however, must be that one manage to communicate with the satellite after it is placed in orbit. To accomplish this, radios and antennas are needed both on the ground as well as on-board the satellite. It is also, of course, a goal that other subsystems are working as intended, but the communication system should be made as independent upon correct operation of the other subsystems as possible.

In the 9th semester specialization project written by the author in 2011, also entitled *Antenna Systems for NUTS* [4], it was demonstrated that *crossed dipole* antennas, also known as *(flat) turnstile* antennas, were much better suited than many other alternatives. Considering that NUTS will orbit the Earth with one side constantly facing down, the turnstile antennas results in a higher link margin (received signal strength) throughout the whole pass, than any of the other alternatives. It was further concluded that the turnstile antennas would be best suited even if the angular orientation of the satellite is not properly controlled. This is because it had the most near-isotropic pattern of the antennas considered.

The intent of this master project is to carry this work further, by actually building the turnstile antennas. This involves a mechanical solution, as well as a fit way to feed the antennas. Turnstile antennas are assumed to be more difficult to feed than for instance dipoles or monopoles, since they must be fed in quadrature. The quadrature feeding of turnstile antennas can typically be achieved by networks made solely of coaxial cables, but such solutions are not feasible on-board the satellite due to size constraints. Alternative ways of doing it must therefore be

[1] A nanosatellite is a small satellite with a mass between one and ten kilograms [1].

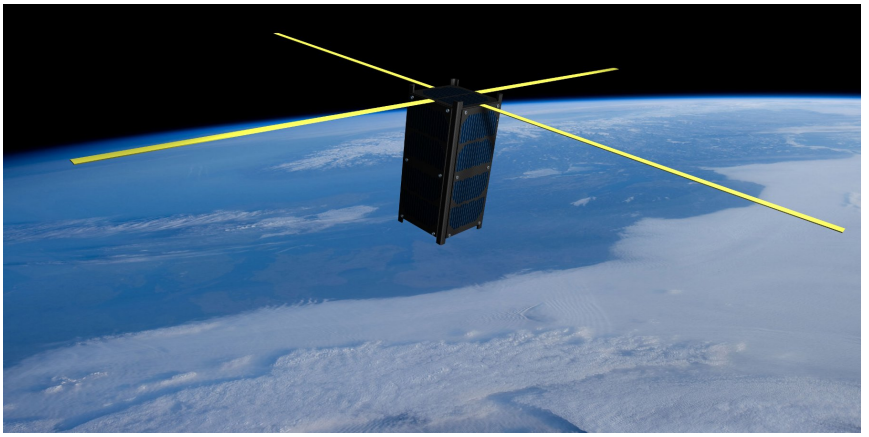

Figure 1.1: An illustration of NUTS. The illustration does not include the UHF antennas. Satellite image: courtesy of Kai Inge Midtgård Rokstad, background image: Astronaut photograph STS131-E-11693 obtained from the ISS, courtesy NASA JSC Image Science & Analysis Laboratory.

studied. Moreover, it is important that the antenna module complies with the CubeSat standard, and with other modules on-board the satellite. This must be taken into account when designing the antenna systems.

1.1 Outline

Ch. 2 presents the necessary background about the satellite, as well as a brief review of microwave and antenna theory. Large parts of Ch. 3 is a summary of the previous work done with the NUTS antenna systems in [4]. It discusses how the orbital dynamics of the satellite-Earth system influences the received signal strength, and how the choice of satellite antenna interacts with it. Finally in Ch. 3, further insight about the link is brought to the NUTS project by analysing the download capacity of the satellite. Ch. 4 presents the mechanical solutions of the antennas, and how it is made compatible with other modules on-board the satellite, as well as the CubeSat standard.

Different possibilities of how to feed the antennas are thoroughly discussed in Ch. 5, with a decision of which network to choose. The chosen network is then rigorously designed with high-quality components in Ch. 6. To verify the design and the calculations, a deterministic simulation is carried out in Ch. 7. A stochastic simulation is also performed, to determine the influence the components tolerance and temperature coefficients had on the performance of the link. Lastly, in Ch. 8 the design is built and tested.

Electromagnetic simulations of the antennas are further presented in Ch. 9, to verify their performance. Further on, their matching will be optimized, and mutual coupling will be studied in order to determine if the antennas are compatible with

each other such that they may co-exist on-board the satellite.

The VHF antenna including the feeding network will be assembled, and mounted on a mock-up of the satellite for measuring the radiation patterns in Ch. 10.

Due to the many parts of this work, results, discussions and conclusions are presented after the various simulations and experiment rather than in separate chapters. But since all the parts in the end constitutes *one* system, a discussion from a systems perspective is given in Ch. 11. Finally, a conclusion is given in Ch. 12.

2 Background

This chapter provides the necessary prerequisites for understanding this thesis. It is divided into three sections; one about the NUTS project, one about microwave theory, and one about antenna theory. Most of the microwave and antenna-theory is likely well know to other antenna-designers, but are included for completeness.

2.1 The NUTS Project

As a payload, NUTS will carry an *Infrared* (IR) camera mounted on the nadir[1] plane of the satellite. Its purpose is the observation of *gravity waves* which is an atmospheric phenomena (not to be confused with gravitational waves from general relativity) [5]. A major part of the capacity of the radio link is therefore expected to be used for transferring image sequences from the camera.

The angular orientation of the satellite in space, known as its *attitude*, will be controlled by the *Attitude Determination and Control System* (ADCS) such that the nadir plane always points towards nadir, by utilizing the magnetic field of the Earth [6]. It is therefore reasonable to assume that the spacecraft antennas will always point in a certain direction, although one should not depend on it. It is desirable that a link can be established even in case of failure of other subsystems.

Other subsystems of the satellite that should be mentioned in this thesis, are the frame and the *Electrical Power System* (EPS). The frame will be made of carbon fibre and covered with *Printed Circuit Boards* (PCBs). All the other modules, including the antenna modules, should be mounted to the frame. Solar panels will be mounted on the outside walls of the satellite, as well as on the zenith plane. Moreover, the solar panels will be connected to the EPS by cables. It is important that the antenna modules are made such that they fit on the frame along with these modules.

[1] Nadir is the direction pointing down towards the Earth, whereas zenith is the opposite direction.

2.1.1 Radio Systems

The NUTS spacecraft will carry two tranceivers for communication purposes. One at approximately 146 MHz and one at approximately 437 MHz [4]. There will also be a beacon broadcasting a morse code at the 437 MHz frequency. Beware that the exact frequencies are not known, since they are yet to be allocated at the *The Norwegian Post and Telecommunications Authority* (P&TT). This thesis will therefore assume them to be exactly 146 MHz and 437 MHz.

Previously, it has been assumed that the exact frequencies 437.305 MHz and 145.980 MHz will used [4, 7], and that the bandwidth available will be 25 kHz. Strictly speaking, it is therefore sufficient for this thesis that the spacecraft antennas are made with a 25 kHz bandwidth. However, since the exact frequencies are not yet known, it would be of interest for the NUTS project to know whether or not the antennas can be used also at other frequencies without modification, or if they have to be re-tuned when the frequencies are allocated. 146 MHz is located in the *Very High Frequencies* (VHF) amateur radio band, and 437 MHz in the *Ultra High Frequencies* (UHF) amateur radio band. The range of these bands, as well as the maximum bandwidth that can be used within them, are listed in Tab. 2.1 [8]. It is therefore certain that the satellite will operate within these limits.

However, the *International Amateur Radio Union* (IARU) have specified certain segments of the amateur radio bands that should be used exclusively by satellites (internationally). These restrictions are also listed in Tab. 2.1. It is therefore reasonable to assume that NUTS will be allocated frequencies and bandwidths according to these restrictions. From the table it is observed that the maximum offset from the assumed center frequency is at 435 MHz, 2 MHz away from the assumed center frequency.

From here on it is considered as a requirement that the antennas have a bandwidth of 25 kHz, but it would be beneficial if the bandwidth covers the whole IARU frequency segments.

Which frequency to use for uplink and downlink is, at the time being, not determined. It has been suggested that VHF is used as uplink for *Telemetry, Tracking and Command* (TT&C) whereas UHF is used as downlink of housekeeping data (temperature, system status, etc.) and payload data. The beacon will be used by the ground station operator as a first means of locating the satellite.

One should also remember the Doppler shift that occur due to the relative velocity of the satellite w.r.t. the ground station. This was computed in [7], and is also listed in Tab. 2.1. This is coped with by continuously shifting the center frequency on the ground station, both for transmission and reception. Thus, the frequency as observed from the satellite will be unaffected by the Doppler shift, and it is not necessary to include this in the bandwidth for equipment made for the satellite.

2.1.2 Launch and the Orbit

NUTS will be carried in a *Poly-Picosatellite Orbital Deployer* (P-POD) by a rocket carrying a commercial satellite, and be ejected at a suitable time. The satellite is

Table 2.1: Frequency specifications

	UHF	VHF
Previously presumed center frequency	437.305 MHz	145.980 MHz
Assumed center frequency	437 MHz	146 MHz
Assumed bandwidth	≤ 25 kHz	≤ 25 kHz
Norwegian amateur radio bands	432–438 MHz	144–146 MHz
Maximum permitted bandwidth in Norway	30 kHz	18 kHz
International satellites exclusively segment	435–438 MHz	145.806–146 MHz
International satellite bandwidth	20 kHz	18 kHz
Doppler shift	≤ 11 kHz	≤ 4 kHz

not allowed to turn on its radio and deploy its antennas until after 30 minutes [3]. The CubeSat will undergo extensive testing, including vibrational test before launch.

How the satellite orbits the Earth can be described by its *orbital elements* which uniquely describes the motion of a two-body problem [9]. The z-axis in Fig. 2.1 is the axis of the rotation of the Earth, whereas x and y points towards fixed coordinates in space, meaning that the Earth rotates within this frame (it is an *inertial* frame) [9]. The angle between the equatorial and orbital planes are known as the *inclination* i [9]. NUTS will have a *polar orbit* meaning that i will be near 90°. For $i = 98°$ the perturbations due to the oblateness of the Earth make the orbital plane rotate such that it has a fixed alignment w.r.t. the Sun. Such orbits, known as *sun-synchronous*, are often used for Earth-observation satellites [10]. Since NUTS will follow a commercial satellite and have polar orbit, it is not unlikely that it will have an inclination of $i \approx 98°$.

CubeSats typically have a very near-circular orbit [11]. The ellipticity of the orbit is described by the *eccentricity*, which is zero for circular orbits.

The altitude for NUTS is not exactly known, since it is yet to be determined which rocket it will follow. Several assumptions has therefore been done within the NUTS team. Reports about the radio systems have typically assumed between 400 km and 800 km [4, 12]. This report, however, will assume the altitude to be in between 350 km and 650 km in accordance with more recent assumptions within the team.

The last element that describe the orientation of the orbital plane is the *Right Ascension of the Ascending Node* (RAAN) Ω. It describes the rotation of the plane about the z-axis as seen in Fig. 2.1 [9]. The orbital plane will remain fixed (except for perturbations) within this reference frame whereas the Earth rotates within it such that the satellite covers the whole Earth [9], by orbiting it approximately 12-14 times a day [4]. Fig. 2.2 illustrates a possible orbit of NUTS.

There are a couple of more orbital elements that describe the satellites motion within the orbital plane. It is sufficient for this thesis, however, to know the ones

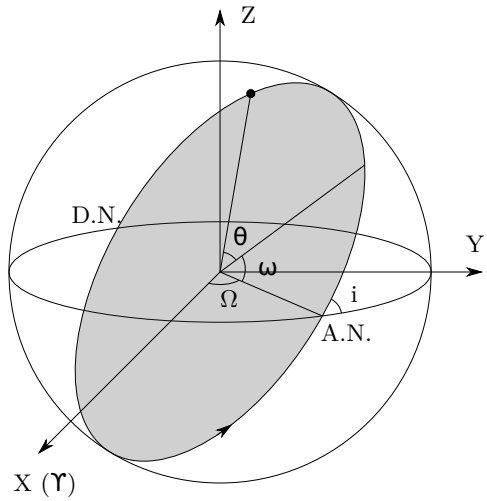

Figure 2.1: The inertial reference system of the satellite orbit

that describe the orbital plane itself. For more information about this topic see [9, 13, 10, 14].

2.2 Microwave Theory

2.2.1 S-parameters

S-parameters (scattering-parameters) are a complete black-box parametrization of linear networks that are specifically suited for *Radio Frequency* (RF) and microwave applications. Consider an N-port network. At each port i, there is an incident (forward travelling) wave, represented by its voltage V_i^+ and a reflected, or scattered (backward travelling) wave represented by V_i^-. They are related by:

$$\begin{bmatrix} V_1^- \\ V_2^- \\ \vdots \\ V_N^- \end{bmatrix} = \begin{bmatrix} S_{11} & S_{12} & \cdots & S_{1N} \\ S_{21} & S_{22} & \cdots & S_{2N} \\ \vdots & \vdots & \ddots & \vdots \\ S_{N1} & S_{N2} & \cdots & S_{NN} \end{bmatrix} \begin{bmatrix} V_1^+ \\ V_2^+ \\ \vdots \\ V_N^+ \end{bmatrix} \tag{2.1}$$

The incident and scattered currents I_i^+ and I_i^- are related to the voltages by the port impedance Z_0, which is assumed to be equal for all ports.

Generalized S-Parameters

If the port impedances are *not* equal the S-parameters as defined above loses some of its meaning. Therefore, it is convenient to introduce incident and reflected *power*

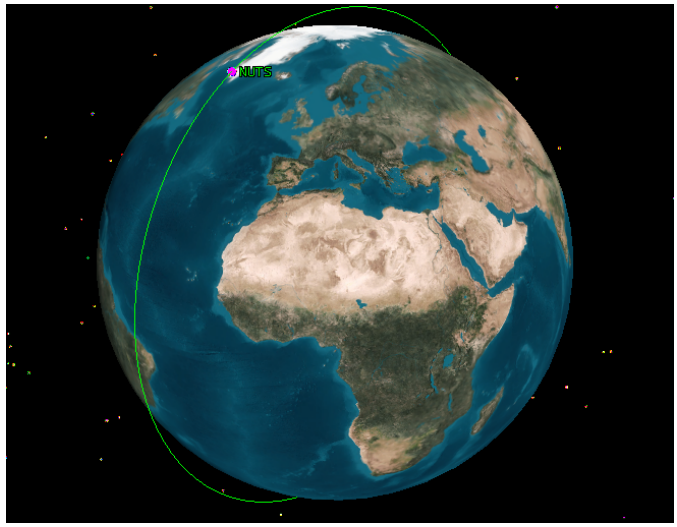

Figure 2.2: An image illustrating NUTS' orbit. The inclination on the picture is 90°. Simulations from STK. Courtesy of Snorre Stavik Rønning.

waves[2] a_i and b_i, respectively, for each port:

$$a_i = \sqrt{V_i^+ I_i^+} = V_i^+ / \sqrt{Z_{0i}} \qquad \left[\sqrt{\mathrm{W}}\right] \quad (2.2)$$

$$b_i = \sqrt{V_i^- I_i^-} = V_i^- / \sqrt{Z_{0i}} \qquad \left[\sqrt{\mathrm{W}}\right] \quad (2.3)$$

where Z_{0i} are the port impedances. Subsequently the *generalized* S-parameters are defined as:

$$\begin{bmatrix} b_1 \\ b_2 \\ \vdots \\ b_N \end{bmatrix} = \begin{bmatrix} S_{11} & S_{12} & \cdots & S_{1N} \\ S_{21} & S_{22} & \cdots & S_{2N} \\ \vdots & \vdots & \ddots & \vdots \\ S_{N1} & S_{N2} & \cdots & S_{NN} \end{bmatrix} \begin{bmatrix} a_1 \\ a_2 \\ \vdots \\ a_N \end{bmatrix} \quad (2.4)$$

which reduce to the same as the non-generalized definition if the port impedances are the same.

Interpretation

The S-parameters may also be written:

[2]Despite that they are called power waves they are still amplitudes quantities, meaning that they should be converted to dB with $20\log(\cdot)$.

$$S_{ij} = \left.\frac{b_i}{a_j}\right|_{a_k=0 \text{ for } k\neq j} \quad [\,] \quad (2.5)$$

from which the following important interpretation follows: $|S_{ij}|$ says how much power, or actually square root of power, that is scattered out of port i from what was incident to port j. If the port impedance Z_{0i} is real $\angle S_{ij}$ is the phase lag in voltage (or current) from j to i. For $a_k = 0$ to be true there must be no reflections at the non-excited ports, which is achieved by terminating them passively by their port impedances (they are matched). S_{ii} is then interpreted as the reflection coefficient seen into port i when all other ports are matched.

It is common to define the *insertion loss* as the amount of power (in dB) that is lost from port j to port i:

$$\mathrm{IL}_{ij} = -20\log_{10}|S_{ij}| \quad [\mathrm{dB}] \quad (2.6)$$

Often times one like to keep this as low as possible since it being something else than zero implies wasted power. Other times, however, not *all* of the power is intended to go from port j to i in the first place. For instance in power splitters, one would often like only half of the power to exit one of the outputs, from which it follows that IL theoretically equals 3 dB. It is then common to talk about *excess* insertion loss as the loss above what is intended. Yet other times, it is intended that *no* power crosses between ports i and j (it is infinite), but then it is usually called *isolation* and denoted I rather than IL (although computed with the same formula).

Moreover, the *return loss* is usually defined as[3]

$$\mathrm{RL}_i = -20\log_{10}|S_{ii}| \quad [\mathrm{dB}] \quad (2.7)$$

and is again a measure of how well a port is matched.

More about S-parameters and its interpretations can be found in [15, 16]. *Mixed-mode* S-parameters will also be mentioned a few times during this thesis, but only for the interested reader. It is not strictly a prerequisite. It is therefore only referred to the original 1995 paper about them; "Combined Differential and Common-Mode Scattering Parameters: Theory and Simulation" [17].

2.2.2 Transmission Lines (TL)

When a cable, or another device, has a comparable length to the wavelength, it becomes necessary to take into account the phase-shift that occur as the wave travels, and wave considerations are necessary. A *Transmission Line* (TL) is used similarly to a normal cable, but takes into account the propagation of *Transverse*

[3]Strictly speaking the return loss should be defined with a reflection coefficient Γ rather than S_{11} but if all ports are well matched the definitions turns out the same.

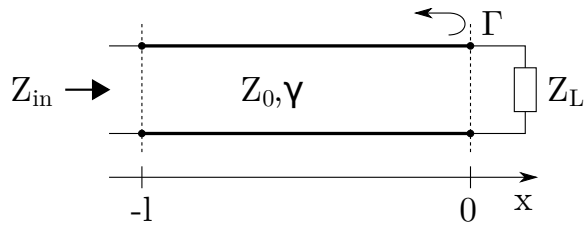

Figure 2.3: A transmission line (TL)

Electromagnetic (TEM) waves. A TL with characteristic impedance Z_0 and complex propagation constant γ is illustrated in Fig. 2.3. It is terminated by an impedance Z_L. γ is often split in a real part α and an imaginary part β. For lossless TLs $\alpha = 0$ and one is left with only β.

As a wave is incident on a lossless TL such that the forward travelling voltage is V^+ at $x = 0$, the voltage at an arbitrary position x can be written:

$$V(x) = V^+(e^{-j\beta x} + \Gamma e^{j\beta x}) \quad [\text{V}] \quad (2.8)$$

where V^+ is the forward travelling voltage at $x = 0$ and Γ is the reflection coefficient seen at the load. It is given by:

$$\Gamma = \frac{Z_L - Z_0}{Z_L + Z_0} \quad [\,] \quad (2.9)$$

It is interesting to see that if the load is matched ($Z_L = Z_0$ such that $\Gamma = 0$) the lossless TL only incorporates a phase-shift.

Further on, the input impedance (seen into the TL) is:

$$Z_{\text{in}} = Z_0 \frac{Z_L + Z_0 \tanh \gamma\ell}{Z_0 + Z_L \tanh \gamma\ell} \overset{\text{lossless}}{\downarrow} = Z_0 \frac{Z_L + jZ_0 \tan \beta\ell}{Z_0 + jZ_L \tan \beta\ell} \quad [\Omega] \quad (2.10)$$

Quarter Wave Transformers (QWT)

Of special interest is the TL being $\lambda/4$ long; the *Quarter Wave(length) Transformer* (QWT). It incorporates, of course, a 90° phase-lag, and has an input impedance given by:

$$Z_{\text{in}} = \frac{Z_0^2}{Z_L} \quad [\Omega] \quad (2.11)$$

The interesting part about this equation is that Z_0 can be chosen in such that the impedance Z_L is transformed to an arbitrary input impedance Z_{in}, which is why it is called an (impedance) transformer.

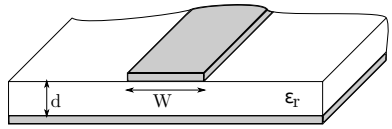

Figure 2.4: Cross-section of a microstrip line

Practical TLs

Examples of practical TLs are the coaxial cable, stripline, and microstrip lines. The characteristic impedance of (lossless) TLs is determined from the capacitance and inductance of the two conductors comprising the TLs, which again is determined by the geometry. It is also important to know that the velocity of the waves is dependent on the media in which it propagates. Therefore, it is customary to introduce the *velocity factor* VF as the number that when multiplied by the speed-of-light yields the velocity of the waves in the media. For instance for coaxial cables:

$$\mathrm{VF} = \frac{1}{\sqrt{\varepsilon_r}} \qquad [\,] \quad (2.12)$$

where ε_r is the *relative permittivity* of the dielectric. Due to the reduction in speed, the *electrical wavelength* λ becomes different from that in vacuum:

$$\lambda = \lambda_0 \mathrm{VF} \qquad [\mathrm{m}] \quad (2.13)$$

where the wavelength in vacuum is given by:

$$\lambda_0 = \frac{c}{f} \qquad [\mathrm{m}] \quad (2.14)$$

where f is the frequency and $c = 299792458\,\mathrm{m/s}$ is the speed-of-light.

Microstrip Lines

Microstrip lines is a TL of particular interest to this thesis. It is a TL made as paths on for instance a PCBs, with a certain substrate thickness d with relative permittivity ε_r. A cross-section is illustrated in Fig. 2.4. The ratio W/d determines the characteristic impedance of microstrip lines. Given that a certain characteristic impedance Z_0 is desired, the ratio is determined by:

$$\frac{W}{d} = \begin{cases} \frac{8e^A}{e^{2A}-2} & , W/d < 2 \\ \frac{2}{\pi}\left[B - 1 - \ln(2B-1) + \frac{\varepsilon_r - 1}{2\varepsilon_r}\left\{\ln(B-1) + 0.39 - \frac{0.61}{\varepsilon_r}\right\}\right] & , W/d > 2 \end{cases} \quad (2.15)$$

where:

$$A = \frac{Z_0}{60}\sqrt{\frac{\varepsilon_r + 1}{2}} + \frac{\varepsilon_r - 1}{\varepsilon_r + 1}\left(0.23 + \frac{0.11}{\varepsilon_r}\right) \tag{2.16}$$

$$B = \frac{377\pi}{2Z_0\sqrt{\varepsilon_r}} \tag{2.17}$$

Note that in order to find the W/d-ratio, one must first assume which formula to use, and then verify if it was the correct one depending on if W/d is greater or smaller than 2.

Once the W/d-ratio is found, the *effective* relative permittivity may be found from the following formula:

$$\varepsilon_e = \frac{\varepsilon_r + 1}{2} + \frac{\varepsilon_r - 1}{2}\frac{1}{\sqrt{1 + 12d/W}} \quad [\,] \tag{2.18}$$

and then the velocity factor for microstrip lines are given by:

$$\mathrm{VF} = \frac{1}{\sqrt{\varepsilon_e}} \quad [\,] \tag{2.19}$$

In theory the geometry shown in Fig. 2.4 should extend to infinity, which is not practical. A question may be, what is close enough to infinity? A rule of thumb that is used throughout this thesis is that three substrate thicknesses ($3d$) is approximately equal to infinite [18, 19].

A variant of the microstrip line is the *covered* microstrip line, which has a metallic cover plate at a short distance from the microstrip. Often used for shielding or protection. This may perturb the operation of the microstrip line.

More information about TLs can be found in [15, 16, 20, 21].

2.2.3 Synthetic Transmission Lines

According to [22, 23] TLs can be replaced by synthetic TLs made of lumped components that have the same properties at the center frequency. Four unit cells for synthetic TLs are presented, that can be used as building blocks in order to replace a distributed network with its lumped equivalent. Two of the unit cells are so-called *Right Handed* (RH), i.e. they act like a normal transmission line, where the **E**-field, **H**-field and wavevector **k** forms a right-handed system [24]. These unit cells are only valid for TLs with an electrical length (a phase-lag) of $\theta \in (0°, 180°)$.

A material with simultaneously negative permittivity ε and permeability μ (meaning that it is a *Metamaterial* (MM)) has a **E**-field, **H**-field and wavevector **k** that forms a *left-handed* system [24]. One of the most notable consequence of this is the fact that the refractive index n will be negative. Another consequence is that the phase-velocity will be negative such that a phase-*advance* occur as a wave propagates[4]. Such a material is naturally referred to as a *Left Handed Material* (LHM).

[4]The group-velocity will still be positive though, meaning that a photon does not appear in space before it is emitted and thus violating causality.

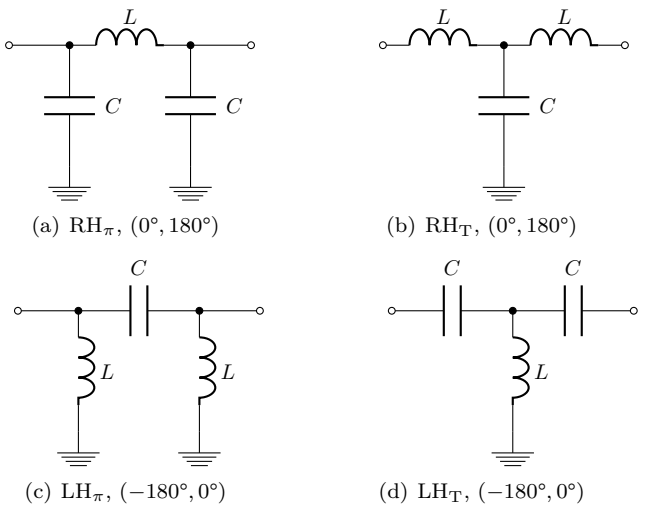

(a) RH_{π}, $(0°, 180°)$ (b) RH_{T}, $(0°, 180°)$

(c) LH_{π}, $(-180°, 0°)$ (d) LH_{T}, $(-180°, 0°)$

Figure 2.5: Synthetic TL Unit Cells

Table 2.2: Trigonometric functions for synthetic TLs

Unit cell	$f_L(\theta)$	$f_C(\theta)$
RH_{π}	$\sin\theta$	$\frac{1-\cos\theta}{\sin\theta}$
RH_{T}	$\frac{1-\cos\theta}{\sin\theta}$	$\sin\theta$
LH_{π}	$\frac{\sin\theta}{1-\cos\theta}$	$\frac{1}{\sin\theta}$
LH_{T}	$\frac{1}{\sin\theta}$	$\frac{\sin\theta}{1-\cos\theta}$

Making a TL with LHM means that there is a phase-*advance* through the TL corresponding to its length rather than a delay. Even though this might sound very exotic, it is possible to make non-homogeneous LHM by making structures in the material much smaller than the wavelength. For example, a TL could be made with a few lumped components on it [24]. In the case of *synthetic* TLs it is even simpler; it is sufficient to interchange the place of capacitors and inductors in the RH unit cells. It is intuitively satisfying that this will be equivalent to having negative ε and μ. The *Left Handed* (LH) unit cells in Fig. 2.5 are valid for a phase-*advance* of $\theta \in (-180°, 0°)$.

Ideally, it does not matter whether a π or T-network is used, but some authors such as [23] and [25] prefer to choose them such that the number of components, or inductors are minimized.

To design a synthetic TL of electrical length θ and characteristic impedance Z_0 the following formulas from [23] can be used:

$$L = \frac{Z_0}{\omega_0} f_L(\theta) \quad \text{[H]} \quad (2.20)$$

$$C = \frac{1}{Z_0 \omega_0} f_C(\theta) \quad \text{[F]} \quad (2.21)$$

where ω_0 is the angular center frequency and the trigonometric functions $f_L(\theta)$ and $f_C(\theta)$ can be found in Tab. 2.2. Notice that $f_L(90°) = f_C(90°) = 1$ irrespective of topology.

2.3 Antenna Theory

2.3.1 Gains, Directivity and Efficiencies

The *radiation intensity* $U(\theta, \phi)$ is the power radiated per unit solid angle (W/sr) [26] in the direction of (θ, ϕ) in a spherical coordinate system. The *directivity* $D(\theta, \phi)$ of an antenna is then a measure for how well the antenna radiates in a certain direction (θ, ϕ) as compared to the average radiation intensity of the antenna [26]:

$$D(\theta, \phi) = \frac{U(\theta, \phi)}{P_{\text{rad}}/4\pi} \quad [\,] \quad (2.22)$$

where P_{rad} is the total *radiated* power, such that $P_{\text{rad}}/4\pi$ becomes the average radiation intensity mentioned.

Beware, however, that it is not certain that all power accepted by the antenna, P_{in}, is radiated. Some of it may be dissipated in non-ideal conductors and dielectrics. It is therefore useful to define the *gain* as how well the antenna radiates in a certain direction as compared to if P_{in} was isotropically radiated (that is; evenly distributed in all directions):

$$G(\theta, \phi) = \frac{U(\theta, \phi)}{P_{\text{in}}/4\pi} = e_{cd} D(\theta, \phi) \quad [\,] \quad (2.23)$$

where $e_{cd} \triangleq P_{\text{rad}}/P_{\text{in}}$ is the *radiation efficiency* that describes how much of the accepted power that is radiated. This is what is usually understood by antenna gain[5].

But again, not all of the power available from the source, P_{av}, is necessarily accepted by the antenna. Some of it, specified by a reflection coefficient Γ, is reflected. The *realized* gain can then be defined as how well the antenna radiates in a certain direction as compared to if P_{av} was isotropically radiated:

[5] According to "IEEE Standard Definitions of Terms for Antennas" [27] this gain is also known as *absolute gain* wheras in [26] the absolute gain is defined to be the same as realized gain. This report will therefore not use the term absolute gain. Sometimes, to emphasize that it is *not* a partial gain, the non-standard term *total gain* will be used.

$$G_{\text{re}}(\theta,\phi) = \frac{U(\theta,\phi)}{P_{\text{av}}/4\pi} = e_r G(\theta,\phi) = e_0 D(\theta,\phi) \qquad [\,] \quad (2.24)$$

where $e_r \triangleq P_{\text{in}}/P_{\text{av}}$ is the fraction of available power that is accepted by the antenna. $e_0 \triangleq e_{cd}e_r$ is called the *total efficiency*.

2.3.2 Input Impedance and Matching

From a circuit perspective, an antenna may be seen as simply an impedance Z_A [26]:

$$Z_A = (R_L + R_r) + jX_L \qquad [\Omega] \quad (2.25)$$

where R_r is called the *radiation impedance* (referred to the input) and is defined as the resistance that will dissipate the same amount of power as what is radiated. R_L models the ohmic losses (which makes $e_{cd} \neq 1$), whereas X_L are the inductive or capacitive net reactance of the antenna.

If Z_A is not matched to its feeding network, a reflection coefficient given by (2.9) will force a fraction $|\Gamma|^2$ of the power to be reflected. Consequently, only a fraction $1 - |\Gamma|^2$ is accepted by the antenna implying that:

$$e_r = 1 - |\Gamma|^2 \qquad [\,] \quad (2.26)$$

The loss this mismatch causes in dB may be called *reflection loss*, *transmission loss* or *(impedance) mismatch loss*[6]:

$$\text{ML} = -10\log_{10}(e_r) = -10\log_{10}(1 - |\Gamma|^2) \qquad [\text{dB}] \quad (2.27)$$

Since antennas can often be considered to be 1-ports one may often replace Γ by S_{11} in these equations. One should be careful doing that, however, if coupling between two (or more) antennas is present as it may then be considered as a 2-port with non-zero S_{12}. If the coupling is weak, however $\Gamma \approx S_{11}$ is a valid approximation.

As for the *bandwidth* of antennas that can generally be defined as the frequency band within which the antenna operate within specified bounds. What exactly these bounds are, depends upon the application. Typically, it is the impedance that is considered to be the limiting factor [26]. When the reflection coefficient of the antenna becomes larger than a specified limit, it is out of the bandwidth of the antenna.

[6] The radiation efficiency, return loss, mismatch loss, reflection coefficient or the *Voltage Standing Wave Ratio* (VSWR) may all be used to describe how well the antenna is matched. VSWR is given by $\text{VSWR} = 1 + |\Gamma|/1 - |\Gamma|$ [26].

Resonance of a Dipole

For a lossless $\lambda/2$-dipoles the impedance is $(73 + j42.5)\,\Omega$, but by shortening the dipole a bit the imaginary part can be eliminated with only a negligible reduction of the real part [26]. This is often the case for practical dipoles. It can then be connected to a $70\,\Omega$ system or to a $50\,\Omega$ system if one accept a bit higher mismatch loss.

Two frequencies are often referred to as the resonance frequency of dipoles. The typical microwave definition from for instance [15] is that resonance is when the imaginary part is zero. It is also common to say that the antenna is at resonance when Γ is at a minimum, since the antenna has the best match then. These two definitions approximately coincide for dipoles, although the latter also depend on the systems impedance. Independently of what one choose to call resonance, one should opt for a best possible match, which occur Γ-minima.

2.3.3 Polarization

Electromagnetic waves consist of both an electromagnetic field vector **E**-field, and a magnetic field vector **H**-field, that in the far-field are orthogonal to each other and to the direction of propagation [26]. The orientation of them is important, which necessitates a definition of polarization. Given that the plane of the polarization is the plane orthogonal to the direction of propagation, the polarization can be defined the shape drawn by **E** in the plane as time passes.

The most general polarization is the *elliptical polarization* (see Fig. 2.6). Considering that the wave is travelling away from our point-of-view, the **E**-vector may draw the ellipse clockwise, or counter-clockwise as time passes. It is more commonly known as *Right Hand Elliptical Polarized* (RHEP) or *Left Hand Elliptical Polarized* (LHEP), respectively. The ellipse is fully described by its *handedness* (or polarization *sense*), its tilt angle τ and its *axial ratio*. The tilt angle is simply the angle between the semi-major axis (largest magnitude) and a specified reference direction in the plane, for example $\hat{\mathbf{a}}_\theta$. The axial ratio is given by [26]:

$$\mathrm{AR} = \frac{\text{semi-major axis}}{\text{semi-minor axis}} \qquad [\,] \quad (2.28)$$

The special case of *circular polarization* occur when $AR = 0$. It is then called *Right Hand Circular Polarized* (RHCP) or *Left Hand Circular Polarized* (LHCP) depending on the handedness. The polarization is called *linear* when $AR \to \infty$. A more mathematical treatise of polarization is given in for instance [26, 4].

The polarization of an antenna is defined as the polarization of a wave radiated by the antenna, and is generally dependent on the direction (θ, ϕ).

Polarization Loss

The gain of an antenna may very well describe how well it radiates in different directions. Due to reciprocity it also describes how well it receives, assuming that the polarization of the incoming wave matches the polarization of the antenna. If

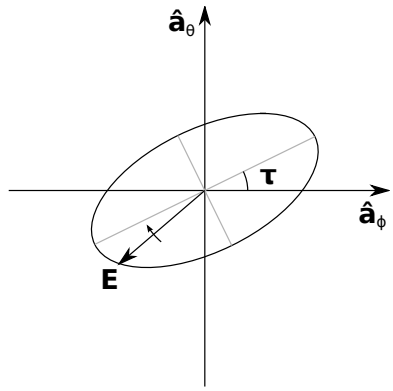

Figure 2.6: The polarization ellipse

Table 2.3: Polarization loss for different combinations of incoming wave and receiving antenna polarizations

Polarization Combination	PLF [dB]
Linear-linear (aligned)	0
Linear-linear (perpendicular)	∞
Linear-linear (in between)	$(0, \infty)$
Linear-circular	3
Circular-circular (same handedness)	0
Circular-circular (opposite handedness)	∞
Circular-elliptical (same handedness)	$(0, 3)$
Circular-elliptical (opposite handedness)	$(3, \infty)$

the polarization of the incoming wave differs from that of the receiving antenna, the receiving antenna will only be able to intercept a projection of the **E**-vector [4, 26]. The additional loss is known as *polarization loss* and is specified by the *Polarization Loss Factor* (PLF). Tab. 2.3 from [4] summarizes the PLF for several combinations of incoming waves and receiving antenna polarizations.

Partial Gains and Directivity

The radiation intensity may be decomposed to two orthogonal polarizations $U = U_1 + U_2$, where U_1 and U_2 is the power per unit solid angle of each kind of polarized waves. Since the gains and directivity are linearly based upon U, they may be decomposed in the same manner [26, 27]. For instance, one can choose to decompose the gain to an RHCP and an LHCP component:

$$G(\theta, \phi) = G_{\text{RHCP}}(\theta, \phi) + G_{\text{LHCP}}(\theta, \phi) \qquad [\,] \quad (2.29)$$

Considering a link with one RHCP receiver antenna and an arbitrary transmitter antenna. Only the RHCP partial gain will be accepted by the RHCP receiver antenna due to the polarization loss [28, 4]. Thence, one may say that G_{RHCP}, often called the right-hand *circular gain*, is simply the gain minus the polarization loss given that the other antenna is perfectly RHCP (note the logarithmic scale) [28, 4]:

$$G_{\text{RHCP}}(\theta, \phi) = G(\theta, \phi) - \text{PLF}_{\text{RHCP}}(\theta, \phi) \quad \text{[dBiC]} \quad (2.30)$$

Polarization for NUTS

The polarization of the incoming wave may often be taken to be the same as the polarization of the transmitting antenna. In other cases, there are environmental effects that may change the polarizations. For instance, the whole polarization plane rotates as it goes through the ionosphere. This is known as *Faraday rotation*.

In [4] it was shown to be a necessity that at least one end in the radio link used circular polarized antennas, since one can not depend upon aligning the polarizations. Not only due to the Faraday rotation, but also because it is difficult to track the relative orientation of the satellite.

Another advantage is that using circular polarization mitigate multipath since the polarization degrades upon reflections with the ground [29] (if the ground is PEC the polarization completely swaps handedness). This may lead to less fading, and a lower link margin may suffice.

3 Link Overview

This chapter is intended to put the rest of the thesis in a context, by looking at the antennas from a systems perspective. It will explain why it was decided to use the turnstile antennas, and how this choice affects other parts of the satellite.

As already mentioned, this thesis is a continuation of the work done (by the author) in the specialization project also called *Antenna Systems for NUTS*[1] [4]. One of the goals of the project was to choose a suited antenna to ensure a link that is as *reliable* as practically possible. This suggests a top-down approach that requires some understanding of how the choice of antenna and orbital mechanics interact and impacts upon the link margin in a dynamical way.

Therefore, to present the choice of antenna, a review of some topics in [4] is required. Sec. 3.1 and Sec. 3.2 presents how the link budget is computed and how it is dynamically changing throughout the pass. Sec. 3.3 is a summary of which antennas were compared and how. The last section on the "download capacity" is *not* a review from [4] but rather a new effort that is done to gain further insight in the data link.

3.1 Link Budget

3.1.1 Link Margin as a Reliability Measure

With reliability of link, it must be understood the amount of data successfully transferred between satellite and ground station. Or more specifically, NUTS is specified to have a *Bit Error Rate* (BER) of 10^{-5} [4], meaning that one (or less) of 100000 bits are, on average, allowed to be detected erroneously. This is equivalent as saying that the *bit-energy-to-noise-density ratio* E_b/N_0 must be equal to, or above, a certain threshold $(E_b/N_0)_{\text{req}}$ [30]. This threshold depends upon the modulation scheme used, and whether or not error correction is implemented. In the time of writing, NUTS is assumed to use *non-coherent Frequency-Shift Keying* (FSK)

[1] This report is published at the NUTS website.

without error correction[2]. That yields $(E_b/N_0)_{\text{req}} = 13.8\,\text{dB}$ in theory plus 1 dB of *implementation loss*. The *link margin*;

$$\text{LM} = \frac{E_b}{N_0} - \left(\frac{E_b}{N_0}\right)_{\text{req}} \quad [\text{dB}] \quad (3.1)$$

from now on serves the purpose as a measure for the reliability of the link. In theory, if $\text{LM} \geq 0$ we achieve the specified BER or better, whereas if $\text{LM} < 0$ the BER will rapidly increase until the link is no longer sustained. In practice however, one does not expect a good link until the link margin is somewhat higher than zero, maybe 6 or 10 dB [4]. The reason is that there are numerous of effects of little significance, or effects one cannot possibly take into account such as fading.

Furthermore, E_b/N_0 can be expressed as a constant times the *Signal-to-Noise Ratio* (SNR) [4]:

$$\frac{E_b}{N_0} = \frac{S}{N} \cdot \frac{B}{R} \quad [\,] \quad (3.2)$$

where B is the noise bandwidth in Hz and R is the datarate in *bits-per-second* (bps). To understand how the choice of antenna affects the link margin it is therefore a necessity to take a closer look at the received signal and noise strengths.

3.1.2 Received Signal

The current NUTS link budget is built on the AMSAT-IARU template for CubeSats. In [4] it was thoroughly derived that the received power in the budget could be expressed as:

$$\begin{aligned} S = P_r = &P_t + G_t + G_r - \text{FSPL} - \text{PLF} \\ &- L_{t,\text{pnt}} - L_{r,\text{pnt}} - L_{t,\text{TL}} - L_{r,\text{TL}} - L_{\text{atm}} - L_{\text{ion}} \quad [\text{dBW or dBm}] \end{aligned} \quad (3.3)$$

P_t is here the transmitted power, and $L_{t,\text{TL}}$ is the passive losses from from the transmitter to the transmitter antenna. Likewise, P_r is the received power and $L_{r,\text{TL}}$ the passive losses from the receiver antenna to the receiver. $G_t(\theta_t, \phi_t)$ is the gain of the of the transmitter antenna in the direction (θ_t, ϕ_t) of the receiver antenna (in the coordinate system of the transmitter antenna). Likewise, $G_r(\theta_r, \phi_r)$ is the gain of the receiver antenna in the direction of the transmitter antenna. An example of an antenna (a dipole) with its angularly dependent gain is shown in Fig. 3.1.

Moreover, it is reasonable to assume that the antennas are slightly misaligned, which manifests itself as deviations in the (θ, ϕ)-angles for the respective antennas. One cannot know what these deviations will be, only that they will be within some bounds. Specifically for the NUTS-project, it is assumed that the antennas at the ground station can be controlled to be within 10° of the intended direction,

[2]It is generally agreed within the NUTS-team that someone in the future should implement error correction.

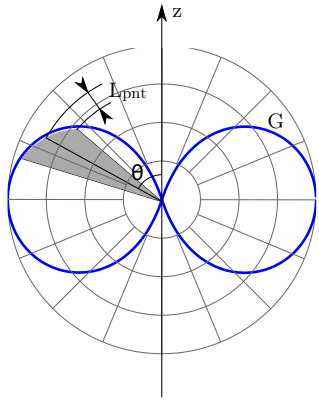

Figure 3.1: The angularly dependent gain of an antenna (a dipole in this example) and the pointing loss illustrated.

Table 3.1: Atmospheric and Ionospheric Losses

Elevation	Loss (L_{atm})
0°	10.2 dB
2.5°	4.6 dB
5°	2.1 dB
10°	1.1 dB
30°	0.4 dB
45°	0.3 dB
90°	0.0 dB

Frequency	Loss (L_{ion})
146 MHz	0.7 dB
438 MHz	0.4 dB

and the satellites attitude in space is accurate up to 10° as well [4]. Since these deviations will change the gain, it is common to introduce the *pointing loss* L_{pnt} as the worst-case reduction in gain that may happen within these bounds. This is also illustrated in Fig. 3.1.

The *Free-Space Path Loss* (FSPL) is as usual given by [4]:

$$\text{FSPL}(r) = 20 \log \left(\frac{4\pi r}{\lambda} \right) \quad [\text{dB}] \quad (3.4)$$

L_{atm} and L_{ion} represents attenuation in the received signal strength because of attenuation due to atmospheric gases and the ionosphere, respectively. L_{atm} is dependent on elevation angle ε, whereas L_{ion} is dependent upon frequency. Empirical values are shown in Tab. 3.1 [4].

Finally comes the *polarization loss* which is represented by the PLF. If an incoming wave has a different polarization than the receiving antenna, only some of the power flux which the receiving antenna intercepts will be available for reception. The PLF$(\theta_t, \phi_t, \theta_r, \phi_r)$ represents the loss of power this causes. Since the polarization of the transmitting and receiving antennas may differ depending on direction, the PLF is a function of $(\theta_t, \phi_t, \theta_r, \phi_r)$. Strictly speaking, it is not dependent on the polarization of the transmitting antenna at (θ_t, ϕ_t) but rather the polarization of the incoming wave, which might be different if the polarization changes after it is radiated. For instance due to *Faraday rotation*.

Faraday rotation is the phenomenon that the plane of polarization rotates as a wave travels through ionized gases, such as in the ionosphere. Therefore, if linear or elliptical polarization is used, the tilt angle of the polarization will be different at reception than when it was transmitted. NUTS circumvents this problem by utilizing circular polarization at the ground station. The PLF can then be assumed to only depend on $(\theta_{\text{sc}}, \phi_{\text{sc}})$ where the subscript "sc" indicates that it is the angles as seen from the spacecraft antenna irrespective of whether it is the transmitter or the receiver. A whole chapter is devoted to the topic of polarization loss and Faraday rotation in [4].

3.1.3 Received Noise

The received noise is given by [4]:

$$N = kT_sB \quad \text{[W]} \tag{3.5}$$

where $k = 1.381 \cdot 10^{-23}\,\text{W/Hz/K} = -228.6\,\text{dBW/Hz/K}$ is Boltzmann's constant and B is the (noise) bandwidth of the receiver. T_s is then the *equivalent system noise temperature*, which is the physical temperature a matched resistor at the input should have in order to produce the same amount of noise as all the contributions together. T_s consists of contributions from the thermal noise of the receiver itself, the antenna, and the passive components in between. In addition, there is a contribution from the noise the antenna intercepts due to noise that is radiated by all of its surroundings (c.f. brightness temperature and black-body radiation).

The antenna designer cannot do anything about the background noise, but by altering the gain of the antenna, noise contributors such as for instance the Sun can be less weighted. Since it is a restriction of the spacecraft antenna that it must be near-isotropic, the designer has little control over the noise it intercepts. Moreover, the thermal noise of wire antennas are typically very low due to the high conductivity in the wires[3]. It is therefore concluded in [4] that the choice of spacecraft antenna has negligible impact on the received noise. An estimate of $T_s = 310\,\text{K}$ has therefore been computed and used in the link budget [4].

[3]If the frequency was higher one might also consider using patch antennas, in which case one should expect some ohmic losses in the dielectric.

3.1.4 Current Link Budgets

NUTS has an uplink and downlink budget on both VHF and UHF since both bands may potentially be used for both transmission directions. In addition beacon at UHF has its own budget, meaning that there is five budgets in total. The parameters in all of these link budgets *before* the work of this thesis is carried out is stored in `link_data.txt` which can be found in App. E.3. It is not the task in this thesis to keep track of all the link budgets. It is only of interest to see how the antennas influence the link margin, which will be the same for all link budgets. Therefore, it is chosen to only reprint results for the UHF downlink margin in this thesis, since that is the lowest one.

3.2 Dynamics of the Link Budget

It is important to realize that as a satellite crosses the sky, several of the parameters in the link budget will change. Since the satellite is observed at a time-dependent angle as the satellite passes the sky, the antenna gain is one of these parameters. The choice of spacecraft antenna therefore has a great impact on how the link margin varies throughout the pass, implying that the antenna should be chosen with this in mind.

The link margin will be constant for a given elevation angle, which in turn depends upon time. The link margin can therefore be viewed as a function of either time or elevation angle. Hence, to analyse which antenna is superior, one can either look at which has the highest link margin versus time for a specific pass, or at which has the highest link margin versus elevation angle. Since the passes differ from time to time, it is more convenient to look at the link margin versus elevation angle.

The orbital dynamics behind the link budget will therefore be studied in this section.

3.2.1 Time-Dependent Parameters

The mechanical parameters used in the link budget are $(r, \theta_{\text{bs}}, \phi_{\text{bs}}, \theta_{\text{sc}}, \phi_{\text{sc}})$ where "bs" and "sc" denote the angles as seen from the coordinate system of the base station or spacecraft, respectively.

The direction $(\theta_{\text{bs}}, \phi_{\text{bs}})$ of the satellite in the coordinate system of the ground station antenna is dependent on the type of antenna. Since the ground station antenna is mechanically steered, the whole coordinate system is rotated such that the position of the satellite remains fixed within that coordinate system, plus minus some steering inaccuracy. For NUTS, this accuracy is within 10° [4]. This is neglected in the parameters $(\theta_{\text{bs}}, \phi_{\text{bs}})$, and the worst case reduction in gain that can occur within 10° is accounted for by means of the pointing loss. $(\theta_{\text{bs}}, \phi_{\text{bs}})$ is therefore *not* dynamical (time-dependent).

It is a very good approximation to claim that NUTS will have perfectly circular orbit [4]. Fig. 3.2 then illustrates how the line-of-sight distance r and the off-

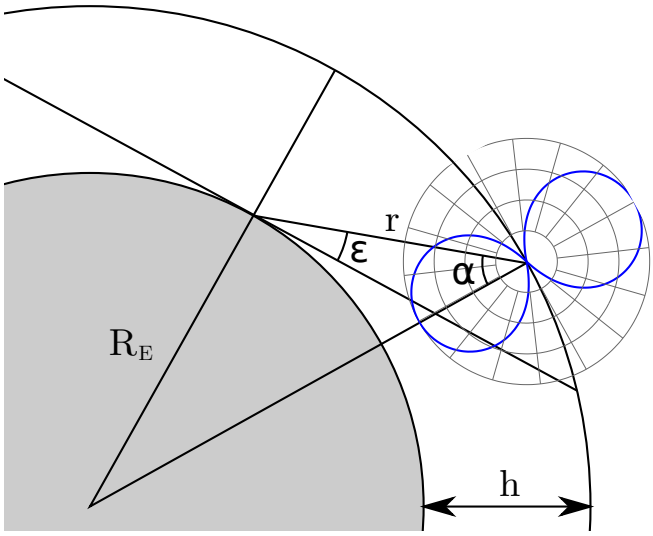

Figure 3.2: Illustration of the complex system which influence the link margin. The gain pattern for the satellite is for a horizontal dipole perpendicular to the paper. Each ring is 3 dB down.

nadir angle α is determined by only one time-dependent variable ε. The following relations was derived in [4]:

$$r = \sqrt{(R_E \sin\varepsilon)^2 + 2R_E h + h^2} - R_E \sin\varepsilon \quad \text{[m]} \quad (3.6)$$

$$\alpha = \arcsin\left(\frac{R_E}{R_E + h}\cos\varepsilon\right) \quad \text{[rad]} \quad (3.7)$$

where $R_E = 6371\,\text{km}$ is the mean radius of the Earth and h is the altitude of the orbit, often assumed to be 600 km in [4]. As seen from (3.4) FSPL is time-dependent, since it depends upon r.

It is obvious from Fig. 3.2 that $(\theta_{\text{sc}}, \phi_{\text{sc}})$ is also time-dependent. In order to reveal the dependence one must relate α to the coordinate system for the specific antenna under consideration[4]. Notice however, that there is one degree of freedom that is not predictable. If, for instance, the antenna's coordinate system is made such that the z-axis points in the nadir direction, then $\theta_{\text{sc}} = \alpha$, but ϕ_{sc} however may be anything, presuming that extraordinary attitude control is not present. During simulations one must therefore choose a value for this degree of freedom such that the gain is minimized. Thence, one is certain that the actual link margin cannot be lower than the calculated one.

[4]Nadir will be in different directions in the coordinate systems of the antennas that are to be considered.

Table 3.2: Dependence on Link Parameters

Variable	Depends on ...	
	Satellite Antenna	Elevation Angle
P_t	–	–
$L_{t,\mathrm{TL}}$	–	–
$L_{r,\mathrm{TL}}$	–	–
G_{bs}	–	[1]
G_{sc}	Yes	Yes
$L_{\mathrm{bs,pnt}}$	–	–
$L_{\mathrm{sc,pnt}}$	Yes	Yes
FSPL	–	Yes
PLF	Yes	Yes
L_{atm}	–	Yes
L_{ion}	–	–
T_s	[2]	[2]
B	–	–
R	–	–
$(E_b/N_0)_{\mathrm{req}}$	–	–

[1] Dependent if the ground station use a phase-steered antenna. Not dependent for a mechanically steered antenna.
[2] Not significantly dependent.

In Sec. 3.1 G_{sc} and PLF are easily seen to be dependent upon $(\theta_{\mathrm{sc}}, \phi_{\mathrm{sc}})$. But the pointing loss will also vary. Why? If the slope of the gain is steeper for some values of $(\theta_{\mathrm{sc}}, \phi_{\mathrm{sc}})$ than others, then adding a few degrees of inaccuracy to those initial values can yield more reduction in gain than for other initial values. To summarize, the dependencies in the link budget are listed in Tab. 3.2.

How ε changes with time is also a very interesting question, and a necessary one in order to determine how the link margin varies with time. In [4] an analytical expression for the elevation-time relation was derived based upon the assumption of a perfect pass, i.e. a pass where the satellite crosses the zenith, and the Earth's rotation is neglected within the duration of the pass. Most passes however, are not close to crossing zenith. Simulations over a time span can be done to get a more realistic picture of the elevation-time relation. This was also done in [4], but more recent simulations will be presented later in this report. Nonetheless, it is sufficient to consider link margin versus elevation angle to conclude which antenna is better suited.

3.3 Analysis of Different Antennas

The method that was used to analyse different antennas in [4] was a combination of simulations in *Computer Simulation Technology Microwave Studio* (CST) and a

tool developed by the author in MATLAB. CST was used as an electromagnetic simulator that can be used to determine the gain of the antennas, while the MATLAB tool takes into account dynamical effects of the link budget. The MATLAB tool computes which angles to use for $(\theta_{\text{sc}}, \phi_{\text{sc}})$ as well as the FSPL as a function of elevation or time as described above. Plots of the link margin versus time or elevation angle can then be made.

3.3.1 Reformulation of Link Parameters

To be able to perform the MATLAB simulations, a few of the link budget parameters had to be reformulated. As seen in Tab. 3.2, G_{sc}, $L_{\text{sc,pnt}}$ and PLF depends upon the spacecraft antenna, meaning that these variables has to be fetched from the CST simulations. CST has the ability to export a partial gain consisting only of the part that can be received from an ideal RHCP polarized antenna. This is known as *circular polarized gain* or just *circular gain* and therefore takes into account both the total gain and the polarization loss that occur assuming a perfectly circular antenna is used in the other end. To be more precise:

$$G_{\text{sc,RHCP}} = G_{\text{sc}} - \text{PLF}_{\text{RHCP}} \qquad \text{[dBiC]} \quad (3.8)$$

where $G_{\text{sc,RHCP}}$ is the RHCP partial gain, given in dBiC, where C indicate circular, and PLF_{RHCP} is the polarization loss given that the other antenna is perfectly RHCP polarized. The first reformulation is therefore that the circular gain is used in the link budget in place of the usual gain, and that the PLF term is not used.

The other reformulation is that $L_{\text{sc,pnt}}$ is also set to zero. Instead, a shift in the angles $(\theta_{\text{sc}}, \phi_{\text{sc}})$ is manually imposed in MATLAB such that the circular gain is decreased as much as possible within the angular accuracy of the satellites attitude. This will account for both lower gain and higher PLF that may occur due to attitude inaccuracy.

3.3.2 Results for Different Antennas

Four different antennas were simulated with the above mentioned MATLAB tool; a theoretical dipole (in the horizontal plane), a theoretical monopole (vertically aligned), a simulated monopole, and a simulated turnstile. Analytical expressions were used for the theoretical dipole and monopole whereas CST simulations was performed for the latter two. The CST models for the simulations are depicted in Fig. 3.3. The monopole was only considered to be used for UHF while the VHF antenna still being a turnstile. The idea was that the VHF turnstile should act like a virtual ground plane for the UHF monopole. In order to verify whether or not the concept worked, it was used both a simulated gain and a theoretical gain for the UHF monopole.

The simulated link margin for the different antennas are shown in Fig. 3.4. Notice how the link margin goes to $-\infty$ dB near 90° elevation for the monopoles. This is reasonable due to the zero in the pattern of a monopole. The reason why it

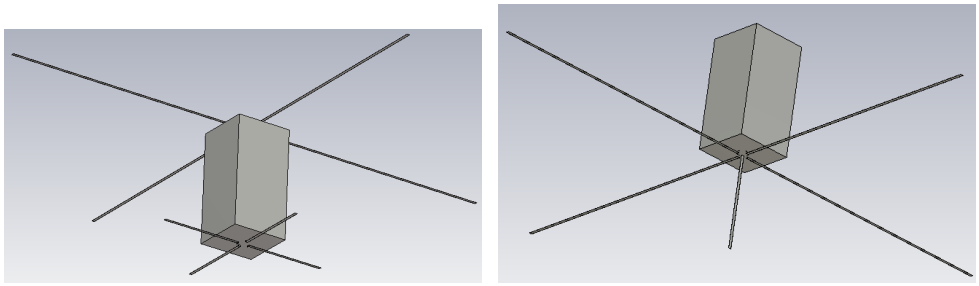

(a) Two turnstile antennas (b) Monopole for UHF

Figure 3.3: Two sets of antennas considered and simulated for NUTS. From CST.

goes to $-\infty$ dB slightly *before* the 90° elevation is due to the pointing loss. When the ground station is within 10° of the nominal direction of the zero (as seen from the satellite) the pointing loss will make sure the link margin is $-\infty$ dB. The simulation presented in Fig. 3.4 is valid for 600 km altitude.

The simulations clearly shows that the turnstile antenna yields the highest link margin for all elevation angles, particularly for the low elevation angles. As pointed out in [4], the link margin for low elevation angles are more important than for high elevation angles since the satellite, most of the time, will be visible only at rather low elevation angles (this can also be seen in Fig. 3.6). Therefore, it was no doubt concerning which antenna to build; namely the turnstile antenna [4]. Simulations was also done for 400 km and 800 km altitude, but did not altered the conclusion and is therefore not included here.

3.4 Downlink Capacity

It has been a problem within the NUTS-team that several vague assumptions has been made regarding how much data one can expect to download from the satellite. But no rigorous analysis has previously been carried out. Part of the problem is that it is not explicitly written in a problem statement for any of the NUTS theses, and it therefore becomes nobody's responsibility. As this knowledge is needed to determine how much the payload data must be compressed, the author and Marianne Bakken who has written the thesis *Signal Processing for Communicating Gravity Wave Images from the NTNU Test Satellite* [5] has done a joint effort to solve this problem. This joint effort is presented in this section.

First of all, it is assumed that UHF will be used for download[5]. It is assumed that the altitude will be in between 350 km and 650 km. The UHF download link margin has therefore again been simulated, for 350, 500 and 650 km as shown in

[5]It is not decided yet which band is to be used for download. Therefore the worst-case in terms of link margin, UHF, is assumed. It is also UHF that has been considered for downlink earlier [4].

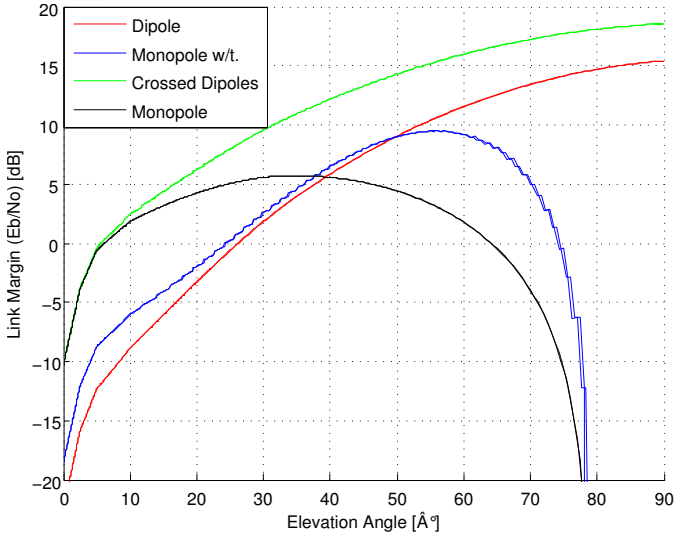

Figure 3.4: The link margin versus elevation angle

Table 3.3: Downlink capacity for different altitudes assuming that $LM > 10\,\text{dB}$ is needed

Altitude	Min. Elevation	Average Capacity
350 km	21°	581 kB/day
500 km	28°	627 kB/day
650 km	34°	636 kB/day

Fig. 3.5. Assuming that a link margin of 10 dB is needed to ensure a robust link, the minimum (threshold) elevation angles are as listed in Tab. 3.3.

Further on, *Analytical Graphics, Inc. Satellite Toolkit* (STK) was used to simulate the elevation angle as a function of time for the same altitudes during a whole week (to get a realistic distribution of good and bad passes). Fig. 3.6 shows, as an example, the passes for the first simulation day for the 500 km altitude simulation. For these simulations, it was assumed that the orbit was perfectly circular (eccentricity equals zero) which is a quite good assumptions for CubeSats [4, 11]. It was also assumed to that it was a sun-synchronous orbit, meaning that the inclination is 98°. This assumption is based upon the fact that NUTS is to be in a polar orbit and that it therefore most likely will be in a sun-synchronous orbit, such as the CP3 CubeSat [31]. The RAAN was simply set to zero since it is unknown, and since this simplification only impose a time-shift of when the orbit passes the ground station.

The ground stations coordinates was taken as $63°25'47"N, 10°23'36"E$ (Trond-

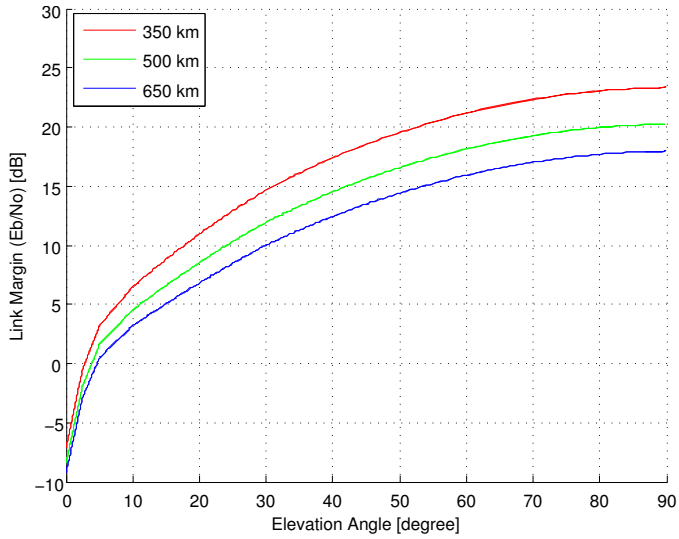

Figure 3.5: UHF download link margin for different elevation angles

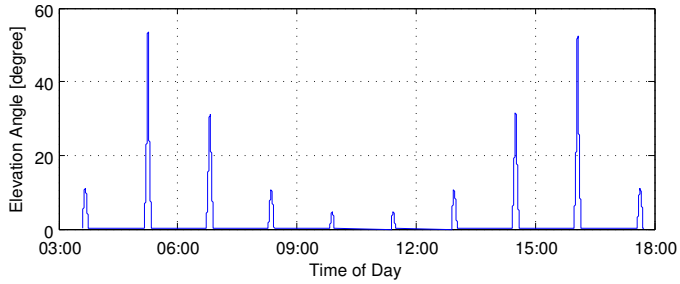

Figure 3.6: An example of elevation versus time.

heim)[6].

The simulated elevation angle versus time, was exported to a text file which was read by the MATLAB function `read_stk_elev()`. `threshold_stk_elev()` is then used to extract the start and stop times for the intervals when the satellite is above a certain threshold elevation angle. Multiplying the duration of all intervals by the bitrate (9600 bps) and dividing by 7 (days in the simulation span) then yields the average data downloaded per day (the capacity). Plots of this is presented in Fig. 3.7. The capacity for the computed minimum elevation angles are also listed in Tab. 3.3.

[6]The step-size was taken as fine as 1 second since an error of several seconds quickly becomes an error of several kB in terms of downlink capacity. The readers interested in orbital dynamics might like to know that orbital perturbations up till the J4 term, including the oblateness of the Earth, was included in the simulations. More information about orbital dynamics can be found in [9, 13, 10, 14].

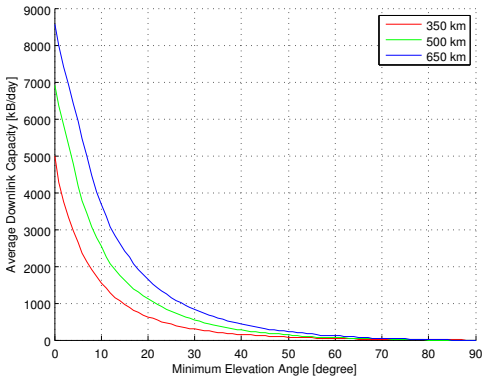

(a) Elevations from 0° to 90°.

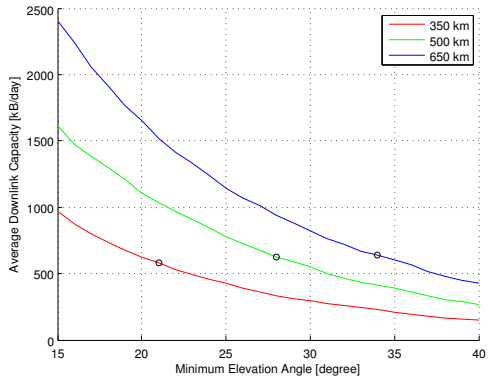

(b) Elevations from 15° to 40°. The circles indicate the computed minimum elevation angle for the different altitudes.

Figure 3.7: Downlink capacity in kB per average day for NUTS.

The conclusion is that there is a balancing effect. Since the FSPL is lower for low altitudes, lower elevation angles can be used for the download, which increases the capacity. On the other hand, the passes will become shorter, and more of them will be concentrated around the really low elevation angles which decreases the capacity. Anyhow, there is a lot to gain by slightly increasing the link margin such that lower angles can be utilized. The limit in download capacity imposes difficulties when several images from the IR camera payload are to be downloaded, which suggests that compression algorithms should be used. More about that in [5].

4 Mechanical Aspects

4.1 Exterior Part

It is already mentioned that the satellite will use two turnstile antennas, one on the nadir plane and one on the zenith plane. However, according to the CubeSat standard, the satellite should be kept within certain size constraints of a double CubeSat during launch. The antennas must also be within that volume during launch, and then deployed when in-orbit. The CubeSat standard specifies that there may be components extruding up to 6.5 mm *outside* the $20 \times 10 \times 10$ box as shown in Fig. 4.1. Within 8.5 mm of the corners there may *not* be any components since the corners will act like rails in the P-POD.

It was suggested in [4] to wrap the satellite with the antennas like a gift. This is illustrated in Fig. 4.2. The UHF antenna, which has the shorter elements, must be folded first. The VHF antenna is folded on top of that. Since each element of the VHF antenna goes more than halfway around the satellite, one of the elements must be folded on top of that on the other side. Also, the two dipoles will overlap

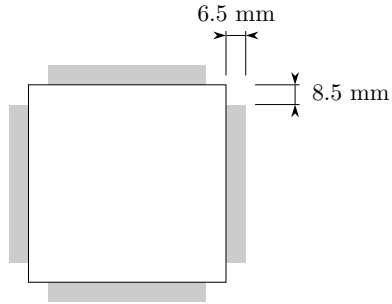

Figure 4.1: The shaded area illustrates the space available on the exterior of the satellite.

with each other in the bottom of the satellite.

In the middle of each side wall, in between the solar cells, there will be room for tightening the measuring tape to the satellites body with nylon thread. For deployment, the nylon thread will be melted by a wire made of *Nickel-Chromium alloy* (Nichrome), which turns hot when current is applied to it. For the sake of redundancy, two Nichrome wires will be twinned around each nylon thread such that at least one of them will burn off the nylon thread upon deployment.

To build and verify that this works like intended, is not a part of this thesis, but was given as a project to a group of students in the NTNU-course "TFE4850 EiT - Studentsatellitt" [32]. It was concluded that it was feasible, and that all of the antennas could be wrapped within the specified 6.5 mm. Further on, it was concluded that there was no danger of cracking the solar cells or jamming the antennas upon deployment, if mounted correctly.

The circuit applying current to the Nichrome wire in [32] consisted only of a transistor and two resistor. In addition, it is assumed to be triggered by an external signal, for instance from a *Microcontroller Unit* (MCU), at the correct time. Moreover, the Nichrome wires should be triggered sequentially, since otherwise, the peak current may be too large for the power supply. Feasible triggering sequences are also studied in [32].

It was decide within the NUTS-team that it is most convenient to put the deployment circuit on the side wall PCBs together with the solar cells. These circuits are therefore not a part of the antenna modules, and hence not a part of this thesis.

4.2 Interior Part

The NUTS-team has agreed that the space that can be used on *each* antenna module *inside* the satellite is a $100 \times 100 \times 6$ mm box (or thinner) except for a connector and some nuts (more about that in Sec. 6.7) and a square centimetre on each corner as shown in Fig. 4.3. The corners are reserved for the frame, and will also be used for mounting the antenna modules to the frame. In addition, one piece of measuring tape will stick out of each (thin) side and be wrapped on the *outside* of the satellite until deployed.

The antennas, along with its feeding networks, should be mounted on a PCB. A potential problem is that another module, also consisting of a PCB with a ground plane, is mounted on top of that, such that the antenna elements, or components in the feeding network are short circuited. Even if that does not happen, one must make sure that the characteristic impedance of the microstrip lines does not change severely due to proximity of other conducting material. Actually it is a *requirement* from the team that it should be possible to put other modules on top of the antenna modules without any separation. Therefore it has been decided to put another PCB with only a ground plane at small distance away from the first one, just sufficient to not change the performance too severely, and let it be a part of the antenna module (see Fig. 4.4). In that way the performance of the antenna modules does not depend upon what is mounted on top of it. It is also assumed

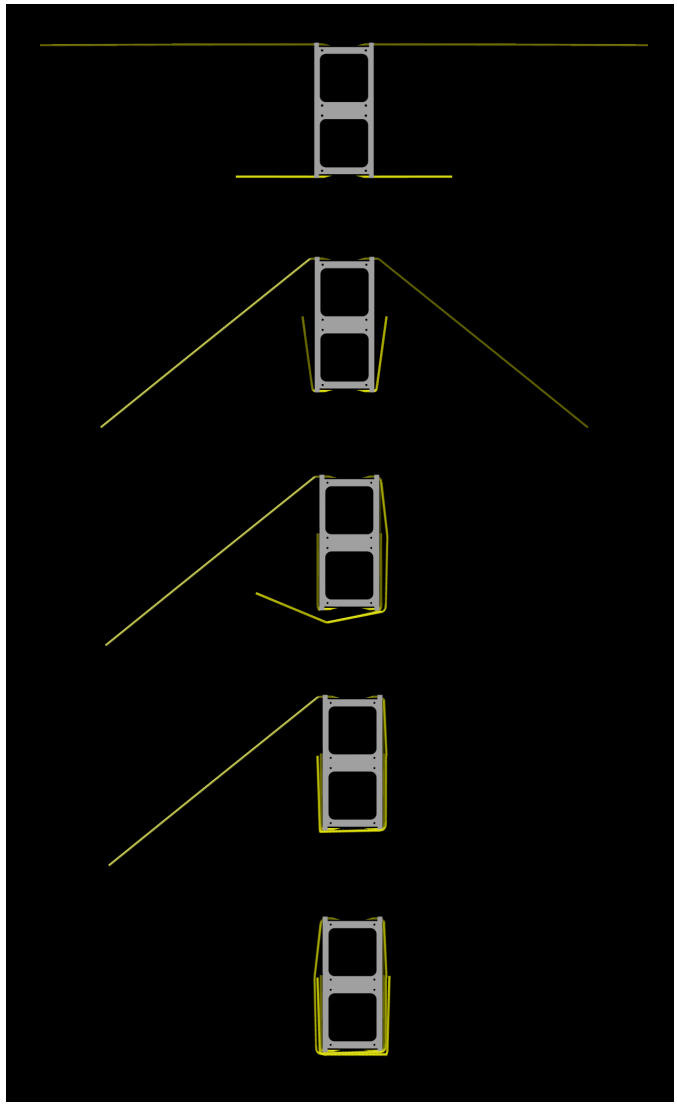

Figure 4.2: The folding of the antennas before deployment. Courtesy of S. Birkeland, T. H. Bryne, T. Grav, K. A. Kvåle and T. B. Martinsen [32].

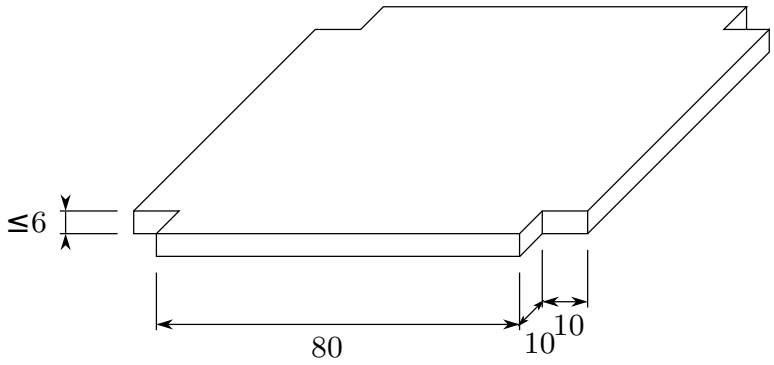

Figure 4.3: Space available for each antenna module. All lengths are in mm and the space available are symmetric.

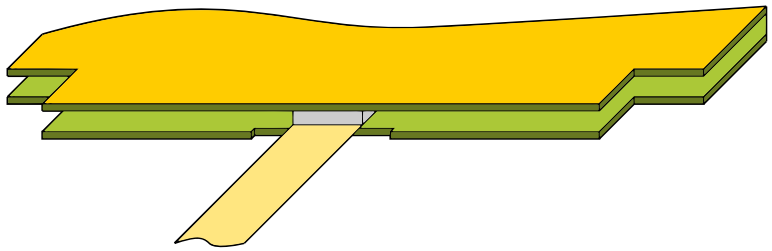

Figure 4.4: The idea for each module is to stack two PCBs

that this extra PCB will provide some sort of shielding against noise albeit it is not perfect due to the opening at the edges of the PCBs. (Remember thought, that this opening is small compared to the wavelength). The extra PCB will also make the module mechanically more robust.

To be more specific, 0.8 mm thick *Flame Retardant 4* (FR4) PCBs will be used, and the spacing between them will be 3 mm. The lower PCB on the drawings will be mounted closest to the satellites center (this is true for both antenna modules, meaning that the UHF PCB will be upside down). The two PCBs will be tightened to each other with bolts and nuts with spacers in between them as illustrated in Fig. 4.5. The nuts will be on the outside of the lower PCB. Since there are no components inside the satellite lying face-to-face to the antenna module the height of the nuts does not count in the total height of the antenna modules, but rather occupies space that will not be used for other modules anyway[1].

There will also be space for an *SubMiniature version A* (SMA) connector in the corner below the lower PCB. This also does not count in the height of the antenna module either. The remaining 1.4 mm that *is* part of the module height will be used for the bolt heads on top of the upper PCBs (since they are thinner than the

[1]This does not mean that the antenna module could have been thicker. The satellite frame will have a wall on the outer edge of the satellite further down.

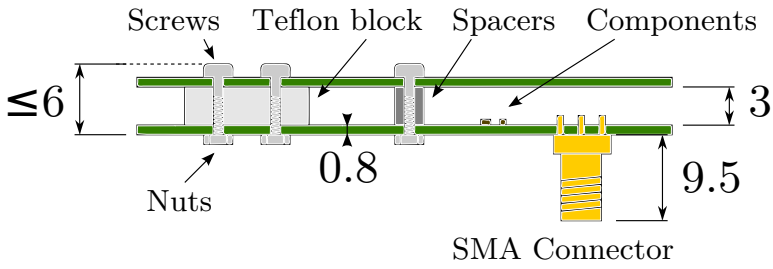

Figure 4.5: The height of the different components that comprise the antenna modules. All lengths are in mm. NB: The components relative positioning is not realistic in this illustration.

nuts). Cylindrical screw heads will be used despite the fact that cone-shaped heads could decrease the space needed as they are recessed into the PCB (and possibly also the spacers/teflon block). They do, however, dramatically increase the risk of cracking the PCB during launch and vibration testing of the satellite, which is why they should not be used.

Moreover, the screws should be of type M2×6 mm (6 mm long and fit for 2 mm holes) and they should be made of steel. It might be tempting to use nylon bolts some places since they are insulating. Nylon bolts, however, are not as strong as steel bolts and are therefore not fit for this purpose.

The feeding network will be made on the *lower* PCB on the layer inside the module. The network will consist of lumped components and microstrip lines. The outer layer of this PCB is the ground for the microstrip lines as well as acting like a shield. SMA connectors to feed and test the circuit will also be mounted on the outer layer.

The *upper* PCB has no circuitry but only a grounded layer of copper on each side of the module. This PCB will be the above mentioned shield, protecting the feeding network.

4.3 Mounting the Antenna Elements

Each piece of measuring tape will be squeezed in between the lower PCB and a small teflon block which fits exactly between the two PCBs. The measuring tape elements will be fed simply by leading the microstrip lines to them. Two bolts will go through the teflon blocks as well as the PCBs, and the measuring tape to fasten the measuring tape properly as shown in Fig. 4.5.

Also notice how a little piece (2 mm wide) is removed from the lower PCB's edge around the measuring tape (See Fig. 4.4). This allows a smoother bend of the measuring tape without the measuring tape going further away from the body of the satellite than necessary. A cross-section of an edge of the satellite is depicted in Fig. 4.6 to illustrate this.

The teflon block is not placed on the edge of the PCB either but *further* 4 millimetres in. The reason for this is to have a stronger mechanical solution. It is the

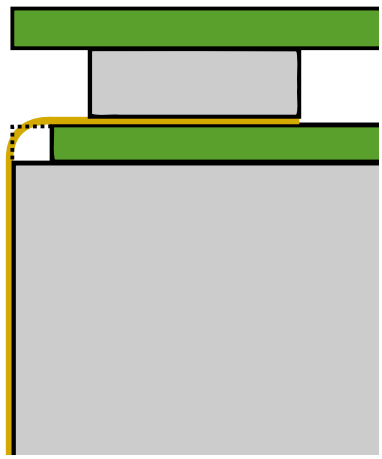

Figure 4.6: How the measuring tape will be bent at the corners of the satellite.

curvature *across* the measuring tapes that make them straighten out when nothing holds them back. When the measuring tape is squeezed in between the PCB and the teflon block this curvature is flattened out, and the measuring tape loses some of its ability to straighten out. The tape quickly restores its curvature where it is not squeezed anymore. Hence, by leaving a few millimetres of free space in front of the teflon box the measuring tape will be slightly stiffer at the bend, and thereby more mechanically robust. The tape will oscillate a bit like a pendulum when the antennas are deployed. The fact that the bend is not immediately after the tape is squeezed will dampen these oscillations since the tape is stiffer[2].

In Fig. 4.7 a more detailed mechanical outline is given. It shows that the measuring tapes should stick 20 mm into the satellite. As already mentioned, a 2 mm piece of the lower PCB is removed, and there is another 4 mm before the teflon box. Due to the fitting of the module within the frame, it is beneficial if as little as possible of the space 6 mm from the edges are used, such that parts (or all) of it can be removed or used for fastening purposes. This area is therefore left untouched except for where the antenna elements exit.

4.4 Mechanical Compatibility with other Modules

The antenna module on the *nadir* plane of the satellite must have a hole for the lens of the infrared camera payload to pass through [5]. See Fig. 4.8. As no hardware is yet determined for the payload, assumptions has to be made regarding this hole. One possibility is to have the hole centered such that the lens passes through the feed gaps of the dipoles. The radius of this hole is 25 mm for two reasons; (1) It is bigger than the lens of the camera which has been considered that has the biggest

[2]The statements must be considered as practical considerations that follows from simple experiments performed by the author with a measuring tape, a table edge, and a small metal ruler.

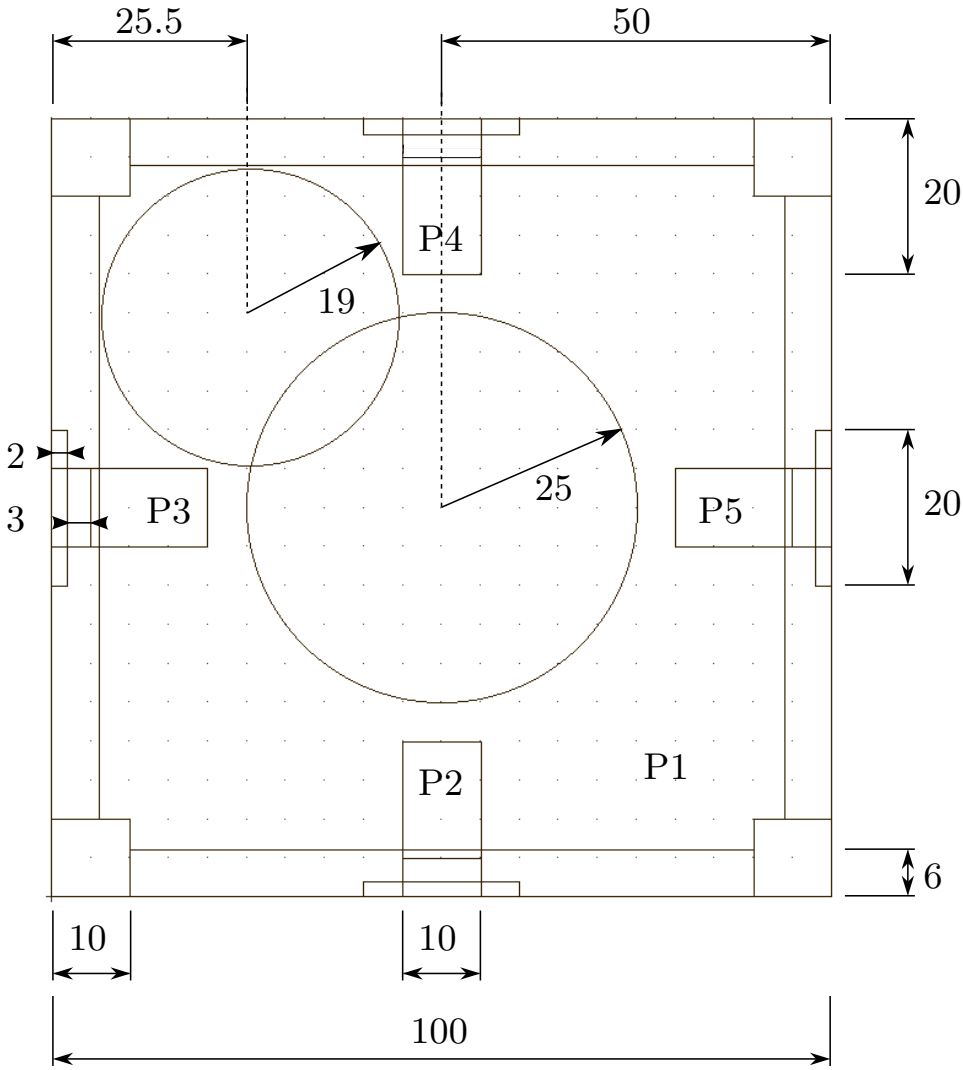

Figure 4.7: The mechanical design of the PCBs as seen looking down on the inner layer of the lower PCB (this is important to get the port labelling correct). All lengths are in mm and the PCBs are symmetric. The physical positioning of ports 1-5 are marked as P1-P5.

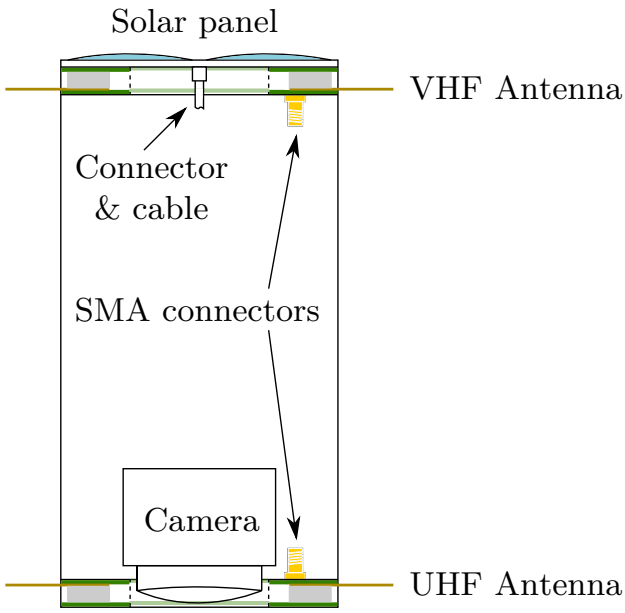

Figure 4.8: How the different modules will be mounted on the satellite and how it interferes with the antenna modules.

lens (45 mm *diameter* [5]) and (2) it is the biggest hole the author could possibly fit in between the antenna elements.

It has also been discussed within the team to have a smaller camera that can fit in the corner of the satellite, as this might make it possible have an S- or C-band patch antenna in the other corner (on top of the UHF antenna module). The only camera that is considered for this has a lens diameter of approximately[3] 20 mm. The hole in the corner can have a radius up to 19 mm *if* the center of the hole is 25.5 mm from the edges. The cable to the patch antenna must then go somewhere through the big hole in the center (see Fig. 4.7). As it is unknown what will be the case, the antenna modules will be will be made with this space unused. There will initially be PCBs in both areas, but it can be removed as needed later on.

The antenna module on the *zenith* plane, will be mounted underneath a PCB of solar panels. On the backside of this PCB there will be a connector in order to connect the solar panels to the EPS. The cable must go through the VHF antenna module, and furthermore, the solar panel module is not thick enough to house the connector[4], meaning that the connector will go through the antenna module, as well. It is estimated that the hole needed for this connector (and cable) is a square hole of approximately 20×10 mm. Since the connector must lie in between

[3]This is approximate since it is found by measuring it on a picture in the datasheet and comparing it in a dime that is also on the picture. This datasheet is available as an appendix in [5].

[4]It was agreed that the PCB with the solar panels can occupy the same amount of space as shown in Fig. 4.3 except that it can only be 4 mm thick.

two rectangular solar cells, and thus can not lie in a corner, this connector must go through the center of the antenna module. It is obvious that the hole already reserved for the camera lens is more than big enough (remember that the same PCBs will be used for both antennas).

Finally, the antenna module must be mounted to the frame somehow. The 1 square centimetre corners will be used for this purpose. Despite the fact that the antenna module itself can not use the corners, it has been agreed that the PCBs should be made *with* the corners, and the designer of the frame will make a fastening mechanism that attach the corners of the antenna modules to the frame. The parts of the corners that needs to be removed in order to make this fit will be removed after production.

4.5 Port and Element Labelling

Finally, it is time to label the antenna elements such that is possible to refer to them later on. Fig. 4.7 depicts the lower PCB (where the feeding network is) as seen from above. I.e. we look down to the layer where the components are mounted. Port 1 (P1) is the SMA-connector that connects the antenna module to the radio tranceiver. It is located somewhere in the lower right corner (opposite to the corner that can be used for the camera lens). Ports 2 to 5 (P2–P5) are the ports that connects the antenna elements (made of measuring tape) to the feeding network. They are connected to the measuring tape by leading microstrip lines to them. Alternatively, an SMA-connector can be soldered in place of the measuring tape for testing purposes (more about this later). These ports are labelled in a clockwise manner as seen in the figure. The antenna elements will also be referred to as element 2-5, correspondingly. Note that this report makes a clear distinction between *antennas*, *dipoles* and *antenna elements* to make it easier for the reader to understand what is meant. The satellite will have *two* turnstile antennas (one for VHF and one for UHF), each consisting of *two* perpendicular dipoles. Each of the dipoles consists of *two* elements that are fed by one port each.

5 A Study of Feeding Networks

Feeding VHF and UHF turnstile antennas on a small satellite poses some problems that are not encountered when these antennas are used on the ground. The main problem is that there is not enough space on-board the satellite for a distributed feeding network (this statement will be justified in Sec. 5.6.1). Because of this, it was necessary to study alternative ways to feed the antennas. First the requirements for the feeding network is identified in Sec. 5.1. Further on, several sub-circuits that has been considered, and how they were meant to be used in a complete feeding network, are presented. The chapter ends by explaining what is the better solution and why. The more rigorous design (and analysis) of the chosen network is presented in Ch. 6.

5.1 Requirements

The feeding network for the antennas has several purposes. It can be grouped into the following requirements:

Quadrature power splitting/combining. The power should be equally split between the two dipoles and the two dipoles must be fed with a mutual phase-shift of 90° (in the transmitting mode) in order to achieve circular polarization. In the receiving mode the device combines the power in a reciprocal manner. A device that does this is called a *Quadrature Power Splitter* (QPS).

Matching. The feeding network must act like a matching device such that both the dipoles and the radio is (more or less) matched, and thereby little power is reflected.

Balun. The signal from the radio is fed to the antenna through a coaxial cable, meaning that it is an unbalanced signal. Dipole antennas are balanced struc-

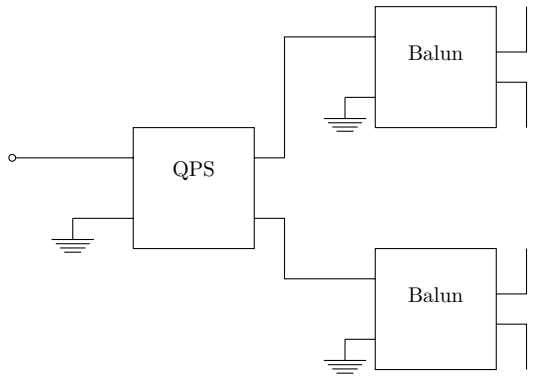

Figure 5.1: How turnstile antennas are typically feed

tures implying that a balun (balanced-unbalanced) should be used in between to ensure that all the current flows in the antenna elements as intended.

Static buildup protection. As the spacecraft will go through plasma the antenna elements may become charged unless they are DC-wise connected to ground [20]. The antenna elements should therefore be connected to ground through an inductor.

All of this is typically achieved as shown in Fig. 5.1. An unbalanced signal is split into quadrature by a QPS and fed to the antennas through balancing devices (baluns) which is made such that the antennas are DC-wise grounded. Moreover the baluns can have different input and output impedances (an inherent impedance transformation) in order to match the dipoles. The theory for various power splitters and baluns will be studied later in this chapter, before different solutions for the complete feeding network is ivestigated.

5.1.1 Environmental Requirements

Ideally, the circuit should also be:

- Small enough to fit within the designated space on-board the satellite
- Mechanically robust to survive the vibration test and launch of the satellite
- Robust against radiation to survive space weather
- Made of components with a large enough operating temperature range in order to survive the temperatures in space
- Made of components with small enough temperature coefficients to ensure sufficient performance
- Made of *Commercially available Off-The-Shelf* (COTS) components, i.e components that are not specially made for space, but readily available

Not all of these requirements go well together. For example; there are specially made components that survive extreme vibrations and space weather called space grade components. These are often very expensive and definitely not COTS components. It is a requirement for all the circuitry on-board the satellite to only use COTS components. Space grade components may only be considered for NUTS if it is necessary, and not too expensive.

The harsh radiation environment in space may cause ionization of electronic components such that a charge occur inside them. This, in turn, may lead to the change of a bit (*Single Event Upset* (SEU)), or even worse, permanent damage for example by damaging a transistor's gate or degrading the crystal structure in silicon or other semiconducting materials [33]. If particles is charged within a passive network it is probably not damaging since the passive components are often larger and without semiconducting material. The feeding network should therefore be comparatively robust against this even if made with COTS components.

Concerning temperature, no study has been done w.r.t. which temperature the different parts of NUTS will experience, so assumptions must be made. A rule of thumb within the NUTS team has been that all components should operate within $-40°C$ to $+85°C$, perhaps except special parts such as the infrared camera where such operating temperature ranges are difficult to find [5]. According to [31], the CubeSat CP3 satellite's exterior experienced temperatures between $-30°C$ to $+20°C$ during normal operation in 2007 (the interior varied less), and almost up to $+50°C$ at times where the satellite constantly was illuminated by the sun. Since CP3 had similar orbital elements[1] as NUTS will have, the assumed temperature range of $-40°C$ to $+85°C$ is likely more than enough.

5.2 Distributed Power Splitters

A *power divider* or *power splitter* is a device that is used to split power into two or more output ports. As mentioned in Sec. 5.1, this will be needed to split power between the two crossed dipoles. This section will focus on distributed 2-way equal-split power dividers although it is possible to have N-way dividers (N outputs) with unequal power division between the output ports.

Of course the divider should be designed such that no power is wasted (theoretically). There are basically two ways a device *may* cause loss of power. One is that the device itself is lossy, i.e. it contains some resistance that dissipate power. The other is that the device is not matched at one or more of its ports and therefore power is reflected and dissipated somewhere else in the circuit. It can be shown that it is impossible to create a lossless, reciprocal, three-port device that is matched on all ports [15]. A reciprocal device is one where the S-matrix i symmetric, i.e. $S_{ij} = S_{ji}$. This happens when the device is made only of passive and anisotropic components. To create anisotropic components, one typically use ferromagnetic materials, which are not considered to be practical within the specified size constraints a satellite due to size and weight[2]. Active components could be used, but

[1] More precisely, it had a *Low Earth Orbit* (LEO) orbit with an inclination of 97.9°.

[2] Also, if ferromagnetic components were used it would likely not be power splitter but a

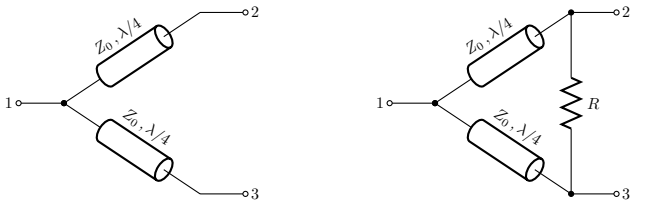

(a) Power Splitting with QWTs (b) Wilkinson Power Splitter (WPS)

Figure 5.2: Two common power splitters

they would increase the complexity, and they are more noisy than passive ones [34]. Therefore, non-reciprocal devices will not be considered, and the 2-way power dividers must either be lossy or not matched at all ports. Beware that this does not mean that there *is* a loss of power, just that the component *may cause* a loss of power (depending on its use and design). This will be illustrated later on.

If a power splitter is made of reciprocal (passive and non-ferromagnetic) components it may also be used as a power combiner. I.e. that ports 2 and 3 act like inputs and the power from them is combined at port 1. Throughout this report a power *splitter* should be understood as a device that can be used for both power *splitting* and *combining* as they are made of reciprocal devices.

5.2.1 Power Splitting with QWTs

A common way to feed two dipoles is by simply matching them with *Quarter Wave(length) Transformers* (QWTs) as shown in Fig. 5.2(a) [26, 20]. Consider two loads of i.e. $Z_{\text{sys}} = 50\,\Omega$ connected to ports 2 and 3, respectively. Each load is then connected to a QWT whose input impedance is accordingly given by (2.11). Since the input of the two QWTs appear in parallel and are identical, the input impedance must be half:

$$Z_{\text{in}} = \frac{Z_0^2}{2Z_{\text{sys}}} \quad [\Omega] \quad (5.1)$$

Assuming that port 1 should be matched to the same impedance as the antenna impedance ($Z_{\text{in}} = Z_{\text{sys}}$) then the characteristic impedance Z_0 of the QWTs must be:

$$Z_0 = \sqrt{2}Z_{\text{sys}} \quad [\Omega] \quad (5.2)$$

Z_{sys} is often called the *system impedance*.

Since no power is reflected at the input (it is matched) and the device is lossless, all the power must be delivered to the load (with equal split due to symmetry).

circulator [15]

And this despite the fact that the splitter is mismatched at the outputs[3]. Thence;

$$S_{21} = S_{31} = \frac{1}{\sqrt{2}} e^{-j90^\circ} \quad [\,] \quad (5.3)$$

where the 90° phase lag is due to the length of the QWTs. This means that if a signal is fed to *one* of the outputs, there will be some reflections (and actually some power will be transmitted to the other output port[4]). If, however, the same signal (common-mode) is fed to both ports 2 and 3, all the power will be transferred to the port 1, since this is the reciprocal mode of operation as exciting port 1. Hence the circuit will also work as a perfect power combiner *if* (and only if) no differential-mode signal is excited across ports 2 and 3.

Due to the striking similarity between this splitter and the previous one, it will simply be assumed that the *Wilkinson Power Splitter* (WPS) is the superior one throughout this chapter. In Sec. 6.3 the impact of setting $R = 0$ is studied in order to properly compare the two.

5.2.2 Wilkinson Power Splitters (WPS)

Contrary to the previous splitter, the 2-way *Wilkinson Power Splitter* (WPS) (shown in Fig. 5.2(b)) is matched on all ports [15]. This is achieved by introducing a resistor between ports 2 and 3 that dissipate the differential mode signal. The resistor makes the divider lossy, but if used correctly (without a differential signal at the output), no power is dissipated in the divider.

Usually the WPS is designed for an equal split and it is assumed that all ports is matched to the same (real) impedance Z_{sys} (typically $50\,\Omega$). In that case the S-parameters of the splitter is given by:

$$S = \begin{bmatrix} 0 & 1 & 1 \\ 1 & 0 & 0 \\ 1 & 0 & 0 \end{bmatrix} \left(-\frac{j}{\sqrt{2}} \right) \quad (5.4)$$

and the design equations are as follows:

$$Z_0 = \sqrt{2} Z_{\text{sys}} \quad [\Omega] \quad (5.5)$$

$$R = 2 Z_{\text{sys}} \quad [\Omega] \quad (5.6)$$

The derivation can be found in [15]. It is also possible to make a WPS with inherent impedance transformation (unlike that in [15]), which is derived in Sec. 6.1.

[3]The power splitter is passive and reciprocal so at least one port must be mismatched. Why is it mismatched at *both* port 2 and 3? By symmetry; if it is mismatched at port 2, it must be mismatched at port 3 and vice versa. Moreover, for a three-port device to be mismatched at only one port (say, port 3) that port must be completely detached from the other two ports ($|S_{33}| = 1$ and $S_{31} = S_{13} = 0$) [15].

[4]The complete S-matrix for such a splitter, possibly with inherent impedance transformation has been derived in Sec. 6.3.

Note that similar to the splitter in Sec. 5.2.1, the WPS delivers *all* the power to the output loads and none are dissipated in R. This is intuitive; due to symmetry the voltage must be equal at the two outputs, and no current flows trough R. A characteristic feature of the WPS is that no power fed to port 2 exits port 3 and vice versa ($S_{23} = S_{32} = 0$). One say that the outputs are *isolated* and in practice one typically measure the degree of isolation between two ports i and j as:

$$I = -20 \log |S_{ij}| \quad \text{[dB]} \quad (5.7)$$

If a common-mode signal is fed to ports 2 and 3, no current will flow through R, and all the power will be perfectly combined at port 1 like in the splitter in Sec. 5.2.1. This is the reciprocal mode of operation as only feeding port 1. A differential signal across ports 2 and 3 however, is dissipated in R.

5.2.3 Quadrature Power Splitters (QPS)

The power splitters until now have been completely symmetric and the output signals have the same phase. One of the requirements for the feeding network is that the dipoles are fed in quadrature, i.e. with a 90° phase-difference. A QPS is a 2-way power splitter with a 90° phase-difference between its outpus. A QPS can simply be made by appending a phase-shifter (for example a TL) on one of its outputs such that it lags behind the other output by 90°. It is, of course, also possible to shift one port by +45° and the other by −45°. Or any other combination as long as the difference is 90°.

5.2.4 N-Way WPSs

Three topologies for making N-way WPSs with all ports matched to the system impedance Z_{sys} has been studied.

WPS with Star Isolating Resistor Network

One way to make an N-Way WPS can be seen in Fig. 5.3(a). This is, in fact, the original WPS which Ernst. J. Wilkinson himself designed in his famous 1960 paper entitled “An N-Way Hybrid Power Divider” [35]. Wilkinson imagined (and built) this device as depicted in Fig. 5.4. Notice how one resistor of value Z_{sys} from each output is connected to a common node in a star-like pattern. To manufacture this in a planar (two-dimensional) structure, such as a PCB, is impossible for $N \geq 3$ unless crossovers are used [15].

The TLs should have a characteristic impedance of $\sqrt{N} Z_{\text{sys}}$.

WPS with Delta Isolating Resistor Network

Another way to make an N-way WPS is by replacing the star-network on the outputs with a delta-network (Fig. 5.3(b)) where there is a $N Z_{\text{sys}}$ resistor between every pair of outputs [36]. For $N = 3$ it has been suggested to eliminate one of

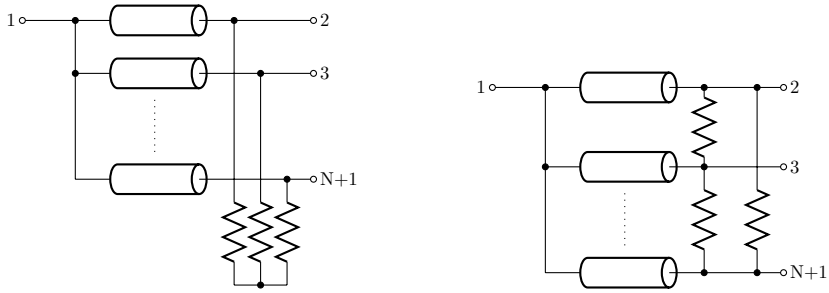

(a) Star Isolating Resistor Network (b) Delta Isolating Resistor Network

Figure 5.3: Two N-Way WPS topologies

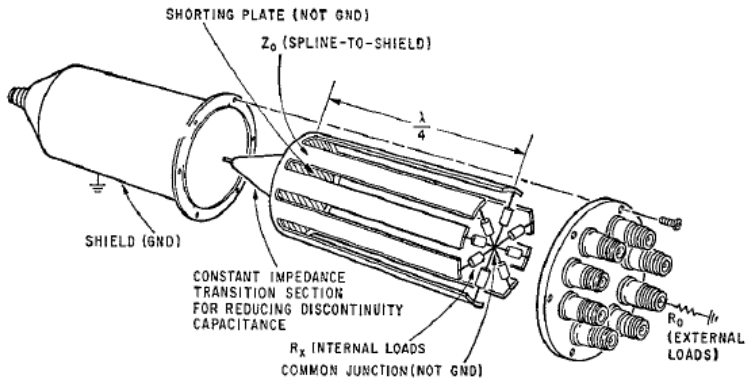

Figure 5.4: How Wilkinson imagined (and built) the N-Way WPS. Courtesy of [35].

the resistors to make it possible to manufacture in a pure planar structure [37]. This *will* degrade the performance of the splitter, but hopefully not too severely. The values of the remaining resistors must be tweaked in order to achieve a good enough result. The author does not know of any attempts to do this for $N = 4$.

Again, the TLs should have a characteristic impedance of $\sqrt{N}Z_{\text{sys}}$.

Corporate WPS

The third way to make an N-way WPS is simply by connecting 2-way WPSs on the outputs of another WPS to make a tree-like, or corporate, structure [15]. This can be done in as many stages as desirable. The corporate N-way WPS can be built in planar structure since the 2-way WPS can be built in planar structure.

5.3 Lumped Power Splitters

As was pointed out in the beginning of this chapter, there is no room for a distributed feeding network on-board the satellite. However, *all* the discussed *distributed* power splitters may be converted to lumped equivalents simply by replacing all TLs in it with synthetic TLs (see Sec. 2.2.3). This allows the designer to first choose amongst different distributed solutions before he continues and make a lumped equivalent of it. Because of this, only a few selected power splitters of special interest has been transformed to lumped equivalents in this thesis.

5.3.1 Lumped Wilkinson Power Splitters (LWPS)

A lumped equivalent of the WPS is known as a *Lumped Wilkinson Power Splitter* (LWPS). Since the TLs in Fig. 5.2(b) are $\lambda/4$ long, it is most intuitive to synthesize them by one of the RH-networks, as only they can possess a 90° phase-lag. But it is also possible to use one of the LH-networks with a 90° phase-*advance*. The reason is that instead of $\lambda/4$-lines the distributed WPS can be made with two $3\lambda/4$-lines (= 270° lag = 90° advance), since the impedance seen into a TL is $\lambda/2$-periodic (see (2.10)).

It is common to try to reduce the number of components and, particularly inductors, since practical inductors are more lossy than practical capacitors (this statement will be justified in Sec. 6.6). The fewest inductors are achieved by choosing either the RH_π or the LH_T-network, but if the RH_π-network is chosen, two capacitors will be in parallel at the input of the splitter, and they can be replaced by a single capacitor, which makes the splitter made of RH_π-networks the optimal one. This splitter is shown (amongst others) in Fig. 5.5.

5.3.2 A Lumped QPS (LQPS)

In 2005 a novel design approach for *Lumped Quadrature Power Splitters* (LQPSs) was presented in a paper entitled "Lumped-Element Quadrature Power Splitters Using Mixed Right/Left-Handed Transmission Lines" [23]. The LQPS presented in the paper consist of an LWPS followed by one phase-shifter at each output port.

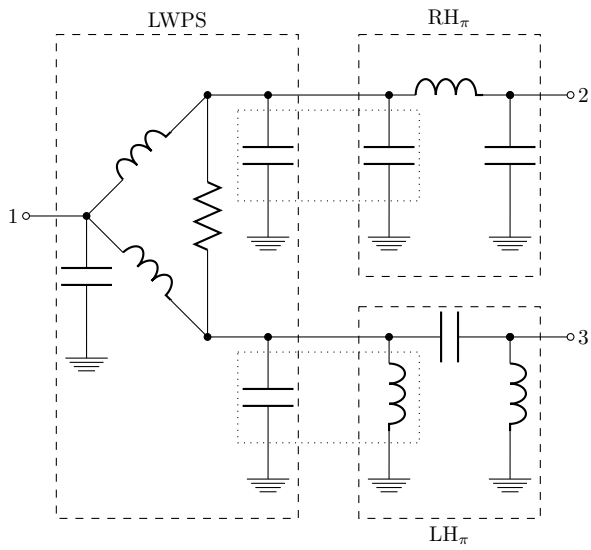

Figure 5.5: LQPS made by a LWPS and two phase-shifters as found in [23]. The dashed boxes show the different units while the dotted boxes shows components to be replaced by an equivalent one.

See Fig. 5.5. Port 2 has a phase-lag of θ_{RH} which is realized as an RH$_\pi$ unit cell whereas port 3 has a phase-lag of $\theta_{\mathrm{LH}} < 0$ (so it is actually a phase-advance) realized as an LH$_\pi$ unit cell. Port 3 leads ahead of port 2 by 90° by imposing the restriction $\theta_{\mathrm{LH}} = \theta_{\mathrm{RH}} - 90°$. θ_{RH} is then a free parameter which the designer can choose to acquire certain desired features. For example, by choosing $\theta_{\mathrm{RH}} = 0°$ or $\theta_{\mathrm{RH}} = 90°$ one of the phase-shifters is eliminated. The greatest bandwidth occur for $\theta_{\mathrm{RH}} = 45°$ *if* the circuit remain as depicted in Fig. 5.5.

It is interesting to note that an LH$_\pi$-cell was chosen rather than an LH$_{\mathrm{T}}$-cell despite the fact that it has one more inductor (and therefore more loss). The advantage of the π-cell is that one of its inductors appear in parallel with a capacitor from the LWPS (see Fig. 5.5) and therefore the total component count can be reduced by replacing them with an equivalent component. Further on, if $\theta_{\mathrm{RH}} > 19.5°$ the equivalent component is a capacitor and thence the total number of inductors is reduced to the same as if the LH$_{\mathrm{T}}$-cell was chosen. If $\theta_{\mathrm{RH}} = 19.5°$ the equivalent component vanish.

It can be shown that if the dotted boxes in Fig. 5.5 are replaced by equivalent capacitors, the bandwidth is maximized at $\theta_{\mathrm{RH}} = 31.4°$. This was done in [23]. An even higher bandwidth can be achieved by using a more broadband modified LWPS as found in [25].

Table 5.1: Impact of θ_{RH} on the LQPS in Fig. 5.5

$\theta_{\mathrm{RH}} = 0°$	The upper phase-shifter vanish.
$\theta_{\mathrm{RH}} = 90°$	The lower phase-shifter vanish.
$\theta_{\mathrm{RH}} = 45°$	Maximized bandwidth if the dotted boxes are *not* replaced by equivalent components.
$\theta_{\mathrm{RH}} = 31.4°$	Maximized bandwidth if the dotted boxes *are* replaced by equivalent components.
$\theta_{\mathrm{RH}} < 19.5°$	The equivalent component in the lower dotted box is an inductor.
$\theta_{\mathrm{RH}} > 19.5°$	The equivalent component in the lower dotted box is a capacitor (less loss than the inductor).
$\theta_{\mathrm{RH}} = 19.5°$	The equivalent component in the lower dotted box vanish (least loss).

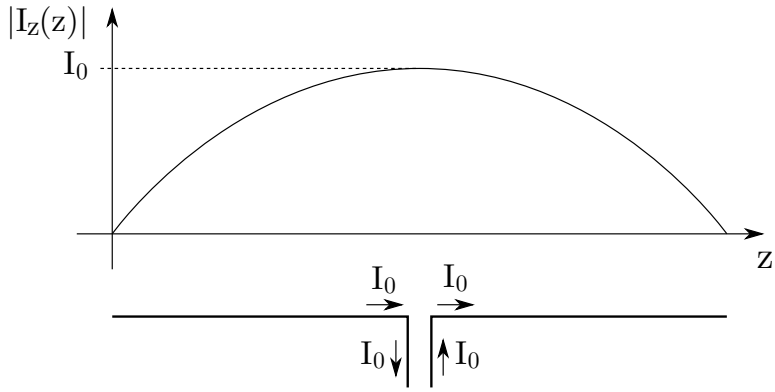

Figure 5.6: Current distribution in a dipole.

5.4 Baluns

A dipole is a balanced structure. Its working principle is based upon the assumption that it has a symmetric current distribution, meaning that it must be fed at its terminals with a purely differential, or balanced, signal like illustrated in Fig. 5.6 [26]. If this is not the case the current distribution in the two halves will not be symmetric, which causes a distorted radiation pattern [38]. If the dipole is fed by a coaxial cable or another unbalanced structure, an imbalance in the currents may occur (as will be further explained). A *balun* (balanced-unbalanced) can be used to resolve the problem.

A typical example of how imbalance currents may occur is illustrated in Fig. 5.7(a). Electromagnetic boundary conditions forces the currents I_1 and I_2 to be equal (but travel in opposite directions) [26]. I_1 is also the current flowing in the left half of

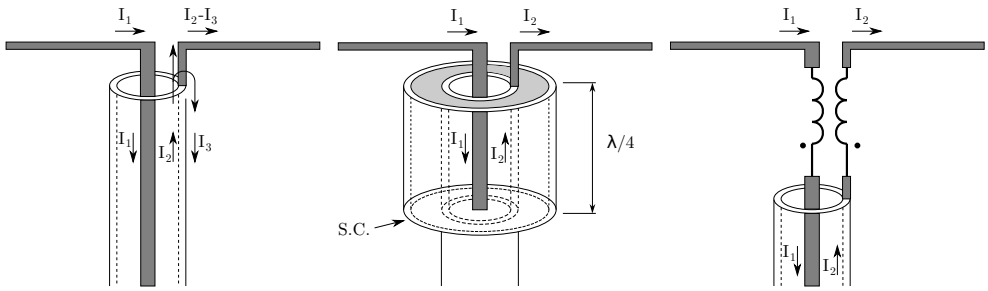

(a) Without balun (b) With a bazooka balun (c) With a current balun

Figure 5.7: Currents in dipoles fed with and without baluns. The size of the cables and baluns are not to scale.

the dipole. The skin effect forces the current I_2 to flow on the (inner) surface only [38]. The inner and outer surface of the outer conductor can be considered to be insulated by the skin effect. At the end of the cable, the inner surface will be connected to both the right half of the dipole as well as to the outer surface. If the current flowing on the outer surface is denoted I_3 only $I_2 - I_3$ will flow to the right half of the dipole. This causes a distorted radiation pattern because there is a current imbalance in the dipole, but also because there is a current flowing on the outer surface of the outer conductor. This current can also radiate and contribute to the pattern distortions, and it may cause a loss of power as the current is fed back to ground.

Despite the fact that this is an example with a coaxial cable, it is important to take this effect into account for feeding networks not using coaxial cables as well. For instance, if one of the dipole halves is simply connected to the ground conductor, one might get an imbalance in the current, distorting the pattern, and causing a mismatch. One should ensure that dipoles are fed in a differential manner.

5.4.1 Bazooka Balun

Typical textbooks about antennas like [26] and [20] suggests numerous baluns. Common for most of them is that they have a physical length of either $\lambda/4$ or $\lambda/2$. Only one of them will be discussed here; the *bazooka*, or *sleeve* balun.

The bazooka balun is simply another piece of cylindrical conductor on the outside of the outer conductor (Fig. 5.7(b)). Along with the outer surface of the shield, this third layer of conductor constitutes a waveguide or TL. It is short circuited (S.C.) by a conducting annulus in the bottom and since it is $\lambda/4$ long it is effectively open circuited in the top end where the dipole is terminated. Because of this, no current can flow on the outer surface of the shield, so I_2 flows solely in the right half of the dipole and the imbalance is eliminated.

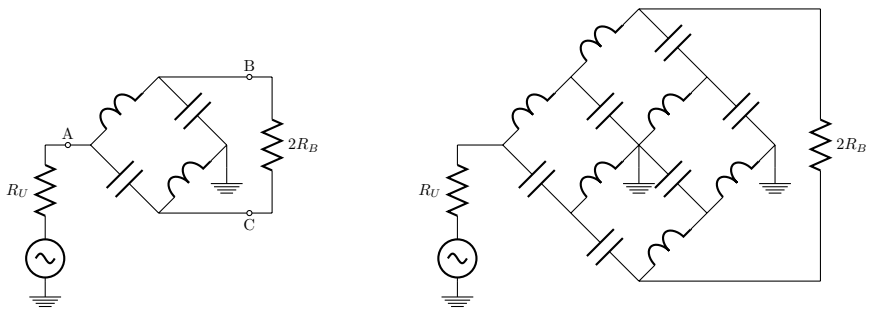

(a) First-order (b) Second-order

Figure 5.8: Lattice Baluns

5.4.2 Lattice Baluns

Due to the quite physical nature of the bazooka balun and other similar baluns it is hard to imagine that they can be synthesized by synthetic TLs in the same way as the previously discussed power splitters. Instead, the lumped baluns works in a different way. The idea is that the dipole is fed directly from a circuit with a differential output, such that the current balance is preserved when fed to the antennas. These circuits are also referred to as baluns. They are commonly used in mixers or other analog/RF-circuitry but they may also be also be used for antennas [34].

The first order lattice balun (shown in Fig. 5.8(a)) comprises two second order filters, one low-pass and one high-pass [34, 39]. Both filters are designed such that the $-3\,\mathrm{dB}$ cut-off frequency of the filters is at the center-frequency of the balun, such that half the power is fed to the load through each filter. This is illustrated in Fig. 5.4.2. Further on, the low-pass filter will exhibit a 90° phase-lag and the high-pass filter a 90° phase-advance at this frequency, such that all the power is differentially fed to the load. This yields the following design equations:

$$L = \frac{Z_0}{\omega_0} \quad [\mathrm{H}] \quad (5.8)$$

$$C = \frac{1}{Z_0 \omega_0} \quad [\mathrm{F}] \quad (5.9)$$

where ω_0 is the angular center-frequency of the balun and Z_0 is an equivalent characteristic impedance given by:

$$Z_0 = \sqrt{2R_B R_U} \quad [\Omega] \quad (5.10)$$

Note that an inherent impedance transformation can be achieved by choosing the balanced load $2R_B$ unequal to the unbalanced impedance R_U.

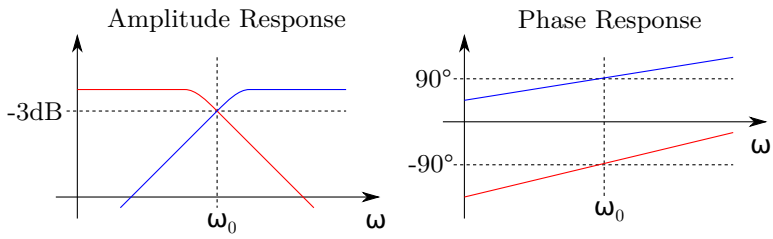

Figure 5.9: Frequency response of the filters that constitutes a first-order lattice balun

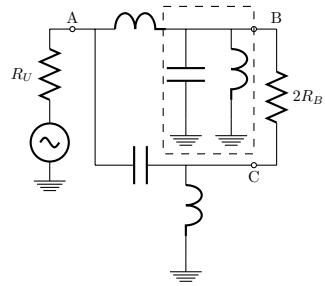

Figure 5.10: Modified first-order lattice balun

The first-order lattice balun is a rather narrowband device due to the fact that the frequency response of each filter quickly deviates. In 2004 the second-order lattice balun (Fig. 5.8(b)) which has a vastly larger bandwidth was presented in [40] and later that year the design was improved to also include an impedance transformation [34]. As the NUTS communication link is rather narrowband this solution will not be studied further.

5.4.3 Modified Lattice Balun

The balun will typically be the device closest to the antenna and thus all the output pins should be DC-wise connected to ground to prevent static build-up. The lattice balun shown in Fig. 5.8(a) has node C DC-wise connected to ground through an inductor whereas node B is not connected to ground. The author suggest that this can be solved simply by replacing one capacitor with a parallel of a capacitor and an inductor as shown in Fig. 5.10. Such an inductor will hereinafter be referred to as a *DC-grounding inductor*. At the center-frequency this parallel should have the same reactance as the capacitor it replaces.

This trick can also be done on other circuits including the second-order lattice balun. Beware that it will affect the bandwidth since the parallel will only be equivalent to the capacitor at one frequency.

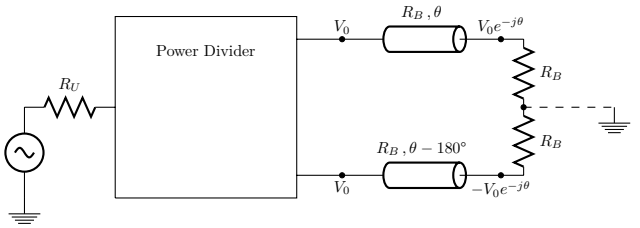

(a) Unbalanced-to-balanced (transmitting) mode

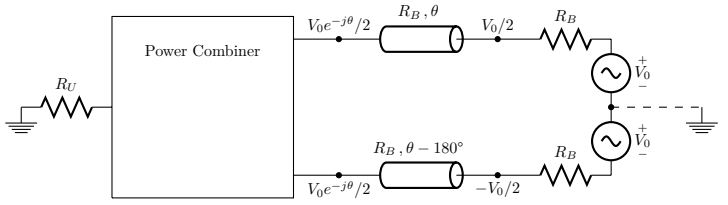

(b) Balanced-to-unbalanced (receiving) mode

Figure 5.11: Using an equal-split 2-way power splitter as a balun

5.4.4 Power Splitters as Baluns

In fact, the lattice balun can be considered as an equal-split two-way power divider where each output port has R_B as its output impedance, and the outputs are 180° apart (a 180° divider). But other kinds of 180° dividers with output impedance R_B can be used as well. For instance, one could use a WPS and separate the outputs' phase by using phase-shifters (for example TLs) such that there is a 180° phase-difference between the outpus. The two outputs can then be used as one differential output (This can be analysed with *mixed-mode* S-parameters, but it is not strictly necessary).

The reason why this works is simple. Fig. 5.11(a) shows an unbalanced signal fed to an equal-split power divider. Because it is an equal power split, and each of the two outputs has the same impedance, the voltages at the outputs are equal. It is denoted V_0. One or both will go through a phase-shifter such that they become a differential signal (they have opposite signs). The differential signal is fed to the load $2R_B$, which is split into two resistors in series in the figure. Due to the symmetry, the voltage at the mid-point must be 0 V and thus virtually ground. The two branches are de-coupled and it is obvious that the power is fed to the load in a balanced way.

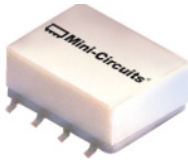

(a) MiniCircuits ADQ-22+

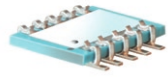

(b) MiniCircuits QBA-07

(c) MiniCircuits SBTCJ-1W+

(d) MiniCircuits SCPJ-2-9+

(e) MiniCircuits ADT1-1WT+

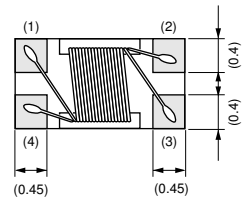

(f) muRata DXW21BN7511T (view from below)

Figure 5.12: The various ICs included in this study. The images are courtesy of their vendors, see the datasheets in App. H.

In the receiving mode (Fig. 5.11(b)), there will be a generator (i.e. an antenna) in series with the $2R_B$ resistor in the output. We will now denote the voltage it generates by $2V_0$. The source can also be split in two equal parts, and since there is an odd symmetry[5] in the circuit, there will be a virtual ground in the midpoint. The two branches are again de-coupled. After the phase shifters it will become a common-mode signal that is fed to the power combiner, and thus all the power will be fed to R_U.

For simplicity, the phase-shifters are shown as TLs in Fig. 5.11(a) and Fig. 5.11(b). Naturally, the phase-shifters, as well as the power splitter/combiner, must be implemented with lumped components to call the device a lumped balun.

5.5 Integrated Circuits (ICs)

Both baluns and various power splitters are commercially available (COTS) as *Integrated Circuits* (ICs) and it is natural to consider them as well. Numerous ICs have been considered, mainly from the manufacturers *MiniCircuits* and *muRata*, and there is no point in discussing all of them in detail in this report. Instead, selected data from a representative selection of ICs are given in Tab. 5.2. The devices are depicted in Fig. 5.12 and their datasheets are found in App. H.

The selected devices consist of two QPSs, two transformer type baluns and two 180° power splitters which, according to Sec. 5.4.4, may be used as baluns. No

[5]Actually, the whole circuit is not quite symmetric due to possibly different phase-shifters in the two branches. However, the impedance looking into the phase shifter (from either end) will be R_B for both branches, which means that the circuit equivalently possess odd symmetry to the right of the phase shifters and even symmetry to the left.

Table 5.2: Selected data for various ICs.

	MiniCircuits ADQ-22+	**MiniCircuits QBA-07**
Description	QPS	QPS
Operating Frequency	95 – 200 MHz	340 – 680 MHz
System Impedance	50 Ω	50 Ω
Max RF Power	0.5 W	21 W
Excess Insertion Loss	max. 0.6 dB	typ. 0.8 dB, std. 0.1 dB[a]
Amplitude Unbalance	max. 1.6 dB	max. 2.0 dB
Phase Unbalance	max. 6°	max. 7°
Operating Temperature	-40°C – 85°C	-55°C – 100°C
Temperature Behaviour	N/A	max power may drop to 9W
Impact of vibration/shock	N/A	N/A
Physical Height	5.46 mm	1.78 mm

	MiniCircuits SBTCJ-1W+	**MiniCircuits SCPJ-2-9+**
Description	180° Splitter	180° Splitter
Operating Frequency	1 – 750 MHz	200 – 900 MHz
System Impedance	50 Ω	50 Ω
Max RF Power	0.5 W	1 W
Excess Insertion Loss	max. 1.8 dB	max. 0.7 dB
Amplitude Unbalance	max. 0.9 dB	max. 2.0 dB
Phase Unbalance	max. 10°	max. 6°
Operating Temperature	-40°C – 85°C	-40°C – 85°C
Temperature Behaviour	Apparently stable[b]	N/A
Impact of vibration/shock	N/A	N/A
Physical Height	3.81 mm	7.11 mm

	MiniCircuits ADT1-1WT+	**muRata DXW21BN7511T**
Description	Transformer Balun	Transformer Balun
Operating Frequency	0.4 – 800 MHz	50 – 870 MHz
System Impedance	75 Ω	75 Ω
Max RF Power	0.5 W	0.5 W
Insertion Loss	max. 0.6 dB	max. 1 dB
Amplitude Unbalance	max. 0.5 dB	CMRR$\geq$ 20 dB[c]
Phase Unbalance	max. 4°	N/A
Operating Temperature	-20°C – 85°C	-40°C – 85°C
Temperature Behaviour	N/A	N/A
Impact of vibration/shock	N/A	N/A
Physical Height	2.84 mm	1.2 ± 0.2 mm

[a] MiniCircuits QBA-07 does not have a maximum excess insertion loss in its datasheet. It does, however, have a typical excess insertion loss and a standard deviation. [b] The datasheet claims that MiniCircuits SBTCJ-1W+ is temperature stable without specifying any numbers. [c] muRata chose to put the *Common-Mode Rejection Ratio* (CMRR) in their datasheets rather than the amplitude unbalance.

4-way power divider for the NUTS frequencies was found.

The datasheets typically operate with both "typical" and "maximum" devations from the ideal values. For instance, the "typical amplitude unbalance" is how much the output amplitudes *typically* differ (they should ideally be equal). They may, however, deviate as much as the "maximum amplitude unbalance". To have some sort of guarantee of the performance (and because of the harsh environment in space, c.f. Sec. 5.1.1) it is chosen to always consider the maximum deviations in this report. Also, the *excess* insertion loss is used for the power splitters, i.e. the loss beyond the 3 dB insertion loss that occur due to the power splitting itself.

Moreover, the vendors are modest with information about how the performance changes when exposed for vibration/shock or abnormal temperatures. Beware that knowing the "operating temperature" is typically not enough. Often, the maximum deviations found in datasheets are the maximum deviations at room temperature, meaning that the performance may be even worse at other temperatures such as $-30°\text{C}$.

5.5.1 Current Balun

It is also interesting to see that the two baluns are *current* baluns, a kind of transformer balun. The current balun is simply a transformer with equal number of turns on both coils as illustrated in Fig. 5.7(c). That means that the current through each of them must be equal, and due to the direction of the windings (c.f. dot convention), the currents must also be of opposite phase. This enforces all of the current I_2 to enter the right half of the dipole and there can be no current on the outside of the shield [38].

5.6 Complete Feeding Networks

At last in this chapter, it is time to put everything together to a complete feeding network and to discuss advantages and disadvantages of different solutions.

5.6.1 Distributed Solutions

A distributed feeding network could be built after the model in Fig. 5.1. The QPS could, for example, be made as a WPS with a 90° TL on one of its output as described in Sec. 5.2.3. The balun could be a bazooka balun. This is a total of 5 TLs or baluns of length $\lambda/4$ (where λ is the *electrical* wavelength and not necessarily the wavelength i vacuum). $\lambda/4$ has been computed (using the formulas in Sec. 2.2.2) for both NUTS frequencies, for both a coaxial cable and a microstrip line for a PCB that is readily available at *Institute for Electronics and Telecommunication (a department at NTNU)* (IET). The results are given in Tab. 5.3. It is obvious that 5 $\lambda/4$ devices of each frequency cannot easily fit inside a $10 \times 10 \times 20\,\text{cm}$ CubeSat. Another question with conventional feeding networks would be; how do one cope with the large feeding gaps of 6 cm?

Table 5.3: TL dimensions

	UHF 437 MHz	VHF 146 MHz
Wavelength in vacuum (λ_0)	69 cm	205 cm
Wavelength (λ) in coaxial cable[a]	45.5 cm	135.3 cm
$\lambda/4$ in coaxial cable[a]	11.4 cm	33.8 cm
Microstrip width (W) for $Z_0 = 50\,\Omega$[b]	1.4 mm	
Microstrip width (W) for $Z_0 = 35\,\Omega$[b]	2.5 mm	
Wavelength (λ) in microstrip[c]	36.3 cm	108.5 cm
$\lambda/4$ in microstrip[c]	9.1 cm	27.1 cm

[a] Assuming a velocity factor VF = 0.66 which is true for many coaxial cables [20].
[b] Assuming FR4 PCB with substrate thickness of $d = 0.8$ mm and $\varepsilon_r = 4.8$.
[c] The wavelength is slightly dependent on characteristic impedance since the effective permittivity ε_e in (2.18) depends on the W/d-ratio. These values are based upon $Z_0 = 50\,\Omega$ but will be close for $Z_0 = 35\,\Omega$ as well. Like for [b] it is assumed to be made on FR4 PCB with substrate thickness of $d = 0.8$ mm and $\varepsilon_r = 4.8$.

The width of microstrip lines has also been computed with the formulas from Sec. 2.2.2, as can be seen in Tab. 5.3. The widths are of practical sizes, so using short TLs of appropriate widths to connect various non-distributed components are feasible.

5.6.2 Integrated Solutions

Using ICs appears to be the easiest solution. Beware that the selected ICs for this study is neither the best suited, nor the worst suited ICs for this mission. It is simply meant to be a *representative* selection such that one can see a trend.

For example, it seems like it is reasonable to expect to find QPSs, 180° power splitters, and transformer baluns for the UHF and VHF frequencies. Moreover, all of the devices can handle 0.5 W or higher powers so that should not be a problem.

When it comes to physical dimensions however, there is a *trend* that the components are higher than 2 mm. In Fig. 4.5 it is seen that there is only 3 mm of height between the two PCBs, meaning that the components should not be higher than 2 mm, leaving 1 mm of clearance. Two of the ICs in Sec. 5.5 are lower than 2 mm, however, indicating that it might be possible to find all of the required components with small enough dimensions if one search long enough.

Moreover, *all* of them has the same impedance on the input and the output. In fact, no power splitters with inherent $50\,\Omega - 35\,\Omega$ impedance transformation or baluns with inherent $50\,\Omega - 70\,\Omega$ impedance transformation was found by the author at all, *implying* that matching must probably be done by a separate lumped network, or simply by tuning the dipole lengths to the best possible match.

Most components have an operating temperature range of −40°C – 85°C or better which is more than sufficient for the expected temperatures of the satellite (−30°C – 20°C). Unfortunately, none of the datasheets specifies whether the max-

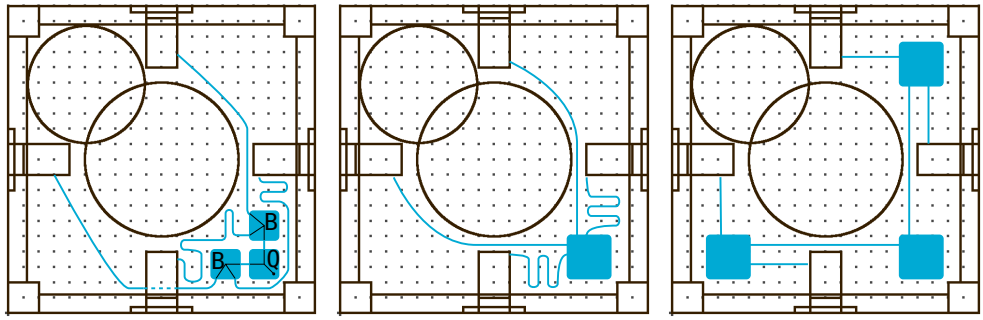

(a) Layout for one QPS and two baluns.

(b) Centralized layout.

(c) Symmetric layout.

Figure 5.13: Various strategies for circuit layout on the PCB

imum deviations from ideal conditions is at room temperature or within the whole operating frequency range. One might be tempted to assume that it must be for the whole operating temperature range, but the fact is that one can not know for sure unless it is specified. Little information is available w.r.t. how a mechanical shock or vibration affects the components.

There is also no data w.r.t. how the components behave at out-of-band frequencies, which could have been useful to resolve possible mutual coupling problems.

Layout

Where to put the different components on the PCB is also a significant challenge. Fig. 5.13(a) shows one idea for how it could be done. The signal is fed through the PCB in the lower right corner within the area labelled "Q". That area contains a QPS. Each of its output goes to a balun ("B"). The baluns feed the dipoles through microstrip lines because of the significant length from the balun to the antenna elements. One must take care that the length of the microstrip lines are the same for each element such that the mutual phase-shift between the elements does not change. On the other hand, the microstrip lines must not be too close or they will experience mutual coupling.

Furthermore, since one balun feeds one dipole, it is impossible not to have a crossover with this circuit topology (Fig. 5.1). Probably the easiest place to have a crossover is below one of the antenna elements, but this assumes that the measuring tape is elevated above the PCB which complicates the whole structure. It would be beneficial if a layout without crossovers was possible with ICs (such as for example Fig. 5.13(b) or Fig. 5.13(c)). Unfortunately, no such solution was found during this study.

To summarize; it *is* possible to use ICs, but it lacks a several qualities; there are no components with inherent impedance transformation, some devices are not available as ICs, and the datasheets are modest with some information. The layout can not possess symmetry, it has one crossover, and its microstrip lines are messy.

5.6.3 Lumped Solutions

An advantage with lumped networks is that the designer has the freedom to customize the circuit in many ways. It has been shown in this chapter that both baluns, phase-shifters and power splitters can easily be designed as lumped networks. Moreover, the designer can adapt the design to whichever impedance and frequency is wanted. The major drawback is that they are time-consuming to study, design, build and test.

Alternative I

The first lumped feeding network that was considered utilizes the QPS from [23] (Fig. 5.5) followed by one first-order lattice balun on each output. As seen by (5.10), the lattice balun can be made such that it incorporates an inherent impedance transformation from $50\,\Omega$ to $70\,\Omega$ to better match the dipoles. For all of the dipoles to be DC-grounded the first-order lattice balun is modified as explained in Sec. 5.4.3. The complete network is shown in Fig. 5.14.

This network was successfully designed, and simulated with Agilent *Agilent Advanced Design System* (ADS). Unfortunately, this network must also be built with a layout similar to what is shown in Fig. 5.13(a) (i.e. with crossovers), and it was therefore discarded. Further details about design and simulations can be found in App. G.2.

Alternative II

This alternative is an attempt to improve the layout issues with alternative I and the integrated solutions. Rather than having the conventional "QPS and baluns" topology (Fig. 5.1) it makes use of the fact that differential outputs of any device makes it unnecessary to use a balun (see Sec. 5.4.4). The idea, is to use a lumped 4-way corporate WPS (which can be built without crossovers) followed by lumped phase-shifters on each output as shown in Fig. 5.15. The phase-shifters will make the outputs pairwise differential, and with a quadrature in between the two pairs. Since the output ports of a WPS are identical the phase-shifters can be shuffled around such that crossovers are avoided. A thought (symmetric) layout is shown in Fig. 5.13(b). If the whole lumped circuit is placed within the blue box in the lower right corner, the outputs can be ordered in such a way that crossovers are unnecessary. We will later see that it can even be built as indicated in Fig. 5.13(c) where the lumped circuitry is spread across three of the corners, with TLs in between. The latter layout avoids winding up the TLs to keep equal lengths from the input to each element.

Conclusively, it is decided that this alternative is the most appropriate one. In Ch. 6 a rigorous design of this feeding network is carried out.

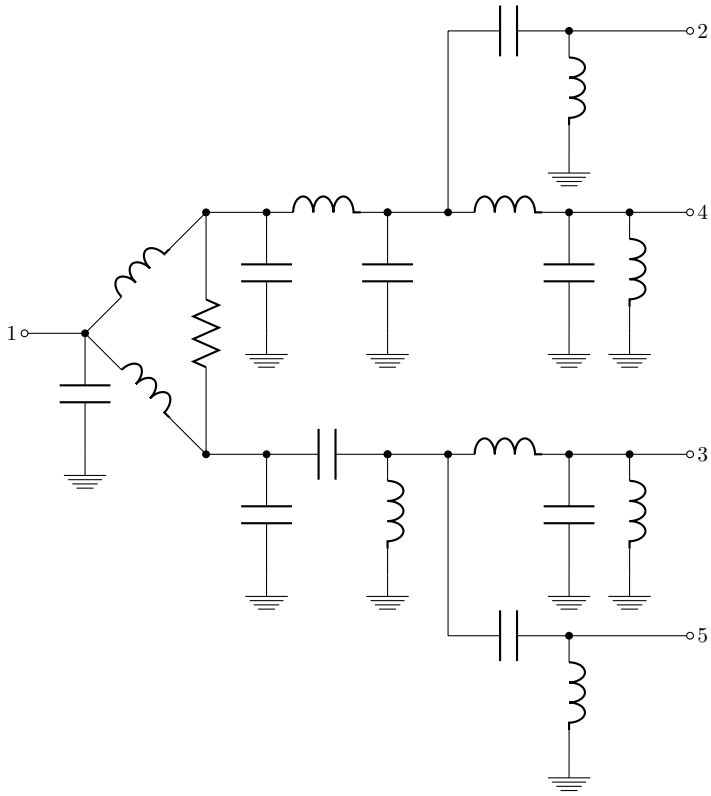

Figure 5.14: Lumped feeding network, alternative I. First comes the LQPS from Fig. 5.5 (where the components in the dotted boxes has been replaced by equivalent capacitors). On each output there is a modified lattice balun as shown in Fig. 5.10. Notice that on a layout, the outputs can not be arbitrarily placed due to possible crossovers.

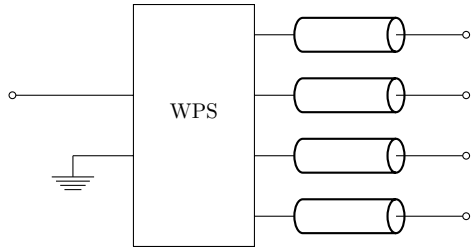

Figure 5.15: Making a feeding network with a 4-way power splitter and four phase-shifters (here: indicated as TLs). Note that contrary to Fig. 5.14 (or Fig. 5.1 in general) the designer can shuffle the outputs to suit the layout.

6 Designing the Feeding Network

In Ch. 5 it was decided to design a feeding network consisting of a corporate 4-way WPS and four phase-shifter. This is shown in Fig. 6.1. The two first stages comprises the corporate WPS whereas the third stage is the phase-shifters. The input (port 1) will be connected to a $50\,\Omega$ system, whereas the outputs should be $35\,\Omega$ in order to better match the dipoles. This impedance transformation takes place in stage 2 by the use of specially designed WPSs.

Given that *all* of the TLs in Fig. 6.1 is synthesized by π-cells (either RH_π or LH_π) the circuit will become as shown in Fig. 6.2. The squares are either a capacitor or an inductor depending on which unit cells are used. The specific components will be further explained throughout the chapter.

First, in this chapter, the splitters and the phase-shifters are designed to yield an RHCP-polarization before components are chosen and a PCB layout is presented.

6.1 Design of Impedance Transforming WPS

It is possible to design a WPS such that it is matched to different impedances at the input and the outputs (it has an inherent impedance transformation). Designing the stage 2 WPSs in Fig. 6.1 with an inherent impedance transformation from $50\,\Omega$ to $35\,\Omega$ will make the feeder better matched to $70\,\Omega$ crossed dipoles. The stage 1 WPS will be a conventional $50\,\Omega$ system impedance splitter without inherent impedance transformation.

Due to the fact that text books such as [15] usually does not mention WPSs with inherent impedance transformation, the derivation is done as a part of this thesis (although it has probably been done before). The derivation is quite similar to the non-impedance transformation case.

Consider again Fig. 5.2(b). Let the input (port 1) be terminated by R_i whereas the outputs (ports 2 and 3) are matched to R_o ($S_{22} = S_{33} = 0$). In order to determine what Z_0 and R must be for these conditions to be met, an odd-even analysis

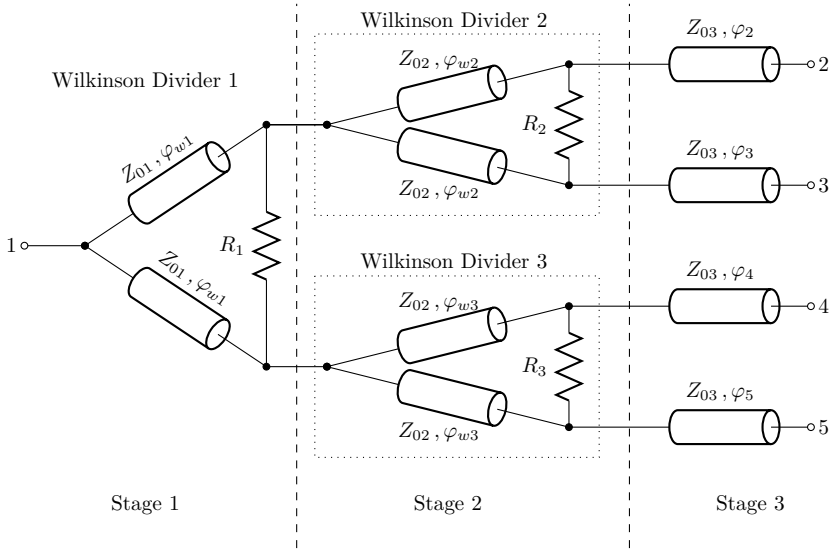

Figure 6.1: Lumped feeding network, alternative II, is to first design a distributed network as shown in this figure, and then synthesize it by synthetic TL.

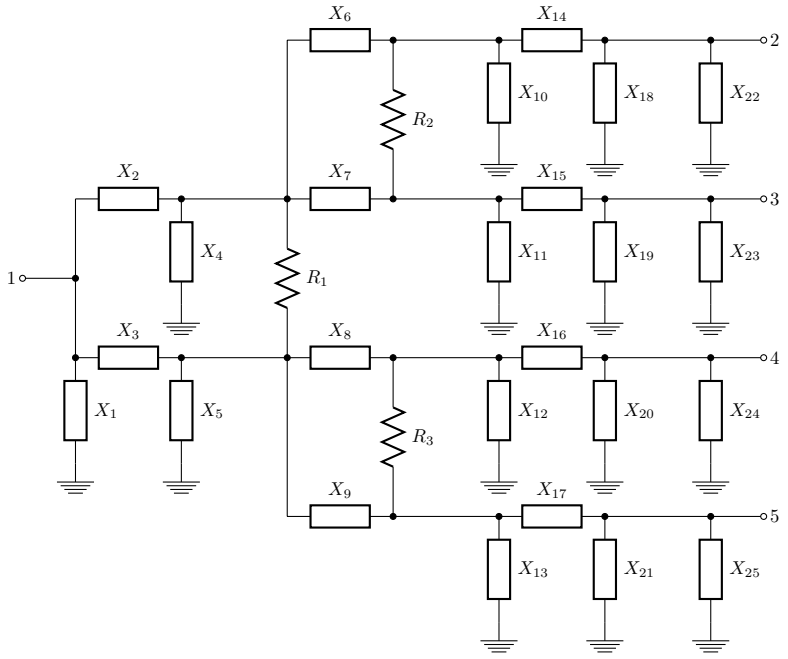

Figure 6.2: The alternative II network, when each TL is synthesized by a π-cell.

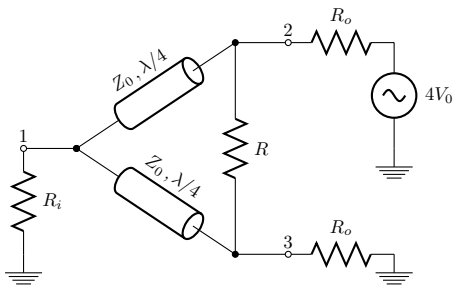

(a) Direct excitation of port 2

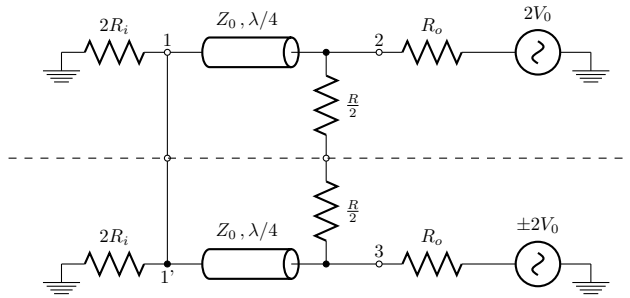

(b) Decomposed to two excitations

Figure 6.3: WPS excited at port 2 in two equivalent ways

method is used. Consider that port 2 is excited by a voltage source $4V_0$ whereas the other ports are terminated by their intended loads as shown in Fig. 6.3(a). Except for the excitation/voltage source, the circuit is symmetric. It is possible to make the excitation symmetric as well by utilizing superposition. First, both ports 2 and 3 are excited by $2V_0$ (even symmetry) and then port 2 is excited by $2V_0$ whereas port 3 is excited by $-2V_0$ (odd symmetry). Adding these two excitation modes is then equivalent to only exciting port 2 by $4V_0$. This is illustrated in Fig. 6.3(b). Notice that R_i and R has been replaced by a parallel and series circuit, respectively, in order to split the circuit into two symmetric pieces.

Even Mode

For the even mode, the voltage at nodes 2 and 3 has to be equal due to the symmetry of the network and thus no current flows through the $R/2$ resistors. By the same reasoning the voltage at node 1 and 1' has to be equal such that no current flows between them either. An equivalent circuit (as seen from port 2) is then obtained by removing the lower half and leaving open circuited (O.C.) connections at the bisection. See Fig. 6.4(a). To achieve a match for the even mode excitation the impedance seen into port 2 must equal R_o, meaning that the QWT has to transform $2R_i$ to R_o. Applying (2.11) yields:

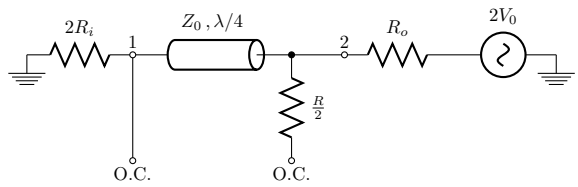

(a) Even mode equivalent

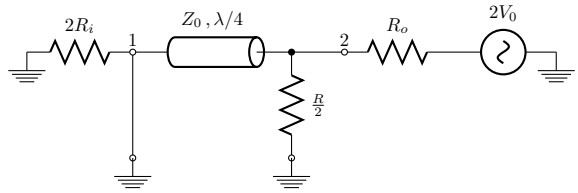

(b) Odd mode equivalent

Figure 6.4: Equivalent networks for symmetric excitations of a WPS

$$Z_0 = \sqrt{2R_oR_i} \quad [\Omega] \quad (6.1)$$

Notice that this equation coincides with (5.5) for $R_i = R_o$.

Odd Mode

For the odd mode, the voltage at node 3 has to be minus the voltage at node 2, due to the odd symmetry of the circuit. Because of the equal voltage division between the resistors $R/2$ the voltage at the bisection must be zero, hence the bisection can be replaced by ground at this node. By the same reasoning, the voltage at node 1 and 1' must be zero so a ground can replace the bisection also here. The equivalent network is shown in Fig. 6.4(b). Since one end of the QWT is short circuited, the other end is effectively open circuited. The only impedance seen into port 2 is then $R/2$, and to achieve match it must be equal to R_o:

$$R = 2R_o \quad [\Omega] \quad (6.2)$$

Again, this equation is similar to (5.6).

6.1.1 Design and Synthesis

Two different distributed WPSs has been designed with (6.1) and (6.2). A conventional WPS with $50\,\Omega$ on all ports will be used in the first stage of the feeding network, whereas the two splitters in the second stage will possess an impedance transformation to $35\,\Omega$ to better match the dipoles. The values of Z_0 and R are shown in Tab. 6.1.

Table 6.1: Component values for two WPSs

		Conventional WPS Stage 1		Unequal impedances Stage 2	
		UHF 437 MHz	VHF 146 MHz	UHF 437 MHz	VHF 146 MHz
Design parameters	R_i	$50\,\Omega$		$50\,\Omega$	
	R_o	$50\,\Omega$		$35\,\Omega$	
Dist. component values	Z_0	$\sqrt{2}\cdot 50\,\Omega \approx 70.7\,\Omega$		$\sqrt{3500\,\Omega} \approx 59.2\,\Omega$	
	R	$R_w = 100\,\Omega$		$R_u = 70\,\Omega$	
Unit cell values	C_w/C_u	5.2 pF	15.4 pF	6.2 pF	18.4 pF
	L_w/L_u	25.7 nH	77.1 nH	21.5 nH	64.5 nH

Both of them was synthesized to LWPSs made by two lumped RH_π-networks, as explained in Sec. 5.3.1. The unit cell inductances and capacitances, as computed with (2.20) and (2.21), are also shown in Tab. 6.1. The variables has subscript w for the first stage dividers and subscript u for the second stage dividers.

6.2 Analysis of Impedance Transforming WPS

The *design* of the impedance-transforming WPS in Tab. 6.1 only took into account the match at the output ports. But that does not prove that the circuit actually *works* like a Wilkinson divider. One could imagine, for example, that the isolation between the output ports is no longer preserved. In this section the impedance-transforming WPS will be analysed to verify that it *does* operate as a WPS.

First of all, Z_0 and R was chosen so that port 2 is matched to R_o for both odd and even signals. This means that when the $4V_0$ source in Fig. 6.3(a) is connected to port 2, power is reflected from neither the even nor the odd component. Thus $S_{22} = 0$ and by symmetry $S_{33} = 0$.

To determine S_{11}, consider that a source is connected to port 1 only, whereas the others are matched (notice that this is the reciprocal mode of operation as compared to the even mode excitation). Due to symmetry, the voltage at nodes 2 and 3 must be equal so no current flows through R. Since R can be effectively removed, the input impedance of *one* of the QWTs is given by (2.11). The input impedance at port 1 is half of this since there are two in parallel:

$$Z_{\text{in}} = \frac{Z_0^2}{2R_o} \overset{(6.1)}{=} R_i \qquad [\Omega] \quad (6.3)$$

from which it follows that $S_{11} = 0$.

Moreover, as the two halves are completely detached for both even and odd

mode excitations, no power flows from port 2 to 3 (the ports are completely isolated) so:

$$S_{23} \overset{\text{symmetry}}{\downarrow} = S_{32} = 0 \qquad [\,] \quad (6.4)$$

Finally, consider again the situation in Fig. 6.3(a). The voltage at node 2 is a superposition of the odd and even modes ($V_2 = V_2^o + V_2^e$). Since port 2 is matched, an impedance equal to R_o is seen into the port, meaning that it acts like a resistive voltage divider, and the voltage at node 2 is half of the generator voltage ($V_2^o = V_2^e = V_0$). Node 1 is grounded for odd modes: $V_1^o = 0$. In order to determine the even mode voltage at node 1 in terms of V_0 it is necessary to utilize (2.8). Let $x = 0$ be at port 1 and $x = -\lambda/4$ at port 2. Then:

$$V_2^e = V(-\lambda/4) = jV^+(1-\Gamma) = V_0 \quad \Rightarrow \quad V^+ = \frac{jV_0}{\Gamma - 1} \qquad [\mathrm{V}] \quad (6.5)$$

$$V_1^e = V(0) = V^+(1+\Gamma) = jV_0\frac{\Gamma+1}{\Gamma-1} \qquad [\mathrm{V}] \quad (6.6)$$

where Γ is given by (2.9) and (6.1) as:

$$\Gamma = \frac{2R_i - \sqrt{2R_iR_o}}{2R_i - \sqrt{2R_iR_o}} \qquad [\,] \quad (6.7)$$

Substituting Γ in (6.6) yields:

$$V_1^e = -jV_0\sqrt{\frac{2R_i}{R_o}} \qquad [\mathrm{V}] \quad (6.8)$$

Finally the *generalized*[1] definition of S-parameters are used to determine S_{12}:

$$\begin{aligned} S_{12} &= \frac{b_1}{a_2} = \frac{V_1^-/\sqrt{R_i}}{V_2^+/\sqrt{R_o}} \\ &= \sqrt{\frac{R_o}{R_i}} \cdot \frac{(V_1^e + V_1^o)}{(V_2^e + V_2^o)} = \sqrt{\frac{R_o}{R_i}} \cdot \frac{-jV_0\sqrt{2R_i/R_o}}{2V_0} \\ &= -j/\sqrt{2} \end{aligned} \qquad [\,] \quad (6.9)$$

And by symmetry and reciprocity $S_{21} = S_{12} = S_{31} = S_{13} = -j/\sqrt{2}$.

[1]Since the input and output impedances are different it is important to use the generalized definition of S-parameters which is based upon incident and reflected *power waves* a and b rather than incident and reflected voltage waves V^+ and V^- as they will not result in the correct S-parameter.

To summarize:

$$S = \begin{bmatrix} 0 & 1 & 1 \\ 1 & 0 & 0 \\ 1 & 0 & 0 \end{bmatrix} \left(-\frac{j}{\sqrt{2}} \right) \tag{6.10}$$

Since the S-matrix is identical to that in Sec. 5.2.2 it is clear that the impedance-transforming WPS presented in this chapter preserves the features of a WPS.

6.3 The Influence of R

In Ch. 5 it was stated that any of the two power splitters in Fig. 5.2 could be used interchangeably. Clearly, the presence of R is the only difference between the two dividers, and it is time to study its influence properly in order to decide whether or not to keep it there. So how does the analysis in the Sec. 6.2 change if R was removed?

First of all, there is no current through R when only port 1 is excited. Thus S_{11}, S_{21} and S_{31} remains unchanged. By reciprocity, S_{12} and S_{13} also remains unchanged.

Now, let port 2 be excited by an incoming power wave whose amplitude is $a_2 = A_0$. This is equivalent of first exciting ports 2 and 3 with $a_2^e = a_3^e = A_0/2$ (even mode) and then $a_2^o = -a_3^o = A_0/2$ (odd mode) and subsequently adding the results. For the even mode, no current flows through R and thereby no power is reflected ($\Gamma^e = 0$). For the odd mode (See Fig. 6.4(b)) the generator sees an open circuit, since the QWT is short circuited at node 1. Thence the odd mode component is fully reflected and $\Gamma^o = 1$. The *total* scattered (outgoing) power waves from ports 2 and 3 can then be written as a superposition of the contributions from the odd and even components:

$$b_2 = a_2^e \Gamma^e + a_2^o \Gamma^o = \frac{A_0}{2}(\Gamma^e + \Gamma^o) \qquad \left[\sqrt{\mathrm{W}}\right] \tag{6.11}$$

$$b_3 = a_3^e \Gamma^e + a_3^o \Gamma^o = \frac{A_0}{2}(\Gamma^e - \Gamma^o) \qquad \left[\sqrt{\mathrm{W}}\right] \tag{6.12}$$

And finally the S-parameters are found by substitution into their definition, and by symmetry:

$$S_{33} \overset{\text{symmetry}}{\overset{\downarrow}{=}} S_{22} = \frac{b_2}{a_2} = \frac{1}{2} \qquad [\,] \tag{6.13}$$

$$S_{23} \overset{\text{symmetry}}{\overset{\downarrow}{=}} S_{32} = \frac{b_3}{a_2} = -\frac{1}{2} \qquad [\,] \tag{6.14}$$

And to summarize:

$$S = \begin{bmatrix} 0 & -j/\sqrt{2} & -j/\sqrt{2} \\ -j/\sqrt{2} & 1/2 & -1/2 \\ -j/\sqrt{2} & -1/2 & 1/2 \end{bmatrix} \tag{6.15}$$

Comparing with (6.10) it is seen that the difference between with, and without R, is that the output ports are no longer matched ($S_{22} = S_{33} = 1/2 \neq 0$) and they are not isolated ($S_{23} = S_{32} = -1/2 \neq 0$). So what are the consequences? Consider the antenna in the transmitting mode, when the device is used as power *splitter* and not as a combiner. Port 1 is excited, and since $|S_{21}| = |S_{31}| = 1/\sqrt{2}$ half the power is fed to each output like intended. Due to electromagnetic reciprocity, the antenna in which the network is used will work equally well in the receiving mode (this may also be verified by computing the mixed mode S-parameters). Thus, there is no apparent disadvantage of eliminating R, *if* the antennas are ideally match and no error is present.

6.3.1 The Influence of R in the Presence of a Fault

Consider again that R is not present. What now, if one of the outputs of the splitter becomes (effectively) open circuited due to some fault[2]? Then the input will become effectively short-circuited. All the incident power will be reflected and none will be delivered to *any* of the outputs. This illustrates the lack of isolation between the output ports. Due to a mistake at one port, the power delivered to the load at the *other* port is altered, in worst case eliminated.

In the presence of R, however, a fault at one of the outputs will not alter the power delivered to the other loads. Port 2 is considered to be passively matched ($S_{22} = 0$) such that the outgoing wave b_2 is all fed to the load at port 2. Hence, $a_2 = 0$. At port 3 a fault has occurred such that a reflection coefficient Γ_3 is seen towards the load. Thus; $a_3 = \Gamma_3 b_3$ re-enters the power-splitter. Consider now a wave a_1 incident to the input (port 1). b_2 is then given by the definition of S-parameters:

$$b_2 = a_1 S_{21} + a_2 S_{22} + a_3 S_{23} = a_1 S_{21} + \Gamma_3 b_3 S_{23} \qquad \left[\sqrt{\mathrm{W}}\right] \quad (6.16)$$

But since $S_{23} = 0$ the reflections at port 3 does not alter the power delivered to the load at port 2. Instead, some of the power a_3 is dissipated in the resistor, while some occur as reflections at the input[3].

Conclusively, it is decided to keep R. Despite the fact that it has no purpose if everything works like intended, it will make sure an error on *one* output does not propagate to the others.

[2]This is actually not so unrealistic. If two antenna elements jam upon deployment and gets short circuited to ground, the stage 1 splitter will have an effectively open circuited output if R is not present.

[3]Actually, it is possible to compute how much is dissipated by the resistor be determining b_1, the square root of the power that is reflected. The power that is not reflected is dissipated in the resistor.

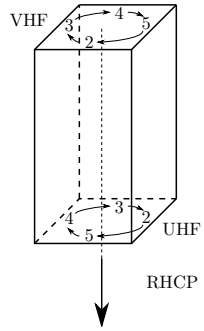

Figure 6.5: This figure illustrates in which order the ports must be excited in order to achieve RHCP-polarization toward the Earth

6.4 Designing Phase-Shifters

6.4.1 Determining Polarization

In order to get RHCP-polarization towards the Earth, each of the four antenna elements must be excited with a 90° mutual phase-lag according to the right-hand rule as illustrated in Fig. 6.5. The figure also shows the placement of the ports (c.f. Fig. 4.7).

The VHF PCB will be mounted on the zenith plane with the microstrip lines up such that the position of the various ports becomes like indicated on Fig. 6.5. For the right-hand rule to apply, it is seen that port 5 must lag behind port 4 by 90° which again lags behind port 3 by 90° which again lags behind port 2 by 90°.

The UHF PCB however, is mounted on the nadir plane with the microstrip lines pointing *downwards* (i.e. the PCB is upside down) and therefore the port numbering goes the other way around. In order for the UHF signal to be RHCP towards the Earth the phase-shifts of the ports must therefore be opposite to that of the VHF network. Port 2 lags behind port 3 by 90° which again lags behind port 4 by 90° which again lags behind port 5 by 90° (yes, it is easy to get confused by this kind of stuff).

6.4.2 The Choice of Phase-Shifters

π unit cell synthetic TLs will be used as phase shifters, since a component of each phase-shifter will appear in parallel with a component from the power-splitter. Moreover, it is easy to add a DC grounding inductor in parallel with the output if one component is already in shunt at the output. The phase-shift will determine whether a RH_π or LH_π cell is to be used (see Fig. 2.5), and the characteristic impedance of the synthetic TLs must be $35\,\Omega$ in order to match the output of stage 2.

It is a requirement that the phase-difference between two consecutive ports are 90°, but except for that there is no requirement of what the phase shift from input

Table 6.2: Unit cell values for the phase-shifters, and whether a DC grounding inductor is needed. n is the port number.

			φ_n	L_n	C_n	DC-Inductor
UHF 437 MHz	Port 2	LH_π	$-45°$	30.77 nH	14.72 pF	No
	Port 3	LH_π	$-135°$	5.28 nH	14.72 pF	No
	Port 4	RH_π	135°	9.01 nH	25.12 pF	Yes
	Port 5	RH_π	45°	9.01 nH	4.31 pF	Yes
VHF 146 MHz	Port 2	RH_π	45°	26.90 nH	12.90 pF	Yes
	Port 3	RH_π	135°	26.90 nH	75.19 pF	Yes
	Port 4	LH_π	$-135°$	15.80 nH	44.05 pF	No
	Port 5	LH_π	$-45°$	92.11 nH	44.05 pF	No

to output must be. One can therefore choose one of the phase-shifts freely and determine the other ones. For example, one could let the phase-lags in stage three be 0°, 90°, 180° and 270°, respectively. A problem with this is that it is not possible to synthesize a 180° phase-shifter with the unit cells described in Sec. 2.2.3. In fact, either the inductance or the capacitance (depending on which unit cell) will rapidly increase as θ approaches $N \cdot 180°$ where N is any integer. Therefore, it is wise to avoid phase-shifts near 180°. It has been decided to use phase-lags of 45°, 135°, -135° and -45°. The former two, will be realized as RH_π-cells whereas the latter are LH_π-cells.

The component values for the unit cell synthetic TLs can be found in Tab. 6.2. They are computed from (2.20) and (2.21). Again it is seen that the phase-shifters have different ordering for the frequency bands to achieve RHCP.

Another, perhaps more elegant choice of phase-shifters can be achieved by using different unit-cells for the two second stage WPSs. This reduces the components but makes the circuit less symmetric. This was therefore not chosen. The interested reader may see App. F.1 for further information.

6.5 Putting it all Together

Just replacing all of the TLs in Fig. 6.1 by their unit cells would work, but leaves several components in parallel, which can be simplified. For example, the two TLs constituting the first WPS each has a shunted capacitor C_w at the input which can be replaced by *one* capacitor $2C_w$ (component X_1 in Fig. 6.2) to save a component.

Further on, components X_2 and X_3 are inductors of size L_w, since they are simply the inductor of the unit cells constituting the first WPS. X_4 and X_5 are a parallel of two C_u capacitors from stage 2 and one C_w capacitor from stage 1. Hence their capacitance is $C_w + 2C_u$. X_6 to X_9 are all L_u-inductors, belonging to the second stage splitters' unit cells.

Consider now the phase shifter at port 2. The component X_{10} are a parallel of the C_u-capacitor from the stage 2 splitter, and the first unit-cell component of the

phase-shifter at port 2. If the phase-shifter at port 2 is an RH_π-cell (see Fig. 2.5) (such as for VHF), this component is the capacitor C_2. If the phase-shifter is an LH_π-cell (such as for UHF), the component is an inductor of size L_2. Thus X_{10} is either a parallel of C_u and C_2 or of C_u and L_2, depending on phase-shifter topology.

Further on, the component X_{14} is a L_2 inductor for RH_π-cell phase-shifters and an C_2 capacitor for an LH_π-cell phase-shifters. Finally, if the phase-shifter is of type LH_π, the component X_{18} is the last component in the LH_π-unit cell (see Fig. 2.5), namely the inductor of size L_2. Notice how this is grounding the element DC-wise. Therefore, the component X_{22} is left open. If the phase-shifter is an RH_π-unit cell, however, the last component would be a capacitor. Thus, X_{22} is taken as an inductor of value L_{DC} to DC-ground the element. The capacitors value, must then be increased accordingly, such that reactance of the parallel remains the same. That is achieved by solving the below equation for two components in parallel.

The component values for the other three output ports follows the same procedure, where the component values for the unit cells, C_n and L_n, are listed in Tab. 6.2.

$$\frac{1}{j\omega_0 C_n} = Z_{\mathrm{parallel}} = \left(\frac{1}{j\omega_0 L_{\mathrm{DC}}} + \frac{1}{(j\omega_0 C_{\mathrm{eff},n})^{-1}}\right)^{-1} \quad [\Omega] \quad (6.17)$$

$$\Rightarrow C_{\mathrm{eff},n} = C_n + \frac{1}{\omega_0^2 L_{\mathrm{DC}}} \quad [\mathrm{F}] \quad (6.18)$$

In theory, L_{DC} can be chosen to any value. Nevertheless, it is wise to choose it not to be too small. The reason is that small deviations from the ideal value in L_{DC} may cause large deviations in Z_{parallel} if L_{DC} is already a quite small value (as seen from the equation above). Moreover, it should be chosen to have the same order of magnitude as other components in the circuit. L_{DC} is therefore chosen to be 100 nH for VHF and 33 nH for UHF.

Due to the many steps of computations necessary in order to determine the component values, a spreadsheet entitled "NUTS Feeding Network Calculator" was made. Screenshots from the spreadsheet can be found in App. B.

6.5.1 Separating Stages 1 and 2

The design so far, fits the layout model in Fig. 5.13(b). All the circuitry is made in one huge block, and TLs can go from the output of the circuitry to the antenna elements. It is possible to make such a layout (the author tried) but it is cumbersome to put all the components in one corner, and it is difficult to fit in the curly TLs.

Looking at Fig. 6.1 it is apparent that it is possible to separate the stages 1 and 2 by two equal-length, 50 Ω TLs and thus, the layout model in Fig. 5.13(c) can be realized. Beware however, that two more lumped components are needed upon synthesis. The reason is that the capacitors C_w at the outputs of WPS 1 is no longer in parallel with the two C_u capacitors of the second stage WPSs, but rather separated by TLs as shown in Fig. 6.6. In this case X_{4a} and X_{5a} is C_w-capacitors whereas X_{4b} and X_{5b} are $2C_u$-capacitors.

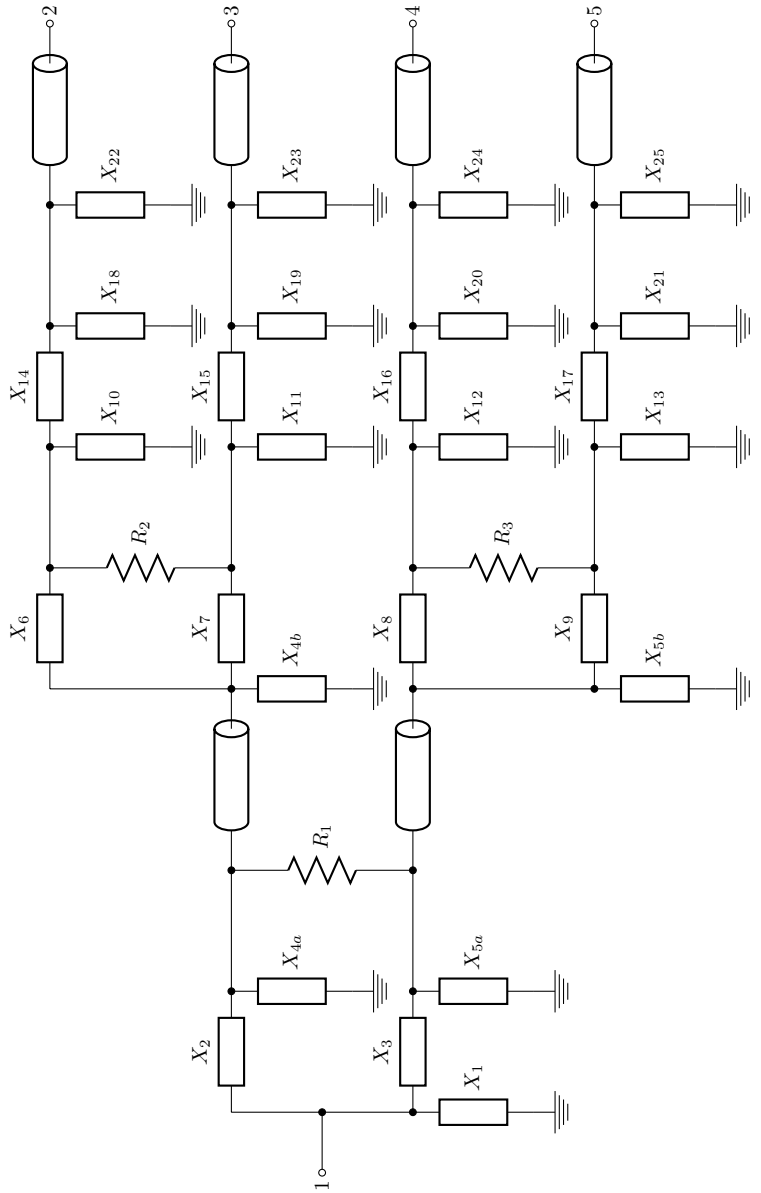

Figure 6.6: A model of the complete feeding network.

The figure also shows a TL on each output. These are the 35 Ω TLs that lead the signal to the antenna elements. All 6 TLs that has been introduced in this section will contribute to the phase-shift from input to output, but since they have the same physical length, the phase-difference between two consecutive antenna elements will remain 90° such that the function of the circuit is preserved.

This is the final design. All the component values are listed in App. A. Note that it is chosen not to distinguish between capacitors and inductors by just labelling all of them X. This is because whether a given component, say X_{10}, is a capacitor or an inductor depends on whether it is the feeding network for VHF or UHF (because of the different order of the phase-shifters).

6.6 The Components

A satellite has unusual requirements for its components. It is already stated that neglect the presence of radiation for passive components will be neglected (c.f. Sec. 5.1). Nevertheless, the components will undergo cyclic temperature changes (likely within $-30°C$–$20°C$), and significant vibrations during launch and vibration test. The choice of components also affects how well the circuit works.

The NUTS-project is also supposed to be comparatively cheap, and therefore use COTS-components (i.e. not specially made). Still it is feasible within NUTS' budget to use rather expensive, high quality COTS components, where it is beneficial. For example, one 100 nH 0603-inductor from Johanson Technology with 5% tolerance costs[4] 0.40 NOK if it is a cheap ceramic one and 1.32 NOK if it is expensive and wirewound. In mass production, this difference may accumulate and become large. In building *one* single satellite, however, these differences are negligible. The components are therefore chosen to be amongst the better components available off-the-shelf. Subsequently follows arguments for why components were chosen as they were, by comparing them with other alternatives.

6.6.1 Inductors

The chosen series of inductors are the 0603-series of *RF Wirewound Inductors* from *Johanson Technology*. It is compared with three other series in Tab. 6.3 to illustrate its advantages.

The inductors are probably the most critical in the design. There are quite a few of them, and practical inductors, tend to be lossy. A way to measure the loss, is by the Q-factor [15]:

$$Q \triangleq \omega \frac{\text{average energy stored}}{\text{energy loss/second}} \qquad [\,] \quad (6.19)$$

A practical inductor can be modelled as an ideal inductor L in series with a resistor

[4] These are prices from `http://www.farnell.no` at the time of writing.

Table 6.3: A comparison of various inductors

	Johanson Technology RF Ceramic Inductors		**Johanson Technology RF Wirewound Inductors**	
Size	0402	0603	0402	**0603**
Available Values	0.6 – 39 nH	1.0 – 120 nH	1.0 – 120 nH	2.0 – 390 nH[a]
Q (min.)	8@100 MHz	12@100 MHz	55@900 MHz	60@900 MHz
SRF[b] (min.)	21 GHz (1 nH)	23 GHz (1 nH)	11 GHz (1 nH)	13 GHz (2 nH)
Op. Temperature	-40 – 100°C		-40 – 125°C	
Best Tolerance	±5% (±0.3 nH below 6.8 nH)		±5%[c] (±0.2 nH below 6.8 nH)	
TCL[d]	N/A		25 – 125 ppm/°C	
Thermal Shock	$L = \pm 10\%$, $Q = \pm 20\%$		$L = \pm 5\%$, $Q = \pm 10\%$	
Drop Test	N/A		$L = \pm 5\%, Q = \pm 10\%$	

[a] Actually 470 nH is also available but then with ferrite core rather than ceramic. This alters the TCL and operating temperature range.
[b] SRF is the frequency where the parasitic capacitive reactance equalizes the inductive reactance.
[c] Actually 2% tolerance is available according to the datasheet but the author could not find any provider that ships component with 2% tolerance to Norway within reasonable amount of time.
[d] *Temperature Coefficient of Inductance (L)* (TCL) is how much the inductance may change due to temperature deviations from $T_0 = 25$°C. Note that this is *not* included in the tolerance of the component.

R. In that case, the Q-factor for the inductor is given by[5] [15]:

$$Q = \frac{\omega L}{R} \qquad [\,] \quad (6.20)$$

These equations indicate that Q increase with frequency. That is true until a certain point, when the inductor is no longer a good inductor electromagnetically (plots that illustrate this are found in the datasheet in App. H).

In Tab. 6.3 it is seen that the wirewound inductors has a higher Q. They are tested on higher frequency, so the comparison is not quit fair, but a closer inspection in the datasheet in App. H reveal that the wirewound has significantly better Q for all frequencies.

Two physical sizes are compared, 0402 (0.04×0.02 in $= 1.0 \times 0.5$ mm) and 0603 (0.06×0.03 in $= 1.6 \times 0.8$ mm). It is also seen that the Q is slightly better for bigger inductors. Moreover, the operating frequency (VHF and UHF) should be well below the *Self-Resonant Frequency* (SRF), the frequency where the parasitic capacitance becomes more dominating than the inductance, to ensure that it behaves properly as an inductor. That requirement is fulfilled for all the components. The operating temperature is also seen to be feasible for all inductors.

Moreover, ceramic 0402-components are not available with higher values than

[5] This definition of Q actually assumes that it is used at resonance in series with an ideal capacitor

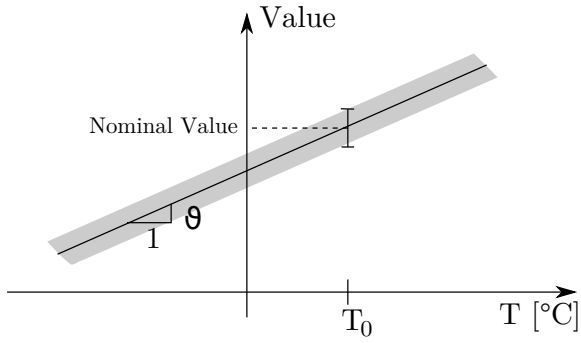

Figure 6.7: To know what a components value may be one must take into account both the tolerance and the temperature coefficient ϑ.

39 nH whereas the highest in the design are 100 nH (see component list in App. A). The other three series covers all the values in the design.

The inductances was found to have (mostly) 5% tolerance at best, meaning that the value can be maximally 5% off the nominal value (the one that is printed on the package) at $T_0 = 25°C$. As illustrated in Fig. 6.7, it may deviate *more* than specified by the tolerance if the temperature changes. The temperature coefficient (named TCL for inductors) specifies how much the inductance is expected to change per degree. At a temperature T, the nominal value of the inductor should be adjusted according to the temperature coefficient. Then the value of the inductor may deviate maximally 5% off *this* value.

Assuming that the components will be in the range of $-30°C$ to $20°C$, the largest possible offset from T_0 is $55°C$. With the TCL specified for the wirewound inductors, that is a deviation of less than 0.7%, which is neglegible compared to the tolerance. The ceramic inductors does not have a TCL specified. Further on, the wirewound inductors are tested for both thermal and mechanical shock (drop test) with the results that the inductance should be off by no more than 5% and the Q-factor no more than 10% after the shock. It is not known how the tests performed by the vendors compare to the stress during a satellite launch. Nonetheless, it is the only indication we have. The ceramic inductors has slightly worse thermal results and are apparently not tested for mechanical stress in any way.

It is seen in Sec. 7.2 that the phase of the outputs of the feeding network are a bit sensitive to the inductances and capacitances of the components and therefore it is beneficial to have as stable valued components as possible. It is therefore concluded that the 0603 or 0402 wirewound inductors the suited ones (the 0603 are slightly better than the 0402). Since the capacitors are chosen to be 0603, the inductors are also chosen to be 0603.

6.6.2 Capacitors

It is chosen to use the 0603-series *Multilayer Capacitors* from *Johanson Technology* with *NP0* dielectric. This series is compared with two others in Tab. 6.4; an 0402-

Table 6.4: A comparison of various capacitors

	Johanson Technology Multilayer Capacitors		
Dielectric	X7R	**NP0**	
Size	0201	0402	**0603**
Available Values	0.2 – 100 pF	0.2 – 33 pF	0.2 – 100 pF
TCC[d]	±15%	30 ppm/°C	
Op. Temperature	-55 – 125°C		
Best Tolerance	±2% (±0.1 pF below 10 pF)[a]		
Q (min.)	1000@1 MHz		
Thermal Cycles	±2.5% or 0.25 pF		
Vibration Test	±2.5% or 0.25 pF		

[a] Actually 1% tolerance (±0.05 pF below 10 pF) is available according to the datasheet but the author could not find any provider which ships that to Norway within reasonable amount of time.
[d] *Temperature Coefficient of Capacitance (C)* (TCC) is how much the capacitance may change due to temperature deviations from $T_0 = 25°C$. Note that this is *not* included in the tolerance of the component.

series of the same kind, and an 0201-series (0.02×0.01 in $= 0.6 \times 0.3$ mm) with X7R dielectric.

It is easy to see that capacitors are more close to ideal than inductors. They have a vastly higher Q-factor implying less loss[6]. Their tolerance and maximum deviations due to thermal and mechanical stress are also better than for the inductors. As already stated, it is important to keep the reactances to be as accurate as practically possible.

When it comes to the range of values, it is seen that the 0402-series' highest value is 33 nH whereas the highest in the design is 100 pF. For the other series all the needed values are available. The operating temperature range is also seen to be more than sufficient.

Choosing the right dielectric, however, seems to be important. Since the capacitance is inversely proportional to the distance between the plates of the capacitors, it is important to have an temperature insensitive dielectric such as NP0. For the X7R, which is not temperature insensitive, the capacitance may deviate as much as 15% within the operating temperature range. Beware that this is way more than the tolerance. In fact, for a satellite that undergoes cyclic temperature variations, the tolerance is almost negligible as compared to the deviations due to temperature. Since the phase of the outputs of the network is somewhat sensitive to the reactances a 15% change is unacceptable. This clearly shows why it is important to choose components carefully. For the NP0 dielectric the TCC is 30 ppm/°C which means that the capacitance may vary less than 0.2% (again, assuming a lowest temperature of $-30°C$, $55°C$ lower than T_0). This is negligible.

[6] $Q = 1/\omega CR$ for the capacitor, again assumed to be in series resonance with a perfect inductor[15].

Table 6.5: A comparison of various resistors

	Multicomp MCMR06	**Panasonic ERJP03**	Vishay CRCW0603-HP e3
Size	0603		
Available Values	All that is of interest plus more		
TCR[a]	200 ppm/°C		
Op. Temperature	-55 – 125°C		
Best Tolerance	1%		
Max Power	100 mW	200 mW	250 mW

[a] *Temperature Coefficient of Resistance (R)* (TCR) is how much the resistance may change due to temperature deviations from $T_0 = 25°C$. Note that this is *not* included in the tolerance of the component.

The conclusion is therefore that only the 0603-series is suitable.

6.6.3 Resistors

It is chosen to use *ERJP03* resistors (of size 0603) from *Panasonic*. It is compared with a resistor from *Multicomp* and one from *Vishay* in Tab. 6.5.

The resistors are probably the least critical components in the design, since they do not contribute to the phase on the outputs. Also, resistors seems to be the component available with highest precision in terms of tolerance. It has a tolerance of 1%, and a temperature coefficient of 200 ppm/°C. Again for a range of $55°C$, that yields 1.1% deviation of resistance (comparable to the tolerance). The temperature range is also way better than necessary, and it seems like it is little difference in 0603 resistors.

It appears to the author as if it is most common that 0603 resistors can handle 100 mW of power, like the Multicomp resistor. The resistors from Panasonic and Vishay are, according to their datasheets in App. H, built to handle higher power. The reason why this might be of interest for the NUTS feeding network is in case of malfunction. The radio will transmit 500 mW of power, and the feeding network will split it in four (125 mW). In case one of the antenna elements are short circuited, the power intended for that element will partly be reflected on port 1, and partly be dissipated in a resistor (as discussed in Sec. 6.3). It will not propagate to other outputs, since they are isolated. This means that if one output is short circuited, the power dissipated in a resistor is at most 125 mW. Choosing a resistor that can handle at least 125 mW is therefore wise. In case of *two* short circuits, at most 250 mW is dissipated (not necessarily in the same resistor). That actually suggests that the resistor from Vishay is best suited. However, that would not ship to Norway within reasonable time. Therefore, the Panasonic-resistor was chosen, with the knowledge that at least one element can be short-circuited in calculated manners. Further qualitative considerations of malfunctions, are presented in Sec. 11.2.

Conclusively, there is a clear difference between the accuracy/stability of the values for various components, but of the chosen ones, it is unlikely to experience a larger deviation than 5%. The reason is as follows: None of them has a higher tolerance than 5% and the temperature coefficients are small enough to be neglected except for the resistors. Temperature variations may cause deviations of about 1% for resistors, in addition to their 1% tolerance. In total; 2% which is still less than 5%. The components are seen to be stable to within 5% or better when exposed to mechanical or thermal stress.

As an endnote about components, the author would like to emphasize that the *ideal* component values as computed earlier in the design, of course is not available for purchase (at least not off-the-shelf). Instead, fixed (*nominal*) values are available for sale, as can be found in the datasheets in App. H. One simply has to pick the closest value available. A list of exactly which components are used can be found in App. A.

6.7 PCB Design

Due to the specific requirements for the geometry of the PCB, the layout had to be drawn manually. This was done in ADS and can be seen in Fig. 6.8. The port 1 is fed to the module through a SMA connector in the lower right corner, where the stage 1 splitter also happens to be placed. Stages 1 and 2 are separated as explained in Sec. 6.5.1 by lines of width 1.4 mm corresponding to 50 Ω (c.f. Tab. 5.3).

Stages 2 and 3 are placed in the lower left, and upper right corners. As seen in Tab. 6.2, the DC grounding inductors are only needed on two of the ports, but which ports differs for the UHF and VHF design. The design was made completely symmetric, including a footprint for a DC grounding inductor on each port. The reason for this is twofold; (1) the same PCB layout can be used for both UHF and VHF, and (2) if, for some reason, one need to change the phase-shifters after production (i.e. to change polarization), this can simply be done by changing component values. The same PCB can be used.

From each of the phase-shifters to the place of the antenna elements there is a 2.5 mm wide 35 Ω microstrip line (according to Tab. 5.3). In order to test the PCB, footprints for SMA connectors are put in the place of each antenna element. When the PCB has been successfully tested, the SMA connectors can be de-soldered and replaced by the measuring tape comprising the antenna elements. The hole for the center-conductor of the SMA connector is 1.6 mm in diameter and should be drilled to 2 mm in diameter to be used for fastening of the measuring tape along with the other hole right behind it. It is important that the footprint of the four grounding pins of the SMA connector are *not* connected to ground, as that would short circuit the antenna element. Their only purpose is to mount the SMA connector. The SMA connector should be grounded on the other side of the PCB.

Note also that there is a discontinuity in the width of the microstrip line right before the SMA connector. This is the end of the footprint of the SMA connector, and is to be used as a reference plane in measurements. Instruments and SMA connectors are all matched to 50 Ω meaning that there will be a mismatch at this

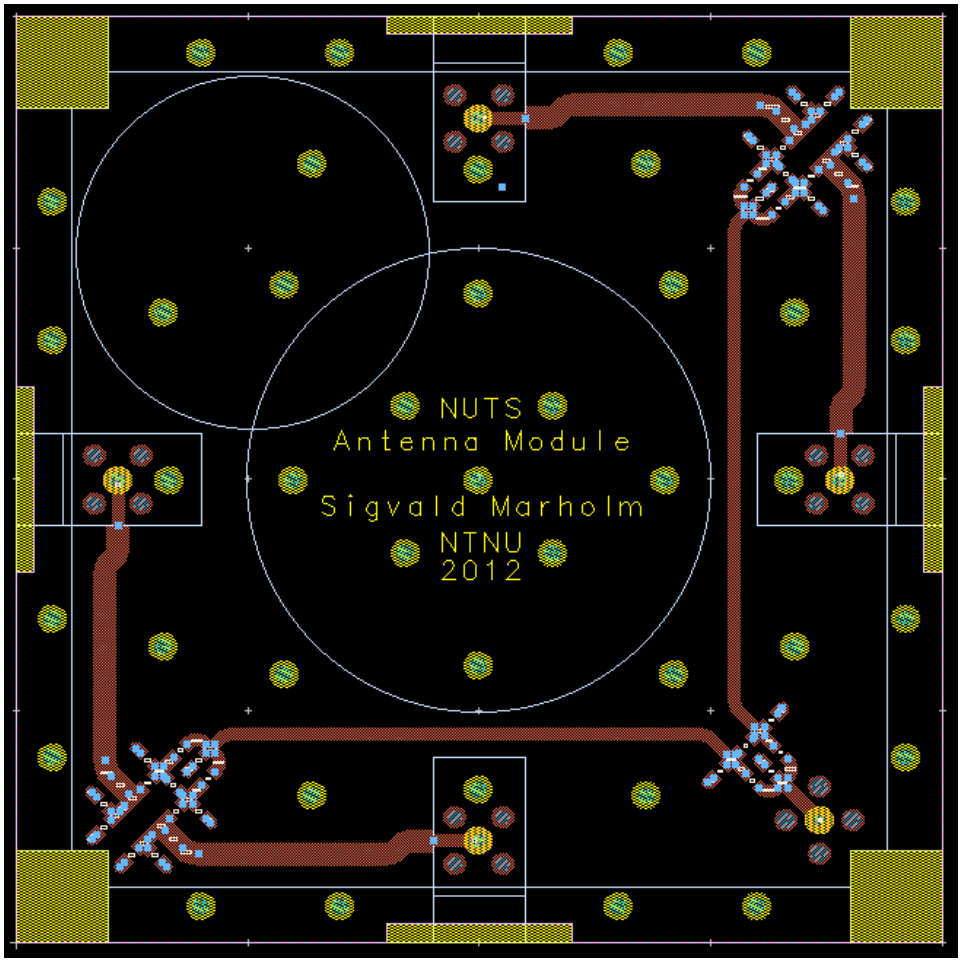

Figure 6.8: The PCB Layout. Red indicates copper on the top layer and yellow indicates where it is *not* copper on the bottom layer. The tiny blue dots are only electrical junctions in between various microstrip lines and components in ADS and does not represent anything on the physical PCB.

Table 6.6: Electrical length (obtained from ADS) of TLs in PCB layout

	UHF 437 MHz	VHF 146 MHz
TLs between stages 1 and 2	56.3 mm	
	56°	18°
TLs from stage 3 to elements	30.2 mm	
	31°	10°

point during measurements. More about that in Sec. 7.2.4.

The dots are the screw holes for which the two stacked PCBs (see Ch. 4) will be mounted. They will be mounted by steel screws of size M2×6 mm. Not all of the holes needs to be used, but many holes are present in the design. As explained in Ch. 4, the two large holes, and the edges may be removed by those who finally integrate all the devices in the satellite. In that case, not so many holes are left for the bolts.

Generally, it is attempted to keep at least three substrate thicknesses (2.4 mm) of distance from the microstrip lines to all surrounding metal. This is achieved, except for at the passage in between the elements and the camera hole. At the smallest, there is only 1.8 mm of spacing in between the microstrip line and the the antenna element/camera hole. Nonetheless, it is assumed to be negligible since this is only for 1 cm of length which is negligible as compared to the wavelengths.

6.7.1 Covered Microstrip Lines

As described in Ch. 4, another PCB will be put on top of the feeding network, with 3 mm of separation, to protect the feeding network both mechanically and performance-wise. Since the purpose of the cover partly is to protect the characteristic impedance of the microstrip lines, it would be unfortunate if the the cover itself affects the characteristic impedance too much.

The characteristic impedance of the microstrip lines was simulated with ADS *LineCalc*. The cover changes the impedance of the 50 Ω-lines to 48.7 Ω (less than 3% change) and that of the 35 Ω-lines to 33.6 Ω (less than 4% change). The reflection coefficient present when one of these covered microstrip lines are terminated to a 50 Ω/35 Ω system is not more than 2%, which by far supersedes the accuracy of the rest of the design.

It is therefore concluded that the cover does not notably influence the performance of the microstrip lines, but rather protects them from other obstacles like intended.

7 Simulations of the Feeding Network

The designed feeding network were simulated in *Agilent Advanced Design System* (ADS). The purpose of the simulations are many. First, one would like to verify that the design from Ch. 6 works like intended; that no mistakes are done in the design procedure. For this, the ideal component values should be used. Second; the component values must be replaced by realistic ones. That is, physical components are labelled with nominal values (which are different from the ideal ones) and they have a certain tolerance. Statistical simulations will help to make sure such deviations in component values does not affect the performance too severely. They will also make it possible to compute worst-case results such as amplitude and phase unbalance that can be used for later study. At last in this chapter, simulations will be presented that can be compared with actual measurement.

Until now, the design is only considered at the center frequency. This is expected to be sufficient since the NUTS radios are narrowband ($\leq 25\,\text{kHz}$, see Sec. 2.1.1), which can also be verified in the plots throughout this chapter. As stated in Sec. 2.1.1, however, the NUTS project has not yet allocated any frequencies at the P&TT. Although it is not a requirement for this thesis to look at out-of-band performance, it is of interest for the NUTS project to know what happens if the allocated frequencies are a few MHz different than what is first anticipated. Therefore it is chosen to simulate with a 10 MHz-frequency span.

7.1 Verification of the Design

The first simulation is a verification that the design works like intended, and that all the calculations are correct. The circuit in Fig. 6.6 is modelled in ADS with *ideal* component values, and terminated by $R_i = 50\,\Omega$ on the input and $R_o = 35\,\Omega$ on each output as illustrated in Fig. 7.1(a) (a screenshot from ADS can be found in App. G.1).

The resistors with a square box around it indicates an S-parameter termination

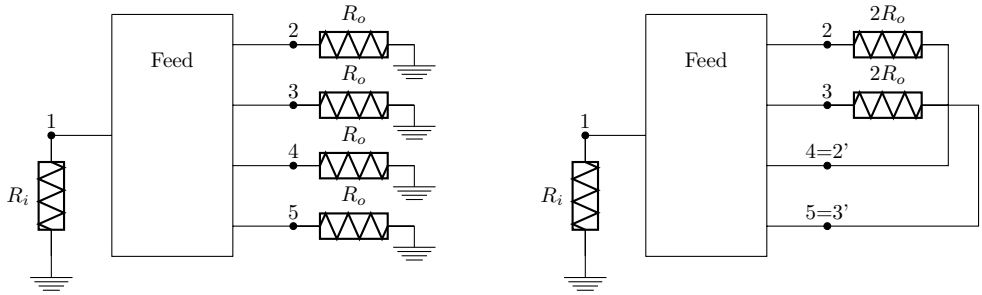

(a) Single-ended setup

(b) Differential setup

Figure 7.1: Various simulation setups. The resistors with a square box around it indicates an S-parameter termination in ADS. The box labelled "Feed" is the circuit illustrated in Fig. 6.6.

in ADS. For example, when ADS determines S_{n1}, the termination in port 1 acts like a generator with resistance R_i that produces the incoming wave (a). The terminations on the other ports are then purely resistive loads. The S-parameters can then be computed from the waves scattered to all the terminations. Which termination acts like a generator, depends on which S-parameter ADS is computing.

7.1.1 What to Expect

As for what to expect of the S-parameter simulations, this can be found either by setting up incident waves (a) and scattered waves (b) for all the dividers and phase-shifters and using the definitions of S-parameters, or it can be found by reasoning, as will be done here.

Consider again Fig. 6.1, but without the phase-shifters on the output. Since it is a 4-way WPS one would expect:

$$S_{21} = S_{31} = S_{41} = S_{51} = \frac{1}{2}e^{-j180^\circ} \qquad [\,] \quad (7.1)$$

where the magnitude (1/2) indicate that the power is split in four, and the angle (-180°) is due to the lag through the TLs. Moreover, matching is expected:

$$S_{ii} = 0 \qquad , \quad \forall i \qquad [\,] \quad (7.2)$$

and isolation between the outputs:

$$S_{ij} = 0 \qquad , \quad \{i, j\} \subset \{2, 3, 4, 5\} \qquad [\,] \quad (7.3)$$

Due to the phase-shifters, S_{n1} experiences an additional lag (a decrease by φ_n in the angle of the S-parameter) as shown in Tab. 6.2. Including that lag for the UHF circuit:

$$\begin{aligned} S_{21} &= 0.5e^{-j135^\circ} \\ S_{31} &= 0.5e^{-j45^\circ} \\ S_{41} &= 0.5e^{j45^\circ} \\ S_{51} &= 0.5e^{j135^\circ} \end{aligned} \tag{7.4}$$

and for the VHF circuit:

$$\begin{aligned} S_{21} &= 0.5e^{j135^\circ} \\ S_{31} &= 0.5e^{j45^\circ} \\ S_{41} &= 0.5e^{-j45^\circ} \\ S_{51} &= 0.5e^{-j135^\circ} \end{aligned} \tag{7.5}$$

and by reciprocity, $S_{1n} = S_{n1}$ for $n \in \{2, 3, 4, 5\}$.

One should also take into account the separating TLs between stages 1 and 2, and between the splitter and the antenna elements. They impose an additional lag which is taken into account by subtracting their length (in degree) from the angle of the S_{n1}-parameters. The lengths are found in Tab. 6.6. For UHF:

$$\begin{aligned} S_{21} &= 0.5e^{j138^\circ} \\ S_{31} &= 0.5e^{-j132^\circ} \\ S_{41} &= 0.5e^{-j42^\circ} \\ S_{51} &= 0.5e^{j48^\circ} \end{aligned} \tag{7.6}$$

and for the VHF circuit:

$$\begin{aligned} S_{21} &= 0.5e^{j107^\circ} \\ S_{31} &= 0.5e^{j17^\circ} \\ S_{41} &= 0.5e^{-j73^\circ} \\ S_{51} &= 0.5e^{-j163^\circ} \end{aligned} \tag{7.7}$$

It might be easier, and more intuitive, to check that $|S_{n1}| = -6\,\text{dB}$ for $n \in \{2, 3, 4, 5\}$ and that the outputs phase-difference is $\pm 90^\circ$. Let us define the phase-difference between ports i and j as:

$$\phi_{ij} \triangleq \angle S_{j1} - \angle S_{i1} \qquad [^\circ] \tag{7.8}$$

then, for UHF:

$$\phi_{23} = \phi_{34} = \phi_{45} = \phi_{52} = 90 \qquad [^\circ] \tag{7.9}$$

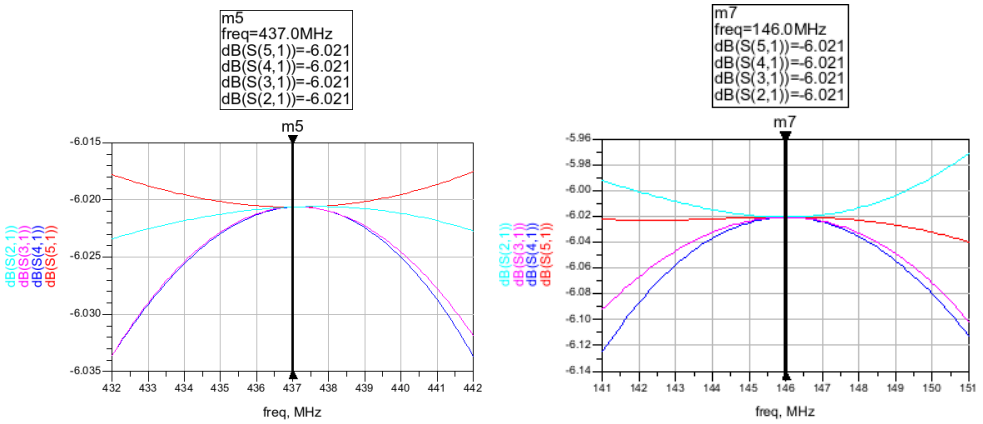

(a) UHF (b) VHF

Figure 7.2: S-parameters from input to outputs in dB. From ADS.

and for VHF:

$$\phi_{23} = \phi_{34} = \phi_{45} = \phi_{52} = -90 \qquad [^\circ] \quad (7.10)$$

Remember that the UHF PCB is mounted upside down, which causes the different signs.

We will both check the phase-differences ϕ_{ij} as well as the absolute phase of the S-parameters, since we will later need them for comparison.

7.1.2 Simulation Results

The magnitude (in dB) and phase of the S_{n1} parameters for $n \in \{2, 3, 4, 5\}$ are shown in Fig. 7.2 and Fig. 7.3, respectively. At the center frequency, it is seen that the magnitude is $-6.021\,\text{dB}$ as compared to the ideal $-6\,\text{dB}$ and the phases are within 1° of what was predicted in the previous section.

Fig. 7.4 shows the simulated phase-differences ϕ_{ij} between the outputs. As predicted, it is at about 90° for the UHF center frequency and −90° for the VHF center frequency (to within 1°) for all i, j.

Finally, it is only noted here that both matching (S_{ii} for all i), and isolation between the output ports (S_{ij} for different i and j, both unequal to 1), all was below $-50\,\text{dB}$ for both UHF and VHF at the center frequency. The output isolation stayed below $-25\,\text{dB}$ for the whole frequency-spans for both bands whereas $S_{ii} < 25\,\text{dB}$ for UHF and $S_{ii} < 15\,\text{dB}$ for VHF for all frequencies in the span and for all i. The plots can be found in App. G.4.

7.1.3 Conclusions of the Simulation

The difference between computed values and simulation results at the center frequencies are negligible, and it is reasonable to assume that they are due to round-off

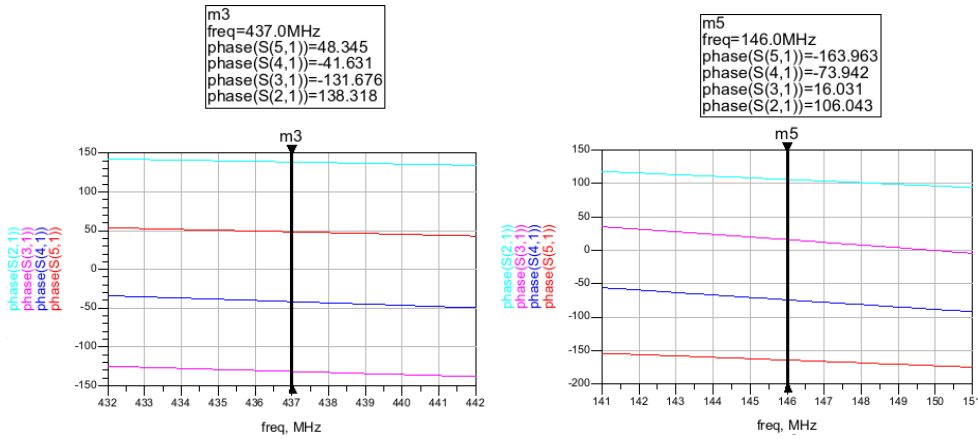

(a) UHF (b) VHF

Figure 7.3: S-parameter phase from input to outputs. From ADS.

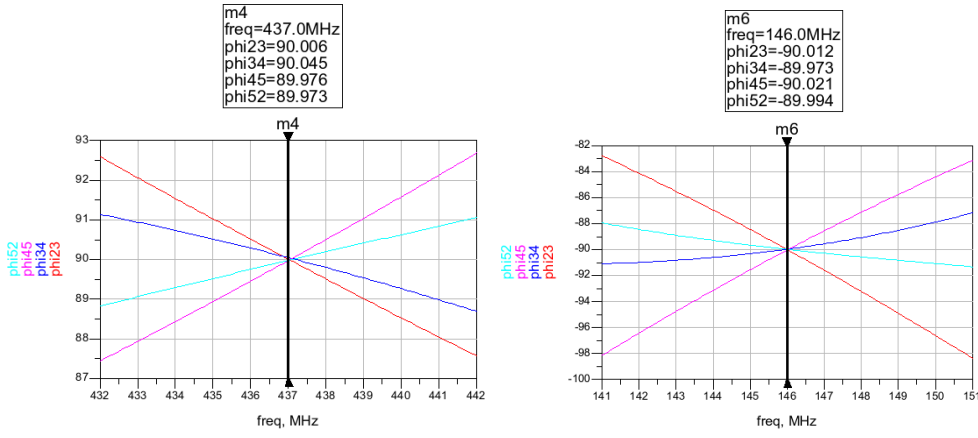

(a) UHF (b) VHF

Figure 7.4: Simulated ϕ_{ij}. From ADS.

errors in calculations, and maybe simulation inaccuracy. It is therefore concluded that the design is correct and no mistakes are present in the computed values.

For deviations of 5 MHz off the center-frequency, up to almost 3° error may occur for UHF and up to about 9° for VHF (if ideal components are assumed). It is reasonable that it is larger for VHF since 10 MHz is a larger *relative* bandwidth for VHF than for UHF.

Whereas the power delivered to each load, as seen in Fig. 7.2, remains almost unchanged within the frequency-span, the phase-difference does not. In other words, if the frequency is gradually shifted, the phase-differences will degrade quicker than the amplitude-balance at the outputs.

What the bandwidth of the circuit is, depends upon how accurately one requires the phase-difference to be, but one can safely conclude that the bandwidth is higher than the required 25 kHz (c.f. Tab. 2.1). In fact, the circuits can likely be used for the whole simulated 10 MHz-ranges, although with slightly degraded phase-performances.

To say something more certain about the bandwidth and performance, one should take into account the fact that the components are not ideal.

7.2 Statistical Simulations

In the previous simulations the component values was taken to be exactly like computed in the design phase (ideal values). However, true components are restricted to certain fixed values (nominal values) available off-the-shelf. In addition, they may deviate from the nominal value for a number of reasons, which has been thoroughly discussed in Sec. 6.6. In Sec. 6.6, it was concluded that up to 5% deviation may occur. One may ask; is this significant? How greatly will this influence the performance of the circuit? Is it even likely that the circuit will work? Remember that the phase is important in this application, and that the reactive components control the phase-shifts throughout the whole circuit. Due to the significant number of reactive components such questions are reasonable to ask. Statistical simulations was therefore carried out in ADS to answer these questions.

7.2.1 Background About the Monte Carlo Analysis

The principles of *Monte Carlo* simulations, as applied on circuits, are the following: All (or selected) component values are assigned a *Probability Density Function* (PDF)[1]. The simulation is run N times (referred to as trials). Each trial the components values are randomly picked according to their PDF. The simulation data for each of the trials is readily available for evaluation, and is typically plotted simultaneously such that the person interpreting the results can see what the trend is [41].

[1] One may also specify a correlation between the component values. The components are here assumed to be uncorrelated.

Yield Analysis

The *yield analysis* is another variant of the Monte Carlo analysis with more rigorousness. It attempts to estimate the percentage Y of built circuits that will work like intended. To do this, one must define requirements the circuit must fulfill in order to be considered successful. These requirements are referred to as "goals". As an example, $S_{11} < 10\,\text{dB}$ could be one goal, and one may have as many goals as desirable [41].

7.2.2 Method of Simulations

In our case, only *one* circuit is to be built, and rather than the percentage of working circuits, Y will represent the probability that the one circuit performs within the specified goals. In fact, one may reformulate it: "what must the goals be for Y to be very high, for instance 95%?". We will then be 95% sure that the circuit will perform within the obtained goals.

According to [41], the number of trials must be chosen according to the following inequality:

$$N > \left(\frac{\epsilon}{E}\right)^2 \hat{Y}(1-\hat{Y}) \qquad [\,] \quad (7.11)$$

where E is the error in %, and ϵ controls the confidence level. It is here chosen that the *estimated* yield should be $\hat{Y} \approx 0.95$ (to within a percent due to round-off) and that the *true* yield is within $E = 0.02$ of this with 95% confidence. $\epsilon = 2$ corresponds to a 95% confidence [41]. That results in the requirement $N > 475$ for these simulations to be reliable. It is therefore chosen to use $N = 500$. More information about this can be found in either App. G.3 or [41].

In ADS, it is possible to assign component values with either normal (Gaussian) distribution or uniform distribution. It is impossible to know what the distribution of the components actually are, since it is not specified in any datasheets. It is therefore *assumed* that the distribution is uniform for two reasons: (1) It is hard to define a boundary for the normal distribution that corresponds to the tolerance limit of the component. One would simply have to say that the tolerance lies a certain number of standard deviations from the center. (2) the uniform distribution provides a greater probability that, for a given trail, the component value is closer to the tolerance limit. It is therefore a more pessimistic assumption, suitable for worst-case scenarios. To summarize; the component values (for each component) was chosen to be uniformly distributed from 5% below the *nominal* value, to 5% above the *nominal* value.

Three statistical simulations has been performed with this method. Two single-ended simulations; with setup as illustrated in Fig. 7.1(a), and one differential simulation, with setup as illustrated in Fig. 7.1(b). The first single-ended setup has all the outputs terminated by $R_o = 35\,\Omega$ loads whereas the second single-ended setup has all outputs terminated by $R_o = 50\,\Omega$ loads (which causes a mismatch). The reason for introducing the mismatch is to have simulation results to compare

Table 7.1: According to yield analysis, it is 95% certain that the circuit will perform within these specifications, when terminated by 35 Ω loads. These specification therefore serves as worst-case.

		UHF		VHF	
		Center 437 MHz	Out-of-band 432–442 MHz	Center 146 MHz	Out-of-band 141–151 MHz
$\lvert S_{n1}\rvert$	min.	−7 dB	−7 dB	−6.6 dB	−6.8 dB
	max.	−5.7 dB	−5.7 dB	−5.7 dB	−5.7 dB
ϕ_{ij}		$90° \pm 29°$	$90° \pm 30°$	$-90° \pm 20°$	$-90° \pm 26°$
$\lvert S_{ii}\rvert$	max.	−8 dB	−8 dB	−10 dB	−8 dB
$\lvert S_{ij}\rvert$	max.	−20 dB	−20 dB	−20 dB	−18 dB

measurements performed by network analyser with, as most network analysers are made with 50 Ω port impedance. None of these results, however, can be directly used to state anything about the performance of the antennas that will be built. A dipole will be seen as a 70 Ω differential load between two of the outputs (when its length is reduced such that it is non-reactive). Therefore, to determine the phase and amplitude unbalance one should expect for the antenna (worst-case), the setup with $2R_o = 70\,\Omega$ differential loads are simulated as well.

Losses in microstrip lines and components are not included in the simulations, since it is not suspected that they may have a fatal consequence on the performance.

7.2.3 35 Ω Single-Ended Results

The worst expected performance of the circuit when terminated by $R_o = 35\,\Omega$ single-ended loads, is shown in Tab. 7.1. It is seen that the power splitting S_{n1} for $n \in \{2, 3, 4, 5\}$ is within 1 dB of the ideal −6 dB for all frequencies. The isolation (S_{ij} for different i and j, both unequal to 1), are seen to be very good. The match (S_{ii} for all i) are also sufficiently good. Nonetheless, the (worst) expected phase-error is observed ranging from 20° to 30° which is quite a lot. It therefore requires further attention to determine what is the effect of this phase-error. In Sec. 7.2.5 a worst-case estimate for the polarization loss it causes is carried out.

Despite the fact that high-quality components were chosen, phase-errors of up to 30° may occur. In order to emphasize the importance of choosing high-quality components, one simulation at the VHF center frequency is performed, where it is assumed that capacitors with X7R dielectric is used. The capacitors with X7R dielectric can, according to Tab. 6.4, deviate up to 15% due to temperature fluctuations. When the components PDF are allowed to be uniform with limits at 15% of the nominal value rather than 5%, the performance in Tab. 7.2 results. It is clearly not sufficient.

Table 7.2: This is an example of what would happen if the components were allowed to deviate by 15% rather than 5%. According to yield analysis, it is 95% certain that the circuit will perform within these specifications, when terminated by 35 Ω loads.

		VHF
		Center 146 MHz
$\lvert S_{n1}\rvert$	min.	−8 dB
	max.	−5 dB
ϕ_{ij}		90° ± 50°
$\lvert S_{ii}\rvert$	max.	−3 dB
$\lvert S_{ij}\rvert$	max.	−15 dB

Table 7.3: According to yield analysis, it is 95% certain that the circuit will perform within these specifications, when connected to a network analyser (50 Ω loads). These specification therefore serves as worst-case.

		UHF		VHF	
		Center 437 MHz	Out-of-band 432–442 MHz	Center 146 MHz	Out-of-band 141–151 MHz
$\lvert S_{n1}\rvert$	min.	−7.5 dB	−7.5 dB	−6.6 dB	−7 dB
	max.	−5.8 dB	−5.8 dB	−5.8 dB	−5.7 dB
ϕ_{ij}		90° ± 32°	90° ± 33°	−90° ± 22°	−90° ± 27°
$\lvert S_{ii}\rvert$	max.	−6 dB	−6 dB	−10 dB	−8 dB
$\lvert S_{ij}\rvert$	max.	−20 dB	−20 dB	−20 dB	−18 dB

7.2.4 50 Ω Single-Ended Results

In order to test the feeding network, the layout is made with a footprint for an SMA-connector at each port, such that it can be connected to a network analyser. Both the SMA-connectors, and the network analyser are made for 50 Ω, meaning that a mismatch will occur at ports 2-5. In order to resolve that problem, simulations has been done with the same port-impedance ($R_o = 50\,\Omega$) as the network analyser. Physical measurements can then be compared with these simulations to verify that the circuit works like intended. The outcome of the simulations is presented in Tab. 7.3.

It is clear that the results are not very different from the 35 Ω case, but it can be seen that the phase-error increases with a couple of degrees, and that the match at UHF can not be expected to be equally good. It might seem suspicious that the match did not degrade for VHF as well, but remember that this is only what is statistically expected as a worst case. The *average* matching is likely better for

35 Ω.

7.2.5 70 Ω Differential Results

In order to determine the consequences to expect due to the imperfections, especially the phase-error, simulations are performed where $2R_o = 70\,\Omega$ loads are differentially terminated across the output (this actually yields a differential-mode part in a mixed-mode S-parameter representation). The reason for this simulation setup is that it can be used to determine the amplitude, and phase unbalance that may occur in the two crossed dipoles, which again can be used to determine the axial ratio and polarization loss.

Note that only *three* ports are present in this ADS simulation. One load is placed in between ports 2 and 4 (hereby referred to as port 2^D for "differential"), and one between ports 3 and 5 (port 3^D). S^D_{21}, for instance, is then the differential-mode S-parameter that express the amount of power incident on port 1 that exits port 2, and is fed to one of the dipoles. The amplitude unbalance can then be defined as the difference between power delivered to the two dipoles when port 1 is excited:

$$A_e = |20\log|S^D_{31}| - 20\log|S^D_{21}|| \quad \text{[dB]} \quad (7.12)$$

And the phase unbalance is defined as the difference between the actual phase-difference and the wanted phase-difference (±90°):

$$\phi_e = \begin{cases} |(\angle S^D_{31} - \angle S^D_{21}) - 90°| & \text{, UHF} \\ |(\angle S^D_{31} - \angle S^D_{21}) - (-90°)| & \text{, VHF} \end{cases} \quad [°] \quad (7.13)$$

Moreover, the maximum excess insertion loss is taken as the insertion loss from port 1 to port 2 or 3 (whichever is highest) minus the 3 dB that stems from the power splitting:

$$\text{EIL} = \max_{n\in\{2,3\}} (-20\log|S^D_{n1}| - 3) \quad \text{[dB]} \quad (7.14)$$

Worst-case estimates of these parameters are then obtained by yield analysis from which the results are shown in Tab. 7.4. It is seen that only 11° phase unbalance between the two dipoles is to be expected in contrast to 30° when used in a single-ended fashion. A discussion of why the phase-error improved this much can be found in App. F.2 for the interested reader.

7.2.6 A Discussion of Loss Caused by the Imperfections

Two losses should be taken into account, which can be derived from the 70 Ω differential simulation results; the excess insertion loss, and the polarization loss. The max. excess insertion loss can simply be used in the link budget as-is, by

Table 7.4: According to yield analysis, it is 95% certain that the circuit will perform within these specifications, when connected to the antenna elements (70 Ω differential loads). These specification therefore serves as worst-case.

	UHF		VHF	
	Center 437 MHz	Out-of-band 432–442 MHz	Center 146 MHz	Out-of-band 141–151 MHz
Max. Amplitude Unbalance	0.7 dB	1 dB	0.5 dB	1 dB
Max. Phase Unbalance	11°	11°	11°	11°
Max. Excess Insertion Loss	1 dB	1 dB	0.6 dB	1 dB

including it as a passive loss in between the spacecraft tranceiver and the antenna gain. The other imperfections give rise to an additional polarization loss that should be computed.

Axial Ratio

According to [42, 43]; four sources are identified that cause degradation of axial-ratio for near-circular polarized antennas. Two of them are the *phase-error* (or unbalance) ϕ_e and *amplitude error* (or unbalance) A_e as simulated above. In addition, there is the *orthogonality error* β_e. The orthogonality error is the physical misalignment of the two crossed dipoles. I.e. if the two dipoles are perfectly perpendicular, then $\beta_e = 0°$. The holes in the PCB that are used to fasten the measuring tape are made by a milling-machine with sub-millimetre accuracy to exactly fit the M2-screws that is used. This is therefore not a source of orthogonality error. There is, however, a slight human factor involved in making the holes in the *measuring tape*. Experience suggests that this can be done with good accuracy. Anyhow; 5° of orthogonality error is taken into account in the computation of the axial ratio because of this human factor. The last source of error is the *polarization error* γ_e, which is an error due to the fact that the two crossed linear polarized antennas are not perfectly linear polarized but rather elliptical polarized with a very high axial ratio. The two linear polarized antennas are in this case the two dipoles and is expected to have such a high axial ratio that the polarization error can be neglected. Then, the axial ratio AR_r of the antenna is given by [42, 43] as:

$$\mathrm{AR}_r = \sqrt{A_e^2 + 0.0225(\phi_e + \beta_e)^2} \quad \text{[dB]} \quad (7.15)$$

where AR_r and A_e is given in dB and ϕ_e and β_e in degrees. Fig. 7.5 illustrates this relation. For the worst-case values found in the simulations, AR is found to be 2.6 dB. Moreover, it is seen from the formula that it is of little use to have a feeding network with excellent phase unbalance unless the antenna elements cannot be excellently aligned.

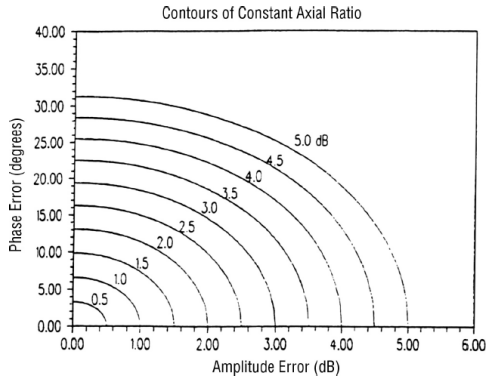

Figure 7.5: Contours of Constant Axial Ratio. The "Phase Error" axis actually includes *both* the phase error and the orthogonality error. Courtesy of [42].

Polarization Loss

Consider now that NUTS is at zenith such that the antenna is perfectly pointing towards the ground station. Ideally, there should be no polarization loss. Taking into account the *non*-ideal axial ratio, the following formula from [29] can then be used to compute the PLF:

$$\mathrm{PLF} = \frac{(1+\mathrm{AR}_w^2)(1+\mathrm{AR}_r^2) + 4\mathrm{AR}_w\mathrm{AR}_r + (1-\mathrm{AR}_w^2)(1-\mathrm{AR}_r^2)\cos(2\tau)}{2(1+\mathrm{AR}_w^2)(1+\mathrm{AR}_r^2)} \quad [\,] \tag{7.16}$$

where AR_r is the axial ratio of the receiving antenna and AR_w is the axial ratio of the incoming wave, both in *linear* scale. τ is the tilt angle between the two polarization ellipses. One can not keep track of the tilt of the near-circular ellipses and take it into account in the link budget. Therefore it is simply assumed to be the worst case; $\tau = 90°$. The formula is graphically illustrated in Fig. 7.6.

Moreover, the spacecraft antenna is taken as the receiving antenna, and the axial ratio of the ground station antenna is taken as a the axial ratio of the incoming wave. Strictly speaking, the wave may change its polarization from the transmitter on its way to the receiver, but the difference between the transmitted and and the incident wave is negligible in *circular* polarized waves for space communications systems (in the case of linear polarization one would have to take into account the Faraday rotation, c.f. Sec. 2.3.3). The polarization loss for various axial ratios on the ground station is listed in Tab. 7.5.

Unfortunately, the axial ratio for the ground station seems not to be documented. Several antennas has been considered for the ground station. At the time of writing, crossed yagi antennas are used, although an 8-turn helix antenna is designed in [12]. According to [26, 20] the axial ratio of an N-turn helix can be approximated by:

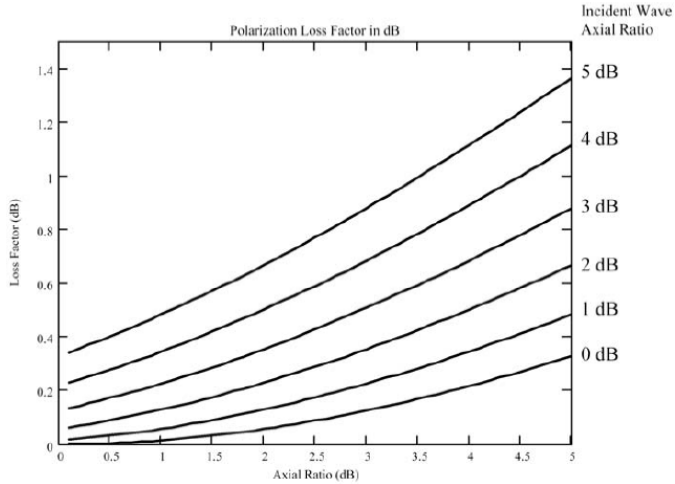

Figure 7.6: Polarization loss for various axial ratios of incident wave and receiving antenna. Courtesy of [29].

Table 7.5: Worst-case PLF due to non-ideal circularity when ground station and spacecraft antennas are aligned such that it should ideally be zero. The axial ratio of the spacecraft is taken to be 2.6 dB.

Assumed AR at ground station	0 dB	1 dB	2 dB	3 dB
Resulting PLF	0.09 dB	0.18 dB	0.30 dB	0.44 dB

$$\mathrm{AR} = \frac{2N+1}{2N} \qquad [\,] \quad (7.17)$$

which yields an approximation of 0.5 dB for the 8-turn helix antenna. At least, it should be below 1 dB, resulting in PLF = 0.18 dB. For the crossed yagi antennas, it is reasonable to assume that they are better than the crossed dipole on-board the satellite since its phase and amplitude can be more accurately controlled by feeding it with accurate length arrangements of coaxial cable. Therefore 3 dB could be used as a worst-case estimate for the axial ratio of the ground stations crossed yagis. Nevertheless, the polarization losses it causes is below 0.5 dB.

As discussed in Sec. 3.3, the satellite is rarely close to zenith, in which case the viewing angle has a much stronger impact of the axial ratio than the unbalance in the feeding network. The losses caused by the unbalances will thereby decrease for decreasing elevation angle. The high axial ratio for low elevation angles and the losses it causes, is already present in the link analysis by using the *circular* gain as presented in Sec. 3.3.1. As a means to take into account the additional polarization losses that occur for high elevation angles due to the unbalances, the *excess* polarization loss is introduced[2]. By subtracting 0.5 dB of *excess* polarization loss from the link margin, the additional losses that can occur in the link budget due to the unbalances in the feeding network is accounted for.

7.2.7 Yield Optimization

Yield optimization (also known as design centering) is, as the name suggests, to optimize the percentage of successful circuits (or in our case the probability of success). This is achieved by shifting component values *off* their ideal values. Fig. 7.7 illustrates why this can possibly optimize the yield. The nominal component values in a circuit is usually calculated such that they result in the ideal, intended performance (solid horizontal line). But the true component value may actually be anywhere within the shaded area. For this particular illustration, the performance is more sensitive to a decrease in component value than to an increase, it is beneficial to shift the nominal component value up such that as many realizations of the true component value as possible will be within the goal. This is illustrated in Fig. 7.7(b).

ADS has a built in yield optimization tool that can do this automatically. In the first iteration a normal yield analysis is run, and ADS estimates the yield as a function of component value for each of the components. Subsequently, ADS shifts the values to optimize the yield, and iterate until convergence.

Since it would be beneficial if the feeding network could be less sensitive to component deviations, such an optimization was attempted for the feeding network. Unfortunately, the optimal component value remained the same as their ideal value. The author believes the reason for this is that the phase is critical, and that changing a components values immediately shifts the phase. It is more

[2]This is not a standard concept, as far as the author knows.

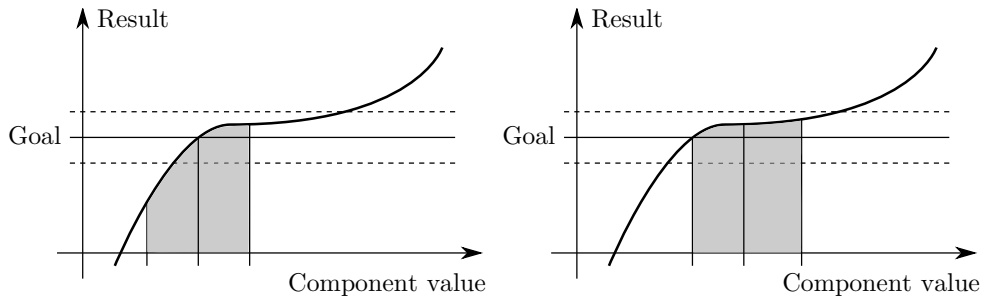

(a) Before yield optimization (b) After yield optimization

Figure 7.7: Sensitivity of component value deviations.

likely that it would have worked if there were only constraints w.r.t. magnitude of the S-parameters, for instance a filter.

7.2.8 Conclusion of Statistical Simulations

One of the most important questions throughout this chapter is; “Is it even likely that the circuit will work?”. And from the discussion in Sec. 7.2.6 it was found that the losses due to a the imperfections in the circuit are low. The conclusion is therefore; yes the circuit will work, and the losses are known. It is important, however, that high-quality components are used.

8 Feeding Network Experiment

8.1 Production

The circuits were produced on FR4 PCBs of thickness 0.8 mm and a relative permittivity of 4.8. The components and SMA-connectors were soldered[1]. One of the produced PCBs is depicted in Fig. 8.1.

8.1.1 TRL Calibration Kit

A *Through-Reflect-Line* (TRL) calibration kit was made to calibrate the network analyzer. Before calibration, it must be assumed to be an error in the measurements, for instance due to the length of the cables. This is illustrated in Fig. 8.2. In order to remedy the errors, the *Device Under Test* (DUT) is replaced by three known standards, and the network analyser de-embed the error-boxes such that measurements are performed *on* the device [15]. The first standard, "through", is made as a short circuit, with the two reference planes for ports 1 and 2 coinciding. The second standard, "reflect", is made with a large reflection at the reference planes. The TRL technique does not require the reflection to be a perfect open circuit. That is an advantage, since there will likely be fringing fields at the end of the microstrip line, making it capacitive.

Further on, the TRL calibration technique assumes that the "line" standard is in between 0° and 180°. In practice, Agilent recommends that it is in between 20° and 160° [44]. The "line" in this experiment is therefore chosen to be 136 mm, which is 90° for the frequency in the middle of 146 MHz and 437 MHZ. Tab. 8.1 shows the length of the line degree. This yields a bandwidth from approximately 70 to 520 MHz where the line is in between 20° and 160°.

Notice that by making a separate TRL kit, the reference plane for the measurements are *on* the microstrip lines where the antennas is to be fed, on the disconti-

[1] It should be noted that due to a mistake in the delivery, the three 100 nH inductors in the VHF-design was not shipped. Instead, series of two inductors had to be used in its place.

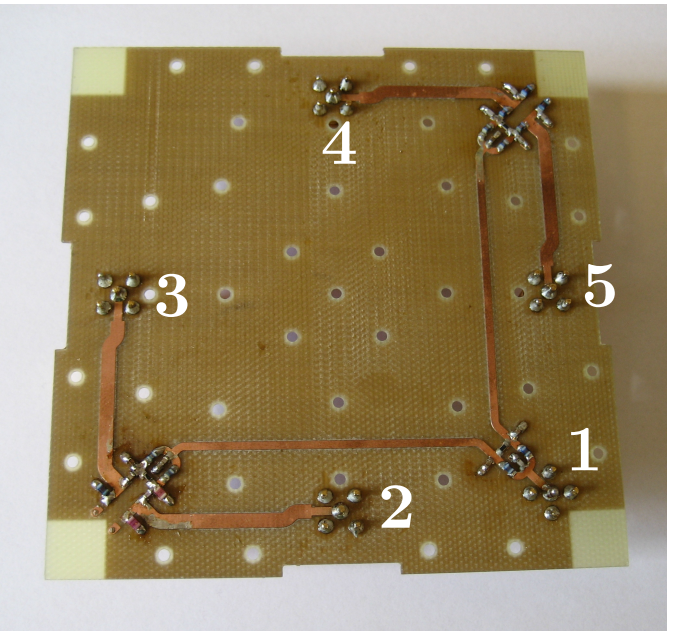

Figure 8.1: The UHF feeding network. The ports are labelled.

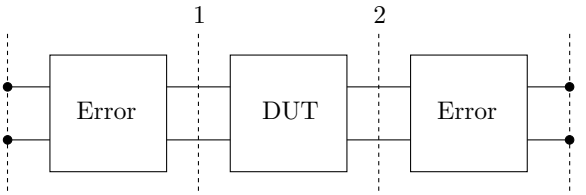

Figure 8.2: Calibration technique: The measurements are to be performed on the reference planes, but error boxes are in between the intended reference planes and the instrument. Various known DUTs are replaced to de-embed the error-boxes

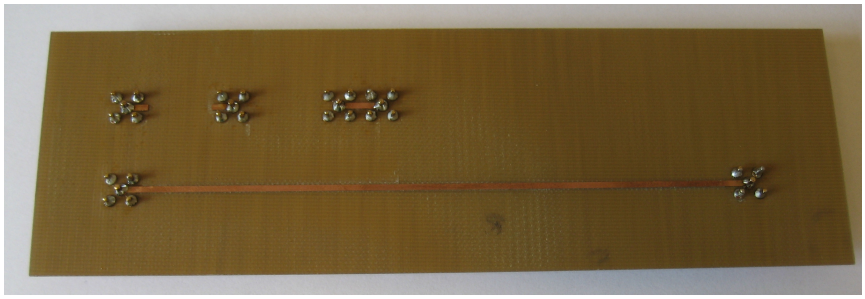

(a) Top side. Note that the reference plane is defined where the microstrip lines stop at the "reflection" standard, or in middle between the "through" standard. The same reference plane is used for the "line" and for feeding network.

(b) Bottom side.

Figure 8.3: TRL calibration kit specially built for the feeding network.

Table 8.1: Electrical length (obtained from ADS) of "line" in TRL kit

Frequency	70 MHz	146 MHz	291 MHz	437 MHz	520 MHz
Length	22°	45°	90°	135°	160°

nuity in Fig. 6.8. Since the TRL technique can de-embed any passive network, the SMA connectors at the output are de-embedded.

8.2 What to Expect

One might be tempted to think that the statistical simulations in ADS are an absolute fact, but it is important to realize that there are certain non-ideal characteristics not accounted for in ADS model. The ADS simulations was intended to answer how the tolerance of the components affect the performance (and it did) but there are some other facts to take into account as well.

The loss in the microstrip lines and in the components (especially the inductors) are note taken into account in the model. This will enforce a downwards shift in

the S_{n1}-parameters and thus increase the maximum excess insertion loss beyond what is predicted in the simulations. This loss might also make the isolation better.

The fact that the losses in the inductors and capacitors can be modelled as a series resistor might cause a slight shift in the phase of the output, although it is assumed not to be critical. It might also cause the circuit to become more or less narrowband.

In Fig. 6.6 it is seen that the circuit in between the microstrip lines are considered to be lumped, i.e. of zero physical size. Of course this is not quite true, and the size of the circuit is big enough to expect some phase shift through it. Because of the high degree of symmetry in the PCB, however, this phase-shift will be the same in all ports, and thereby not degrade the performance of the circuit.

Lastly, it is possible that the three inductors on the VHF PCB that was replaced by a series of slightly different inductance also slightly affects both phase and magnitude of all the S-parameters.

None of the factors discussed herein is expected to be prone to large statistical variability such as the phase. It can therefore be taken into account simply increasing the excess insertion loss.

8.3 Method

The following network analyser was used for the measurements:

- Agilent Technologies E8364B, S/N: MY43040217

The network analyser was calibrated with the above mentioned TRL kit. The full 5×5 S-matrix for the device was measured for a span of 10 MHz about the center frequency, by connecting the analyser to every pair of ports of the feeding network while terminating the other ports by $50\,\Omega$ loads. The results was stored to `.s2p`-files for further analysis. The files was then imported to MATLAB by the function `import_s2p()` which is enclosed in App. D and plots were made by the script `plot_s_params.m` (also in appendix). The script utilizes the MATLAB toolbox *RF Utilities V1.2* by Neill Tucker, available at the MATLAB Central[2].

8.4 Results for VHF

The measurement results for the VHF network are plotted in Fig. 8.4.

8.5 Discussion of the VHF Results

To start with the obvious, it is easy to see that the matching and the isolation are in accordance with the predicted results from Tab. 7.3. In fact, S_{11} is at an amazing -28 dB at the center frequency. As for the transmission S-parameters

[2]More precisely, RF Utilities V1.2 can be found at: `http://www.mathworks.com/matlabcentral/fileexchange/22996-rf-utilities-v1-2`.

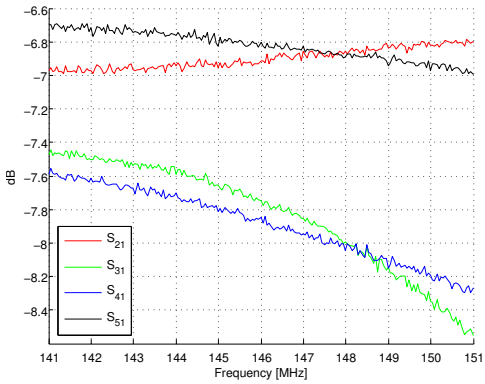

(a) S_{n1}-parameters in dB

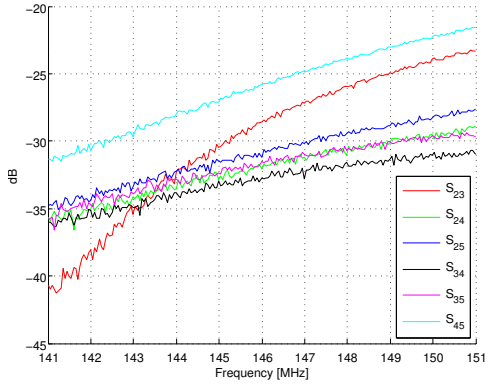

(b) Isolation

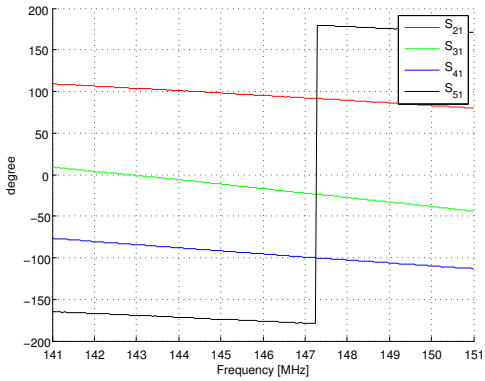

(c) S_{n1}-parameters' phase

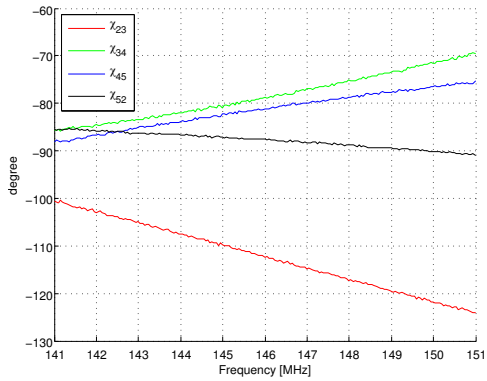

(d) ϕ_{ij}

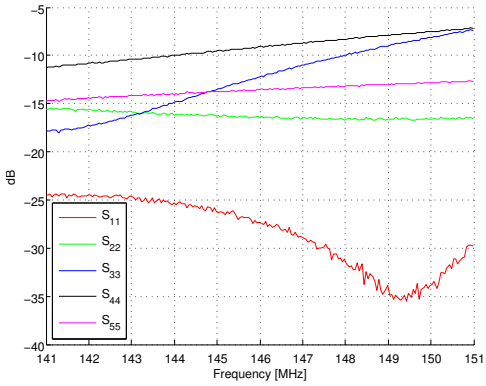

(e) Match

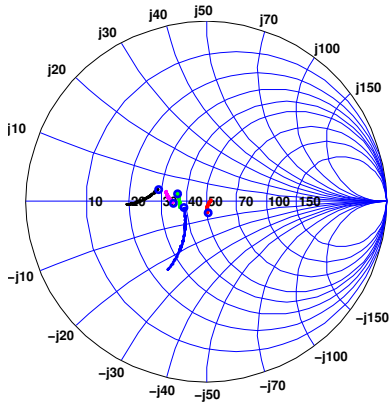

(f) Match (in Smith chart). The ports 1 to 5 are red, green, blue, black and magenta (in that order). The circle is at the lowest frequency.

Figure 8.4: Measurement results for VHF

S_{n1}, the excess insertion loss is seen to be less than 2 dB at the center frequency but not less than 1 dB as predicted. It seems like 2 dB excess insertion loss should be expected as worst case rather than 1 dB.

Moreover, it is clear that the phase has shifted a lot contrary to that predicted in (7.7). This was expected, due to the physical size of the lumped circuitry, but is unimportant since what matters is the phase-differences ϕ_{ij}. The phase-differences ϕ_{34}, ϕ_{45} and ϕ_{52} seems to be very well within the predicted values, which suggest that the simulations are pessimistic enough. ϕ_{23} is within the predicted values up till about 148 MHz. It is of course possible that this very circuit belongs to the last 5th percentile which does not perform as well as the rest. It is, however, more reasonable to believe that this slightly higher phase-error is due to the improvised series-connected inductors.

8.6 Conclusion for the VHF Measurements

The conclusion is that the VHF circuit *do* work like intended, although with higher insertion loss than expected. Most of the losses in the link budget that are due to the feeding network is because of the insertion loss, and not because of the axial ratio. Moreover, it seems like most of the losses are due to non-ideal behaviour in the lumped components rather than the loss in the microstrip lines, since high S_{n1} are achieved in the lower end of the span. It also seems like the circuit has been accidentally centered for a lower frequency than intended, also due to non-ideal component values. Since quite accurate components was bought, it is not expected to be able to improve upon this by buying better components (unless components are measured and hand picked). It is, however, easier and less time-demanding to regain a decibel somewhere else in the link budget, i.e. by buying an *Low Noise Amplifier* (LNA) to the ground station or by implementing error-correction. In order not to delay the NUTS project, it is recommended to accept the somewhat high excess insertion loss.

8.6.1 A Review of ICs

Due to the slightly high excess insertion loss, one might wonder if it would have been better to use ICs anyway. As no 4-way power splitter was found as an IC, one would necessarily have two stages of ICs to build the circuit, and possibly a third stage of lumped matching network. The average excess insertion loss of the ICs seen in Tab. 5.2, is about 1 dB. For two stages of ICs that is 2 dB maximum, and possibly more in practice. It is therefore likely to believe that using ICs is not a better alternative in terms of excess insertion loss.

The maximum phase unbalance of the ICs is in average at about 7°. Therefore, two in cascade yields 14° which is worse then the 11° of the realized feeding network. The maximum amplitude unbalance averages to 1.4 dB per IC. It is apparent that the performance of the lumped network *is* better than that of the IC solutions also in this respect.

8.7 Discussion of the UHF Troubleshooting

The UHF feeding network was also built, but unfortunately it did not work like intended. The S_{n1}-parameters was as low as almost $-12\,\text{dB}$ at worst, and phase errors of up to 90° took place. Weeks was spent trying to resolve this malfunction, but without success. Therefore, since a working circuit cannot be presented in this report, some of the troubleshooting of it will be.

Both ports 3 and 4 had the mistake where S_{n1} was below $-10\,\text{dB}$ and with large phase-errors. On the other hand, both ports 2 and 5 had S_{n1} parameters above $-8\,\text{dB}$ and a reasonable phase. Both ports 3 and 4 are on different branches of the first stage WPS in the design. Since both ports 2 and 5 worked like intended, it was reasonable to believe that all of the WPSs worked like intended.

First, all vias and solderings was checked to unreveal bad connections and short circuits. It was also attempted to replace the components that comprise the phase-shifters for ports 3 and 4 with new ones, but without success. The author had suspicion that the components had been mistakenly labelled at the store. It was therefore attempted to get completely new components, but also that was without success.

Further on, the error appeared on the two outputs furthest away from the input, which makes the error mirrored about the symmetry axis of the circuit (see Fig. 8.1). In order to verify that it was not something wrong with the layout of the PCB, it was therefore attempted to swap the phase-shifters at ports 2 and 3. The behaviour of the ports swapped accordingly. Port 2 got the error that had previously been at port 3 while port 3 was operating the way port 2 previously did. This indicated that it was not something wrong the the PCB layout, but rather the components.

It was also attempted to remove excess lead to reduce parasitic capacitances (but without notable changes) and it was verified that the isolation between the output ports were good. It was concluded to be even more unlikely that the WPSs was malfunctioning since port 2 worked like intended, and port 3 worked like port 2 should when the phase-shifters were swapped. In other words; both outputs of the same WPS had been tested. The WPSs was therefore not replaced.

Many has been consulted w.r.t. this malfunction, but no reason for the error was determined. It can, however, be concluded that the error follows the phase-shifters of lag $\pm 135°$. The DC-grounding inductor is not believed to be related to the error since ports 4 and 5 are the ones with DC-grounding inductor and port 5 functioned like intended.

It has, of course, several times been checked that the components used on the PCB have the same values as that in the ADS design used to verify the calculations of the component values. Unfortunately, time did not permit for more troubleshooting.

8.7.1 Future Troubleshooting

More troubleshooting should be performed on the UHF feeding network in the future to make it work. The author has little doubt that it should be possible to

repair it. Since the VHF PCB operated like intended, the concept is proved.

Since the phase-shifters have already been tested in several different ways, one might want to verify the function of the WPSs. Although the WPSs seemed to work for two of the ports, it might be of interest to test them further, in case there is an error with them which manifests itself stronger when connected to an $\pm 135°$ phase-shifter. This might be done by removing all the components of the phase-shifters, and bridging the footprints needed such that outputs of the splitters are lead to the SMA connectors.

In fact, it might be a good idea to start with a clean PCB, and only add the first stage splitter, and then measure it. Footprints must be bridged/short circuited so that the outputs are lead to SMA connectors. The bridges might not be ideal, but since they are short compared to the wavelength, it is expected to work more or less. Once the functioning of the first WPS has been verified, it is known that an error on one of its outputs cannot propagate to the other, due to the isolation. Thence, the second stage WPSs can be added and verified in a similar manner. Once they are verified as well, the phase-shifters should be added.

The author guess that by this time, the error has been resolved. If that is *not* the case, a problem might be parasitic capacitances on the components that become significant somewhere between the VHF and UHF frequency. The components chosen are high-quality components, and ADS models of them that includes parasitic effects are downloadable from Johanson's webpage. From the mentioned troubleshooting, it should by now be known which part of the feeding network is problematic. Is it, for instance, the $\pm 135°$ phase-shifters? Whichever the part it is, an ADS model of that part should be made with the models downloaded from Johanson. If this model successfully predicts the error, then the parasitic effects are probably what caused them. If so, the component values for the respective part(s) may now be manually tuned such that matching and correct phase-shift is achieved for the faulty sub-circuit. A test PCB with only this part could be made to verify the simulations. In fact, test PCB's could be made for several sub-circuits, if necessary. By following these steps, the error should be eliminated.

9 Antenna Simulations

From CST simulations in [4], which is also briefly presented in Sec. 3.3, it was shown that (flat) turnstile antennas yields the highest link margin for *all* elevation angles. It was therefore decided to use flat turnstile antennas (crossed dipoles) for both UHF and VHF.

Further simulations in [4] were executed where *both* antennas was mounted on a metal box[1], whence it followed that the VHF antenna remained practically identical to the ideal result. For the UHF antenna, however, there were some distortions in the pattern. Since these distortions will occur if a single dipole is used as well, it is concluded that the turnstile antenna, despite the pattern distortions, remains the best suited antenna of those considered.

At the time the simulations in [4] was performed, it was not yet known exactly how the antennas were to be mounted on the satellite, and the model was therefore inaccurate. For instance, it was not at the time known that the elements would be fastened in between two PCBs, and it was not known that the feed gap would be 6 cm (see Fig. 4.7). It is expected that these facts will slightly change the resonance frequency of the antennas. Moreover, the dipoles that constitutes the turnstiles were shortened to achieve a $50\,\Omega$ match in [4]. Since a slight mismatched occured in the [4] due to not using $70\,\Omega$ ports, the feeding network has now been designed $70\,\Omega$ feeding networks.

A new model, depicted in Fig. 9.1, has now been made in CST, as a refinement of the previous one. The lengths of the dipoles has also been re-optimized (to the closest millimetre) such that the match is as good as possible for the intended center frequencies (meaning that the reflection coefficient is as low as possible).

[1] It should be noted that the satellite frame will likely be made of a composite material. Nevertheless it can very well be approximated as a metal box, since all the sides will be covered by a PCB with either solar panels or feeding networks. The gaps in between the PCBs will be very small compared to the wavelengths.

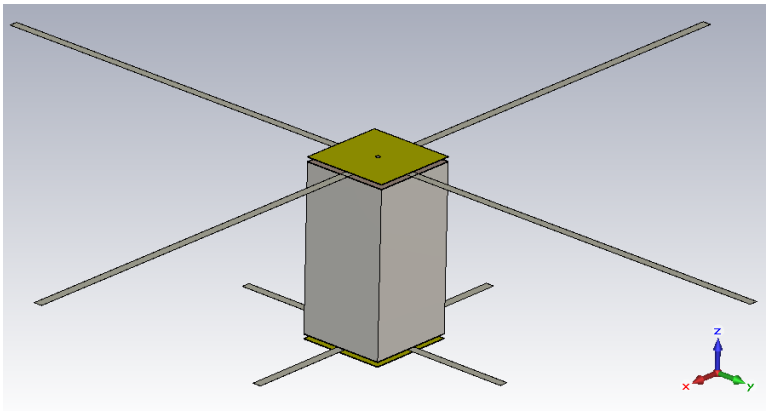

Figure 9.1: Refined CST model of the turnstile antennas mounted on NUTS. The Z-axis is taken towards zenith. From CST.

9.1 Patterns

The total and partial directivities will be plotted in selected plane cuts in this chapter. It should be noted, that the radiation efficiencies e_{cd} was simulated to be 100% for VHF and 99% for UHF, meaning that the directivities are practically equal to the gains. The reflection efficiency e_r will be treated later. Also, the Z-axis is taken to be towards zenith in this chapter.

The 3D patterns for both UHF and VHF are depicted in Fig. 9.2, whereas 2D patterns in different plane cuts are shown in Fig. 9.4 and Fig. 9.3. Fig. 9.4 shows the plane containing nadir and the Y-aligned dipoles (the YZ-plane), whereas Fig. 9.3 shows the horizontal plane cut (the XY-plane). It is of no use to plot *both* the YZ and XZ-planes since they will be equal due to symmetry.

Since it is linear polarization in the horizontal plane, there is a 3 dB polarization loss, whereas the polarization loss is varying within the YZ-plane. Therefore, the circular directivity for this plane is plotted in Fig. 9.5.

Since the the VHF patterns are visually indistinguishable from the theoretical case, no plots for ideal turnstile antennas are included. A slight difference in the maximum gain can be mentioned; whereas it theoretically is 2.2 dBi [4] it has increased to 2.5 dBi for the VHF turnstile antenna. It is clearly not visible by sight.

9.1.1 Discussion

Albeit the VHF pattern is undistinguishable from the ideal case, there is clearly distortions in the UHF pattern. The distortions is such, however, that the UHF antenna is *more* directive towards the Earth. Especially if the circular directivity is considered, which is only an advantage. For some viewing angles, however, there may still be less gain than for the VHF antenna. Take for instance the direction $\phi = 45°$ during a time when the satellite has a low elevation angle, and thus θ is

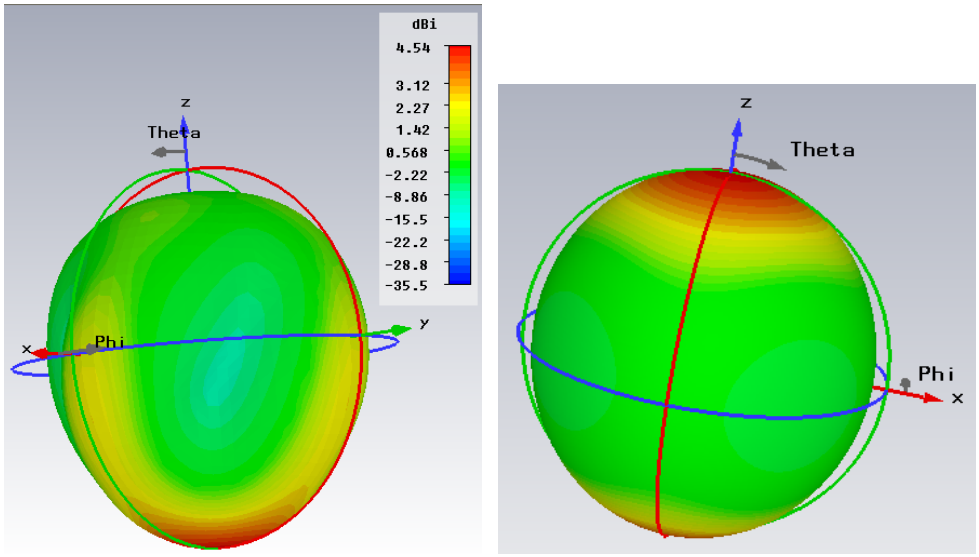

(a) UHF (b) VHF

Figure 9.2: 3D directivities for the two antennas. Simulations from CST.

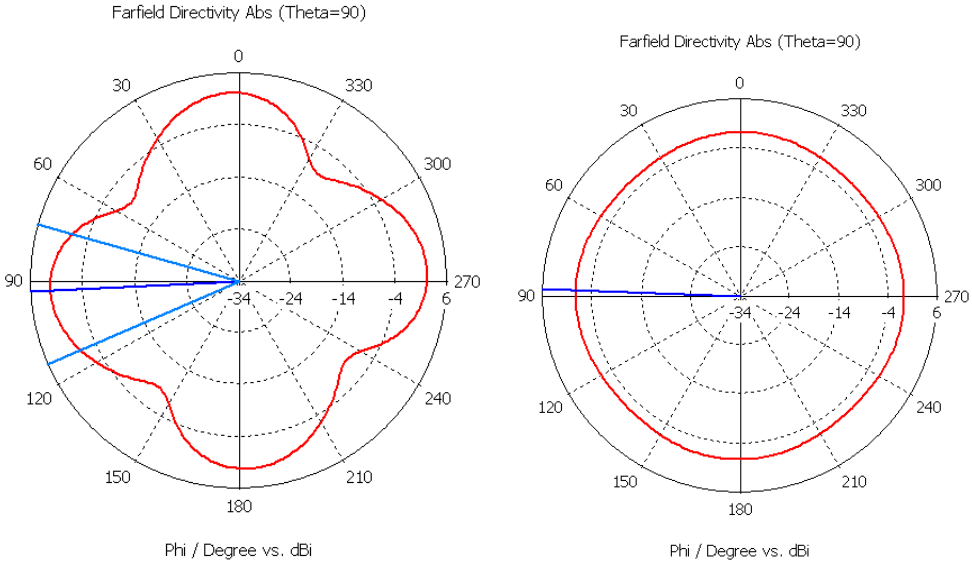

(a) UHF (b) VHF. No more than 1.1 dB variation.

Figure 9.3: Directivities in the (horizontal) XY-plane. The antennas are linear polarized in this plane. Simulations from CST.

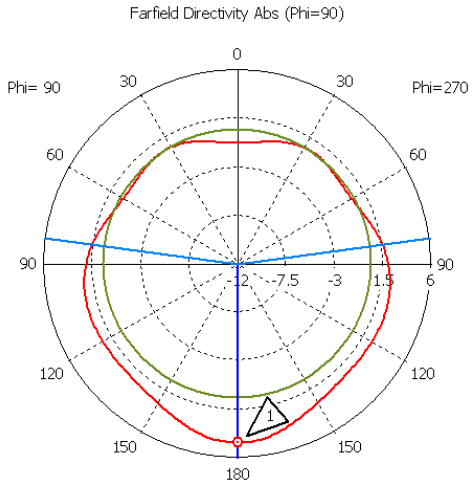

(a) UHF. 1: 4.5 dBi

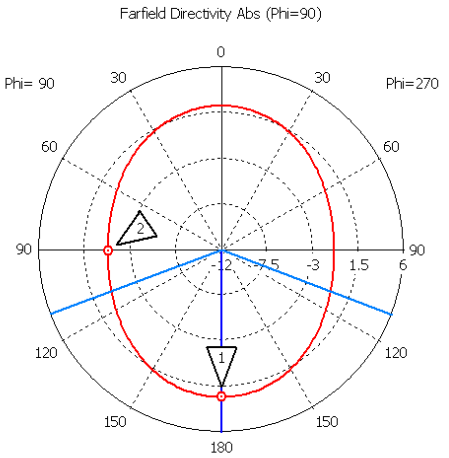

(b) VHF. 1: 2.5 dBi, 2: −0.9 dBi

Figure 9.4: Directivities in the YZ-planes. Nadir is at $\theta = 180°$. Simulations from CST.

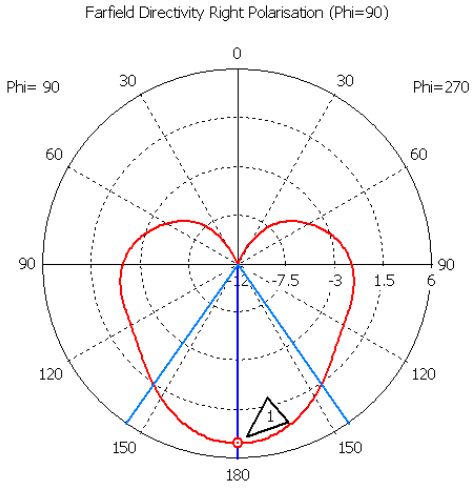

(a) UHF. 1: 4.5 dBiC

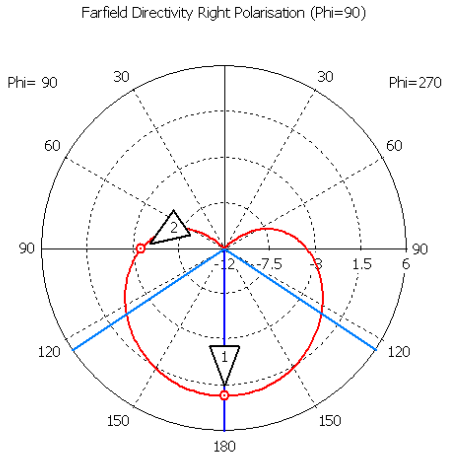

(b) VHF. 1: 2.5 dBiC, 2: −3.9 dBiC

Figure 9.5: RHCP partial directivities in the YZ-plane. I.e. the directivity minus the polarization loss. Nadir is at $\theta = 90°$. Simulations from CST.

approaching 90°[2]. In that direction the gain (or partial gain) will become lower for UHF than for VHF, as can be seen from Fig. 9.3. This does not mean, however, that another antenna should have been chosen. In the case a dipole had been chosen, the pattern would exhibit a zero rather than a minima in the horizontal plane. The pattern distortions also corresponds well with what was discovered in [4], at which time it was decided to use the turnstile antennas.

As for the radiation efficiencies, they are expected to be about 100%. One might think that the 99% radiation efficiency for the UHF is due to numerical errors. It is also not impossible that it is lost in the FR4 substrate which is included in the simulations. In that case, it is reasonable that it is very little, since only a very small part of the antenna is on the PCB. It is also reasonable that it is less efficient for the UHF than for the VHF.

9.1.2 Conclusion

The conclusion is that the antennas, despite the distortions in the UHF pattern, serves the purpose of being the best suited antennas of those considered, in terms of providing the ground station with the highest possible received signal strength. the turnstile antenna is still the most suited for its task, since it has no zeros in its (total) pattern, contrary to most other antennas. Besides, this was already known from [4].

9.2 Patterns for Comparison

Patterns of the VHF turnstile antenna has been measured and is presented in Ch. 10. However, the experiment only makes use of a linear polarized source antenna, meaning that the patterns shown in Fig. 9.4 and Fig. 9.5 cannot be measured. The polarization of the source antenna in the experiment, is such that only one of the two dipoles constituting the turnstile is visible in the measurements (see Ch. 10). Moreover, that visible dipole is measured in the plane containing the **E**-vector (E-plane) and the direction towards nadir. In order to have something to compare those measurements with, a simulation is performed where only the X-aligned dipole is excited. Fig. 9.6 shows the E-plane pattern of the X-aligned dipole that also contains the nadir-direction (XZ-plane).

Finally, it is noted that the pattern when both dipoles are excited *can* be measured in the horizontal plane (Fig. 9.3) since the polarization in that plane is linear.

9.2.1 Discussion

It is seen that when only one VHF dipole is excited, the pattern is again undistinguishable from an ideal dipole. For the UHF antenna that is not so. In fact, the distortions become even more predominant when only one dipole is seen. The

[2] Actually, θ will never become *very* close to 90°, even for small elevation angles, as can be seen from (3.7).

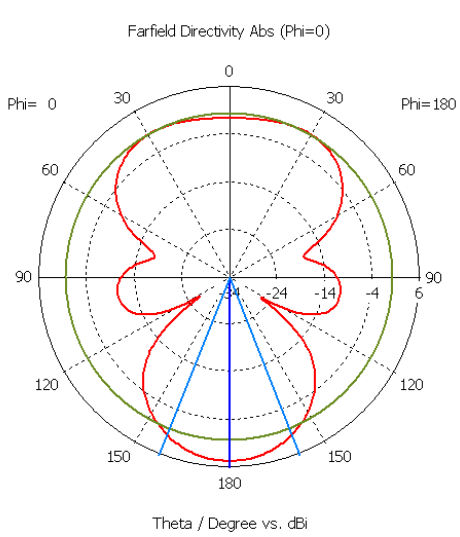

(a) UHF. Max: 4.5 dBi.

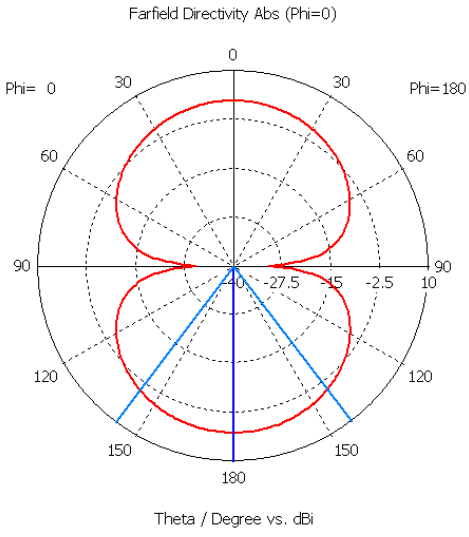

(b) VHF. Max: 2.5 dBi.

Figure 9.6: E-plane patterns when only one dipole is excited. Nadir is at $\theta = 180°$. Simulations from CST.

zeros seems to have shifted downwards. In addition, a new minima has appeared. Remember, however, that when two perpendicular dipoles are fed in quadrature, the zeros of the two dipoles will cancel each other out, and the pattern will become like seen in for instance Fig. 9.2. Therefore, no conclusions are made based upon these simulation results, they are only for comparison with measurement results. Conclusions regarding how they behave in the link budget must be made upon the RHCP patterns.

9.3 Matching

As for the simulations concerning impedance, a simplification was made by removing one dipole from each turnstile (Fig. 9.7). The reason why this is a valid simplification is as follows: Consider that the X-aligned dipole in Fig. 9.8 is excited by a current $I_X \neq 0$, and let the current that is induced in the Y-aligned dipole be called I_Y. Further on; let the whole antenna be rotated 180° around the X-axis, such that the current I_Y now points downwards. But this is the same as the original geometry, whence an upwards going current I_Y is induced. Thus, $I_Y = -I_Y$, enforcing $I_Y = 0$ as the only solution. Thus, there are no coupling.

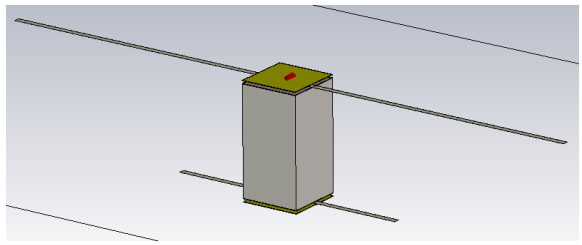

Figure 9.7: CST model with simplification fit for impedance considerations.

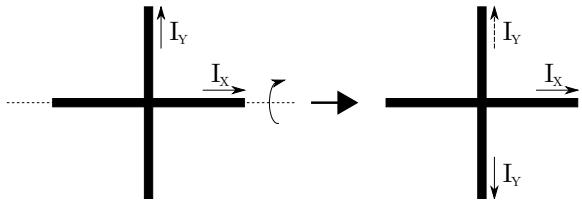

Figure 9.8: Symmetry argument makes two dipoles superfluous for impedance considerations.

With this simplification, it is possible to use only *one* port for each antenna in the CST simulations contrary to four for non-simplified model[3]. This makes it easier to consider the matching of the antenna, and it is almost a necessity when considering coupling.

Nonetheless, the UHF antennas terminal is for the rest of this chapter referred to as port 1, while port 2 goes for the VHF antenna. S_{11} and S_{22} then represents how well the antennas are matched, and is depicted in Fig. 9.9.

9.3.1 Discussion

The VHF antenna is very well matched, with S_{11} below $-14\,\text{dB}$ for approximately $7.2\,\text{MHz}$ around the center frequency (it is narrowband, but remember that the required bandwidth is only $25\,\text{kHz}$). By using (2.26) and (2.27) it is found that the mismatch loss within this band is only $0.2\,\text{dB}$ (the efficiency is $e_r = 0.96$). This is the reduction the mismatch causes in the link margin, which is considered quite acceptable.

As for the UHF antenna, the results are not very good as compared to the VHF. It seems like either the large feed gap, or the stacked PCBs in between which the antenna is mounted, or possibly both, has a negative effect on the matching of the antenna. The S_{11}-parameter only went down to $-7.6\,\text{dB}$ at the center (with an efficiency of $e_r = 0.80$). On the other hand, it has become much more broadband, with a $-7\,\text{dB}$ bandwidth of more than $40\,\text{MHz}$. That is not necessary for this application though. It can be seen from the smith chart that it would probably have been better matched if the outputs of the feeding network was made to be $50\,\Omega$ differentially rather than $70\,\Omega$, which is unfortunate. It should be mentioned, though, that this effect could not have been discovered until it was decided how to feed the antennas. Also, the design of the feeding network had already come far when it became known that there should be a cover on top of the feeding network. This actually illustrates how realistic problems may require several iterations to find the optimum solution.

Nevertheless, if the feeding network *was* optimized for $50\,\Omega$ it would still have a rather large mismatch due to the large inductance that can be seen in the smith chart. Shortening the elements might reduce the *reactive part* of the antenna impedance, but remember that the length of the antennas are already optimized to yield the lowest reflection.

Despite the fact that the UHF antenna was not very well matched, it does not cause more than $1\,\text{dB}$ mismatch loss (c.f. (2.27)), which is still small compared to many other terms in the link budget. A modest improvement in e_r might happen if the feeding networks second stage WPSs is redesigned for another differential output impedance, maybe around 40–$50\,\Omega$. The improvement this yields in the link margin, however, is only a fraction of a dB. Since changing the real part of the output impedance does not eliminate the inductance in the antenna, it cannot be expected to be as well matched as the VHF antenna, thus an improvement of

[3]The non-simplified model uses four ports on each turnstile antenna since two ports cannot intersect each other. Therefore there is a common node in the center to which each element is connected to by one port.

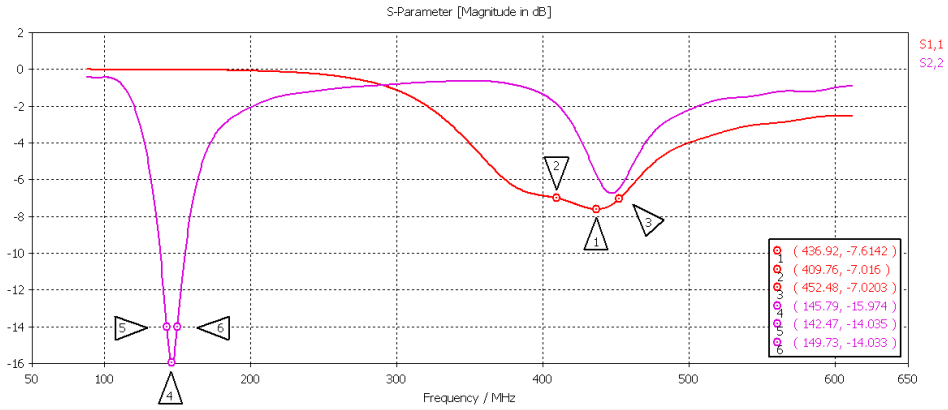

(a) Rectangular Plot in dB.

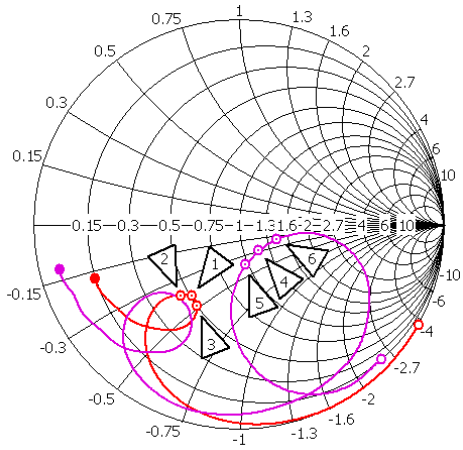

(b) Smith Chart with 70 Ω in the center.

Figure 9.9: Simulated matching of the antennas. S_{11} indicate the matching of UHF and S_{22} that of VHF. Markers 1 and 4 indicate the center frequencies while markers 2 and 3 indicate the -7 dB bandwidth at UHF and markers 5 and 6 indicate the -14 dB bandwidth for VHF.

Table 9.1: Physical dimensions of the dipoles that constitutes the turnstile antennas.

	UHF	VHF
Dipole length	409 mm	1040 mm
Gapsize	60 mm	
Width of tape	10 mm	
Thickness of tape	0.2 mm	

less than 0.8 dB will result. A remedy against the inductive part of the antenna impedance *might* be to put capacitors in series or shunt with the elements. However, this is expected to influence the phase of the outputs, and care must be taken not to destroy the mutual phase-difference between the output ports.

If such a modification is attempted, the influence these components has on the phase must be studied. It must be evaluated by the team if such an effort is worthwhile for an improvement of a fraction of a dB. The author suggests to accept the mismatch since there is a lot more to gain other places in the system, such as by implementing error-correction or buying an LNA for the ground station.

The easiest solution would probably be to remove the cover. If it is decided not to build a patch antenna on the nadir plane, there will be no modules outside the UHF antenna and the cover can be removed such that the microstrip lines are visible from the Earth.

9.3.2 Conclusion

The conclusion is therefore; the VHF is very well matched, whereas the UHF is matched to an acceptable level. An improvement in the link budget of a fraction of a dB might be feasible if the feeding network is redesigned, but it is probably not worth the effort.

9.4 Mutual Coupling

It is important that the two antennas can co-exist on-board the satellite. Since they are close to each other (less than a wavelength for either frequency), it is reasonable to expect that there will be some mutual coupling in between the two antennas. Simulations has therefore been performed to reveal how the coupling affects the performance of the antennas.

Consider first, that the UHF antenna is excited. Some of the power impinges upon the parasitic VHF antenna by inducing a current, and is then reflected according to a reflection coefficient $\Gamma_{\text{parasitic}}$. Some of the reflected power, is again re-radiated and impinges back upon the UHF antenna. This changes the voltage/current ratio on the UHF dipole which means that the input impedance of the antenna changes, and the UHF antenna may no longer be matched. It might be

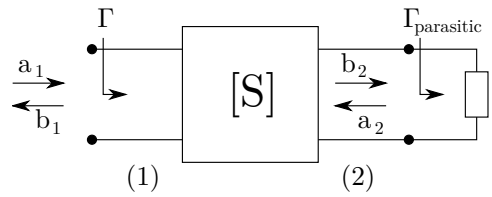

Figure 9.10: The coupling between the UHF antenna (1) and VHF antenna (2) can be considered through a 2-port microwave network consideration

tempting to state that $\Gamma_{\text{parasitic}} \approx 0$ since the VHF antenna must be matched, but remember that the VHF antenna is only matched for 146 MHz, not for 437 MHz.

Mutual coupling is often discussed in relation with arrays. Beware that there is distinct differences between mutual coupling in arrays and for the NUTS antennas. In arrays, all elements are to be used on the same frequency, implying that they are matched when they are used separately. However, since all of them are excited simultaneously (at the same frequency), currents are coupled from one element to the other, changing the voltage/current ratio and hence also the input impedance of the elements [26]. One typically says that if only one element is driven, the input impedance of the driven element will be approximately equal to what it would be in absence of the parasitic elements [26]. But in this case, $\Gamma_{\text{parasitic}} = 0$.

Since the two dipoles in the simulation is *not* matched to the same frequency, one cannot assume $\Gamma_{\text{parasitic}} = 0$. An advantage, however, is that only one element is driven (for the considered frequency). One can therefore consider the problem as a 2-port microwave network, as depicted in Fig. 9.10, where port 1 is excited by a wave a_1. There is no source on port 2, only a passive (unknown) load with reflection coefficient $\Gamma_{\text{parasitic}}$. Thus:

$$a_2 = \Gamma_{\text{parasitic}} b_2 \qquad \left[\sqrt{\text{W}}\right] \quad (9.1)$$

Moreover, the reflection seen at the input of the UHF antenna can be written:

$$\begin{aligned}
\Gamma = \frac{b_1}{a_1} &= \frac{S_{11}a_1 + S_{12}a_2}{a_1} \\
&= \frac{S_{11}a_1 + S_{12}\Gamma_{\text{parasitic}}b_2}{a_1} \\
&= \frac{S_{11}a_1 + S_{12}S_{21}\Gamma_{\text{parasitic}}a_1}{a_1} \\
&\overset{\text{reciprocity}}{\downarrow} \\
&= S_{11} + S_{12}^2\Gamma_{\text{parasitic}} \qquad [\,] \quad (9.2)
\end{aligned}$$

where the definitions of S-parameters has been used.

The term S_{11} represents the reflection due to the mismatch of the UHF antenna itself, as shown in Fig. 9.9. From the second term it is now seen that the UHF

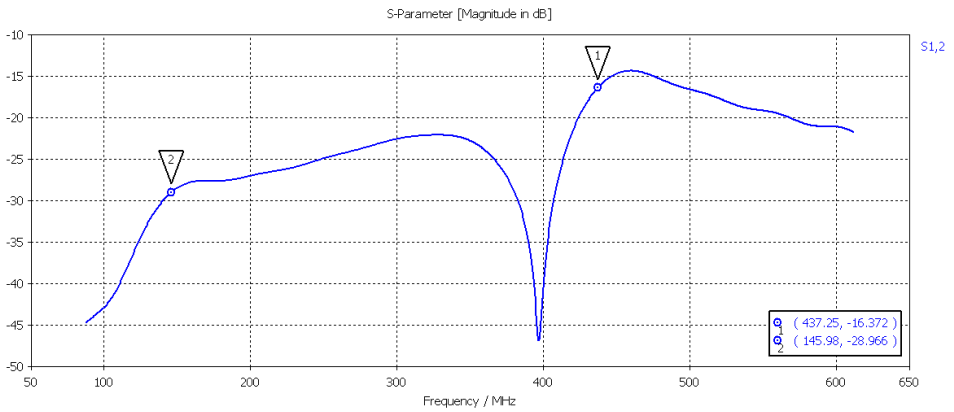

Figure 9.11: Simulated coupling between the two antennas.

antenna may, in fact, be even worse matched than what is predicted by Fig. 9.9. It is therefore of interest to determine the maximum degradation in match due to the coupling. Taking the magnitude of the above expression yields:

$$|\Gamma| = |S_{11} + S_{12}^2 \Gamma_{\text{parasitic}}| \leq |S_{11}| + |S_{12}|^2 \cdot |\Gamma_{\text{parasitic}}| \qquad [\,] \quad (9.3)$$

where the second term represents the maximum change in the match due to the coupling. As mentioned, $\Gamma_{\text{parasitic}}$ is unknown, but it is known to be passive. Hence; $|\Gamma_{\text{parasitic}}| \leq 1$. Therefore, the maximum change in the match (in linear scale) is given by:

$$\Delta|\Gamma| \triangleq |S_{12}|^2 \qquad [\,] \quad (9.4)$$

Although this equation was derived when the UHF antenna was driven and the VHF antenna was parasitic, the same equation would result if the roles of the antennas were interchanged. Hence, this equation can be used to determine the change in the reflection coefficient seen at the input of both antennas. S_{12} must be taken at the frequency of the driven antenna.

Simulations of S_{12} is presented in Fig. 9.11 shows that:

$$|S_{12}| = \begin{cases} -16\,\text{dB} & \text{, UHF} \\ -29\,\text{dB} & \text{, VHF} \end{cases} \qquad (9.5)$$

The maximum (linear) change in reflection coefficient for the two antennas therefore becomes:

$$\Delta|\Gamma| = \begin{cases} 25 \cdot 10^{-3} & \text{, UHF} \\ 1.3 \cdot 10^{-3} & \text{, VHF} \end{cases} \qquad (9.6)$$

9.4.1 Conclusion

Clearly, the change in reflection coefficient, and therefore input impedances, is negligibly low. The proximity of the antennas has no negative effect on the matching of the antennas.

It is already observed that the VHF antenna distorts the pattern of the UHF antenna, and one might imagine that the parasitic reflection coefficient may affect the distortions. However, since the power intercepted by the parasitic antenna in the first place is so low (at least 16 dB lower than that of the driven antenna), variability $\Gamma_{\text{parasitic}}$ is not expected to influence the pattern notably.

The conclusion is therefore that the antennas will co-exist well on-board the satellite.

10 Antenna Experiment

A part of the thesis is to perform antenna measurements on a mock-up of the satellite to verify that it works like intended. A test range for antennas in the VHF and UHF range was not readily available at NTNU, and it was therefore necessary to design and rig up the measurement site as a part of this thesis. This chapter covers the whole experiment, including mounting the antenna. Unfortunately, since the UHF feeding network did not work, only the VHF antenna could be measured.

10.1 Assembly of the Antenna Module

When the feeding network PCB for VHF was successfully tested, the SMA connectors of ports 2-5 were de-soldered, and the hole for the center conductor were expanded from 1.6 mm to 2 mm by careful drilling (c.f. Sec. 6.7). It was punched holes in the end of the measuring tape, and the paint was removed by a glass blower, to ensure electrical connection between the microstrip and the measuring tape. A photograph of all the components is shown in Fig. 10.1.

The different grounding layers will be electrically connected to each other simply by the bolts and spacers. In order for the antenna elements *not* to be grounded by the bolts, very thin plastic washers, cut out of transparent paper[1], was used. It is illustrated in Fig. 10.2 how the elements will be mounted. Since the copper is removed near the screw holes in the PCB layout there is no danger that the bolt accidentally get in touch with the copper layer. It might be tempting to use nylon bolts, but remember that they are not strong enough for space applications.

Another note; the measuring tape was *not* cut to only 10 mm of width which is the design. The reason is simple: the VHF antenna will likely bend due to gravity, and it becomes difficult to measure the antenna. This difference is not expected to have any impact on the performance. Moreover, it is expected that in

[1]The operating temperature of transparent paper is likely larger than the temperature the satellite will experience. Nevertheless, it might be wise finding some better washers for later.

Figure 10.1: The pieces from which the antennas are built (UHF on the picture).

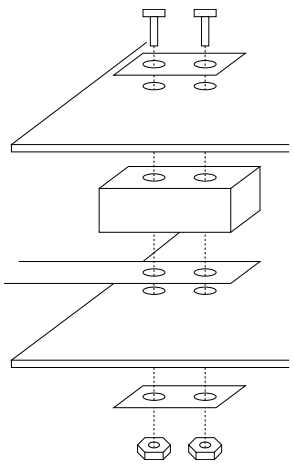

Figure 10.2: Illustration of how the antenna elements are assembled. The double-hole washers on the top and bottom, followed by a layer of PCB, and antenna element and teflon block in the middle.

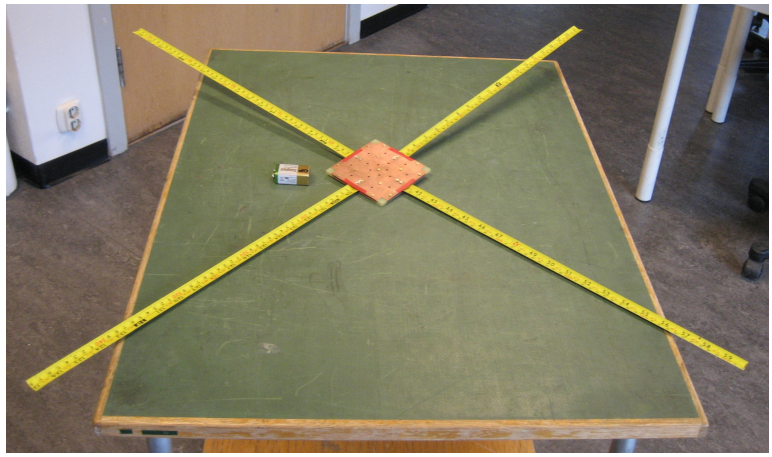

Figure 10.3: The finished VHF antenna

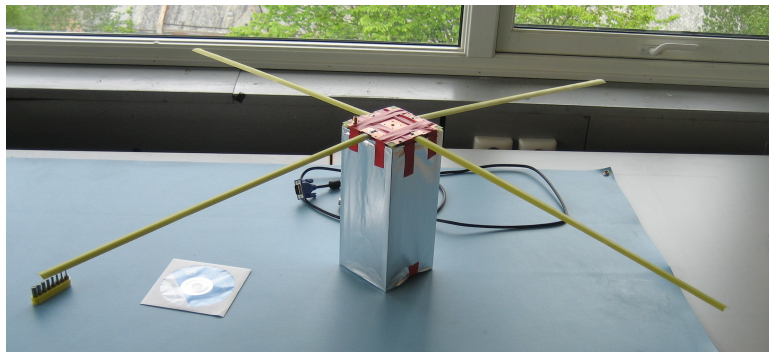

Figure 10.4: A mock-up of the VHF antenna on a double CubeSat frame.

the very last stage of mounting the satellite, the measuring tape will be specially made in *Beryllium Copper* (BeCu) alloy. Contrary to steel, BeCu is non-magnetic but still highly conductive and has been used as antenna for CubeSats before [45]. The reason for having a non-magnetic material is in order not to disturb the magnetometers of the ADCS system. The finished antenna can be seen in Fig. 10.3.

It was chosen *not* to assemble the UHF antenna since the feeding network is not working. De-soldering the connectors on the feeding network and expanding the hole of the center conductor makes it impossible to repair later in the NUTS project.

In order to test the antenna on a mock-up of the satellite, a double CubeSat aluminum frame was covered with aluminum foil and the VHF antenna was fastened to it like depicted in Fig. 10.4.

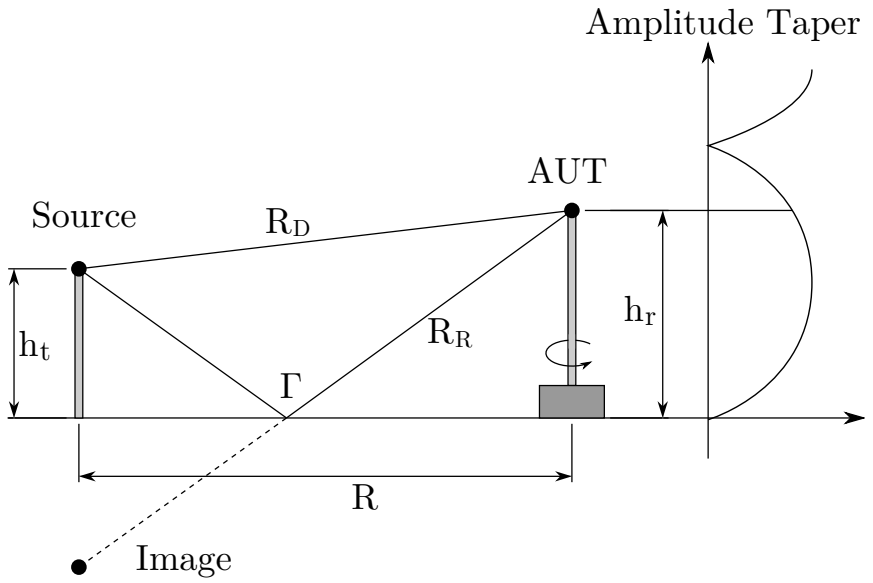

Figure 10.5: Ground-reflection test range. Amplitude taper not realistic.

10.2 Design of the Test Range

Since a ground plane of approximately $5 \times 30\,\mathrm{m}$ is already present on the roof of one of the buildings at NTNU, it was decided to design a *ground-reflection test range* that (as far as feasible) complies with "IEEE Standard Test Procedures for Antennas" [46]. Whereas some test ranges is designed to suppress the effects of the surroundings (*free-space ranges*), the ground-reflection range is on purpose designed such that a reflection occur at the ground plane [46, 26]. This is illustrated in Fig. 10.5. The source antenna is connected to a *Continuous Wave* (CW) signal generator and the direct ray R_D and reflected ray R_R adds up vectorially at a distance R from the source antenna at which the *Antenna Under Test* (AUT) is to be placed. In order for the two rays to add up constructively IEEE suggests that the following relation between the height of the two antennas are maintained:

$$h_t \approx \frac{\lambda R}{4 h_r} \qquad [\mathrm{m}] \quad (10.1)$$

where h_r and h_t are the heights of the AUT and the source, respectively.

Moreover, there will be a vertical interference pattern, or amplitude taper at the AUT's position. It is recommended in [46] that the height of the AUT $h_r > 3.3D$ or preferably $h_r > 4D$ where D is the largest dimension of the AUT. This is for the amplitude taper to vary less than 0.25 dB within the aperture of the AUT, to minimize measurement errors. Since the longest obtainable rod to mount the AUT on only was $h_r = 199\,\mathrm{cm}$ and $D = 104\,\mathrm{cm}$ this requirement was not fulfilled. The

requirement $h > 2D$, however, is almost fulfilled. According to [46] the amplitude taper varies less than 1 dB within the AUT aperture when this requirement is fulfilled. Some error is expected due to this.

Further on, the phase will also vary across the AUT aperture, since the waves propagate more or less spherically from the source. In order for these variations to be sufficiently small (within $\pi/8$ rad), it is necessary that the AUT is in the far-field region of the source antenna ($R > 2D^2/\lambda$). It is also necessary that it is in the far-field to get low reactive coupling between the antennas. However, as [47] points out, $R > 2D^2/\lambda$ is not always an sufficient restriction, especially when the antenna is small compared to the wavelength. To be sure that the AUT is sufficiently far away from the source, *all* of the below constraints should be fulfilled [47]:

$$R > \frac{2D^2}{\lambda} \quad \text{[m]} \quad (10.2)$$

$$R > 5D \quad \text{[m]} \quad (10.3)$$

$$R > 1.6\lambda \quad \text{[m]} \quad (10.4)$$

It is tempting to make R almost as large as the ground plane. The problem is that h_t grows large as R increases (10.1). $R = 6$ m satisfies all of the above mentioned criteria while keeping h_t to a feasible value. To summarize the test range dimensions used:

$$R = 6 \quad \text{[m]} \quad (10.5)$$

$$h_r = 1.99 \quad \text{[m]} \quad (10.6)$$

$$h_t = 1.29 \quad \text{[m]} \quad (10.7)$$

Finally, for the *horizontal* amplitude taper not to vary more than 0.25 dB within the AUT aperture, the following inequality should hold:

$$d \leq 0.37KD \quad \text{[m]} \quad (10.8)$$

where $d = 1.37$ m is the maximum dimension of the source antenna and K is another measure for the distance R as given by:

$$R = \frac{KD^2}{\lambda} \quad \text{[m]} \quad (10.9)$$

Since (10.8) is satisfied for the chosen values of the test range, the *horizontal* amplitude taper varies less than 0.25 dB (which is better than the vertical taper). The test range was rigged up, from which a photograph is found in Fig. 10.6.

Figure 10.6: The test range. The range is placed at an angle to lower specular reflections from the wall.

10.3 Design of the Tests

Which tests to perform must also be designed, but first it is important to realize the limitations of the equipment. The following equipment was available for measurement purposes:

- Scientific Atlanta Antenna Positioner Model 5103-1-R1, S/N: 256-5
- Scientific Atlanta 4131-2 Positioner Controller, S/N: 15898GL
- Hewlett Packard 8565E Spectrum Analyzer, S/N: 05806
- Anritsu Signal Generator MG3602A, S/N: 4021
- STODDART Biconical Antenna model 94455-1, 25–200 MHz, including matching transformer balun

The linear polarized source antenna was fed by the signal generator as explained in the previous section. The AUT can be rotated in the azimuthal direction by the turntable (Antenna Positioner) which is driven by the Positioner Controller. The signal level intercepted by the AUT can be measured by the spectrum analyser while being rotated. Both the spectrum analyser and the turntable controller is connected to a computer through *General Purpose Interface Bus* (GPIB) which controls the azimuth while recording the received power level. It should also be noted that the rod on top of which the AUT is mounted is made by plastic that is transparent to radio waves.

Restrictions imposed by the equipment is for example that the AUT can only be rotated about one axis at a time. The source can be made horizontal, or vertical polarized, or in between, but not circular polarized. It is therefore possible to measure different linear components of the pattern, but not the circular components directly. It has, however, been decided only to use the source antenna in the horizontal direction to make all the results more comparable. This means that in order to measure different linear components, the AUT must be re-mounted on the rod with a different orientation. Beware that this will make the azimuth rotate about another axis, such that axial ratios cannot be swept without changing the polarization of the source.

To measure the handedness of the polarization can be done either by comparing the received signal strength both with RHCP and LHCP source antennas, or by measuring two linear polarized components with phase-difference information. Since none of the two are possible with the above mentioned equipment, the handedness will not be measured. Due to extensive testing with network analyser, however, it is safe to conclude that the it is RHCP. The tests in this chapter will also reveal if the polarization is far from circular.

The measurements are likely not accurate enough to measure the gain. Thus, only the patterns will be measured. Moreover, the plots in this chapter is made in MATLAB by functions found in App. D.

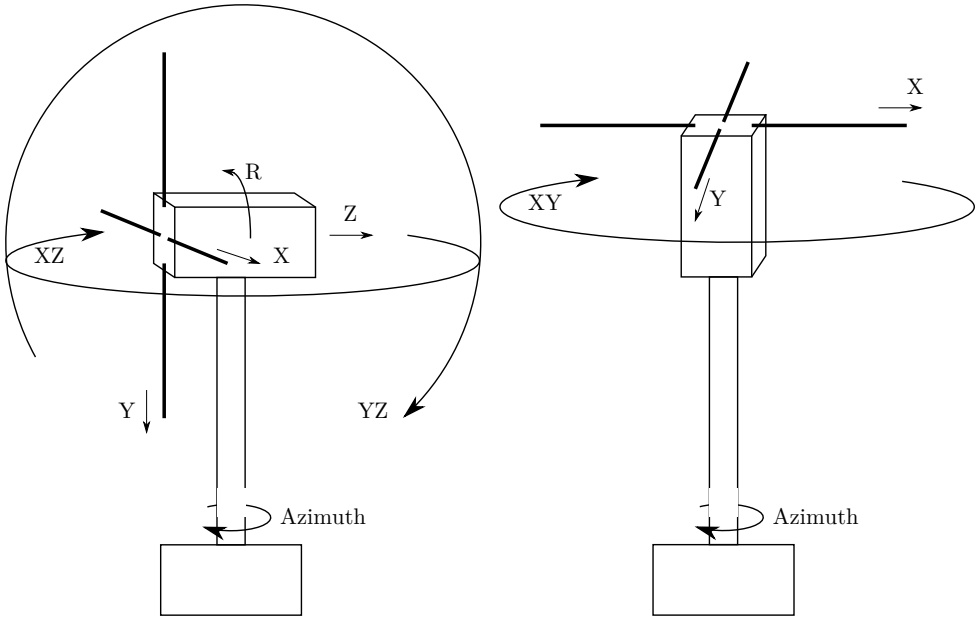

(a) Measurement setup in the XZ- and YZ-planes. (b) Measurement setup in the XY-plane.

Figure 10.7: The measurement setups. The arrows indicate the direction of increasing azimuth angle.

10.3.1 Test 1: The XZ-plane

The first test is to measure the radiation in the XZ-plane, when the antenna is mounted like shown in Fig. 10.7(a). Notice that the Z-direction is taken toward nadir. Since the source is horizontal, the Y-aligned dipole should be practically invisible in these measurements. As the XZ-plane is swept by increasing the azimuth angle, it is therefore expected to see the well known figure-of-eight pattern in the E-plane of a dipole. Remember that the box (and the UHF antenna) had little impact of the diagram for VHF, c.f. Sec. 9.2. This test will thereby verify that the X-aligned dipole radiates as it should. Lastly, it should be mentioned that azimuth is defined to be zero when the Z-axis points towards the source.

10.3.2 Test 2: The YZ-plane

The Y-aligned dipole will be verified to radiate in the same way as the X-aligned dipole was verified to radiate. Specifically, the satellite is rotated 90° as indicated by R on the figure, such that the X-axis points upwards. As the azimuth angle increases the YZ-plane is swept, also indicated on the figure. Again, a figure-of-eight pattern indicates that dipole Y works like intended. Azimuth is zero when Z point towards the source.

Notice that both measurements 1 and 2 measures the pattern at $\theta = 0°$ (the

Z-axis), but the two tests measure different components of the **E**-field. I.e test 1 measures the X-polarized reception at $\theta = 0°$ whereas test 2 measures the Y-polarized reception. If the axial ratio is 0 dB (perfectly circular), the two received power levels at $\theta = 0°$ should be equal. The converse, however, is not true. If, for instance, the two dipoles are fed in-phase instead of in quadrature-phase, the antenna will be linear polarized with a 45° tilt angle w.r.t. ground. Then, the intercepted power will also be equal for the two tested planes, despite AR $\to \infty$.

Nevertheless, the simulations and measurements on the feeding network provide good answers to what the axial ratio might be, and if in addition the two received power levels at $\theta = 0°$ are close then that is a good indication that both dipoles works and constitutes a circular polarized turnstile antenna.

10.3.3 Test 3: The XY-plane

In the third test the antenna is mounted on the rod like illustrated in Fig. 10.7(b), with the X-axis pointing towards the source when the azimuth is zero[2]. According to Sec. 9.1, it was stated that the pattern in this plane should vary by approximately 1 dB. If one of the dipoles did *not* work, however, one would expect to see a figure-of-eight pattern, or at least two nulls in this plane.

This test can also be used as an indication for whether or not the antenna is properly fed in quadrature. Consider now what happens if the dipoles are excited in-phase rather than in quadrature-phase. The fields would interfere destructively in either the directions $\phi = 45°$ and $\phi = -135°$ or $\phi = -45°$ and $\phi = 135°$ such that two nulls again would occur in the pattern. It would be similar to if a single dipole was aligned at an 45° angle between the two crossed dipoles. Therefore, it is reasonable to expect that two minima will become more and more predominant the less circularly the antennas are fed.

Quantitative measurements for the axial ratio of the antennas has already been carried out in the measurements of the feeding-network. Nevertheless, it is pleasant to have additional qualitative measurements to verify them. Of course one should expect more than 1 dB variation in this plane, since it is known that neither the feeding network, the test range nor the antenna are perfect. Nonetheless, the deviations is expected to be quite low within this plane.

10.4 Results

The measured signal strength versus azimuth for the three sweeps is given in Fig. 10.8 and it can already be noted that the XY-sweep is rather flat and that the XZ and YZ sweeps have very close value at 0° azimuth. Both are indications of a good axial ratio.

[2] Actually the azimuth and the ϕ angles has opposite signs in this test since antenna is mounted with the Z-axis downwards.

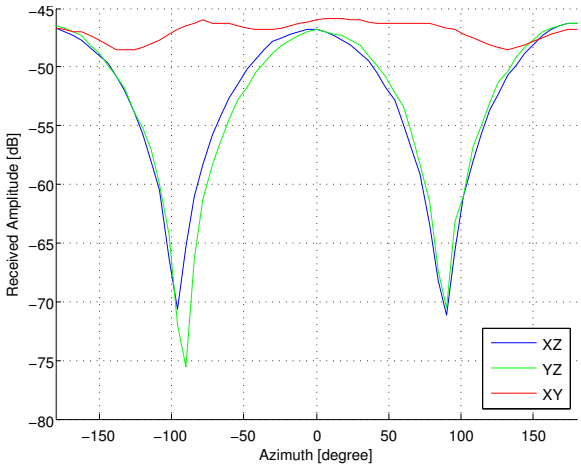

Figure 10.8: Received signal strength for all sweeps.

In fact, the ratio between the XZ, and YZ sweeps at zero azimuth is less than 0.7 dB. [3]. Moreover, Fig. 10.9 shows the measured patterns in the XZ and YZ-planes, and they have been compared to the pattern of a theoretical dipole, indicating that both dipoles radiate well. Finally, the XY-sweep is illustrated in Fig. 10.10.

10.5 Mechanical Measurements

A requirement for the antennas was that it should not be thicker than 6 mm including the bolt heads but not the nuts (see Fig. 4.5). The thickness of the finished antenna module measured to 5.8 mm and thereby fulfilled the requirement.

No requirement was given w.r.t. the weight of the antennas, other than they should probably not weigh too much. Undoubtedly, a mass budget for the satellite should be made, since double unit CubeSats are specified to weigh no more than 2.66 kg, and have a mass center within a certain radius of the geometrical center of the satellite [3]. For those making a mass budget sometime in the future, the VHF antenna module is weighed to be 81 g.

It should be expected to be lighter when it is mounted on the satellite, since the measuring tape used in the experiment is 19 mm wide rather than the designed 10 mm. The tape used, is measured to weigh approximately 14 g per 75 cm. Scaling the mass of by the ratio of the widths yields approximately 7.4 g per 75 cm for the designed tape width. Using the lengths in Tab. 9.1 and subtracting weight of the present antenna yield 44.4 g for the module without the elements. Adding back the elements with the weight of the designed width yields an estimate of 64 g for the

[3] Remember that this is *not* the axial ratio, only one of several measurements that fits with the antenna being circular polarized. Quantitative numbers for the axial ratio must be taken from the statistical simulations to be less or equal to 2.6 dB.

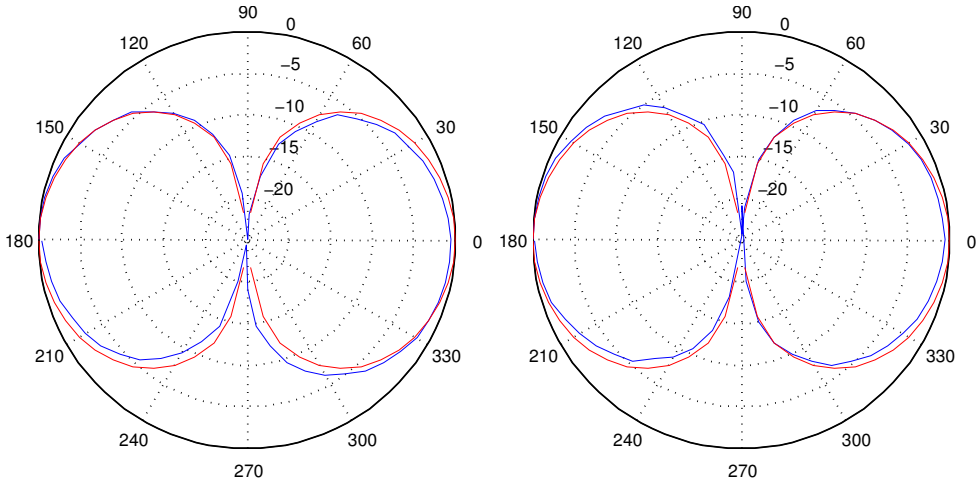

(a) XZ-plane (b) YZ-plane

Figure 10.9: Measured horizontal polarized antenna patterns (blue) compared with ideal dipoles (red) versus azimuth.

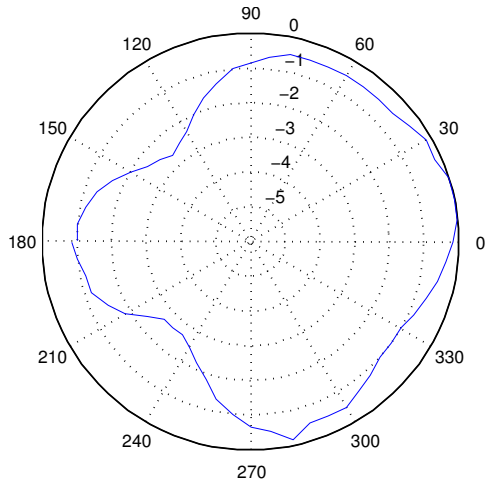

Figure 10.10: Measured horizontal polarized pattern in the XY-plane versus azimuth. Beware of the radial axis.

VHF antenna and 51 g for the UHF antenna that can be used in the mass budget. It will likely be even lighter since the holes for camera and the solar cell connector will be removed from the PCB[4].

10.6 Conclusion

Clearly, both the X-aligned and Y-aligned dipoles radiate as they should. All the measurements match well with the antenna being circular polarized, but the quantitatively measurements of axial ratio are better done on the feeding network.

Moreover, the XY-sweep is seen to vary only 2.5 dB which is considered acceptable. That the variations are larger than the theoretically predicted 1 dB is probably due to tolerances in the feeding network. The antennas also fulfils the mechanical requirements.

Since the UHF antenna could not be built due to the malfunctioning feeding network, its pattern should be measured in the future. These measurements should also be made with the VHF antenna present, in order that its pattern is similar to that shown in Fig. 9.6. One might also consider measuring the VHF pattern again, although it is not expected to change.

[4]Despite the fact that 0.8 mm PCBs was used, the internal module of the satellite feels quite rigid when it is assembled as two stacked PCBs.

11 A Systems Discussion

Discussions have been made for each part of the systems throughout the thesis, and there is no point in repeating all of them here. However, this might be an appropriate time to lift the focus from the detailed level and back to the systems level, in order to see what is achieved, and how the antennas perform from a systems perspective.

11.1 Performance of the Antennas

Monopoles, dipoles and turnstile antennas were considered for the satellite. The antennas were chosen to be the turnstile antennas since they yields the highest received link margin for all elevation angles according to the link margin analysis presented in Ch. 3. The gain patterns[1] of the antennas were obtained by simulations in Ch. 9 with the outcome that the VHF antenna were unaffected by the mechanical structures around it. It's link margin vs. elevation curve is therefore expected to be quite similar to that simulated in Ch. 3 (except for a shift). The UHF antenna had some pattern distortions due to surrounding material, but it was found to still have a superior pattern as compared to dipoles and monopoles.

The link margin simulations in Ch. 3 included a passive loss $L_{\mathrm{sc,TL}}$ in between the spacecraft radio and the antenna. Since the simulations was performed before the feeding network was built, it was unknown what this constant was. It was therefore set to be the parameter used in the current (and not updated) link budget, which according to App. E.3 is 1.1 dB. Now that the antennas and the feeding network is built, however, it is possible to determine a more realistic value for these losses.

The passive losses in between the tranceiver and the antenna comprises the mismatch loss ML in between the antenna and the feeding network, the excess insertion loss EIL through the feeding network, and losses in the cable L_{cable} between

[1] Actually the directivity patterns, but since $e_{cd} \approx 1$ they are practically the same.

Table 11.1: A summary of losses in the antenna systems

		UHF	VHF
Mismatch loss	ML	1 dB	0.2 dB
Excess insertion loss	EIL	2 dB	2 dB
Assumed cable loss	L_{cable}	0.2 dB	0.2 dB
Total passive loss	$L_{\text{sc,TL}}$	3.2 dB	2.4 dB
Excess Polarization Loss	EPLF	0.5 dB	0.5 dB

the radio and the feeding network:

$$L_{\text{sc,TL}} = \text{ML} + \text{EIL} + L_{\text{cable}} \quad [\text{dB}] \quad (11.1)$$

Beware that it is *not* the realized gain that is used in the link budget. The realized gain includes the reflection efficiency e_r, which is equivalent to including the mismatch loss in dB. If the realized gain was used in the link budget, the mismatch loss would therefore be included twice.

The mismatch loss was determined in Ch. 9 and is listed in Tab. 11.1. As mentioned in Ch. 9, it is a bit high for the UHF antenna and optimizing the feeding network further may yield an improvement of a fraction of a dB. The excess insertion loss was determined to be maximum 1 dB by the statistical simulations in Sec. 7.2. However, the statistical simulations did not take into account losses in the components, which seems to be just as dominant as the statistical deviations in component value, in this respect. From the measurements of the VHF network in Ch. 8, it is seen that 2 dB is a better worst case estimate for this value. It is a bit more difficult to know for the UHF, but since the two ports that worked like intended both had insertion losses below 8 dB, it is reasonable to assume that the two broken ports would also have insertion losses below 8 dB if they worked. Since 6 dB is the ideal loss, that excess insertion loss would be 2 dB also for UHF.

The cable loss L_{cable} is not known, but assuming that it would be 0.2 dB, the total passive loss $L_{\text{sc,TL}}$ to be used in the link budget is listed in Tab. 11.1. In addition, one should subtract the excess polarization loss from the link margin to take into account possible losses due to unbalances in the feeding network, as discussed in Sec. 7.2.

11.1.1 Review of Other Antennas

Since the passive losses added up to 3.2 dB for UHF and 2.4 dB for VHF, one might ask; would it not be better to just use dipoles? Then one could probably lower the passive loses.

While it is true that dipoles would have a simpler feeding network implying a lower loss, it is not true that using a dipole is just as good. The cable loss must be assumed to be the same for both alternatives, leaving a difference of 3 dB in passive losses between them. This 3 dB difference, is not accounted for in the plot

of link margin versus elevation angle (Fig. 3.4). However, the difference between link margin for the dipole and for the turnstile antenna as shown in Fig. 3.4, is at the worst 3 dB. For lower elevation angles (i.e. 10°), the difference is seen to be more than 10 dB. Thus, the turnstile antenna, if the difference is accounted for, will still be superior to the dipole for all elevation angles, especially for low ones. Since it was seen in the data capacity analysis in Sec. 3.4 that it is important to raise the link margin for lower elevation angles, there is no doubt that the turnstile antenna, despite the losses, are better than a single dipole.

One might also review using a monopole for UHF, where the VHF turnstile antenna acts like a virtual ground plane. If the monopole acted similarly to a theoretical monopole (black line in Fig. 3.4) that might actually be an option. However, the simulated monopole (blue line) has almost as low link margin as the dipole for low elevation angles. It is therefore also less suited than the turnstile antenna.

11.1.2 Bandwidth

The antennas are seen to have a bandwidth of more than the 25 kHz that is used in the link budget. For the VHF there is a 7 MHz bandwidth where the mismatch loss is below 0.2 dB. The bandwidth were also found fit for use within a 10 MHz range, although the performance degrade at the edges of this band. A new center frequency within the IARU VHF satellite band will maximally be off by 0.2 MHz as seen in Tab. 2.1. The VHF antenna system should therefore be unaffected of new frequency change within this region.

The match for the UHF antenna does not change quickly, as shown in Fig. 9.9, and it should be no problem to change the center frequency by 5 MHz. Since the feeding network for UHF does not work it is difficult to make 100% waterproof statement about its bandwidth. The statistical simulations in Sec. 7.2 in addition to the experience with the VHF bandwidth, however, suggests that a couple of MHz should be no problem. Thence, if NUTS is assigned a new center frequency within the IARU UHF satellite band the performance of the antenna system will remain practically the same.

11.2 Qualitative Error Analysis

The antennas will be used in space and exposed to extreme conditions both during, and after launch. In case of a malfunction, there will be no way back. It is therefore worthwhile discussing, at least qualitatively, what will happen in case of an error. It can be considered part of the environmental requirement that the antenna systems cannot be repaired after launch, and therefore should be comparatively robust against errors.

Since the primary technical goal of NUTS is to establish a communication link with the satellite, it is of utmost importance that the link does not completely disappear. Whether the link margin is sufficient to receive the expected amount of

data or not, is a secondary concern, as long as it is possible to hear the beacon. A few possible scenarios are therefore briefly discussed below.

Short circuited antenna elements. The short circuited antenna element cannot be expected to radiate. Due to the isolation between the output ports, however, the power delivered to the other antenna elements will not be affected, as discussed in Sec. 6.3. Thus, if one element is short circuited, a quarter of the power will be dissipated. Some of it will dissipate in one of the resistors in the network, some will appear as a slight reflection on the input of the feeding network. Power will be delivered as intended to the other three antenna elements. Two of them, will act like a dipole, while the third will likely act like a poor (horizontal) monopole. This will both affect the pattern and the polarization loss, which in turn is expected to reduce the capacity of the link. Since three quarters of the power will still be fed to the antenna, it is nevertheless considered feasible to maintain a link. The same reasoning can be applied if more than one element is short circuited.

One of R_1-R_3 in the feeding network is broken. See Fig. 6.6. These resistors provide the isolation between the output ports. The isolation is not needed if no other error is present, since there will only be a common-mode signal across the resistors in the transmitting mode. The receiving mode will then also work like intended, due to electromagnetic reciprocity.

One of X_1-X_3 in the feeding network is broken. The first stage WPS is broken. Depending on exactly what the error is one might not expect any power radiated. For instance if X_1 is short-circuited, as can be readily understood by considering Fig. 6.6. This is the most critical error that can happen to the feeding network. As a remedy the author suggest that the software for the radios is made such that both bands can be used both for reception and transmission. This will also be a redundancy in case of other errors with respect to the radio.

One of X_4-X_9 in the feeding network is broken. This will manifest itself as a changed load impedance on one of the outputs of the first-stage WPS (See Fig. 6.2 or Fig. 6.6). Due to the isolation, the other output will work as intended and two of the elements will be properly excited. The other two elements may radiate some or not at all depending on the error. Changed patterns and polarizations should be expected, but some signal can be expected at the ground.

One of X_{10}-X_{25} in the feeding network is broken. This will manifest itself as a changed load impedance on one of four outputs (the one where the broken component is) of the second stage divider, and ruin the feeding of the element connected to that port (see Fig. 6.2). The other three elements, however, will be fed like intended. Some signal may be expected on ground.

Jamming during deployment. Elements that are not properly deployed may be short circuited and behave according to the first point. If this happens

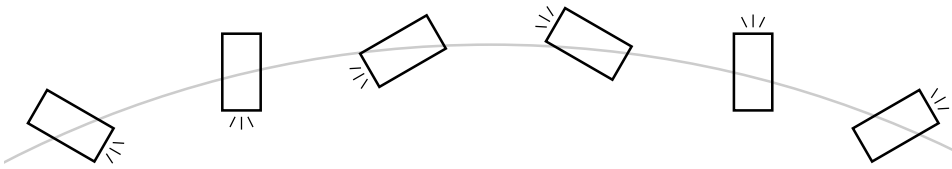

Figure 11.1: NUTS is spinning about a horizontal axis.

with one or two elements a signal may still be expected on the ground. The concern, however, may be that since some elements are folded on top of others, the first element does not deploy. The probability of this is significantly reduced by the fact that two Nichrome wires are used to burn off each nylon thread.

Most of the errors only imply a reduced signal strength on ground. The author suggests that in order to cope with this (and potentially other radio errors) the bitrate is not initially set to its intended value (9600 bps) but somewhat lower. If the received signal strength on ground permits it, the bitrate can be increased to its intended value by transmitting a telecommand.

11.2.1 Defect ADCS Performance

There is one more error that should be considered, namely what happens in case of an ADCS failure. The ADCS is a highly complex system which makes it rather vulnerable to errors. Nevertheless, it is beneficial if the radio link can be maintained even if the ADCS does not work.

In [4] it was concluded that the turnstile antenna is by far the better antenna also in case of an ADCS failure. The total gain of an (ideal) turnstile antenna was found in [4] to only vary 4 dB as a function of (θ, ϕ) whereas the dipole and monopoles *both* have two zeros in their patterns. Although the turnstile antenna does not have a zero in its *total* gain pattern, it has *one* zero in its *circular* gain pattern, as can be seen in Fig. 9.5.

Consider now that the antenna is spinning as indicated in Fig. 11.1. The ground station will experience a fading due to the antenna rotating in and out of the zeros/minima. In case of dipoles or monopoles, there will be two outages per revolution. In the case of a turnstile antenna, there will be one outage per revolution.

For the turnstile antenna, it is possible to remedy this by switching polarization on the ground station. If the polarization is switched to LHCP, the pattern shown in Fig. 9.5 will flip upside down[2]. In that case, the author suggests that the vertical

[2]This is true for an ideal turnstile antenna and therefore also applies to the near-ideal VHF antenna. For the UHF antenna, however, the pattern distortions are likely such that the pattern is not exactly flipped. Nonetheless, the direction of the zero in the circular gain pattern will flip, making it a useful principle also for the UHF antenna.

and horizontal polarized Yagi antennas that are present on the ground station are connected to a 90° hybrid such as the branch-line coupler (c.f. [15]). The intercepted power will then be decomposed into an RHCP-signal and an LHCP-signal. Using two receivers, one for each signal, and connecting them to the same computer, the computer can continuously choose the strongest signal.

12 Conclusion

The turnstile antennas were found to yield a higher link margin than both dipoles and monopoles throughout the whole pass of the satellite, from which it was decided to build turnstile antennas for both VHF and UHF.

The turnstile antennas were more difficult to feed than first anticipated, largely due to the fact that distributed feeding networks consume too much space. Because of that, a study of feeding network was carried out, from which it was concluded that a lumped feeding network, consisting of a corporate 4-way WPS and four phase-shifters, would be a fit solution. This was designed to match 70 Ω dipoles.

Simulations of the designed feeding network proved the theory behind the design, but it was also necessary to study the impact of non-ideal components. It was found by statistical simulations that an amplitude unbalance of less than 1 dB and a phase unbalance of less than 11° was reasonable to expect within a 10 MHz span of the center frequency for both bands. This, however, only imposed a slight reduction of less than 0.5 dB in the received signal strength on ground.

Moreover, the feeding networks were built and tested. The VHF feeding network operated successfully within the IARU frequency band, with an excess insertion loss of less than 2 dB. This is considered to be a bit high, but it is not expected that it would be lower if ICs were used instead of lumped components. Unfortunately, two of the output ports of the UHF feeding network did not work. They had erroneous phase and magnitude. Anyhow, less than 2 dB of excess insertion loss is also expected for the UHF feeding network.

New simulations of the antennas were performed, where the lengths of the dipoles were optimized to yield the best possible match. The mismatch loss is simulated to be less than 0.2 dB for VHF which must be considered very good. For UHF it was found to be less than 1 dB which is not that good, but acceptable. The total passive losses between the tranceiver and the antenna, assuming an additional cable loss of 0.2 dB, adds up to 3.2 dB for UHF and 2.4 dB for VHF. Although this would likely be lower for a dipole or monopole, the turnstile antennas are still best suited, in terms of link margin.

A test range were also designed according to IEEE recommendations, on which the pattern for the VHF antenna was measured. The simulations showed that both dipole radiated like intended and that the antenna was successful. Unfortunately the pattern for the UHF antenna could not be measured since the feeding network did not function.

It should also be mentioned that the design was made such that the antenna module is compliant with other modules on-board the satellite. Space is reserved for the camera, for a connector to the solar panel, and for fastening mechanisms to mount the antenna to the frame. Moreover, the design is made redundant against errors, and the components are carefully chosen to survive the environmental requirements in space.

12.1 Future Work

The most notable remaining work is reparation of the UHF feeding network, as discussed in Sec. 8.7.1. Once this is done, the pattern of UHF antenna should be measured on a mock-up of the satellite with both antennas mounted. It might also be considered to measure the pattern of the VHF antenna again, when both antennas are mounted. The measured patterns can be compared to the simulations in this thesis to determine if it works like intended.

It is also possible to redesign the UHF feeding network for another output impedance in order to achieve a better matching of the antenna. However, there is only a fraction of a dB to earn from it, so its necessity must be evaluated by the NUTS team against the effort required.

Finally, an updated link budget should be made for NUTS. To update the link budget was not a part of this thesis, the link budgets were only used as a tool. Nevertheless, the project will need an updated link budget, and some of the parameters to put in the link budget has been obtained through the work done in this report.

Bibliography

[1] K. Gulzar, "Camera design for pica and nano satellite applications," Master's thesis, University of Würzburg, Germany, 2009.

[2] R. Birkeland, "Nuts-1 mission statement," 2011.

[3] C. P. S. The CubeSat Program, "Cubesat design specication rev. 12," 2011. `http://www.cubesat.org/images/developers/cds_rev12.pdf`.

[4] S. Marholm, "Specializaton project: Antenna systems for nuts." `http://nuts.cubesat.no/publications-and-reports`, 2011.

[5] M. Bakken, "Master's thesis: Signal processing for communicating gravity wave images from the ntnu test satellite," 2012.

[6] G. Bråthen, "Specializaton project: Nonlinear attitude control of a double cubesat." `http://www.iaru.org/bandplans.html`, 2011.

[7] R. Birkeland, E. K. Blom, and E. Narverud, "Small student satellite," *NTNU*, 2006.

[8] "Forskrift om tillatelse for radioamatør.." `http://www.lovdata.no/ltavd1/filer/sf-20011105-1251.html`. Retrieved 19.12.2011.

[9] K. Wakker, *Astrodynamics-I*. Delft University of Technology, 2010.

[10] O. Montenbruck and E. Gill, *Satellite Orbits – Models, Methods and Applications*. Springer, 2000.

[11] J. Gießelmann, "Development of an active magnetic attitude determination and control system for picosatellites on highly inclined circular low earth orbits," Master's thesis, RMIT University, 2006.

[12] L. Beathe Hagen Stenhaug, "Antenna system for a ground station communicating with the ntnu test satellite (nuts)," Master's thesis, 2011.

[13] K. Wakker, *Astrodynamics-II*. Delft University of Technology, 2010.

[14] G. Seeber, *Satellite Geodesy*. Walter de Gruyter GmbH, 2 ed., 2003.

[15] D. M. Pozar, *Microwave Engineering*. John Wiley & Sons, Inc., 3 ed., 2005.

[16] D. M. Pozar, *Microwave and RF Design of Wireless Systems*. John Wiley & Sons, Inc., 2001.

[17] D. Bockelman and W. Eisenstadt, "Combined differential and common-mode scattering parameters: theory and simulation," *Microwave Theory and Techniques, IEEE Transactions on*, vol. 43, pp. 1530 –1539, jul 1995.

[18] T. Mathiesen. Oral statement.

[19] I. Jensen. Oral statement.

[20] R. D. Straw and A. R. R. League, *ARRL Antenna Book*. American Radio Relay League (ARRL), 2003.

[21] D. K. Cheng, *Field and Wave Electromagnetics (2nd Edition)*. Addison-Wesley, 1989.

[22] S. Parisi, "180 deg; lumped element hybrid," in *Microwave Symposium Digest, 1989., IEEE MTT-S International*, pp. 1243 –1246 vol.3, jun 1989.

[23] D. Kuylenstierna, S. Gunnarsson, and H. Zirath, "Lumped-element quadrature power splitters using mixed right/left-handed transmission lines," *Microwave Theory and Techniques, IEEE Transactions on*, vol. 53, pp. 2616 – 2621, aug. 2005.

[24] A. Lai, T. Itoh, and C. Caloz, "Composite right/left-handed transmission line metamaterials," *Microwave Magazine, IEEE*, vol. 5, pp. 34 – 50, sept. 2004.

[25] T. Kawai, H. Mizuno, I. Ohta, and A. Enokihara, "Lumped-element quadrature wilkinson power divider," in *Microwave Conference, 2009. APMC 2009. Asia Pacific*, pp. 1012 –1015, dec. 2009.

[26] C. A. Balanis, *Antenna Theory – Analysis and Design*. Wiley-Interscience, 3 ed., 2005.

[27] "Ieee standard definitions of terms for antennas," *IEEE Std 145-1983*, 1983.

[28] C. S. T. AG, *Computer Simulation Technology AG: User Manual*.

[29] J. S. Seybold, *Introduction to RF Propagation*. Wiley-Interscience, 2005.

[30] S. Haykin, *Communication Systems*. 4 ed.

[31] J. Friedel and S. McKibbon, "Senior project: Thermal analysis of the cubesat cp3 satellite," 2011.

[32] S. Birkeland, T. H. Bryne, T. Grav, K. A. Kvåle, and T. B. Martinsen, "Tfe4850 eit - studentsatellitt, prosjektrapport: Antenneutløsermekanisme." 2012.

[33] E. J. Daly, A. Hilgers, G. Drolshagen, and H. D. R. Evans, "Space environment analysis: Experience and trends." `http://esamultimedia.esa.int/conferences/96a09/Abstracts/abstract45/paper/`. Retrieved 02.07.2012.

[34] D. Kuylenstierna and P. Linner, "Design of broad-band lumped-element baluns with inherent impedance transformation," *Microwave Theory and Techniques, IEEE Transactions on*, vol. 52, pp. 2739 – 2745, dec. 2004.

[35] E. Wilkinson, "An n-way hybrid power divider," *Microwave Theory and Techniques, IRE Transactions on*, vol. 8, pp. 116 –118, january 1960.

[36] H. Mgombelo and J. Gardiner, "Three-way power dividers and combiners constructed on the basis of a three-way luzzato divider," in *RF Combining, IEE Colloquium on*, pp. 4/1 –410, apr 1990.

[37] Microwaves101. `http://www.microwaves101.com/encyclopedia/wilkinson_nway.cfm`, 2010.

[38] W. Roy W. Lewallen, "Baluns: What they do and how they do it," 1985.

[39] P. Vizmuller, *RF Design Guide: Systems, Circuits, and Equations*. Artech House, 1995.

[40] D. Kuylenstierna and P. Linner, "Design of broadband lumped element baluns," in *Microwave Symposium Digest, 2004 IEEE MTT-S International*, vol. 2, pp. 899 – 902 Vol.2, june 2004.

[41] A. Technologies, "Tuning, optimization, and statistical design." `cp.literature.agilent.com/litweb/pdf/ads2005a/pdf/optstat.pdf`, 2005.

[42] *Microstrip Antennas: The Analysis and Design of Microstrip Antennas and Arrays*. Wiley-IEEE Press, 1995.

[43] S. Parekh, "Simple formulae for circular-polarization axial-ratio calculations," *Antennas and Propagation Magazine, IEEE*, vol. 33, pp. 30 –32, feb. 1991.

[44] Microwaves101. `http://na.tm.agilent.com/pna/help/latest/S3_Cals/TRL_Calibration.htm`, 2010.

[45] A. R. Aslan, B. Yagci, A. Sofyali, M. Suer, E. Umit, C. Tola, O. Ceylan, A. S. Durna, G. Celik, D. C. S. Ozturk, and I. N. Group, "Developement of a 3unit cubesat for leo communication,"

[46] "Ieee standard test procedures for antennas," *ANSI/IEEE Std 149-1979*, 1979.

[47] R. Bansal, "The far-field: How far is far enough?," *Applied Microwave and Wireless*, pp. 58–60, Nov. 1999.

[48] E. Kreyszig, *Advanced Engineering Mathematics*. John Wiley & Sons, 2006.

A

Assembly Instructions and Components

This chapter contains the most essential information needed to re-build the antenna modules. Of course, new layout must be produced. The GERBER files will be preserved by the NUTS-team. The teflon blocks should be reproduced, measuring $10 \times 14 \times 3$ mm, with an accuracy of 0.1 mm. Two 2 mm holes should be made, both in the teflon blocks and in the measuring tape. One at 3.5 mm from the short edge, and one at 9 mm from the same edge. The double-hole insulating washers, are made from transparent paper by scissor and a bradawl. The paint must be removed from the tape by a glass blower. Sand paper and similar is not sufficient. The components and their placement is shown in the table and the figures within this chapter. The resistors are of type Panasonic ERPJ03F****V, the inductors of type Johanson L14W****V4E and the capacitors of type Johanson 241R14S****V4T, where **** can be found in the table.

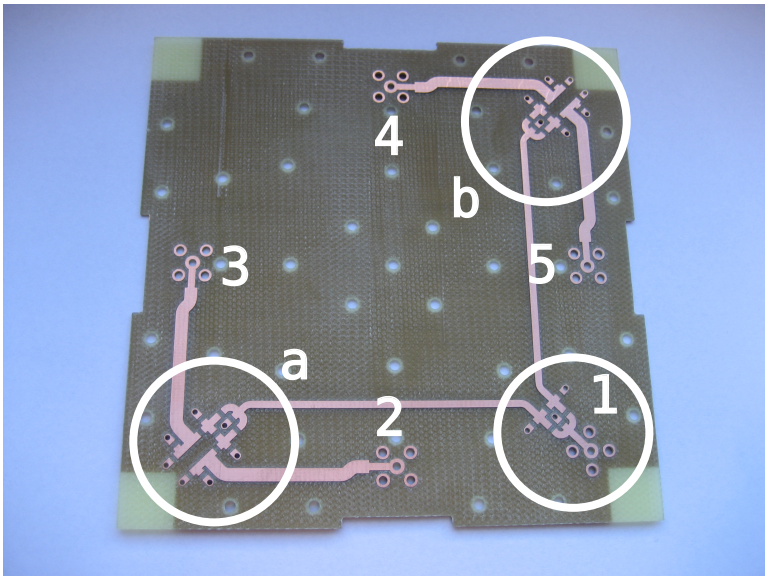

Figure A.1: The PCB. The ports are labelled 1-5. Stage 1 is in the lower right corner together with port 1. Stages 2 and 3 are split into pieces a and b indicated with circles.

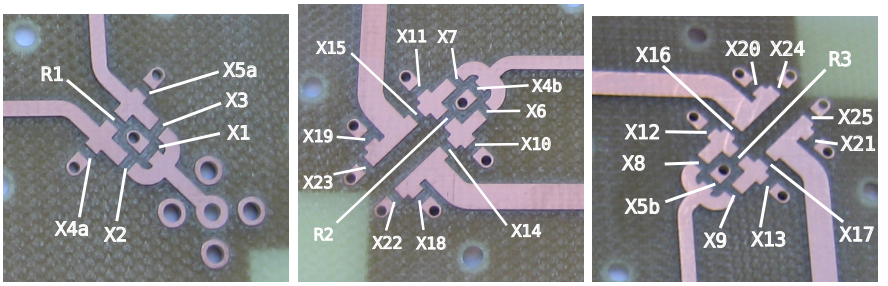

(a) Stage 1 (b) Stage 2&3 part a (c) Stage 2&3 part b

Figure A.2: Component placement

Table A.1: Component values

	VHF			UHF		
	Ideal	True	Part.nr.	Ideal	True	Part.nr.
R1	100 Ω	100 Ω	1000	100 Ω	100 Ω	1000
R2	70 Ω	68 Ω	68R0	70 Ω	68 Ω	68R0
R3	70 Ω	68 Ω	68R0	70 Ω	68 Ω	68R0
X1	30.83 pF	30 pF	300G	10.30 pF	10 pF	100G
X2	77.08 nH	82 nH	82NJ	25.75 nH	27 nH	27NJ
X3	77.08 nH	82 nH	82NJ	25.75 nH	27 nH	27NJ
X4a	15.42 pF	15 pF	150G	5.15 pF	5.6 pF	5R6C
X4b	36.85 pF	36 pF	360G	12.31 pF	12 pF	120G
X5a	15.42 pF	15 pF	150G	5.15 pF	5.6 pF	5R6C
X5b	36.85 pF	36 pF	360G	12.31 pF	12 pF	120G
X6	64.49 nH	68 nH	68NJ	21.55 nH	22 nH	22NJ
X7	64.49 nH	68 nH	68NJ	21.55 nH	22 nH	22NJ
X8	64.49 nH	68 nH	68NJ	21.55 nH	22 nH	22NJ
X9	64.49 nH	68 nH	68NJ	21.55 nH	22 nH	22NJ
X10	31.33 pF	30 pF	300G	1.85 pF	1.8 pF	1R8B
X11	93.62 pF	100 pF	101G	6.99 nH	6.8 nH	6N8J
X12	20.93 nH	22 nH	22NJ	31.28 pF	30 pF	300G
X13	5.53 pF	5.6 pF	5R6C	10.47 pF	10 pF	100G
X14	26.98 nH	27 nH	27NJ	14.71 pF	15 pF	150G
X15	26.98 nH	27 nH	27NJ	14.71 pF	15 pF	150G
X16	44.05 pF	43 pF	430G	9.01 nH	8.2 nH	8N2J
X17	44.05 pF	43 pF	430G	9.01 nH	8.2 nH	8N2J
X18	24.78 pF	24 pF	240J	30.77 nH	33 nH	33NJ
X19	87.08 pF	82 pF	820J	5.28 nH	5.6 nH	5N6C
X20	15.80 nH	15 nH	15NJ	29.14 pF	30 pF	300G
X21	92.11 nH	100 nH	R10J	8.33 pF	8.2 pF	8R2C
X22	100 nH	100 nH	R10J	O.C.	O.C.	
X23	100 nH	100 nH	R10J	O.C.	O.C.	
X24	O.C.	O.C.		33 nH	33 nH	33NJ
X25	O.C.	O.C.		33 nH	33 nH	33NJ

B

Feeding Network Calculator

Due to the large number of formulas to use in order to find the component values for the components of the feeding network, a feeding network calculator was made in *OpenOffice.org Spreadsheet* (a Linux-friendly competitor to *Microsoft Office*). Two screenshots are shown in Fig. B.1 and Fig. B.2.

The spreadsheet consist of several boxes that can be collapsed if they are not wanted (some of the less interesting are collapsed in the screenshots), as well as circuit diagrams of the distributed and lumped feeding network and the unit cells used (not shown on the screenshots). The user inserts the independent variables such as frequency, the value of the DC-grounding inductors and phase-lag in phase-shifters. She/he may also specify whether the WPSs should incorporate 90° or 270° phase-shifts, and what are the characteristic impedance at the input, output and between stages 1 and 2. The little red dots will reveal boxes with further information when the user holds the arrow above them.

The calculator automatically detects which unit cells must be used, and whether or not DC-grounding inductors are necessary. Further on it computes the theoretical S-parameters and component values for both distributed and lumped feeding network.

The example values used in the screenshots presents the minimum number of components achievable. The calculator does not support separating TLs between the stages, but this is planned for the future.

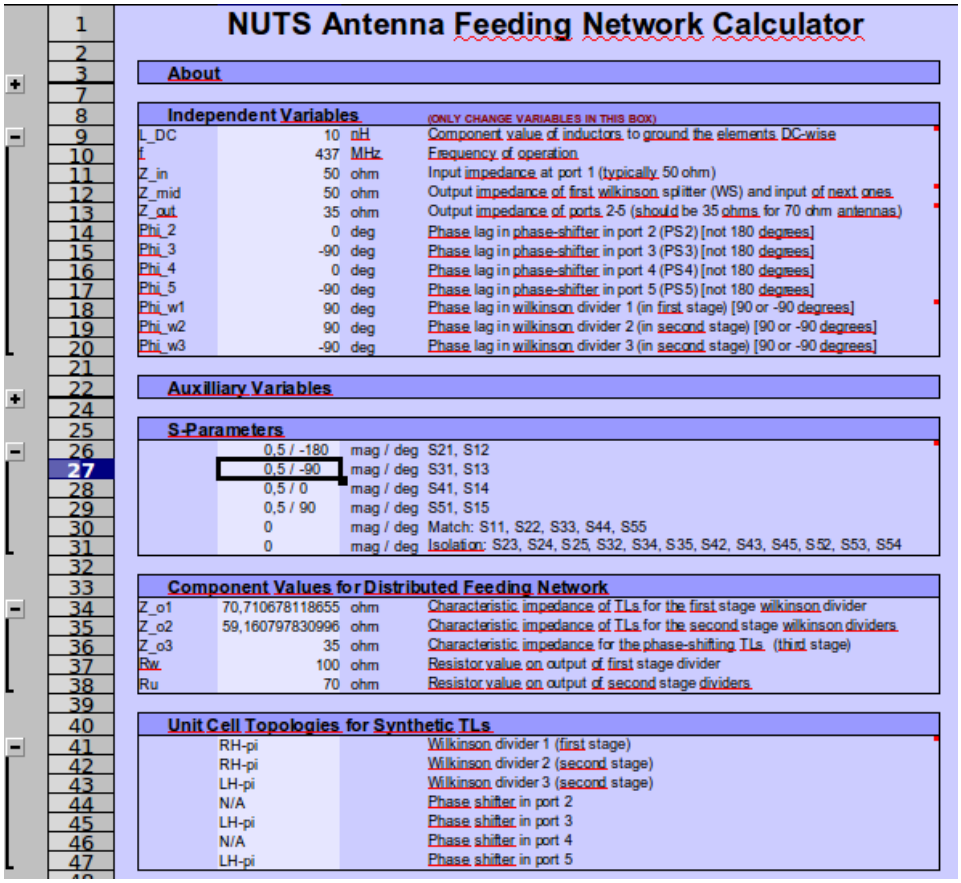

NUTS Antenna Feeding Network Calculator

About

Independent Variables (ONLY CHANGE VARIABLES IN THIS BOX)

L_DC	10	nH	Component value of inductors to ground the elements DC-wise
f	437	MHz	Frequency of operation
Z_in	50	ohm	Input impedance at port 1 (typically 50 ohm)
Z_mid	50	ohm	Output impedance of first wilkinson splitter (WS) and input of next ones
Z_out	35	ohm	Output impedance of ports 2-5 (should be 35 ohms for 70 ohm antennas)
Phi_2	0	deg	Phase lag in phase-shifter in port 2 (PS2) [not 180 degrees]
Phi_3	-90	deg	Phase lag in phase-shifter in port 3 (PS3) [not 180 degrees]
Phi_4	0	deg	Phase lag in phase-shifter in port 4 (PS4) [not 180 degrees]
Phi_5	-90	deg	Phase lag in phase-shifter in port 5 (PS5) [not 180 degrees]
Phi_w1	90	deg	Phase lag in wilkinson divider 1 (in first stage) [90 or -90 degrees]
Phi_w2	90	deg	Phase lag in wilkinson divider 2 (in second stage) [90 or -90 degrees]
Phi_w3	-90	deg	Phase lag in wilkinson divider 3 (in second stage) [90 or -90 degrees]

Auxilliary Variables

S-Parameters

0,5 / -180	mag / deg	S21, S12
0,5 / -90	mag / deg	S31, S13
0,5 / 0	mag / deg	S41, S14
0,5 / 90	mag / deg	S51, S15
0	mag / deg	Match: S11, S22, S33, S44, S55
0	mag / deg	Isolation: S23, S24, S25, S32, S34, S35, S42, S43, S45, S52, S53, S54

Component Values for Distributed Feeding Network

Z_o1	70,710678118655	ohm	Characteristic impedance of TLs for the first stage wilkinson divider
Z_o2	59,160797830996	ohm	Characteristic impedance of TLs for the second stage wilkinson dividers
Z_o3	35	ohm	Characteristic impedance for the phase-shifting TLs (third stage)
Rw	100	ohm	Resistor value on output of first stage divider
Ru	70	ohm	Resistor value on output of second stage dividers

Unit Cell Topologies for Synthetic TLs

RH-pi	Wilkinson divider 1 (first stage)
RH-pi	Wilkinson divider 2 (second stage)
LH-pi	Wilkinson divider 3 (second stage)
N/A	Phase shifter in port 2
LH-pi	Phase shifter in port 3
N/A	Phase shifter in port 4
LH-pi	Phase shifter in port 5

Figure B.1: Screenshot of the NUTS Feeding Network Calculator, Part 1.

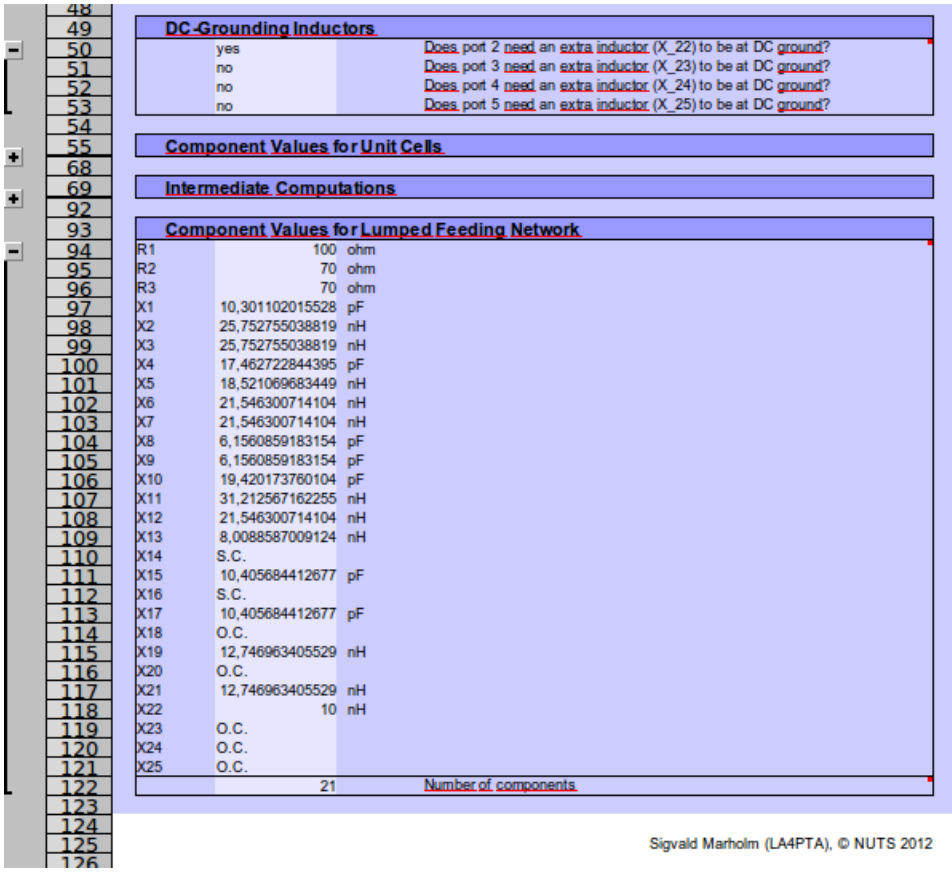

DC-Grounding Inductors

yes	Does port 2 need an extra inductor (X_22) to be at DC ground?
no	Does port 3 need an extra inductor (X_23) to be at DC ground?
no	Does port 4 need an extra inductor (X_24) to be at DC ground?
no	Does port 5 need an extra inductor (X_25) to be at DC ground?

Component Values for Unit Cells

Intermediate Computations

Component Values for Lumped Feeding Network

R1	100	ohm
R2	70	ohm
R3	70	ohm
X1	10,301102015528	pF
X2	25,752755038819	nH
X3	25,752755038819	nH
X4	17,462722844395	pF
X5	18,521069683449	nH
X6	21,546300714104	nH
X7	21,546300714104	nH
X8	6,1560859183154	pF
X9	6,1560859183154	pF
X10	19,420173760104	pF
X11	31,212567162255	nH
X12	21,546300714104	nH
X13	8,0088587009124	nH
X14	S.C.	
X15	10,405684412677	pF
X16	S.C.	
X17	10,405684412677	pF
X18	O.C.	
X19	12,746963405529	nH
X20	O.C.	
X21	12,746963405529	nH
X22	10	nH
X23	O.C.	
X24	O.C.	
X25	O.C.	
	21	Number of components

Sigvald Marholm (LA4PTA), © NUTS 2012

Figure B.2: Screenshot of the NUTS Feeding Network Calculator, Part 2.

C Download Capacity Tool

This appendix contains the MATLAB tools developed by the author and Marianne Bakken and used for the download capacity simulations in Sec. 3.4.

C.1 `read_stk_elev.m`

```
function [data sep] = read_stk_elev(fname)
% Function to read STK data files containing elevation. For now it only
% supports elevation. The usage is as follows:
%
% You set up a scenario with a satellite and a ground station facility in
% STK and you export the elevation as seen from the ground station to a
% .dat file. You have to export ONLY the elevation and not azimuth and
% range since read_stk_elev() doesn't support that. If done correctly, all
% the lines in the .dat file should look like the following:
%
%   Elevation (deg) 47  1.1.2012 03:36:15,000    2,27845993613939
%
% The first number is simple an index, the number of the sample.
% Subsequently follows the date and time, and finally the elevation angle
% in degrees.
%
% There is an issue with the format of the .dat file STK produces; they
% cannot be read by MATLAB. To fix that, open them in a text-editor and
% save them with UTF-8 encoding before using read_stk_elev().
%
% Import the data to a MATLAB matrix called data by
%
%   data = read_stk_elev(fname)
%
% where fname is a variable (of type string) containing the filename (or
% URL) of the .dat-file exported from STK.
%
% data will be a N x 7 matrix where N is the number of samples in the
% .dat-file from STK. The first dimension is the number of samples whereas
% the second dimension holds different information (fields) about the
% samples:
%
%   1 - Year
%   2 - Month
%   3 - Day
%   4 - Hour
%   5 - Minute
%   6 - Second
%   7 - Elevation
%
% For example, data(23,7) yields the elevation of the 23rd sample.
%
% Note that between the passes, when the satellite is not empty, STK
% produces an empty (separator) sample. For these samples all the fields
```

```
45  % are set to 0 in the data matrix. In some cases, it will be useful for the
46  % user to know which samples are separators. Instead of testing for it, the
47  % user can get a list of separators, sep, in the following way:
48  %
49  %   [data sep] = read_stk_elev(fname)
50  %
51  % Made by:
52  %   Marianne Bakken <mariba@stud.ntnu.no>, MSc. thesis for NUTS 2012
53  %   Sigvald Marholm <marholm@stud.ntnu.no>, MSc. thesis for NUTS 2012
54  %
55  % Copyright 2012, NUTS - NTNU Test Satellite
56  %
57
58
59
60  % A typical line may look like the following, followed by regexp blocks and
61  % name of variables they will be stored into.
62
63  % Elevation (deg)    47  1.1.2012 03:36:15,000    2,27845993613939
64  % ---%s---- -%s--   %d  ---%s--- -----%s-----   -------%s-------
65  %                  index   date       time           elevation
66
67  % The two first blocks are just waste
68  % The %d can be used as index in a matrix
69  % The three last blocks are read as strings to be parsed later
70
71  pattern='%s %s %d %s %s %s';
72
73  fid = fopen(fname);
74  unparsed = textscan(fid, pattern);
75  fclose(fid);
76
77  % Read out the regexp blocks
78  index = unparsed(3);
79  date = unparsed(4);
80  time = unparsed(5);
81  elevation = unparsed(6);
82
83  % MATLAB stores them as a 1-element cell-array for some reason.
84  % Read out the one cell element.
85  index = index{1};
86  date = date{1};
87  time = time{1};
88  elevation = elevation{1};
89
90  N = size(index,1);  % The output is a Nx7 matrix
91
92  % Reads out the data in a Nx7 matrix of the form data(index,parameter)
93  % where index is the same index as in the file, parameter is a value of
94  % the following:
95  %
96  %   1 - year
97  %   2 - month
98  %   3 - day
99  %   4 - hour
100 %   5 - minute
101 %   6 - second
102 %   7 - elevation
103 %
104 % So for example data(23,:) yields the time and elevation for sample 23.
105
106 % Initialize data matrix and sep vector
107 data = zeros(N,7);
108 sep = [];
109
110 for i=index.'
111
112     date_ = date(i);
113     time_ = time(i);
114     elevation_ = elevation(i);
115
116     % For some reason MATLAB stores this into 1-dimensional cell arrays as well
117     date_ = date_{1};
118     time_ = time_{1};
119     elevation_ = elevation_{1};
120
121     if(isempty(elevation_))
122         % STK Produces an empty row with just an index when the satellite
123         % is not visible. Reg.exp. functions run into trouble if they try
124         % to parse an empty string. The convention will be that the matrix
125         % is left with zeros at these places. A vector sep is available as
126         % an output for the user. This is an easy way for the user to keep
127         % track of where these samples are.
128         sep = [sep i];
129     else
130
131         % Replace delimiters with space
132         date_ = regexprep(date_,'\.',' ');          % '1.1.2012' => '1 1 2012'
133         time_ = regexprep(time_,':',' ');          % '03:36:15,000' => '03 36 ...
                15,000'
```

```
134
135         % Replace decimal , with .
136         time_ = regexprep(time_,',','.');            % '03 36 15,000' => '03 36 ...
                15.000'
137         elevation_ = regexprep(elevation_,',','.'); % '2,27845993613939' => ...
                '2.27845993613939'
138
139         % Read out 'day month year' from date_
140         temp = textscan(date_,'%d %d %d','CollectOutput',1);
141         temp = temp{1};
142
143         data(i,1) = temp(3);    % year
144         data(i,2) = temp(2);    % month
145         data(i,3) = temp(1);    % day
146
147         % Read out 'hour minute second' from time_
148         temp = textscan(time_,'%f %f %f','CollectOutput',1);
149         temp = temp{1};
150
151         data(i,4) = temp(1);    % hour
152         data(i,5) = temp(2);    % minute
153         data(i,6) = temp(3);    % second
154
155         % Read out 'elevation' from elevation_
156         temp = textscan(elevation_,'%f','CollectOutput',1);
157         temp = temp{1};
158
159         data(i,7) = temp(1);    % elevation
160
161     end
162
163 end
164
165 end
```

C.2 threshold_stk_elev.m

```
1  function intervals = threshold_stk_elev(data,threshold)
2  % Given a set of elevation data from STK simulations and read with
3  % read_stk_data(), this function determines the time intervals when the
4  % elevation is higher than a certain threshold, i.e. 10 degrees.
5  %
6  % Usage:
7  %
8  %   intervals = threshold_stk_elev(data,threshold)
9  %
10 % where data is the output data matrix from read_stk_data() and threshold
11 % is the elevation threshold.
12 %
13 % The output is a matrix where each interval is represented by one row of
14 % 12 elements. The first 6 elements of the row are the year, month, day,
15 % hour, minute and second of the start of the period. The 6 last elements
16 % represent the end of the period in the same manner.
17 %
18 % Example output:
19 %
20 % intervals =
21 %
22 %   1   1   2012    13  43  23  1   1   2012    13  48  43
23 %   1   1   2012    15  32  11  1   1   2012    15  42  12
24 %
25 % This example shows that the data contains two intervals where the
26 % elevation is higher than the user-specified threshold elevation. The
27 % second interval, for example, starts on 1.1.2012 15:32:11 and ends
28 % 15:42:12 the same day.
29
30 intervals = [];
31
32 % The algorithm works by iterating through all samples and detect when the
33 % elevation increase above, or decrease below, the given threshold. When
34 % that happens, it writes to the intervals array. It remembers whether or
35 % not the elevation is above the threshold by a flag called above.
36
37 above = 0;  % Nominally not in an interval
38 N = size(data,1);
39
40 data=stk_remove_spurious(data);
41
42 for i=1:N
43
44     if( (data(i,7)>=threshold) && ~above  )
45
```

```
46          if(~all(data(i,1:6)==[0 0 0 0 0 0]))    % Ignore empty samples
47
48              % Sometimes STK produces spurious output (unbelievably enough).
49              % When the elevation passes below 1 degree it starts typing them in
50              % exponential form, i.e. 7,442341e-001 except that sometimes it
51              % doesn't get the exponent right. Instead the exponent becomes 0,
52              % and there is a single sample before the satellite goes down where
53              % the elevation is supposedly 7 degrees. This function handles that
54              % by checking that the next sample is also above the threshold.
55
56              if (i+1)<=N % Check that there is a next sample and ignore if not.
57
58                  if( data(i+1,7)>=threshold )
59
60                      % An interval starts at this sample. Add a new row in
61                      % intervals and add the time in the six first columns.
62
63                      intervals(end+1,1:6) = data(i,1:6);
64                      above = 1;
65                  end
66              end
67          end
68
69      elseif( (data(i,7)<threshold) && above )
70
71          % An interval stops at this sample. Add the time to the six last
72          % columns in the last row.
73          intervals(end,7:12) = data(i,1:6);
74          above = 0;
75
76      elseif( all(data(i,1:6)==[0 0 0 0 0 0]) && above )
77
78          % if threshold = 0 the above mechanism to detect an end of the
79          % interval doesn't work since STK doesn't save samples with
80          % negative elevation, and hence all samples will have values >=0.
81          % Instead, STK saves a separator sample between every pass where
82          % all fields (year, etc.) are simply zero. When such an sample
83          % occur, and the above flag is still set, you know that the
84          % PREVIOUS sample was the last one.
85
86          intervals(end,7:12) = data(i-1,1:6);
87          above = 0;
88
89      end
90
91  end
```

C.3 plot_stk_elev.m

```
1   function plot_stk_elev(data)
2
3   N = size(data,1);
4
5   % Remove spurious elevations caused by a bug in STK
6   data = stk_remove_spurious(data);
7
8   % This line eliminates all rows that are filled with just zeros. They are
9   % separators to separate between the passes.
10  data(all(ismember(data,[0 0 0 0 0 0 0]),2),:)=[];
11
12  % Takes in the date vector (first six elements) and converts it to MATLABs
13  % serial date format.
14  time_axis = datenum(data(:,1:6));
15
16  plot(time_axis,data(:,7));
17  datetick('x','HH:MM');
18
19  end
```

C.4 stk_remove_spurious.m

```
1   function data = stk_remove_spurious(data)
```

```
% This function remove spurios spikes that STK produces due to a bug in the
% elevation angle at the beginning/end of a pass.

N = size(data,1);

% This is a logical vector (filled with ones and zeros) that indicate where
% there is an increase from a given sample to the next one.
increase = data(1:end-1,7)<data(2:end,7);

% This logical vector indicate where there is a decrease from a given
% sample to the next one.
decrease = [~increase; 0];

% Now it represents whether a given sample has increased w.r.t. the
% previous sample. I.e. if increase(34)==1 then data(34,7) is larger than
% the previous elevation, data(33,7).
increase = [0;increase];

% This is a logical vector representing all the separators
sep = all(ismember(data,[0 0 0 0 0 0 0]),2);

% These are logical vectors representing the samples before and after the
% separators
presep = [sep(2:end);0];
postsep = [0;sep(1:end-1)];

% This is a logical vector representing the elements where the sample
% before the separator increased w.r.t. the one before that. That is a
% spurious elevation angle, a bug from STK. We know that it is below 1, we
% will set it to 0 to fix it.
% spur = or(and(presep,increase),and(postsep,~increase));
spur = or(and(presep,increase),and(postsep,decrease));
data(spur,7)=0;

end
```

C.5 plot_data_down.m

```
% This is a script that plots the downloaded data per average day for
% different orbital heights and threshold elevation angles.

%clear all
close all

% SIMULATION INPUT GOES HERE (AND IN STK)
altitudes = [350 500 650];      % different orbital altitudes
thresholds = 0:90;              % different threshold elevation angles
zoom = 15:40;                   % Make a plot for these angles only
schemes = strvcat('r','g','b'); % Different plot colors (and dots etc.)

% D and I is hold the average kB downloaded during an average day and an
% average pass, respectively, for various altitudes and thresholds.
D = zeros(length(altitudes),length(thresholds));
I = D;

% Loads the data. If the variable already exist, the program will assume it
% is from the previous run, and save time by not loading it again. The
% "clear all" command at the top of the script must be commented for that.
if(~exist('data'))
    for i=1:length(altitudes)
        data{i}= read_stk_elev([num2str(altitudes(i)) 'c.txt']);
        disp(['Datafile for altitude ' num2str(altitudes(i)) ' km loaded.']);
    end
else
    disp(['Data already loaded. If not true; run "clear data".']);
end

for alt=1:length(altitudes)

    for thr=1:length(thresholds)

        intervals = threshold_stk_elev(data{alt},thresholds(thr));

        if(isempty(intervals))  % Elevation never passes threshold
            start=0;
            stop=0;
        else
            start = datenum(intervals(:,1:6));
            stop = datenum(intervals(:,7:12));
        end

```

```
44          duration_d = stop-start;        % This is the duration of the passes in ...
                days.
45          duration_h = duration_d*24;     % ... and in hours
46          duration_m = duration_h*60;     % ... and in minutes.
47          duration_s = duration_m*60;     % ... and in seconds.
48
49          T = sum(duration_s);    % Total duration of pass in seconds
50          N = size(intervals,1); % The number of passes during the
51                                 % simulation time (1 week)
52
53          R = 9600;          % Assuming bitrate of 9600 bps
54          W = R*T;           % Bits downloaded during simulation time (1 week)
55          W = (W/8)/1024; % W is now kB per week.
56          D(alt,thr) = W/7; % D is kB per average day.
57          I(alt,thr) = W/N; % I is kB download per average pass.
58
59      end
60
61      disp(['Simulation for altitude ' num2str(altitudes(alt)) ' km finished.']);
62
63  end
64
65  % Creating legends
66  legs = [];
67  for alt=1:length(altitudes)
68      legs = strvcat(legs,[num2str(altitudes(alt)) ' km']);
69  end
70
71  % Plot Data per Day
72  figure
73  hold on
74  grid on
75  for alt=1:length(altitudes)
76      plot(thresholds,D(alt,:),schemes(alt,:));
77  end
78  xlabel('Minimum Elevation Angle [degree]');
79  ylabel('Average Downlink Capacity [kB/day]');
80  % title('Average Data per Day for Different Criterea');
81  legend(legs);
82
83  % Plot Data per Day (with zoom)
84  first = find(thresholds==zoom(1));
85  last = find(thresholds==zoom(end));
86
87  figure
88  hold on
89  grid on
90  for alt=1:length(altitudes)
91      plot(thresholds(first:last),D(alt,first:last),schemes(alt,:));
92  end
93  xlabel('Minimum Elevation Angle [degree]');
94  ylabel('Average Downlink Capacity [kB/day]');
95  % title('Average Data per Day for Different Criterea');
96  legend(legs);
97  % a = [18,24,30];
98  % b = [D(1,19) D(2,25) D(3,31)];
99  a = [21,28,34];
100 b = [D(1,22) D(2,29) D(3,35)];
101 plot(a,b,'ok');
102
103 % Plot Data per Pass
104 figure
105 hold on
106 grid on
107 for alt=1:length(altitudes)
108     plot(thresholds,I(alt,:),schemes(alt,:));
109 end
110 xlabel('Minimum Elevation Angle [degree]');
111 ylabel('Average Downlink Capacity [kB/pass]');
112 % title('Average Data per (Usable) Pass for Different Criteria');
113 legend(legs);
```

D Pattern and S-parameter Tools

This appendix contains the MATLAB tools developed by the author to import files from network analysers and pattern measurements made with ANAUT (a SINTEF computer program) and plot them. These tools are used in Ch. 8 and Ch. 10. It utilizes *RF Utilities V1.2* by Neill Tucker which is available at the MATLAB Central. It also utilizes `polar2.m` by Daniel Aarmyr, also available at the MATLAB Central. Finally, it utilizes the `pattern_dipole.m` function from the link budget tool in App. E.

D.1 `import_ana.m`

```
function [angle,data] = import_ana(filename)
%IMPORT_ANA Summary of this function goes here
%   Detailed explanation goes here

fh = fopen(filename,'r');

% This variable holds which part of the file we're currently in
section = 'preamble';

% skip two empty lines and the date line
L = fgetl(fh);
L = fgetl(fh);
L = fgetl(fh);

% this line contains the number of samples (integer)
L = fgetl(fh);
N = sscanf(L,'%d');

% declare angle and data
angle = zeros(N,1);
data = zeros(N,1);

% this line says that now starts the angles values in degrees
L = fgetl(fh);

% read all the angles
for i=1:N
    L = fgetl(fh);
    scan = sscanf(L,'%f');
    angle(i) = scan(1,1);
end

% this line says that now starts the data values (and the frequency)
L = fgetl(fh);
```

```
35
36  % read all the data
37  for i=1:N
38      L = fgetl(fh);
39      scan = sscanf(L,'%f');
40      data(i) = scan(1,1);
41  end
42
43  fclose(fh);
44
45  end
```

D.2 import_s2p.m

```
1   function [S11,S21,S12,S22,Freq] = import_s2p(pathname)
2   % This file imports .s2p-files (2-port S-parameters).
3   %
4   % Usage: [S11,S21,S12,S22,Freq]= import_s2p(pathname)
5   %
6   % It is handy to use along with the RFutils pacakge by N.Tucker. RFutils
7   % already have a function, loads2p(), to load S-parameter files. However,
8   % loads2p() assumes that the S-parameters are stored as magnitudes and
9   % phase. This function assumes that the S-parameters are stored as real and
10  % imaginary parts (but none of the functions check the S-parameter files to
11  % verify it).
12  %
13  % Typically, an .s2p-file contains the following line:
14  %
15  %   # Hz S   RI   R 50
16  %
17  % which indicates that the frequency is given in Hz, that the file contains
18  % S-parameters, and that it stores real and imaginary (RI) parts. The
19  % reference impedance for the S-parameters is R=50 ohms. RI is replaced
20  % with MA if magnitude and phase is stored (then: use loads2p) and DB if
21  % magnitude in dB and phase is stored (then: create your own function).
22  %
23  % This function assumes that data starts on line 7.
24
25  fh=fopen(pathname,'r');
26  if fh~=(-1)
27      for i=1:6   % skip 6 lines
28          L=fgetl(fh);
29      end
30
31    Index = 1;
32    Freq=[0];
33    while L~=(-1);
34       L=fgetl(fh);
35       if L~=(-1);
36         SS=sscanf(L,'%f');
37
38         Freq(Index)=SS(1,1);
39
40         S11(Index)=SS(2,1)+1j*SS(3,1);
41         S21(Index)=SS(4,1)+1j*SS(5,1);
42         S12(Index)=SS(6,1)+1j*SS(7,1);
43         S22(Index)=SS(8,1)+1j*SS(9,1);
44
45         Index=Index+1;
46       end
47    end
48    fclose(fh);
49  end
50
51  end
52
53  %function [S11,S21,S12,S22,Freq]=loads2p(pathname)
54  % Load S2P file (2-Port)
55  %
56  % Usage: [S11,S21,S12,S22,Freq]=loads2p(pathname)
57  %
58  % The files need to be for a 2-port measurement saved with
59  % 'Data Only', 'ASCII' options set.
60  %
61  % e.g. [S11,S21,S12,S22,Freq]=loads2p('c:\matlab\toolbox\rfutils_s\data05.s2p')
62
63  % N.Tucker www.activefrance.com 2008
64
65  % fid_in=fopen(pathname,'r');
66  % if fid_in~=(-1)
67  %   fprintf('\nLoading S2P file %s\n\n',pathname);
```

```
%       L=fgetl(fid_in);
%       L=fgetl(fid_in);
%
%    Index=1;
%    L='dummy';
%
%    S11mag=[0];
%    S11pha=[0];
%
%    S21mag=[0];
%    S21pha=[0];
%
%    S12mag=[0];
%    S12pha=[0];
%
%    S22mag=[0];
%    S22pha=[0];
%
%    Freq=[0];
%    while L~=(-1);
%       L=fgetl(fid_in);
%       if L~=(-1);
%         SS=sscanf(L,'%f');
%
%         Freq(Index)=SS(1,1);
%
%         S11mag(Index)=SS(2,1);
%         S11pha(Index)=SS(3,1)*pi/180;
%
%         S21mag(Index)=SS(4,1);
%         S21pha(Index)=SS(5,1)*pi/180;
%
%         S12mag(Index)=SS(6,1);
%         S12pha(Index)=SS(7,1)*pi/180;
%
%         S22mag(Index)=SS(8,1);
%         S22pha(Index)=SS(9,1)*pi/180;
%
%         Index=Index+1;
%       end
%    end
%     S11=S11mag.*(cos(S11pha)+j*sin(S11pha));   % Convert S-param to complex form
%
%
%     S21=S21mag.*(cos(S21pha)+j*sin(S21pha));   % Convert S-param to complex form
%
%
%     S12=S12mag.*(cos(S12pha)+j*sin(S12pha));   % Convert S-param to complex form
%
%
%     S22=S22mag.*(cos(S22pha)+j*sin(S22pha));   % Convert S-param to complex form
%
%
%
%    fclose(fid_in);
% else
%     fprintf('\nError opening file, file not found.\n');
% end
```

D.3 pattern_meas.m

```
% Script that deals with antenna measurements

clear all;
close all;
clc;

% Loads all the measurements
% Horizontal source antenna
% XZ, YZ and XZ plane measurements

[angle,xz] = import_ana('./s2p/13.06.2012_ana/xz_H.ana');
[angle,yz] = import_ana('./s2p/13.06.2012_ana/yz_H.ana');
[angle,xy] = import_ana('./s2p/13.06.2012_ana/xy_H.ana');
% the variable angle is re-used since this is equal for all

% Computes Axial Ratio (actually this is not AR since the tilt is unknown)
i = find(angle==90);
a = xz(i);
b = yz(i);
AR = a/b;
```

```
21  disp('AR in linear scale:');
22  AR = AR^sign(AR-1) % AR is defined to be >=1. Invert if not.
23  disp('AR in dB:');
24  AR = 20*log10(AR)
25
26  % max gain in the whole measurement
27  maxg = max([max(xz) max(yz) max(xy)]);
28
29  % figure
30  % polar_dB(angle*pi/180,xz/maxg,12,3);
31  % figure
32  % polar_dB(angle*pi/180,yz/maxg,12,3);
33  % figure
34  % polar_dB(angle*pi/180,xy/maxg,6,2);
35
36  % Convert from amplitude to dB
37  xz = 20*log10(xz);
38  yz = 20*log10(yz);
39  xy = 20*log10(xy);
40  maxg = 20*log10(maxg);
41
42  figure
43  grid on;
44  hold on;
45  plot(angle,xz,'b');
46  axis([-180 180 -80 -45]);
47  plot(angle,yz,'g');
48  plot(angle,xy,'r');
49  legend('XZ','YZ','XY');
50  xlabel('Azimuth [degree]');
51  ylabel('Received Amplitude [dB]');
52
53  anglef = (-180:180);
54  ideal = pattern_dipole(angle,1,1);
55
56  figure
57  polar2(angle*pi/180,xz-max(xz),[-25 0]);
58  hold on
59  polar2(angle*pi/180,ideal,'r');
60
61  figure
62  polar2(angle*pi/180,yz-max(yz),[-25 0])
63  hold on
64  polar2(angle*pi/180,ideal,'r');
65
66  figure
67  polar2(angle*pi/180,xy-max(xy),[-6 0])
68
69  disp('Max deviations between measurement and ideal...');
70  disp('in XZ:');
71  diff = xz-ideal-max(xz);
72  diff(diff==Inf)=0;
73  max(diff)
74  disp('in YZ:');
75  diff = yz-ideal-max(yz);
76  diff(diff==Inf)=0;
77  max(diff)
```

D.4 plot_s_params.m

```
1   clear all;
2   close all;
3
4   base = 's2p/21.05.2012/VHF PCB/VHF Range/';
5
6   % Some parameters, such as S11 is actually measured several times.
7   % was is a "garbage" variable used where some S-parameter appears more than
8   % once.
9   [S11,S21,S12,S22,Freq]=import_s2p([base 'S21.s2p']);
10  [was,S31,S13,S33,Freq]=import_s2p([base 'S31.s2p']);
11  [was,S41,S14,S44,Freq]=import_s2p([base 'S41.s2p']);
12  [was,S51,S15,S55,Freq]=import_s2p([base 'S51.s2p']);
13
14  [was,S32,S23,was,Freq]=import_s2p([base 'S32.s2p']);
15  [was,S42,S24,was,Freq]=import_s2p([base 'S42.s2p']);
16  [was,S52,S25,was,Freq]=import_s2p([base 'S52.s2p']);
17
18  [was,S43,S34,was,Freq]=import_s2p([base 'S43.s2p']);
19  [was,S53,S35,was,Freq]=import_s2p([base 'S53.s2p']);
20
21  [was,S54,S45,was,Freq]=import_s2p([base 'S54.s2p']);
```

```
22
23  Zo = 50;
24
25  Z11 = s2z(S11,Zo);
26  Z22 = s2z(S22,Zo);
27  Z33 = s2z(S33,Zo);
28  Z44 = s2z(S44,Zo);
29  Z55 = s2z(S55,Zo);
30
31  x_ax=Freq*1e-6;
32
33  % Anonymous functions
34  dB = @(x)(20*log10(abs(x)));    % Converts S-parameter to dB
35  deg = @(x)(angle(x)*180/pi);    % Converts S-parameter to degree
36
37  phi23=deg(S31)-deg(S21);
38  phi34=deg(S41)-deg(S31);
39  phi45=deg(S51)-deg(S41);
40  phi52=deg(S21)-deg(S51);
41
42
43  figure
44  smith(1,Zo)
45  hold on
46  smdrawc(Z11,Zo,'r')
47  smdrawc(Z22,Zo,'g')
48  smdrawc(Z33,Zo,'b')
49  smdrawc(Z44,Zo,'k')
50  smdrawc(Z55,Zo,'m')
51  % title('S_{ii}-Parameters');
52  % legend('S_{11}','S_{22}','S_{33}','S_{44}','S_{55}');
53  % mfreq = 146e6;  % Marker frequency
54  % smarker1(Z11,Freq,Zo,mfreq,1);
55  % smarker1(Z22,Freq,Zo,mfreq,2);
56  % smarker1(Z33,Freq,Zo,mfreq,3);
57  % smarker1(Z44,Freq,Zo,mfreq,4);
58  % smarker1(Z55,Freq,Zo,mfreq,5);
59
60
61
62  % figure
63  % hold on
64  % grid on
65  % plot(x_ax,dB(S11_2),'r');
66  % plot(x_ax,dB(S11_3),'g');
67  % plot(x_ax,dB(S11_4),'b');
68  % plot(x_ax,dB(S11_5),'k');
69  % xlabel('Frequency [MHz]');
70  % ylabel('dB');
71  % title('Debugging. Check difference of S_{11}');
72  % legend('S_{11,2}','S_{11,3}','S_{11,4}','S_{11,5}');
73
74  figure
75  hold on
76  grid on
77  plot(x_ax,dB(S21),'r');
78  plot(x_ax,dB(S31),'g');
79  plot(x_ax,dB(S41),'b');
80  plot(x_ax,dB(S51),'k');
81  xlabel('Frequency [MHz]');
82  ylabel('dB');
83  % title('S_{n1}-Parameter Magnitudes');
84  legend('S_{21}','S_{31}','S_{41}','S_{51}');
85
86  figure
87  hold on
88  grid on
89  plot(x_ax,deg(S21),'r');
90  plot(x_ax,deg(S31),'g');
91  plot(x_ax,deg(S41),'b');
92  plot(x_ax,deg(S51),'k');
93  xlabel('Frequency [MHz]');
94  ylabel('degree');
95  % title('S_{n1}-Parameter Phases');
96  legend('S_{21}','S_{31}','S_{41}','S_{51}');
97
98  figure
99  hold on
100 grid on
101 plot(x_ax,dB(S11),'r');
102 plot(x_ax,dB(S22),'g');
103 plot(x_ax,dB(S33),'b');
104 plot(x_ax,dB(S44),'k');
105 plot(x_ax,dB(S55),'m');
106 xlabel('Frequency [MHz]');
107 ylabel('dB');
108 % title('Matching');
109 legend('S_{11}','S_{22}','S_{33}','S_{44}','S_{55}');
110
111 figure
```

```
112  hold on
113  grid on
114  plot(x_ax,dB(S23),'r');
115  plot(x_ax,dB(S24),'g');
116  plot(x_ax,dB(S25),'b');
117  plot(x_ax,dB(S34),'k');
118  plot(x_ax,dB(S35),'m');
119  plot(x_ax,dB(S45),'c');
120  xlabel('Frequency [MHz]');
121  ylabel('dB');
122  % title('Isolation');
123  legend('S_{23}','S_{24}','S_{25}','S_{34}','S_{35}','S_{45}');
124
125  figure
126  hold on
127  grid on
128  plot(x_ax,phi23,'r');
129  plot(x_ax,phi34,'g');
130  plot(x_ax,mod(phi45,360)-360,'b');
131  plot(x_ax,mod(phi52,360)-360,'k');
132  xlabel('Frequency [MHz]');
133  ylabel('degree');
134  % title('Phase-Difference Between Ports (\phi_{ij})');
135  legend('\phi_{23}','\phi_{34}','\phi_{45}','\phi_{52}');
```

E Link Budget Tool

This appendix contains the MATLAB tools developed by the author during the work with [4] in order to dynamically simulate the link margin as explained in Ch. 3. The simulations perfomed of link margin for varying height, however, is new and is found in the file `master_thesis_elevations.m`. Some of the files utilizes `polar_dB.m` from Hakan Cakan, available from the MATLAB Central.

E.1 `master_thesis_elevations.m`

```
1
2   clear all
3   close all
4   clc
5
6   import\_link\_vars('link\_data.txt','UHF','Downlink');
7
8   h = [400 600 800]*1e3;                          % Heights
9   h = [350 500 650]*1e3;                          % Heights
10  t = 0:1000;                                     % Time after rise [s]
11
12  for i=1:3
13
14      adcs\_acc = 10;                                  % Accuracy of ADCS [degree]
15      % neglect for now
16
17      el = elevation\_vs\_time(t,h(i));                 % Elevation [degree]
18      los = los\_vs\_elevation(el,h(i));               % Line-of-sight distance [m]
19      theta = offset\_angle\_vs\_elevation(el,h(i)); % Antenna offset-angle [degree]
20      theta = theta + adcs\_acc;                      % Add ADCS uncertainty [degree]
21
22      % DIPOLE
23
24      % Replace Link Budget variables
25      L\_plf = 3;
26      L\_tx\_pnt = 0;                                   % Included in G\_tx
27      G\_tx = pattern\_dipole(theta,true,true);        % Diagram (normalized)
28      G\_tx = G\_tx+2.15;                              % De-normalize
29      L\_fspl = fspl\_vs\_los(los,f);                   % FSPL [dB]
30      L\_atm = atmloss\_vs\_elevation(el,f);            % Atmospheric losses [dB]
31      L\_ion = 0;                                     % Ionospheric losses [dB]
32                                                    % Ionosph. are included
33                                                    % in atm
34
35      exec\_link\_budget;   % dipole
36
37      E\_LM\_snr(1,i,:) = LM\_snr;
38      E\_LM\_ebno(1,i,:) = LM\_ebno;
```

```
39
40      % MONOPOLE
41
42      G = import\_far\_field('monopole\_with\_virtual\_gnd.txt');
43      phi = 6;    % worst case phi
44
45      % Replace Link Budget variables
46      L\_plf = 0;  % NB: Monopole has 3 dB PLF but this is not quite monopole so ...
            circular gain is used instead
47      G\_tx = G(180-round(theta)+1,phi+1,4);           % Extracting RHCP gain vs. ...
            time
48      G\_tx = G\_tx.';
49
50      exec\_link\_budget;   % monopole
51
52      E\_LM\_snr(2,i,:) = LM\_snr;
53      E\_LM\_ebno(2,i,:) = LM\_ebno;
54
55      % TURNSTILE
56
57      G = import\_far\_field('second\_attempt\_far\_field.txt');
58      phi = 45;    % worst case phi
59
60      % Replace Link Budget variables
61      L\_plf = 0;                                          % Using circular gain instead
62      G\_tx = G(round(theta)+1,phi+1,4);                   % Extracting RHCP gain vs. time
63                                                  % Note that what points down for
64                                                  % this is 0 degree.... LHCP is at
65                                                  % 180 degree, but it doesn't
66                                                  % matter
67      G\_tx = G\_tx.';
68
69      exec\_link\_budget;   % monopole
70
71      E\_LM\_snr(3,i,:) = LM\_snr;
72      E\_LM\_ebno(3,i,:) = LM\_ebno;
73      E\_el(i,:) = el;
74
75
76      % MONOPOLE (THEORETICAL)
77
78      % Replace Link Budget variables
79      L\_plf = 3;
80      L\_tx\_pnt = 0;                                       % Included in G\_tx
81      G\_tx = pattern\_dipole(theta,false,true);           % Diagram (normalized)
82      G\_tx = G\_tx+2.15;                                  % De-normalize
83      L\_fspl = fspl\_vs\_los(los,f);                      % FSPL [dB]
84      L\_atm = atmloss\_vs\_elevation(el,f);               % Atmospheric losses [dB]
85      L\_ion = 0;                                          % Ionospheric losses [dB]
86                                                  % Ionosph. are included
87                                                  % in atm
88
89      exec\_link\_budget;   % monopole (theoretical)
90
91      E\_LM\_snr(4,i,:) = LM\_snr;
92      E\_LM\_ebno(4,i,:) = LM\_ebno;
93  end
94
95
96  figure
97  hold on
98  plot(E\_el(1,:),squeeze(E\_LM\_ebno(3,1,:)),'r');
99  plot(E\_el(2,:),squeeze(E\_LM\_ebno(3,2,:)),'g');
100 plot(E\_el(3,:),squeeze(E\_LM\_ebno(3,3,:)),'b');
101 xlabel('Elevation Angle [degree]');
102 ylabel('Link Margin (Eb/No) [dB]');
103 axis([0 90 -10 30]);
104 legend('350 km','500 km','650 km');
105 grid on
106
107 for i=1:3   % Prints the elevation when LM>10dB for all altitudes
108     vec = E\_LM\_ebno(3,i,:);
109     ind = find(vec>10,1);
110     E\_el(i,ind)
111 end
```

E.2 offset_angle_vs_elevation.m

```
1  function theta = offset_angle_vs_elevation(el,h)
2
3      constants;
```

```
4
5       if(nargin<2)
6           h = h_default;
7       end
8
9       theta = asin((Re/(Re+h))*cos(el*pi/180))*180/pi;
10
11  end
```

E.3 link_data.txt

Variable Name	UHF Down	UHF Up	VHF Down	VHF Up	BEACON Down	BEACON Up	UNIT	DESCRIPTION
f	437.45	437.5	145.8	145.8	437.45	437.5	MHz	Carrier frequency
A_el	20	20	20	20	5	5	degree	Assumed elevation angle throughout calculations
A_h	800	800	800	800	800	800	km	Assumed height above ground the satellite will orbit in
P_tx_w	0.5	75	0.2	100	0.1	75	W	Transmitted power (in linear scale)
L_tx_tl	1.1	7.4	1.3	4.9	1.1	7.4	dB	Transmitter transmission line losses
G_tx	2.2	16	2.2	13.1	2.2	16	dBi	Transmitter antenna gain
L_tx_pnt	0.1	0.3	0.1	0.3	0.1	0.3	dB	Transmitter antenna misalignment/pointing loss
L_plf	3	3	3	3	3	1.9	dB	Polarization loss factor (PLF)
L_fspl	150.2	150.2	140.7	140.7	154.2	154.2	dB	Free-Space Loss (FSPL)
L_atm	1.1	1.1	1.1	1.1	2.1	2.1	dB	Atmospheric loss (gases etc.)
L_ion	0.4	0.4	0.7	0.7	0.4	0.4	dB	Ionospheric loss
L_rain	0	0	0	0	0	0	dB	Rain loss
L_rx_pnt	0.1	0.1	0.1	0.1	0.1	0.1	dB	Receiver antenna misalignment/pointing loss
G_rx	16	2.2	13.1	2.2	16	2.2	dBi	Receiver antenna gain
L_rx_tl	2.8	1.3	2.3	1.3	2.8	1.3	dB	Receiver transmission line losses
T	337	310	574	461	337	310	K	Effective Noise Temperature in receiver
R	9600	9600	9600	9600	100	9600	bps	Data rate
B	15	25	15	25	1.2	25	kHz	Spectral (noise) bandwidth in receiver
EbNo_thr	14.8	14.8	13.8	14.8	14.8	14.8	dB	Required/minimum/threshold Eb/No
SNR_thr	14.8	14.8	13	14.8	14.8	14.8	dB	Required/minimum/threshold S/N

```
Syntax:
    Everything between the two bars are interpreted as variables, and the
    rest as comments. The following syntax is used for the variable names:
        f - Frequency
        P - Power
        L - Loss
        G - Gain
        T - Temperature
        R - Datarate
        B - Bandwidth
        A - Parameters that are assumed to be something
        SNR - Signal-to-noise ratio
        EbNo - Bit-energy-to-noise-density ratio
    Moreover descriptive subscripts are used to further specify what it is.
    The following abbreviations are common:
        rx - receiver
        tx - transmitter
    For downlink the spacecraft is the transmitter and the ground station
    is the receiver. Note that for the uplink it's the other way around.

Note:
    This document is made to be conformal with the official NUTS' link
    budgets, meaning that all variables might not be up to date. In
    particular, the BEACON Uplink budget is not in use.
```

E.4 exec_link_budget.m

```
%
% SIGNAL PATH
%

P_tx = 10*log10(P_tx_w);                % Transmitted Power [dBW]

P_eirp ...                              % EIRP [dBW]
    = P_tx ...                          % Transmitted Power [dBW]
    - L_tx_tl ...                       % TX Transmission Line Losses [dB]
    + G_tx;                             % TX Antenna Gain [dBi]

P_rx_iso ...                            % Isotropically Received Power  [dBW]
    = P_eirp ...                        % EIRP [dBW]
    - L_tx_pnt ...                      % TX Pointing Loss [dB]
    - L_rain ...                        % Rain Loss [dB]
    - L_fspl ...                        % FSPL [dB]
    - L_plf ...                         % PLF [dB]
    - L_atm ...                         % Atmospheric Loss [dB]
    - L_ion;                            % Ionospheric Loss [dB]

P_rx ...                                % Received Power [dBW]
    = P_rx_iso ...                      % Isotropically Received Power [dBW]
    + G_rx ...                          % RX Antenna Gain [dBi]
    - L_rx_pnt ...                      % RX Pointing Loss [dB]
    - L_rx_tl;                          % RX Transmission Line Losses [dB]

%
% NOISE PATH
%

K = -228.6;                             % Boltzman's constant [dBW/K/Hz]
T_db = 10*log10(T);                     % Effective Noise Temperature [dBK]
B_db = 10*log10(B);                     % RX (Noise) Bandwidth [dBHz]

No ...                                  % Noise density [dBW/Hz] (No=kT)
    = K ...                             % Boltzman's constant [dBW/K/Hz]
    + T_db;                             % Effective Noise Temperature [dBK]

N ...                                   % Received Noise Power [dBW] (N = kTB)
    = No ...                            % Noise density [dBW/Hz]
    + B_db;                             % RX (Noise) Bandwidth [dBHz]

%
% SNR
%

SNR = P_rx - N;                         % Signal-to-Noise ratio [dB]
LM_snr = SNR - SNR_thr;                 % Link Margin (in SNR) [dB]

%
% Eb/No
%

R_db = 10*log10(R);                     % Data rate [dBHz]

SNo = P_rx - No;                        % Signal-to-noise-density ratio [dBHz]
EbNo = SNo - R_db;                      % Bit-energy-to-noise-density ratio [dB]
LM_ebno = EbNo - EbNo_thr;              % Link Margin (in Eb/No) [dB]

%
% G/T
%

GT = G_rx - L_rx_tl - T_db;             % G/T - Figure of Merit
```

E.5 import_vars.m

```
function import_vars(fname,column)
% import_vars(fname,column)
%
% This function is primarily written for importing link budget parameters
% but can be used in a more generic manner as-is.
%
% fname is the name of the file to be imported.
%
```

```
% The file can have several sections separated by lines of ==========
% The variables are stored in the 2nd section like this:
%
% Header Comments (myfile.txt)
%       Set 1   Set 2   Set 3
% ================================
% cool  100     200     300
% fun   40.4    5.5     6e3
% ================================
% Footer Comments
%
% The column argument is which column to import as the variable's values.
% In our example, import_vars('myfile.txt',2) will be equivalent to writing
%   cool = 200;
%   fun = 5.5;
%

% Create the regexp pattern that extracts the variable name and value
pattern = '%s';                             % Extract var. name
for i=1:column-1
    pattern = strcat(pattern,' %*f');       % Ignore (column-1) values
end
pattern = strcat(pattern,' %f');            % Extract column value

section = 1;        % Which section of file.
                    % Each section is seperated by =======

fh = fopen(fname);
while 1
    fline = fgetl(fh);

    if(fline==-1)       % End-of-file
        fclose(fh);
        break;
    end

    if(length(fline)>0)

        if(fline(1)=='=')
            section = section + 1;   % Section separation detected
        else

            if(section==2)           % This is where the variables are at
                A = textscan(fline,pattern,'MultipleDelimsAsOne',true);
                varname = A(1);
                varvalue = A(2);
                varname = varname{1}{1};
                varvalue = varvalue{1};
                varvalue = varvalue(1);
                evalin('caller', strcat(varname,'=',num2str(varvalue),';'));
            end

    end
end

end

end
```

E.6 import_link_vars.m

```
function import_link_vars(fname,band,dir)
%
% import_link_vars(fname,column)
% import_link_vars(fname,band,dir)
%
% Imports the link budget variables from the file 'fname' to the workspace.
% The variables B, A_h and f are converted to SI units such that all
% variables are stored to workspace with SI units.
%
% One can specify which column (1-6) to load from the file manually or one
% can specify which band and what direction of the link one wants to use in
% the input parameters 'band' and 'dir'.
% The possible values are:
%
% Bands: 'UHF','VHF','Beacon'
% Directions: 'U','Up','Uplink' or 'D','Down','Downlink'
%
% The values are case-insensitive
%
% The columns have the following settings:
```

```
21  %    1.  UHF Downlink
22  %    2.  UHF Uplink
23  %    3.  VHF Downlink
24  %    4.  VHF Uplink
25  %    5.  Beacon Downlink
26  %    6.  Beacon Uplink
27  %
28
29      column = 0;
30
31      if(nargin==2)       % column is specified
32
33          column = band;
34
35      elseif(nargin==3)   % band and direction is specified, determine column
36
37          switch(upper(band))
38              case 'UHF'
39                  column = 1;
40              case 'VHF'
41                  column = 2;
42              case 'BEACON'
43                  column = 3;
44              otherwise
45                  error('Invalid link budget band. Must be UHF, VHF or Beacon.');
46          end
47
48          column = column*2;
49
50          switch(upper(dir))
51              case {'UP','UPLINK','U'}
52              case {'DOWN','DOWNLINK','D'}
53                  column = column-1;
54              otherwise
55                  error('Invalid direction. Must be uplink or downlink.');
56          end
57
58      else
59          error('Invalid number of arguments in.');
60      end
61
62      column = num2str(column);
63
64      % Load variables into callers workspace (WS)
65      evalin('caller',strcat('import_vars(''',fname,''',',column,')'));
66
67      % Variables in the link data files are not all in SI-units.
68      % Convert them to SI-units.
69
70      evalin('caller','f = f*1e6;');       % MHz -> Hz
71      evalin('caller','A_h = A_h*1e3;');   % km -> m
72      evalin('caller','B = B*1e3;');       % kHz -> Hz
73
74  end
```

E.7 `obtain_directivity.m` and the Ideal Antenna

This function is used to determine the directivity of an antenna once the pattern is known. In [4], the theoretically ideal pattern for NUTS was derived using this function. The ideal antenna can be defined as one that yields constant link margin versus elevation angle, above a certain threshold elevation angle, i.e. 10°. To compute the pattern of this antenna, first, the link margin as a function of elevation angle is determined for an isotropic radiator. An arbitrarily chosen constant link margin minus the isotropic link margin is then the difference that must be accounted for by the ideal antenna. Choosing the z-axis towards nadir, the link margin difference may be mapped from elevation angle to θ-angle and the pattern of the ideal antenna is then determined. The directivity can then be obtained from this function. This was done in [4] and the ideal pattern is shown in Fig. E.1. Unfortunately, it is impossible to synthesize this pattern. For more details, see [4].

And then the explanation of the function: From [26] it is known that the total

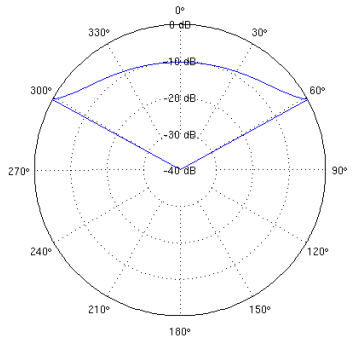

Figure E.1: The ideal antenna pattern (normalized to 0 dB)

power radiated by an antenna can be written:

$$P_{\text{rad}} = \oint_S \mathbf{W}_{\text{rad}} \cdot \mathrm{d}\mathbf{s} = \oint_\Omega U \, \mathrm{d}\Omega \qquad [W] \quad \text{(E.1)}$$

Further on, the directivity can be expressed [26]:

$$D(\theta, \phi) = \frac{U}{U_0} = \frac{4\pi U}{P_{\text{rad}}} \qquad \text{(E.2)}$$

Assume that $D(\theta, \phi) \propto F(\theta, \phi)$ where the shape F is known but not D, i.e. the scaling factor is not known. As $D \propto U$ one can write $U(\theta, \phi) = B_0 F(\theta, \phi)$ where B_0 is unknown. Using (E.1), (E.2) and removing B_0 both in the numerator and in the denominator:

$$D(\theta, \phi) = \frac{4\pi}{\oint_\Omega F(\theta', \phi') \, \mathrm{d}\Omega} F(\theta, \phi) \qquad [\,] \quad \text{(E.3)}$$

Hence, the only thing that needs to be done is to determine the integral S in the denominator, and the directivity has been determined. This is easily done with the trapezoidal rule well known from fundamental calculus [48], where the function is split to several segments and the area of each segment is approximated by a trapezoidal. F and D is further assumed to be independent of ϕ.

$$\begin{aligned} S &= \int_0^{2\pi} \int_0^{\pi} F(\theta) \sin\theta \, \mathrm{d}\theta \, \mathrm{d}\phi \\ &\approx \pi \Delta\theta \sum_{n=1}^{N} \left[F(n\Delta\theta) \sin(n\Delta\theta) + F((n-1)\Delta\theta) \sin((n-1)\Delta\theta) \right] \end{aligned} \qquad \left[\frac{\mathrm{W}}{\mathrm{sr}}\right] \quad \text{(E.4)}$$

where

$$\Delta\theta = \frac{\pi}{N} \qquad [\text{rad}] \quad \text{(E.5)}$$

The trapezoidal approximation yield an error of $\mathcal{O}(\Delta\theta^2)$[48]. The method has been implemented in `obtain_directivity()` and verified by determining the directivity for a dipole. A similar approach is done in [26] which does not approximate integration by sum of a trapezoidal, but by a sum of squares.

```
function D = obtain_directivity(F,theta,varargin)
% Given a function F(theta) that uniquely determine the shape of the
% pattern, but not its scale the obtain_directivity() function can
% numerically "normalize" F(theta) and return the directivity D(theta).
%
% D = obtain_directivity(F,theta)
%
% theta is a vector containing all the theta values. This is assumed to be
% linearly spaced elements running from 0 to 180 degrees. The lowest must
% be 0 and the highest must be 180. F is a vector of the same size that
% describes the shape of the pattern for the corresponding thetas. D will
% be a vector of directivity also corresponding to different thetas. The
% function is not implemented for functions F(theta,phi) only F(theta).
%
% F and D are in decibels

% Which numerical method to use. Using midpoint rule or trapezoidal rule
% results in O(n^2) error. I expect using function evaluations at trailing
% edge has slightly lower accuracy (but maybe still O(n^2)). Using midpoint
% rule means that function evaluations are not at same place as integration
% limits. Therefore I implemented trapezoidal rule which is not mentioned
% in Balanis.
method = 'trapezoidal';

for i=1:length(varargin)
    if(isequal(varargin{i},'trailing'))
        method = 'trailing';
    end
    if(isequal(varargin{i},'midpoint'))
        error('midpoint rule note implemented');
    end
end

if(isequal(method,'trapezoidal'))

    F = 10.^(F./10);        % Linear scale
    theta = theta*pi/180;   % Radians

    delta_theta = theta(2)-theta(1);
    %N = numel(theta)-1; % not needed

    f = F.*sin(theta);

    S = sum(f(2:end)+f(1:end-1))*delta_theta;

    D = (4/S)*F;

    D = 10*log10(D);        % dB scale

end

if(isequal(method,'trailing'))

    F = 10.^(F./10);        % Linear scale
    theta = theta*pi/180;   % Radians

    delta_theta = theta(2)-theta(1);
    %N = numel(theta)-1; % not needed

    f = F.*sin(theta);

    S = sum(f)*delta_theta;

    D = (2/S)*F;

    D = 10*log10(D);        % dB scale

end
```

E.8 `elevation_vs_time.m` and Time-Elevation Relation for the Perfect Pass

As a simplification, a perfect pass is assumed, i.e. that the rotation of the Earth is negligible during the time the satellite is visible, and it that the satellite would pass exactly through zenith. Then, defining a time t as the time since the satellite ascended the horizon at 0° elevation, it was derived the following relation in [4]:

$$t(\varepsilon) = \sqrt{\frac{(R_E+h)^3}{\mu}}\left[\arccos\left(\frac{R_E}{R_E+h}\right) + \varepsilon + \arcsin\left(\frac{R_E}{R_E+h}\cos\varepsilon\right) - \frac{\pi}{2}\right] \quad [\text{s}] \tag{E.6}$$

where n is the angular velocity given by:

$$n = \sqrt{\frac{\mu}{(R_E+h)^3}} \quad \left[\frac{\text{rad}}{\text{s}}\right] \tag{E.7}$$

and where $\mu = 398000.4418\,\text{km}^3/\text{s}^2$ [4, 9] is the gravitational parameter of the Earth, and ε is allowed to be greater than 90° (or $\pi/2$ radians in the formula) to represent a descending satellite.

The function of time versus elevation angle is implemented in `time_vs_elevation.m`, also found in this appendix. The function $t = f(\varepsilon)$ as given in (E.6) is, however, not analytically solvable for ε. It is, however, seen to be strictly monotonically increasing for $\varepsilon \in [0, \pi]$ (remember that ε is defined to go above 90° for descending elevation angles), meaning that

$$\varepsilon_a > \varepsilon_b \Leftrightarrow f(\varepsilon_a) > f(\varepsilon_b) \tag{E.8}$$

Thence, for a given t, start iteration in the middle of the range, with $\varepsilon_0 = \pi/2$ as the inital value. The maximum possible error at this step is naturally $e_0 = \pi/2$, half of the range. Compute $t_0 = f(\varepsilon_0)$ and set the stepsize to $\Delta_1 = \pi/4$. If $t > t_0$ then $\varepsilon > \varepsilon_0$ and ε must be in the upper half of the range. Move it to the middle of this half by *adding* the stepsize. If t is not greater than t_0 then the ε should be moved to the middle of the lower half of the range by *subtracting* the stepsize:

$$\varepsilon_i = \begin{cases} \varepsilon_{i-1} + \Delta_i & \text{if } t > t_{i-1} \\ \varepsilon_{i-1} - \Delta_i & \text{if } t \leq t_{i-1} \end{cases} \quad [\text{rad}] \tag{E.9}$$

For each iteration the interval in which the true ε can be shrinks to half of the previous, hence the name step-halving. The values of the stepsize for, and error after iteration i follows intuitively:

$$\Delta_i = \frac{\Delta_{i-1}}{2} \quad [\text{rad}] \tag{E.10}$$

$$e_i = \frac{e_{i-1}}{2} = \Delta_i \quad [\text{rad}] \tag{E.11}$$

This has been implemented in `elevation_vs_time()`. Note that the function iterates each entry in a vector simultaneously so that the function is compatible with vector inputs.

```
function el = elevation_vs_time(t,h)
% This function returns elevation as function of time. If possible, it's
% better to use time_vs_elevation as this one simply iterates that function
% until a solution is found. The accuracy of iteration is 1e-5. The time
% is zero at elevation 0 and increasing towards the maximum.

if(nargin<2)
    h = 600e3;
end

t_lower = 0;
t_middle = time_vs_elevation(90,h);
t_upper = time_vs_elevation(180,h);

% if(min(t)<t_lower || max(t)>t_upper)
%     error('t is out of bounds');
% end

% Initially, start with an elevation of 90 degrees. The first output from
% time_vs_elevation is monotonously increasing with input el from 0 to 180
% degrees where 90 to 180 degrees represent the downward track. If the same
% convention is adopted here, we have a monotonously increasing function
% and can use the principle of halving the step each time. That is,
% Initially we set el=90 and the elevation time step to 45. Then
% time_vs_elevation is used to compute t_it which is the time that
% correspond to el. If t>t_it then el>90 and we increment el by the time
% step. If t<t_it then el<90 and we decrement el by the time step. For the
% next iteration the time step is halved. In such a manner the region where
% el has to be is halved each iteration until sufficient accuracy is met.
% Notice that the true elevation has to be within 2*el_step away from the
% current positon.

el = 90;
el_step = 45;
converged = false;
accuracy = 1e-10;    % accuracy in degree

% A factor 4 because the true elevation is within 2*el_step of the current
% iteration. el_step has already been prepared for next iteration here.
while(4*el_step>accuracy)

    t_it = time_vs_elevation(el,h);

% The commented way doesn't work on several values at once (vectors) but is
% left as an overview as it is easier to understand.

%     if(t>t_it)
%         el = el + el_step;
%     else
%         el = el - el_step;
%     end

% In the case of several elevations to find, all arranged in a vector, a
% sign vector is created to decide in which direction each element should
% iterate.

    sign = (t>t_it)*2-1;
    el = el + sign*el_step;

    el_step = el_step/2;

end

% Elevations above 90 are not physical but correspond to decsending part of
% the pass. Wrap it to the physical elevation.

% Again this doesn't work for vectors
% if(el>90)
%     el = 180-el;
% end

% Here's the vector solution

el(el>90) = 180-el(el>90);

% Force elevation to zero where t is out of bounds
el(t>t_upper) = 0;
el(t<t_lower) = 0;
```

E.9 time_vs_elevation.m

```
function el = elevation_vs_time(t,h)
% This function returns elevation as function of time. If possible, it's
% better to use time_vs_elevation as this one simply iterates that function
% until a solution is found. The accuracy of iteration is 1e-5. The time
% is zero at elevation 0 and increasing towards the maximum.

if(nargin<2)
    h = 600e3;
end

t_lower = 0;
t_middle = time_vs_elevation(90,h);
t_upper = time_vs_elevation(180,h);

% if(min(t)<t_lower || max(t)>t_upper)
%     error('t is out of bounds');
% end

% Initially, start with an elevation of 90 degrees. The first output from
% time_vs_elevation is monotonously increasing with input el from 0 to 180
% degrees where 90 to 180 degrees represent the downward track. If the same
% convention is adopted here, we have a monotonously increasing function
% and can use the principle of halving the step each time. That is,
% Initially we set el=90 and the elevation time step to 45. Then
% time_vs_elevation is used to compute t_it which is the time that
% correspond to el. If t>t_it then el>90 and we increment el by the time
% step. If t<t_it then el<90 and we decrement el by the time step. For the
% next iteration the time step is halved. In such a manner the region where
% el has to be is halved each iteration until sufficient accuracy is met.
% Notice that the true elevation has to be within 2*el_step away from the
% current positon.

el = 90;
el_step = 45;
converged = false;
accuracy = 1e-10;    % accuracy in degree

% A factor 4 because the true elevation is within 2*el_step of the current
% iteration. el_step has already been prepared for next iteration here.
while(4*el_step>accuracy)

    t_it = time_vs_elevation(el,h);

% The commented way doesn't work on several values at once (vectors) but is
% left as an overview as it is easier to understand.

%     if(t>t_it)
%         el = el + el_step;
%     else
%         el = el - el_step;
%     end

% In the case of several elevations to find, all arranged in a vector, a
% sign vector is created to decide in which direction each element should
% iterate.

    sign = (t>t_it)*2-1;
    el = el + sign*el_step;

    el_step = el_step/2;

end

% Elevations above 90 are not physical but correspond to decsending part of
% the pass. Wrap it to the physical elevation.

% Again this doesn't work for vectors
% if(el>90)
%     el = 180-el;
% end

% Here's the vector solution

el(el>90) = 180-el(el>90);

% Force elevation to zero where t is out of bounds
el(t>t_upper) = 0;
el(t<t_lower) = 0;
```

E.10 atmloss_vs_elevation.m

```
function losslist = atmloss_vs_elevation(el,f)

ellist = el;
for i=1:length(el)
    el = ellist(i);
    % IONOSPHERE

    % Given preset values:
    % 146 MHz - 0.7 dB
    % 438 MHz - 0.4 dB
    % 2410 MHz - 0.1 dB

    list_f = [146e6 438e6 2410e6];
    list_loss = [0.7 0.4 0.1];

    % Eventhough the function is not known they are just linearly interpolated
    % for these frequencies for simplicity.

    % a and b are indices for values to interpolate between
    a=find(list_f<f,1,'last');
    b=find(list_f>=f,1,'first');

    if(f<list_f(1))
        loss = list_loss(1);
    elseif(f>list_f(end))
        loss = list_loss(end);
    else
        slope = (list_loss(b)-list_loss(a))/(list_f(b)-list_f(a));
        loss = list_loss(a)+slope*(f-list_f(a));
    end
    losstemp = loss;

    % ATMOSPHERIC GASES

    % Given preset values

    list_el = [0 2.5 5 10 30 45 90];
    list_loss = [10.2 4.6 2.1 1.1 0.4 0.3 0];

    % a and b are indices for values to interpolate between
    a=find(list_el<el,1,'last');
    b=find(list_el>=el,1,'first');

    if(el<=list_el(1))
        loss = list_loss(1);
    elseif(el>list_el(end))
        loss = list_loss(end);
    else
        slope = (list_loss(b)-list_loss(a))/(list_el(b)-list_el(a));
        loss = list_loss(a)+slope*(el-list_el(a));
    end

    loss = loss+losstemp;
    losslist(i) = loss;
end

end
```

E.11 fspl_vs_los.m

```
function fspl = fspl_vs_los(l,f,varargin)
%
% Free-space loss (FSPL) (dB is default) versus line-of-sight (LOS)
% distance (in meters).
%
% SYNTAX:
%   fspl = fspl_vs_los(l,f)
%   fspl = fspl_vs_los(l,f,'lin')
%
% l      - line-of-sight (LOS) distance [m]
% f      - frequency [Hz]
% 'lin' - keyword to get FSPL in linear scale instead of dB
%
% l can be a vector of different distances. Then fspl will also be a vector
% of the corresponding FSPLs.
```

```
16 %
17 % Author: Sigvald Marholm
18 % Copyright: 04.11.2011
19 %
20
21 constants;
22
23 % Keyword parser
24 linscale = false;
25 for i=1:length(varargin)
26     if(isequal(varargin{i},'lin'))
27         linscale = true;
28     end
29 end
30
31 if(linscale)
32     fspl = (4*pi.*l.*f./c_0).^2;
33 else
34     fspl = 20*log10(l)+20*log10(f)-147.5522167781166;
35 end
36
37 end
```

E.12 los_vs_elevation.m

```
1  function l = los_vs_elevation(el,h)
2  %
3  % Line-of-sight (LOS) distance (in meters) versus elevation angle (in
4  % degrees). Assuming circular orbit (or constant altitude).
5  %
6  % SYNTAX:
7  %   l = los_vs_elevation(el)
8  %   l = los_vs_elevation(el,h)
9  %
10 % h     - height/altitude of satellite [m] (default: 600e3)
11 % el    - elevation angle [degree]
12 %
13 % el can be a vector of different elevation angles. Then l will also be a
14 % vector of the corresponding line-of-sight distances.
15 %
16 % Author: Sigvald Marholm
17 % Copyright: 04.11.2011
18 %
19
20 constants;
21
22 if(nargin<2)
23     h=h_default;
24 end
25
26 el = el*pi/180;
27
28 l = sqrt( (Re*sin(el)).^2 + 2*Re*h + h.^2 ) - Re*sin(el);
29
30 end
```

E.13 pattern_dipole.m

```
1  function U = pattern_dipole(theta,varargin)
2  % Returns the radiation intensity U of a dipole (not normalized)
3  %
4  %   Possible inputs:
5  %   theta - the theta direction of the intensity (radians)
6  %   zaxis - Use the z-axis in the nadir-direction? (true/false)
7  %   length - length of dipole in number of wavelength (default: 0.5)
8  %
9  %   Usually the z-axis for a dipole antenna is oriented along its minima
10 %   and theta=90 is at its maxima. The offset angle is referred to nadir
11 %   such that an offset of 0 degree is at maxima. By setting z-axis=true
12 %   theta is rotated such that theta=0 at pattern maxima. And theta can be
13 %   set equal to the offset angle. Default behaviour is, false, the
14 %   standard in antenna theory. If it is set to true then z-axis will will
15 %   point in nadir such that when theta~=0 then the pattern will actually
```

```
16  %   depend upon another variable phi. This variable is not taken care off
17  %   and the worst case is assumed.
18
19  % Handling optional arguments
20  optargs = {false, false, 0.5};                  % default arguments
21  newvals = cellfun(@(x) ~isempty(x), varargin);  % get indices to non-empty ...
        arguments
22  optargs(newvals) = varargin(newvals);           % replace default values
23  [zaxis, db, length] = optargs{:};               % store in variables
24
25  if(zaxis)   % Use nadir as z-axis (theta=0)
26      theta = theta + 90;
27  end
28
29  theta = theta*pi/180;   % convert to rad
30
31  kl = 2*pi*length;
32
33  U = ((cos( (kl/2)*cos(theta) ) - cos( (kl/2) ))./sin(theta)).^2;
34
35  U(theta==0) = 0;     % Set U=0 for elements where theta=0 due to 0/0-expression ...
        which returns NaN
36
37  if(db)
38      U = 10*log10(U);
39  end
40
41  end
```

E.14 import_far_field.m

```
1   function A = import_far_field(fname)
2   % A = import_far_field(fname)
3   %
4   % Assume that file is exported from CST in 3D with one degree separation in
5   % data points both in theta and phi directions.
6   %
7   % A will be an array which contains the whole pattern.
8   %
9   % The first argument is (theta+1) in degrees. theta is in [0,180].
10  % The second argument is (phi+1) in degrees. phi is in [0,359].
11  % The third argument decides which data you get according to this list:
12  %    1. Absolute Gain i dB
13  %    2. LHCP Gain in dB
14  %    3. LHCP Phase in dB
15  %    4. RHCP Gain in dB
16  %    5. RHCP Phase in dB
17  %    6. Axial Ratio in dB
18
19  % Example, A(91,1,2) will return the LHCP Gain for theta=90 and phi=0
20
21  A = zeros(181,360,6);
22
23  % RegExp
24  % %s - string
25  % %f - float
26  % %d - int
27
28  [theta,phi,absgain,absleft,phleft,absright,phright,ar] = textread(fname,'%f %f ...
        %f %f %f %f %f %f','headerlines',2);
29
30  for i=1:length(theta)
31      a=theta(i)+1;
32      b=phi(i)+1;
33
34      A(a,b,1)=absgain(i);
35      A(a,b,2)=absleft(i);
36      A(a,b,3)=phleft(i);
37      A(a,b,4)=absright(i);
38      A(a,b,5)=phright(i);
39      A(a,b,6)=ar(i);
40  end
```

E.15 constants.m

```
%
% Defines physical constants used by other functions. All constants will be
% stored as a variable into the work space when executed.
%
% SYNTAX:
%   constants;
%
% Author: Sigvald Marholm
% Copyright: 04.11.2011
%

Re = 6371.00e3;          % Mean Earth Radius [m]
mu = 398600.4418e9;      % Gravitational Parameter of the Earth [m^3/s^2]
h_default = 600e3;       % Default height/altitude of orbit [m]
c_0 = 299792458;         % Speed-of-light in vacuum [m/s]
```

E.16 link_budget_ideal_pattern.m

```
%
% GENERIC LINK BUDGET CALCULATIONS TEMPLATE
%
% This template implements the basic link budget in MATLAB and can be
% further extended in order to extract parameters in the link budget and to
% tweak parameters in the link budget. All the link budget parameters will
% be available in this workspace for manipulation. Without further
% manipulations the two lines of code will compute the link budget as is
% the excel sheet provided by øAsbjrn Dahl.
%

% Overview of different budgets:
%
%   1 - UHF Downlink
%   2 - UHF Uplink
%   3 - VHF Downlink
%   4 - VHF Uplink
%   5 - Beacon Downlink
%   6 - Beacon Uplink
%
% import_link_vars() can take either budget numer or strings as arguments

clear all
close all
clc

%
% LOAD NECESSARY VARIABLES WITH DEFAULT VALUES
%
% See link_data.txt for details about the variables.
% All variables are converted to SI-units.
%

import_link_vars('link_data.txt','UHF','Downlink');

theta = 0:0.1:180;                              % All off-nadir angles [degree]
el = elevation_vs_offset_angle(theta,A_h,10);% Elevation [degree]
elt = el(~isnan(el));                           % Only true elevation angles
thetat = theta(~isnan(el));                     % Only true off-naidr angles
los = los_vs_elevation(elt,A_h);                % Line-of-sight distance [m]
% Neglecting ADCS uncertainty

% Replace Link Budget variables
L_tx_pnt = 0;                                   % Included in G_tx (neglect)
L_plf = 0;
G_tx = 1;                                       % Isotropic antenna
L_fspl = fspl_vs_los(los,f);                    % FSPL [dB]
L_atm = atmloss_vs_elevation(elt,f);            % Atmospheric losses [dB]
L_ion = 0;                                      % Ionospheric losses [dB]
                                                % Ionosph. are included in atm
%
% EXECUTE ALL CALCULATIONS IN LINK BUDGET
%
% See exec_link_budget.m to see which quantities are computed.
%
exec_link_budget

figure
hold on
plot(elt,LM_snr,'k');
xlabel('Elevation Angle [degree]');
ylabel('Link Margin (SNR) [dB]');
grid on
```

```
64
65
66  figure
67  hold on
68  plot(thetat,LM_snr,'k');
69  xlabel('Off-nadir Angle [degree]');
70  ylabel('Link Margin (SNR) [dB]');
71  grid on
72
73  %%%
74
75  LM_ideal = 20;  % doesn't really matter what this number is
76  LM_diff = LM_ideal-LM_snr;
77  U = LM_diff - max(LM_diff);   % Normalized gain vs. elevation
78
79  figure
80  hold on
81  plot(thetat,U,'k');
82  xlabel('Off-nadir Angle [degree]');
83  ylabel('Link Margin Difference Normalized (SNR) [dB]');
84  grid on
85
86  %U = 10.^(U./10);    % convert from dB to unitless for plotting
87  U = [U -inf*ones(1,length(theta)-length(U))];   % extend to theta=0:180
88
89  % obtain directivity
90  D = obtain_directivity(U,theta);
91
92  figure
93  hold on
94  plot_polar(theta,U,'mirror');
95
96  figure
97  hold on
98  plot(theta,U);
99
100 disp(['Max directivity is ' num2str(max(D)) ' dB'])
101
102 figure
103 hold on
104 plot_polar(theta,D,'mirror');
105
106 figure
107 hold on
108 plot(theta,D);
109
110 G_tx = D(~isnan(el));
111
112 exec_link_budget
113
114 figure
115 hold on
116 plot(elt,LM_snr,'k');
117 xlabel('Elevation Angle [degree]');
118 ylabel('Link Margin (SNR) [dB]');
119 grid on
```

E.17 link_budget_antenna_compare.m

```
1  %
2  % GENERIC LINK BUDGET CALCULATIONS TEMPLATE
3  %
4  % This template implements the basic link budget in MATLAB and can be
5  % further extended in order to extract parameters in the link budget and to
6  % tweak parameters in the link budget. All the link budget parameters will
7  % be available in this workspace for manipulation. Without further
8  % manipulations the two lines of code will compute the link budget as is
9  % the excel sheet provided by øAsbjrn Dahl.
10 %
11 % Example of use 1: Extract SNR link margin
12 %   It is found in exec_link_budget.m that the SNR link margin is stored in
13 %   the variable LM_snr. This will be stored to workspace and can simply by
14 %   read by executing "LM_snr" on the end of the script.
15 %
16 % Example of use 2: Compare different budgets
17 %   Add a loop around the whole script and iterate through all budgets of
18 %   interest. The link budget variable names will be overwritten in each
19 %   iteration so store the variables of interest into an array that will
20 %   contain them after the loop has run. NB: import_link_vars() can also
21 %   take the budget number as argument instead of two text strings
22 %   describing which budget it is. It plays nicer with loops.
```

```
23  %
24  % Example of use 3: Plot link budget variable versus elevation
25  %   Create a vector of different elevation angles. Import link budget
26  %   variables with import_link_vars() as usual but overwrite the
27  %   elevation-dependent variables with vectors corresponding to the
28  %   different elevations afterwards. There are functions created for this.
29  %   Run exec_link_budget as usual and plot elevation versus the variable of
30  %   interest, i.e. link margin.
31  %
32  % Example of use 4: Plot link budget varibles versus time
33  %   Assume circular orbit. Compute elevation angles versus time and follow
34  %   example 3 but plot versus time instead of elevation. There are
35  %   functions created for this.
36  %
37  % Example of use 5: Synthesize ideal antenna gain (advanced)
38  %   Load variables and replace the satellite antenna with an isotropic one
39  %   and compute link margin for a sweep of elevation angles. Define the
40  %   ideal link margin to be constant (at least above some cut-off elevation
41  %   angle) and take the difference between ideal and isotropic link margin
42  %   to be the preliminary antenna gain versus elevation. Convert to gain
43  %   versus theta. Antenna gain will be unphysical as the ideal link
44  %   margin is arbitrarily chosen. Normalize such that average gain is 1.
45  %   Recompute link budget with exec_link_budget with new parameters to get
46  %   actual link margin
47  %
48
49  % Overview of different budgets:
50  %
51  %   1 - UHF Downlink
52  %   2 - UHF Uplink
53  %   3 - VHF Downlink
54  %   4 - VHF Uplink
55  %   5 - Beacon Downlink
56  %   6 - Beacon Uplink
57  %
58  % import_link_vars() can take either budget numer or strings as arguments
59
60  %
61  % LOAD NECESSARY VARIABLES WITH DEFAULT VALUES
62  %
63  % See link_data.txt for details about the variables.
64  % All variables are converted to SI-units.
65  %
66
67  clear all
68  close all
69  clc
70
71  import_link_vars('link_data.txt','UHF','Downlink');
72
73  h = [400 600 800]*1e3;                          % Heights
74  t = 0:1000;                                     % Time after rise [s]
75
76  for i=1:3
77
78      adcs_acc = 0;                                 % Accuracy of ADCS [degree]
79      % neglect for now
80
81      el = elevation_vs_time(t,h(i));               % Elevation [degree]
82      los = los_vs_elevation(el,h(i));              % Line-of-sight distance [m]
83      theta = offset_angle_vs_elevation(el,h(i)); % Antenna offset-angle [degree]
84      theta = theta + adcs_acc;                     % Add ADCS uncertainty [degree]
85
86      % DIPOLE
87
88      % Replace Link Budget variables
89      L_plf = 3;
90      L_tx_pnt = 0;                                 % Included in G_tx
91      G_tx = pattern_dipole(theta,true,true);       % Diagram (normalized)
92      G_tx = G_tx+2.15;                             % De-normalize
93      L_fspl = fspl_vs_los(los,f);                  % FSPL [dB]
94      L_atm = atmloss_vs_elevation(el,f);           % Atmospheric losses [dB]
95      L_ion = 0;                                    % Ionospheric losses [dB]
96                                                    % Ionosph. are included
97                                                    % in atm
98
99      exec_link_budget;   % dipole
100
101     E_LM_snr(1,i,:) = LM_snr;
102     E_LM_ebno(1,i,:) = LM_ebno;
103
104     % MONOPOLE
105
106     G = import_far_field('monopole_with_virtual_gnd.txt');
107     phi = 6;    % worst case phi
108
109     % Replace Link Budget variables
110     L_plf = 0;  % NB: Monopole has 3 dB PLF but this is not quite monopole so ...
            circular gain is used instead
111     G_tx = G(180-round(theta)+1,phi+1,4);           % Extracting RHCP gain vs. time
```

```
112         G_tx = G_tx.';
113
114         exec_link_budget;   % monopole
115
116         E_LM_snr(2,i,:) = LM_snr;
117         E_LM_ebno(2,i,:) = LM_ebno;
118
119         % TURNSTILE
120
121         G = import_far_field('second_attempt_far_field.txt');
122         phi = 45;     % worst case phi
123
124         % Replace Link Budget variables
125         L_plf = 0;                                  % Using circular gain instead
126         G_tx = G(round(theta)+1,phi+1,4);           % Extracting RHCP gain vs. time
127                                                 % Note that what points down for
128                                                 % this is 0 degree.... LHCP is at
129                                                 % 180 degree, but it doesn't
130                                                 % matter
131         G_tx = G_tx.';
132
133         exec_link_budget;   % monopole
134
135         E_LM_snr(3,i,:) = LM_snr;
136         E_LM_ebno(3,i,:) = LM_ebno;
137         E_el(i,:) = el;
138
139
140         % MONOPOLE (THEORETICAL)
141
142         % Replace Link Budget variables
143         L_plf = 3;
144         L_tx_pnt = 0;                                   % Included in G_tx
145         G_tx = pattern_dipole(theta,false,true);        % Diagram (normalized)
146         G_tx = G_tx+2.15;                               % De-normalize
147         L_fspl = fspl_vs_los(los,f);                    % FSPL [dB]
148         L_atm = atmloss_vs_elevation(el,f);             % Atmospheric losses [dB]
149         L_ion = 0;                                      % Ionospheric losses [dB]
150                                                         % Ionosph. are included
151                                                         % in atm
152
153         exec_link_budget;   % monopole (theoretical)
154
155         E_LM_snr(4,i,:) = LM_snr;
156         E_LM_ebno(4,i,:) = LM_ebno;
157     end
158
159     num = 3;
160
161     %
162     % PLOT SNR LINK MARGIN vs. TIME
163     %
164
165     figure
166     hold on
167     % plot(t/60,squeeze(E_LM_snr(1,1,:)),'Color',[1 0.8 0.8]);
168     plot(t/60,squeeze(E_LM_snr(1,2,:)),'r');
169     % plot(t/60,squeeze(E_LM_snr(1,3,:)),'Color',[1 0.8 0.8]);
170     % plot(t/60,squeeze(E_LM_snr(2,1,:)),'Color',[0.8 0.8 1]);
171     plot(t/60,squeeze(E_LM_snr(2,2,:)),'b');
172     % plot(t/60,squeeze(E_LM_snr(2,3,:)),'Color',[0.8 0.8 1]);
173     % plot(t/60,squeeze(E_LM_snr(3,1,:)),'Color',[0.8 1 0.8]);
174     plot(t/60,squeeze(E_LM_snr(3,2,:)),'g');
175     % plot(t/60,squeeze(E_LM_snr(3,3,:)),'Color',[0.8 1 0.8]);
176     % plot(t/60,squeeze(E_LM_snr(4,1,:)),'Color',[0.8 0.8 0.8]);
177     plot(t/60,squeeze(E_LM_snr(4,2,:)),'k');
178     % plot(t/60,squeeze(E_LM_snr(4,3,:)),'Color',[0.8 0.8 0.8]);
179     xlabel('Passage time [min]');
180     ylabel('Link Margin (SNR) [dB]');
181     axis([min(t)/60 max(t)/60 -20 20]);
182     %title(titles(budget,:));
183     legend('Dipole','Monopole w/t.','Crossed Dipoles','Monopole');
184     grid on
185
186     %
187     % PLOT EbNo LINK MARGIN vs. TIME
188     %
189
190     figure
191     hold on
192     % plot(t/60,squeeze(E_LM_ebno(1,1,:)),'Color',[1 0.8 0.8]);
193     plot(t/60,squeeze(E_LM_ebno(1,2,:)),'r');
194     % plot(t/60,squeeze(E_LM_ebno(1,3,:)),'Color',[1 0.8 0.8]);
195     % plot(t/60,squeeze(E_LM_ebno(2,1,:)),'Color',[0.8 0.8 1]);
196     plot(t/60,squeeze(E_LM_ebno(2,2,:)),'b');
197     % plot(t/60,squeeze(E_LM_ebno(2,3,:)),'Color',[0.8 0.8 1]);
198     % plot(t/60,squeeze(E_LM_ebno(3,1,:)),'Color',[0.8 1 0.8]);
199     plot(t/60,squeeze(E_LM_ebno(3,2,:)),'g');
200     % plot(t/60,squeeze(E_LM_ebno(3,3,:)),'Color',[0.8 1 0.8]);
201     % plot(t/60,squeeze(E_LM_ebno(4,1,:)),'Color',[0.8 0.8 0.8]);
```

```
202  plot(t/60,squeeze(E_LM_ebno(4,2,:)),'k');
203  % plot(t/60,squeeze(E_LM_ebno(4,3,:)),'Color',[0.8 0.8 0.8]);
204  xlabel('Passage time [min]');
205  ylabel('Link Margin (Eb/No) [dB]');
206  axis([min(t)/60 max(t)/60 -20 20]);
207  %title(titles(budget,:));
208  legend('Dipole','Monopole w/t.','Crossed Dipoles','Monopole');
209  grid on
210
211  %
212  % PLOT SNR LINK MARGIN vs. ELEVATION
213  %
214
215  figure
216  hold on
217  % plot(E_el(1,:),squeeze(E_LM_snr(1,1,:)),'Color',[1 0.8 0.8]);
218  plot(E_el(2,:),squeeze(E_LM_snr(1,2,:)),'r');
219  % plot(E_el(3,:),squeeze(E_LM_snr(1,3,:)),'Color',[1 0.8 0.8]);
220  % plot(E_el(1,:),squeeze(E_LM_snr(2,1,:)),'Color',[0.8 0.8 1]);
221  plot(E_el(2,:),squeeze(E_LM_snr(2,2,:)),'b');
222  % plot(E_el(3,:),squeeze(E_LM_snr(2,3,:)),'Color',[0.8 0.8 1]);
223  % plot(E_el(1,:),squeeze(E_LM_snr(3,1,:)),'Color',[0.8 1 0.8]);
224  plot(E_el(2,:),squeeze(E_LM_snr(3,2,:)),'g');
225  % plot(E_el(3,:),squeeze(E_LM_snr(3,3,:)),'Color',[0.8 1 0.8]);
226  % plot(E_el(1,:),squeeze(E_LM_snr(4,1,:)),'Color',[0.8 0.8 0.8]);
227  plot(E_el(2,:),squeeze(E_LM_snr(4,2,:)),'k');
228  % plot(E_el(3,:),squeeze(E_LM_snr(4,3,:)),'Color',[0.8 0.8 0.8]);
229  xlabel('Elevation Angle [degrees]');
230  ylabel('Link Margin (SNR) [dB]');
231  axis([0 90 -20 20]);
232  %title(titles(budget,:));
233  legend('Dipole','Monopole w/t.','Crossed Dipoles','Monopole');
234  grid on
235
236  %
237  % PLOT EbNo LINK MARGIN vs. ELEVATION
238  %
239
240  figure
241  hold on
242  % plot(E_el(1,:),squeeze(E_LM_ebno(1,1,:)),'Color',[1 0.8 0.8]);
243  plot(E\_el(2,:),squeeze(E\_LM\_ebno(1,2,:)),'r');
244  % plot(E_el(3,:),squeeze(E_LM_ebno(1,3,:)),'Color',[1 0.8 0.8]);
245  % plot(E_el(1,:),squeeze(E_LM_ebno(2,1,:)),'Color',[0.8 0.8 1]);
246  plot(E\_el(2,:),squeeze(E\_LM\_ebno(2,2,:)),'b');
247  % plot(E_el(3,:),squeeze(E_LM_ebno(2,3,:)),'Color',[0.8 0.8 1]);
248  % plot(E_el(1,:),squeeze(E_LM_ebno(3,1,:)),'Color',[0.8 1 0.8]);
249  plot(E\_el(2,:),squeeze(E\_LM\_ebno(3,2,:)),'g');
250  % plot(E_el(3,:),squeeze(E_LM_ebno(3,3,:)),'Color',[0.8 1 0.8]);
251  % plot(E_el(1,:),squeeze(E_LM_ebno(4,1,:)),'Color',[0.8 0.8 0.8]);
252  plot(E\_el(2,:),squeeze(E\_LM\_ebno(4,2,:)),'k');
253  % plot(E_el(3,:),squeeze(E_LM_ebno(4,3,:)),'Color',[0.8 0.8 0.8]);
254  xlabel('Elevation Angle [degrees]');
255  ylabel('Link Margin (Eb/No) [dB]');
256  axis([0 90 -20 20]);
257  %title(titles(budget,:));
258  legend('Dipole','Monopole w/t.','Crossed Dipoles','Monopole');
259  grid on
```

F

Further Discussions

F.1 Alternative Phase-Shifting for the Feeding Network

If the third WPS in Fig. 6.1 is made by $3\lambda/4$ lines rather than $\lambda/4$ lines, there will be a 180° phase-difference between the output of WPS 2 and WPS 3. The phase-shifters on ports 2 and 4 may be omitted, and $-90°$ phase shifters are realized by LH_π-cells on ports 3 and 5. This yields a 90° phase-difference between all outputs by using only two components. Moreover, three of the outputs will already have shunt inductor due to the many LH_π-cells. Therefore, only port 2 needs a DC-grounding inductor and thus this becomes the minimal solution in terms of component count that utilizes this circuit topology. Although this i more elegant in terms of circuit design, the author chose not to use it since it is less symmetric than the chosen one. This example is the one shown in the feeding network calculator in App. B.

F.2 The Improved Phase-Difference for Differential Mode

In Sec. 7.2.5 it was observed that the phase-error of the feeding network was improved from 30° to 11° simply by using it with differential loads, rather than single-ended. This might seem curious at first, and this discussion is therefore an attempt to explain why this might be possible, for those interested.

Consider that a signal is fed to port 1 such that some output port (A) ideally should have 90° phase and another (B) 270°. Unfortunately, the circuit is non-ideal and the phase at each of them is given by a PDF. This PDF is illustrated for port A in Fig. F.1. (There is a PDF for the amplitude as well, but this is not considered here). The PDF is likely not properly centered since the nominal values of the components are unequal to the ideal values.

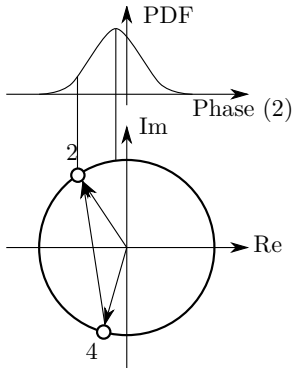

Figure F.1: An illustration of which effects that influence the phase at the load

Further on, a given realization of the circuit might have complex amplitudes as depicted in the figure. The phase-error is then the deviation from 90° and 270° of the two arrows from the origin (ground) to the two complex output amplitudes A and B. Using ports A and B differentially means that the complex amplitude across the load is the long arrow in the figure (the resultant). It is obvious from the geometry that this has a phase closer to 90° (at the cost of a slightly reduced magnitude). For the resultant to have as large phase-error as, for instance amplitude A alone, it is required that amplitude B has an equally large and opposite phase error. The *joint probability* of this is very small for large phase-errors, which is why the statistical simulations had a 95th percentile with much lower phase-error for the differential loads.

G Additional ADS Material

G.1 Screenshot from ADS Schematic

Fig. G.1 shows the schematic used in ADS during simulations. Dependently of which simulations was performed, blocks were added to or removed from the design. Component values and parameters was also adjusted according to the specific simulations. Including all different cases here are included superfluous.

G.2 Lumped Design, Alternative I

The component values for the alternative I lumped feeding network considered in Sec. 5.6.3 were computed. The component values for the LQPS was computed like described in [23], whereas the lattice baluns were computed according to that descirbed in Ch. 5. The ADS simulation schematic including the computed component values are shown in Fig. G.2 whereas the result that showed that the circuit performed like intended are shown in Fig. G.3. The advantage above alternative II is less components. The disadvantages are that the PCB layout becomes problematic, and not all output ports are isolated.

G.3 Statistical Theory for the Yield Analysis

It is of little use to have an estimator $\hat{Y}$ if it is unknown how certain it is that it is close to correct. Assuming a big number of trials, one can apply the central limit theorem and assume that $\hat{Y}$ is normal distributed around the expectation value Y with the following variance [**?**]:

$$\sigma^2 = \frac{\hat{Y}(1-\hat{Y})}{N} \qquad [\%^2] \quad \text{(G.1)}$$

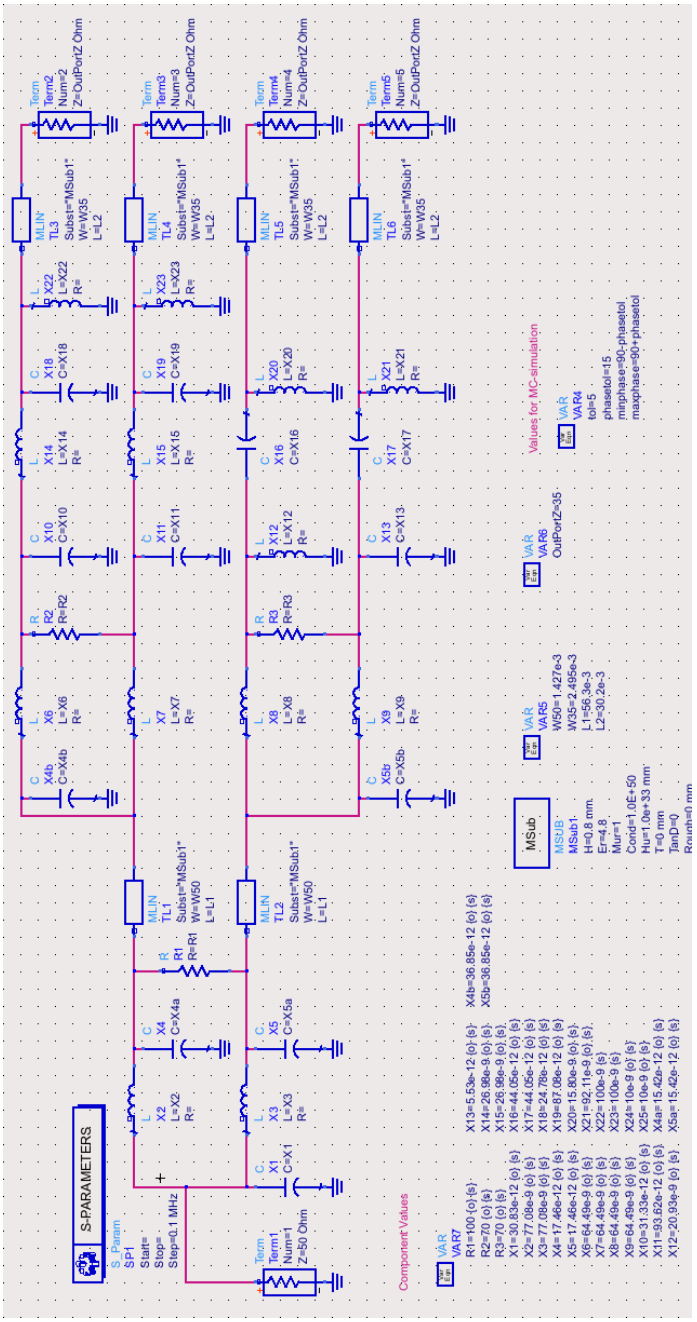

Figure G.1: Screenshot from the ADS Schematic Used During Simulations.

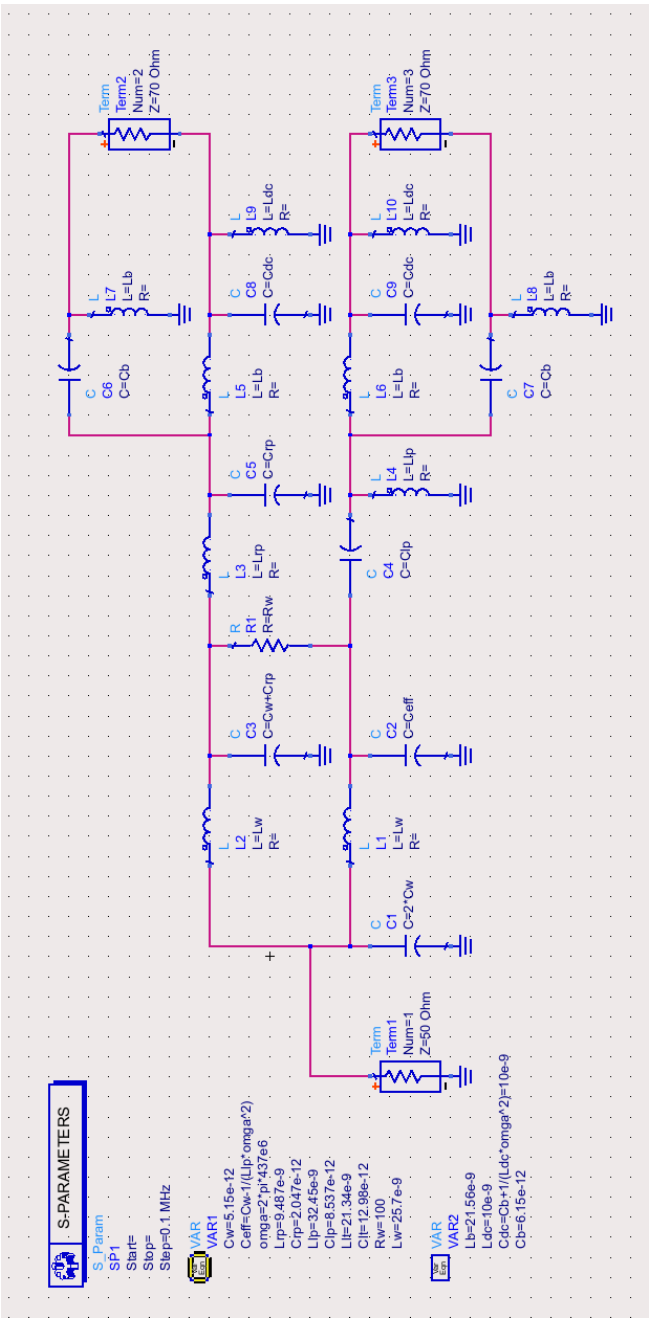

Figure G.2: Lumped network alternative I ADS schematic.

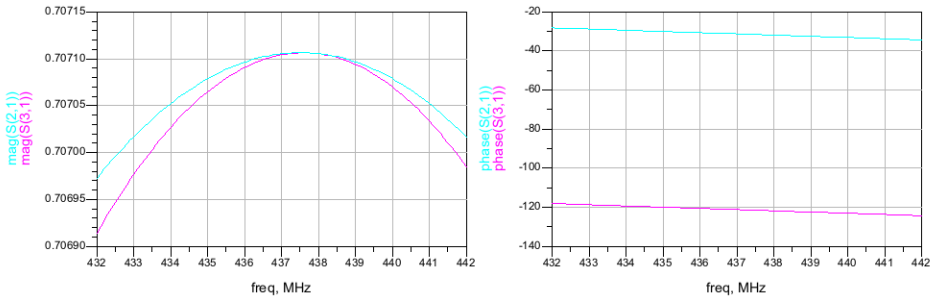

Figure G.3: Simulation results for alternative I feeding network.

Further on, one may define a confidence interval that spans ϵ standard deviations away from the expectation value:

$$\hat{Y} - \epsilon\sigma < Y < \hat{Y} + \epsilon\sigma \qquad [\%] \quad \text{(G.2)}$$

or equivalently:

$$E < \epsilon\sigma \qquad [\%] \quad \text{(G.3)}$$

where $E \triangleq |Y - \hat{Y}|$ is simply the error in the yield. The confidence level (probability that Y actually *is* within the confidence interval) is then given by the normal distribution. ϵ is typically chosen to be 1, 2 or 3, which yields confidence levels of 68%, 95% and 99% respectively. Substituting (G.1) into (G.3) and reordering the term, yields the minimum number of trials:

$$N > \left(\frac{\epsilon}{E}\right)^2 \hat{Y}(1 - \hat{Y}) \qquad [\,] \quad \text{(G.4)}$$

I.e. if the yield is estimated to be $\hat{Y}$ and it is desirable that *true* yield Y is within E of $\hat{Y}$ with for instance 95% certainty ($\epsilon = 2$), then N must be big enough to satisfy the above mentioned inequality [**?**].

G.3.1 The Method of the NUTS Simulations

It is important to realize the difference between the way Monte Carlo simulations are applied here and in typical industrial applications. In industry, $1 - \hat{Y}$ is usually an estimate for how many circuits must be thrown away, and the purpose is therefore mostly of economical nature. But only *one* satellite is to be built (and only one circuit for each frequency band). $\hat{Y}$ therefore becomes the *estimated probability* that the *one* circuit will work. Moreover, $E = 0.02$ and $\epsilon = 2$ is chosen, such that it is expected that this is wrong by maximally 2% with a confidence of 95%.

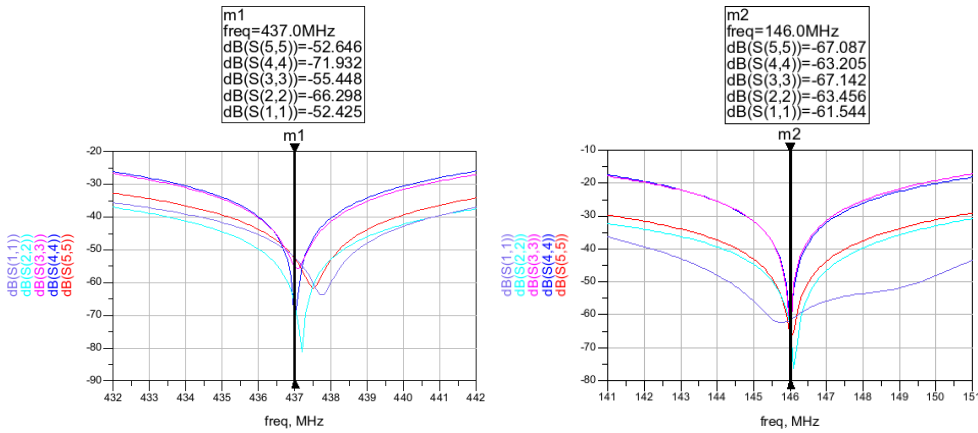

(a) UHF (b) VHF

Figure G.4: Simulated match of the ports

Remember also, that rather than "how many circuits will perform within the specified goals?" we want answer the question "how good performance can we expect?". To answer this, it is *chosen* to achieve $\hat{Y} = 95\%$. This is how strongly we expect it. Subsequently; the goals are adjusted until the desired $\hat{Y}$ is reached. The goals are then what we can expect from our circuit.

Substituting the obtained values into (G.4) results in $N > 475$. It is chosen to use $N = 500$. To summarize; by choosing $N = 500$, we can be 95% confident that the probability that the *one* circuit performs at least as good as the obtained goals is within 93–97% ($\hat{Y} \pm E$).

G.4 Verification of the Design, Further Results

Additional S-parameter simulations from the verification of the design in ADS that is described in Sec. 7.1, are shown in Fig. G.4 to Fig. G.6.

G.5 Monte Carlo Analysis, Further Results

Additional S-parameter simulations from the Monte Carlo simulations of the design in ADS that is described in Sec. 7.2, are shown in Fig. G.7 to Fig. G.22.

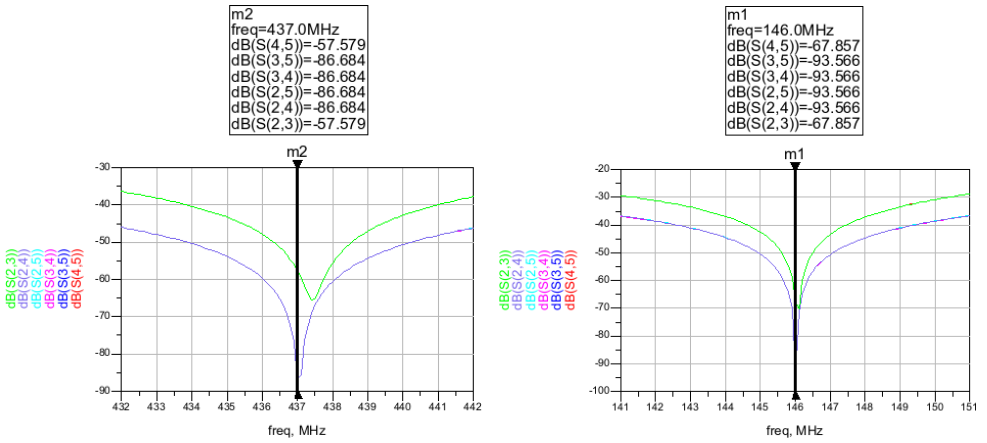

(a) UHF (b) VHF

Figure G.5: Simulated isolation between the ports

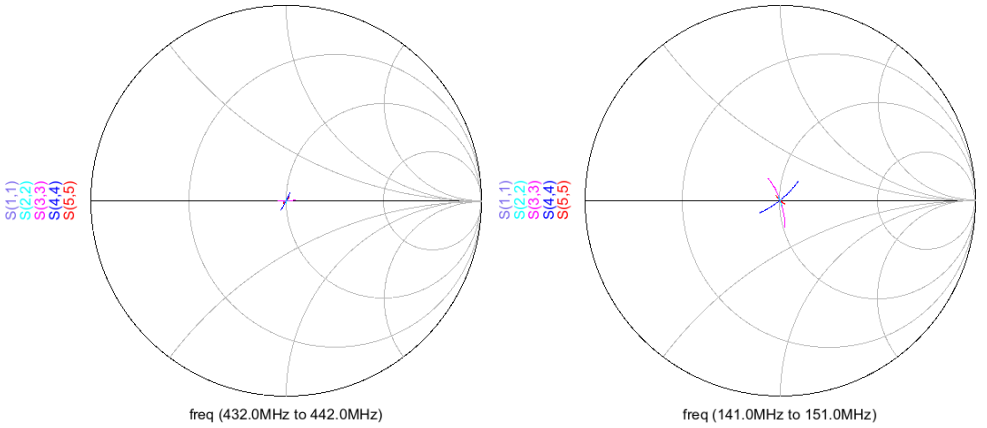

(a) UHF (b) VHF

Figure G.6: S-parameter in smith-chart

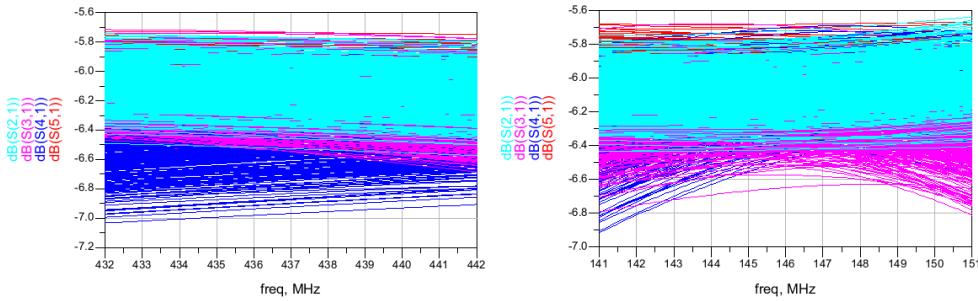

(a) UHF (b) VHF

Figure G.7: S-parameters from input to outputs in dB. Single-ended 35 Ω loads.

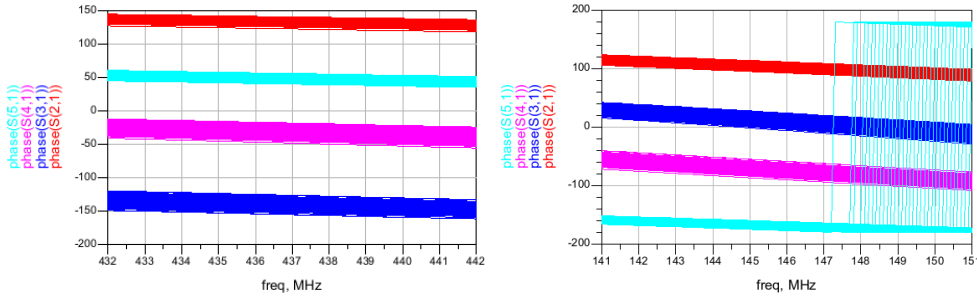

(a) UHF (b) VHF

Figure G.8: S-parameter phase from input to outputs. Single-ended 35 Ω loads.

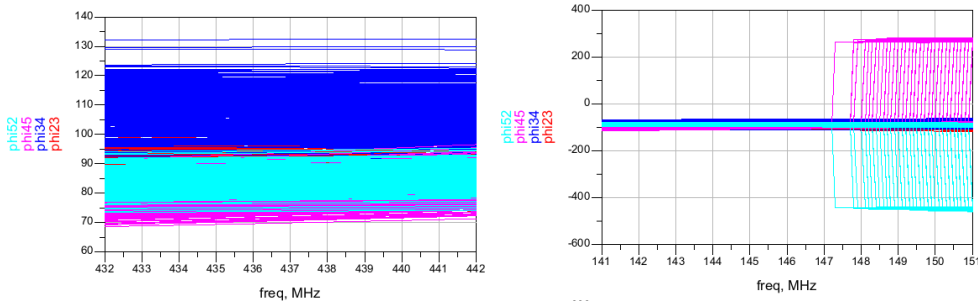

(a) UHF (b) VHF

Figure G.9: Simulated ϕ_{ij}. Single-ended 35 Ω loads.

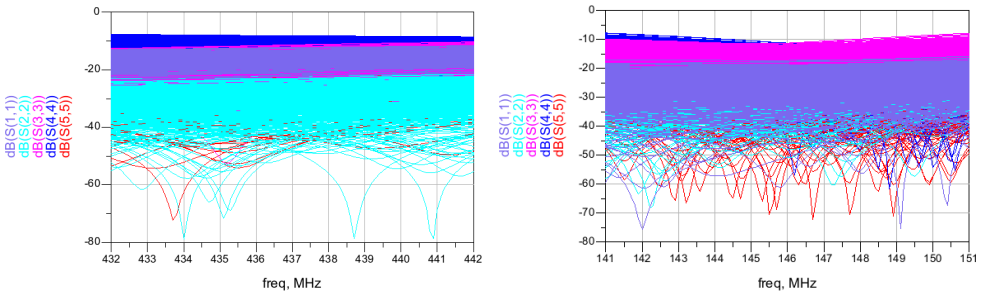

(a) UHF (b) VHF

Figure G.10: Simulated match of the ports. Single-ended 35 Ω loads.

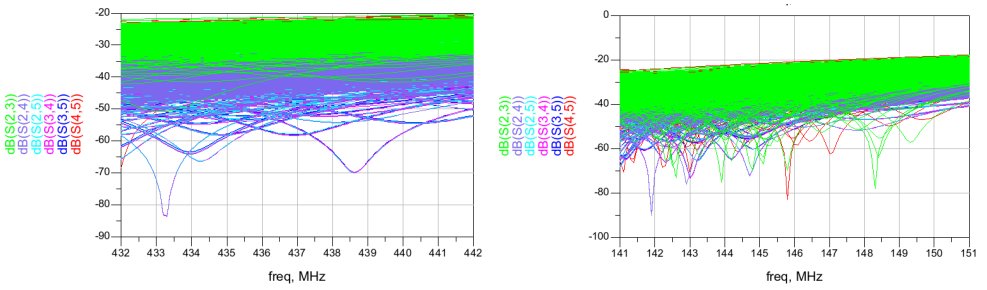

(a) UHF (b) VHF

Figure G.11: Simulated isolation between the ports. Single-ended 35 Ω loads.

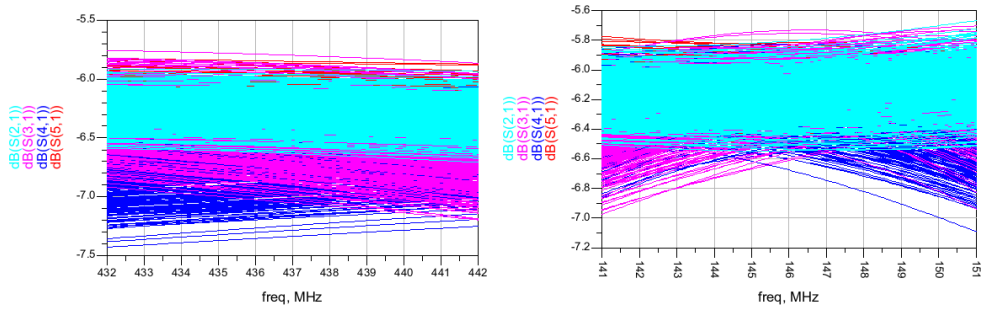

(a) UHF (b) VHF

Figure G.12: S-parameters from input to outputs in dB. Single-ended 50 Ω loads.

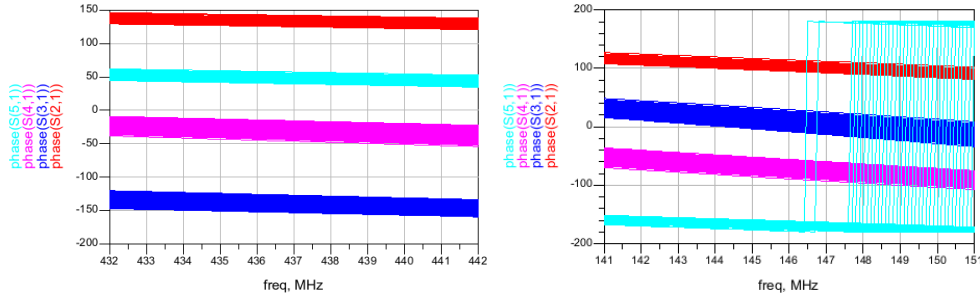

(a) UHF (b) VHF

Figure G.13: S-parameter phase from input to outputs. Single-ended 50 Ω loads.

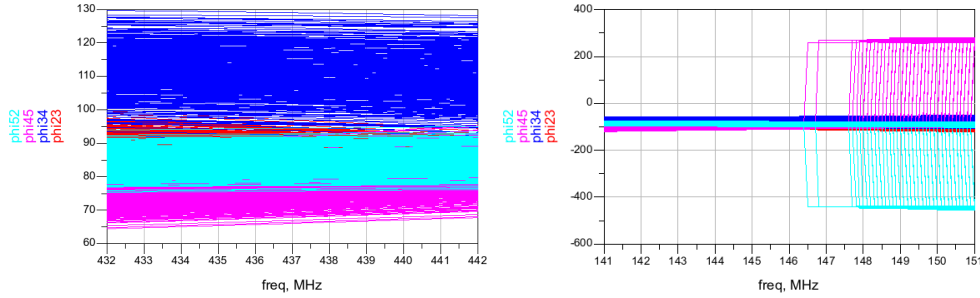

(a) UHF (b) VHF

Figure G.14: Simulated ϕ_{ij}. Single-ended 50 Ω loads.

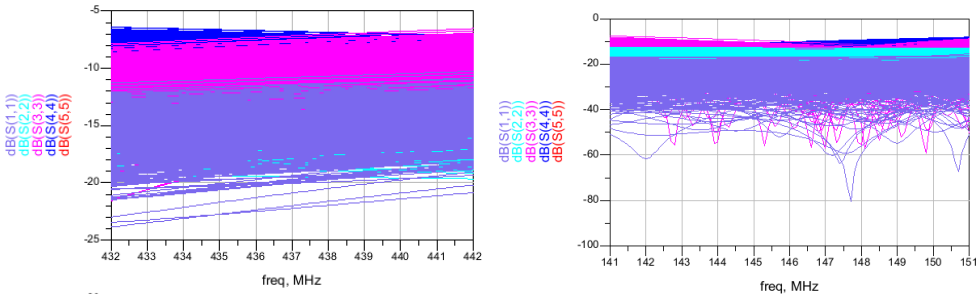

(a) UHF (b) VHF

Figure G.15: Simulated match of the ports. Single-ended 50 Ω loads.

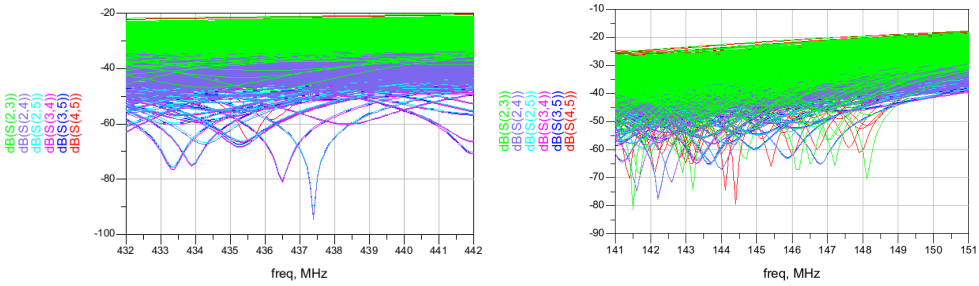

(a) UHF (b) VHF

Figure G.16: Simulated isolation between the ports. Single-ended 50 Ω loads.

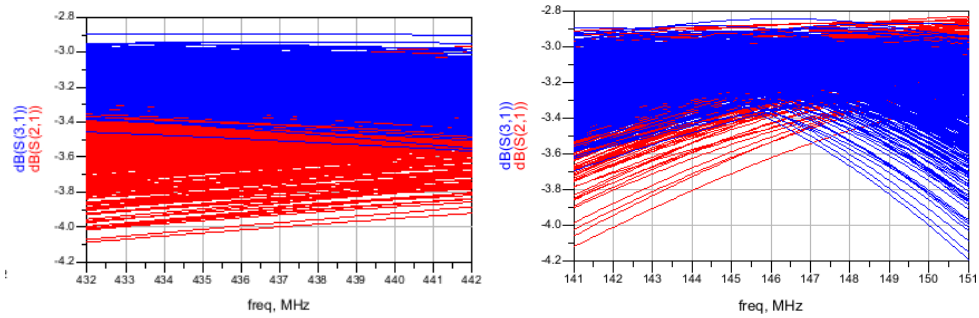

(a) UHF (b) VHF

Figure G.17: S-parameters from input to outputs in dB. Differential 70 Ω loads.

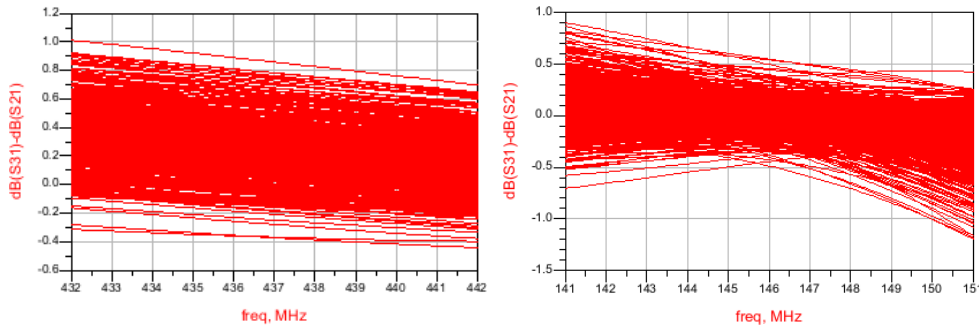

(a) UHF (b) VHF

Figure G.18: Amplitude unbalance. Differential 70 Ω loads.

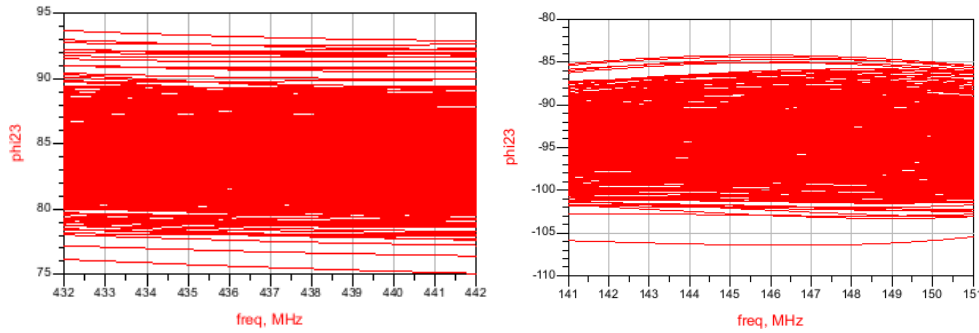

(a) UHF (b) VHF

Figure G.19: Phase unbalance. Differential 70 Ω loads.

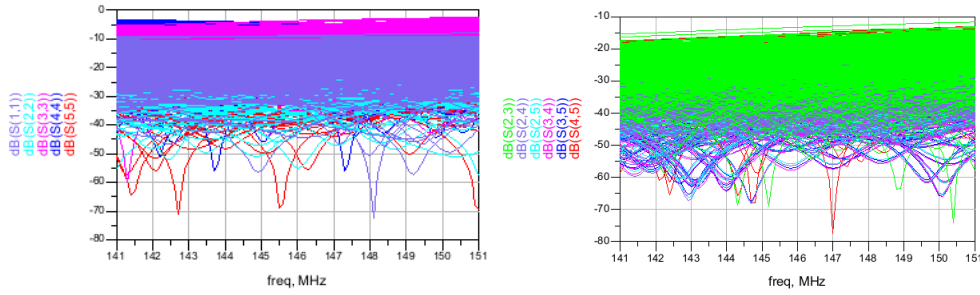

(a) Simulated match of the port. (b) Simulated Isolation between the ports.

Figure G.20: Single-ended 35 Ω loads, VHF. The components are allowed to deviate by 15%.

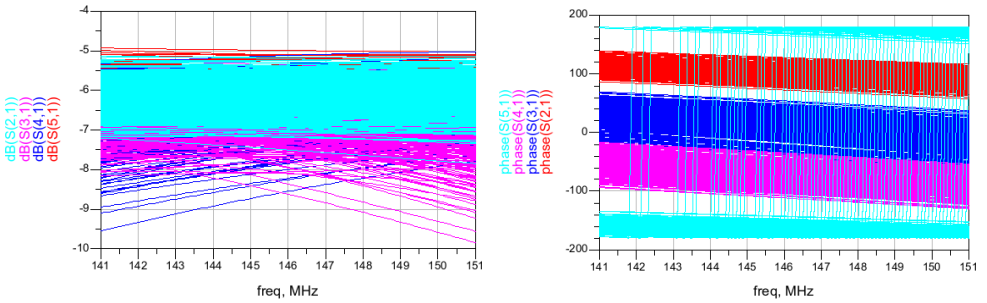

(a) S-parameters from input to output in dB. (b) S-parameter phase from input to output.

Figure G.21: Single-ended 35 Ω loads, VHF. The components are allowed to deviate by 15%.

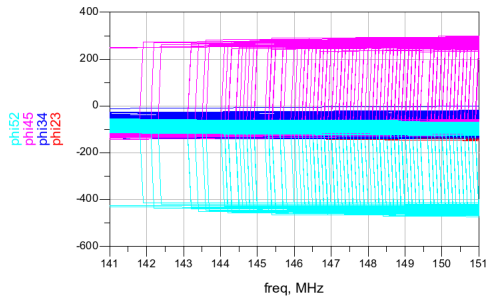

Figure G.22: Simulated ϕ_{ij}. Single-ended 35 Ω loads, VHF. The components are allowed to deviate by 15%.

H

Datasheets

The subsequent pages contains datasheets for the following ICs:

- MiniCircuits ADQ-22+
- MiniCircuits QBA-07
- MiniCircuits SBTCJ-1W+
- MiniCircuits SCPJ-2-9+
- MiniCircuits ADT1-1WT+
- muRata DXW21BN7511T

Surface Mount

Power Splitter/Combiner

2 Way-90° 50Ω 95 to 200 MHz

ADQ-22+

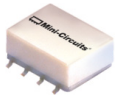

CASE STYLE: CJ725
PRICE: $9.95 ea. QTY (1-9)

+RoHS Compliant
The +Suffix identifies RoHS Compliance. See our web site for RoHS Compliance methodologies and qualifications

Maximum Ratings

Operating Temperature	-40°C to 85°C
Storage Temperature	-55°C to 100°C
Power Input (as a splitter)	1W max.

Permanent damage may occur if any of these limits are exceeded.

Pin Connections

SUMPORT	1
PORT 1 (0°)	5
PORT 2 (+90°)	8
GROUND EXTERNAL	2,3,6,7
50 OHM TERM EXTERNAL	4

Features

- low insertion loss, 0.3 dB typ.
- high isolation, 28 dB typ.
- excellent VSWR, 1.10 typ.
- small size surface mount

Applications

- point to point microwave link

Outline Drawing

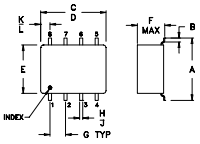

PCB Land Pattern

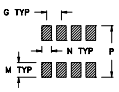

Suggested Layout

Outline Dimensions (inch / mm)

A	B	C	D	E	F	G
.397	.032	.385	.435	.310	.215	.100
10.08	0.81	9.78	11.05	7.87	5.46	2.54

H	J	K	L	M	N	P	wt
.015	.025	.035	.075	.120	.060	.420	grams
0.38	0.64	0.89	1.91	3.05	1.52	10.67	0.45

Demo Board MCL P/N: TB-83
Suggested PCB Layout (PL-063)

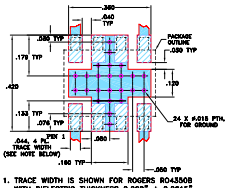

NOTES: 1. TRACE WIDTH IS SHOWN FOR ROGERS RO4350B WITH DIELECTRIC THICKNESS 0.020" ± 0.0015", COPPER: 1/2 OZ. EACH SIDE. FOR OTHER MATERIALS TRACE WIDTH MAY NEED TO BE MODIFIED.
2. BOTTOM SIDE OF THE PCB IS CONTINUOUS GROUND PLANE.

DENOTES PCB COPPER LAYOUT WITH SMOBC (SOLDER MASK OVER BARE COPPER)

DENOTES COPPER LAND PATTERN FREE OF SOLDER MASK

Electrical Specifications

FREQ. RANGE (MHz)	ISOLATION (dB)		INSERTION LOSS (dB) Avg. of Coupled Outputs ABOVE 3 dB		PHASE UNBALANCE (Degrees)		AMPLITUDE UNBALANCE (dB)		VSWR (:1)	
f_L-f_U	Typ.	Min.	Typ.	Max.	Typ.	Max.	Typ.	Max.	S-Port Typ.	Output Typ.
95-200	28	24	0.3	0.6	2	6	0.7	1.6	1.1	1.1

Typical Performance Data

Frequency (MHz)	Total Loss[1] (dB) S-1	Total Loss[1] (dB) S-2	Amplitude Unbalance (dB)	Isolation (dB)	Phase Unbalance (deg.)	VSWR S	VSWR 1	VSWR 2
95.00	2.63	3.78	1.15	31.31	90.78	1.09	1.09	1.06
100.00	2.76	3.61	0.85	31.02	90.87	1.09	1.09	1.06
105.00	2.89	3.47	0.57	30.81	90.96	1.09	1.09	1.06
110.00	3.02	3.35	0.33	30.57	91.06	1.09	1.09	1.06
120.00	3.23	3.15	0.08	30.11	91.27	1.10	1.10	1.06
130.00	3.39	3.02	0.37	29.73	91.48	1.10	1.10	1.06
140.00	3.51	2.94	0.57	29.50	91.70	1.10	1.10	1.06
150.00	3.57	2.91	0.66	29.36	91.97	1.10	1.10	1.06
160.00	3.58	2.93	0.65	29.32	92.23	1.10	1.10	1.06
170.00	3.53	3.01	0.52	29.43	92.53	1.11	1.11	1.05
180.00	3.42	3.15	0.26	29.74	92.88	1.11	1.11	1.05
185.00	3.34	3.26	0.08	30.01	93.05	1.11	1.10	1.05
190.00	3.24	3.38	0.14	30.37	93.26	1.11	1.10	1.05
195.00	3.13	3.53	0.41	30.87	93.48	1.11	1.10	1.04
200.00	2.99	3.72	0.72	31.54	93.71	1.11	1.10	1.04

1. Total Loss = Insertion Loss + 3dB splitter loss.

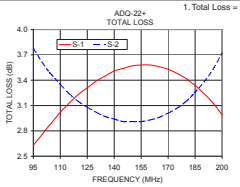

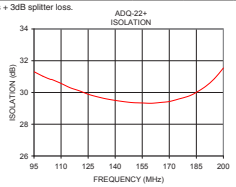

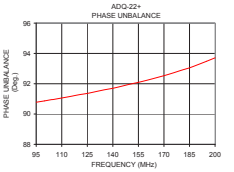

electrical schematic

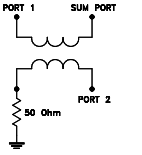

For detailed performance specs & shopping online see web site

Mini-Circuits®
ISO 9001 ISO 14001 AS9100 CERTIFIED

P.O. Box 350166, Brooklyn, New York 11235-0003 (718) 934-4500 Fax (718) 332-4661 *The Design Engineers Search Engine Provides ACTUAL Data Instantly at* minicircuits.com

IF/RF MICROWAVE COMPONENTS

Notes: 1. Performance and quality attributes and conditions not expressly stated in this specification sheet are intended to be excluded and do not form a part of this specification sheet. **2.** Electrical specifications and performance data contained herein are based on Mini-Circuit's applicable established test performance criteria and measurement instructions. **3.** The parts covered by this specification sheet are subject to Mini-Circuits standard limited warranty and terms and conditions (collectively, "Standard Terms"); Purchasers of this part are entitled to the rights and benefits contained therein. For a full statement of the Standard Terms and the exclusive rights and remedies thereunder, please visit Mini-Circuits' website at www.minicircuits.com/MCLStore/terms.jsp.

REV. A
M127604
ED-12462/1
ADQ-22+
HY/IZ/CP/AM
120322

Surface Mount

Power Splitter/Combiner

QBA-07+
QBA-07

2 Way-90° 50Ω 340 to 680 MHz

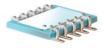

CASE STYLE: SM1L
PRICE: $6.95 ea. QTY (10-49)

+ RoHS compliant in accordance with EU Directive (2002/95/EC)

The +Suffix identifies RoHS Compliance. See our web site for RoHS Compliance methodologies and qualifications.

Maximum Ratings

Operating Temperature	-55°C to 100°C
Storage Temperature	-55°C to 100°C

Permanent damage may occur if any of these limits are exceeded.

Pin Connections

SUM PORT	1
PORT 1 (+90°)	10
PORT 2 (0°)	6
GROUND	2,3,4,7,8,9
50 OHM TERM EXTERNAL	5

Features

- low insertion loss, 0.5 dB typ.
- high power capability, 27W
- hermetically sealed
- low variation with temperature
- low profile, 0.07" height
- aqueous washable
- protected by U.S. Patent 5,534,830

Applications

- NMT
- land mobile radio
- broadcasting

Outline Drawing

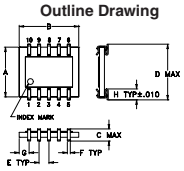

PCB Land Pattern

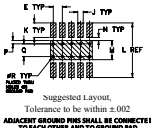

Suggested Layout,
Tolerance to be within ±.002

ADJACENT GROUND PINS SHALL BE CONNECTED TO EACH OTHER AND TO GROUND PAD

Outline Dimensions (inch / mm)

A	B	C	D	E	F	G	H	
.250	.300	.070	.320	.050	.015	.050	.075	
6.35	7.62	1.78	8.13	1.27	0.38	1.27	1.91	
J	K	L	M	N	P	Q	R	wt
.030	.095	.330	.100	.020	.015	.070	.014	grams
0.76	2.41	8.38	2.54	0.51	0.38	1.78	0.36	0.3

Demo Board MCL P/N: TB-115+
Suggested PCB Layout (PL-004)

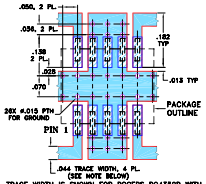

NOTE: 1. TRACE WIDTH IS SHOWN FOR ROGERS RO4350B WITH DIELECTRIC THICKNESS .020 ± .0015; COPPER: 1/2 OZ. EACH SIDE. FOR OTHER MATERIALS TRACE WIDTH MAY NEED TO BE MODIFIED.
2. BOTTOM SIDE OF THE PCB IS CONTINUOUS GROUND PLANE.

DENOTES PCB COPPER LAYOUT WITH SMOBC (SOLDER MASK OVER BARE COPPER)

DENOTES COPPER LAND PATTERN FREE OF SOLDER MASK

Electrical Specifications

FREQ. RANGE (MHz)	ISOLATION (dB)		INSERTION LOSS (dB) Avg. of Coupled Outputs ABOVE 3 dB		PHASE UNBALANCE (Degrees)		AMPLITUDE UNBALANCE (dB)		THERMAL RESISTANCE θjc, °C/W	POWER (W)
f_L-f_U	Typ.	Min.	$\overline{X}$	σ	Typ.	Max.	Typ.	Max.	Typ.	
340-680	**22**	**16**	**0.8**	**0.1**	**3.0**	**7.0**	**0.7**	**2.0**	**20**	**21***
340-530	23	18	0.5	0.1	1.7	4.0	0.7	2.0	20	27**

* Derate linearly to 9W at 100°C
** Derate linearly to 12W at 100°C

Typical Performance Data

Frequency (MHz)	Total Loss[1] (dB) S-1	Total Loss[1] (dB) S-2	Amplitude Unbalance (dB)	Isolation (dB)	Phase Unbalance (deg.)	VSWR S	VSWR 1	VSWR 2
340.00	3.99	3.00	0.99	23.80	90.39	1.14	1.08	1.12
400.00	3.53	3.46	0.07	22.78	90.93	1.17	1.10	1.14
430.00	3.36	3.64	0.27	22.29	91.23	1.19	1.11	1.14
460.00	3.24	3.80	0.56	21.83	91.60	1.20	1.12	1.15
500.00	3.15	3.98	0.83	21.25	91.99	1.22	1.14	1.17
530.00	3.10	4.05	0.96	20.80	92.41	1.24	1.15	1.18
590.00	3.12	4.17	1.05	19.93	93.19	1.27	1.18	1.20
600.00	3.13	4.17	1.04	19.79	93.37	1.27	1.19	1.21
640.00	3.20	4.14	0.94	19.19	94.07	1.29	1.21	1.22
660.00	3.28	4.13	0.85	18.91	94.38	1.30	1.22	1.23
680.00	3.37	4.09	0.73	18.63	94.75	1.31	1.23	1.24

1. Total Loss = Insertion Loss + 3dB splitter loss.

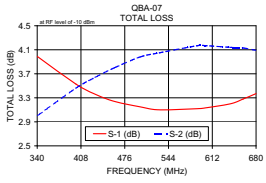

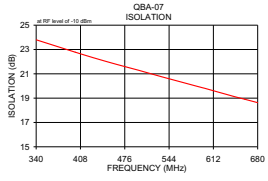

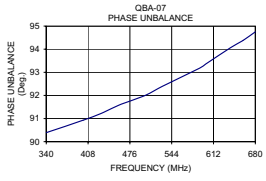

electrical schematic

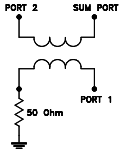

For detailed performance specs & shopping online see web site

Mini-Circuits®
ISO 9001 ISO 14001 AS9100 CERTIFIED

P.O. Box 350166, Brooklyn, New York 11235-0003 (718) 934-4500 Fax (718) 332-4661 *The Design Engineers Search Engine Provides ACTUAL Data Instantly at* minicircuits.com

IF/RF MICROWAVE COMPONENTS

Notes: 1. Performance and quality attributes and conditions not expressly stated in this specification sheet are intended to be excluded and do not form a part of this specification sheet. **2.** Electrical specifications and performance data contained herein are based on Mini-Circuit's applicable established test performance criteria and measurement instructions. **3.** The parts covered by this specification sheet are subject to Mini-Circuits standard limited warranty and terms and conditions (collectively, "Standard Terms"); Purchasers of this part are entitled to the rights and benefits contained therein. For a full statement of the Standard Terms and the exclusive rights and remedies thereunder, please visit Mini-Circuits' website at www.minicircuits.com/MCLStore/terms.jsp.

REV. E
M127604
ED-8943/03
QBA-07
LC/TD/CP
100622

Surface Mount, Micro-Miniature

Power Splitter/Combiner

SBTCJ-1W+

2 Way-180° 50Ω 1 to 750 MHz

CASE STYLE: AT790
PRICE: $ 10.95 ea. QTY. (1-9)

+ RoHS compliant in accordance with EU Directive (2002/95/EC)

The +Suffix has been added in order to identify RoHS Compliance. See our web site for RoHS Compliance methodologies and qualifications.

Maximum Ratings

Operating Temperature	-40°C to 85°C
Storage Temperature	-55°C to 100°C
Power Input (as a splitter)	0.5W max.
Internal Dissipation	0.125W max.

Permanent damage may occur if any of these limits are exceeded.

Pin Connections

SUM PORT	6
PORT 1	1
PORT 2	3
GROUND	2,4
NOT USED	5

Features

- low insertion loss, 0.7 dB typ.
- good isolation, 23 dB typ.
- good VSWR, 1.25 typ. all ports
- small size, 0.15X0.15"X0.15"
- temperature stable, LTCC base
- low cost
- protected by US Patent, 6,806,790

Applications

- cellular
- UHF/VHF receivers/transmitters
- protected by US Patent, 6,806,790

Electrical Specifications

FREQ. RANGE (MHz)	ISOLATION* (dB)						INSERTION LOSS (dB) ABOVE 3.0 dB						PHASE UNBALANCE (Degrees)			AMPLITUDE UNBALANCE (dB)		
	L		M		U		L		M		U		L	M	U	L	M	U
f_L-f_U	Typ.	Min	Typ.	Min	Typ.	Min	Typ.	Max.	Typ.	Max.	Typ.	Max.	Max.	Max.	Max.	Max.	Max.	Max.
1-750	23	20	22	20	24	20	0.6	1.7	0.6	1.2	0.9	1.8	3	7	10	0.2	0.4	0.9

L = low range [f_L to 10 f_L] M = mid range [10 f_L to f_U/2] U= upper range [f_U/2 to f_U]
*Isolation, 17 dB min. at 1 - 3 MHz.

Outline Drawing

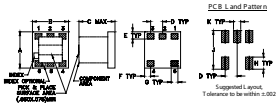

Outline Dimensions (inch / mm)

A	B	C	D	E	F
.150	.150	.150	.050	.030	.025
3.81	3.81	3.81	1.27	0.76	0.64

G	H	J	K	
.028	.050	.160	.030	wt
0.71	1.27	4.06	0.76	grams
				0.10

Typical Performance Data

Frequency (MHz)	Total Loss[1] (dB)		Amplitude Unbalance (dB)	Isolation (dB)	Phase Unbalance (deg.)	VSWR S	VSWR 1	VSWR 2
	S-1	S-2						
1.00	3.84	3.80	0.04	24.15	179.96	1.24	1.15	1.14
5.00	3.57	3.56	0.01	22.73	179.96	1.11	1.07	1.06
10.00	3.54	3.54	0.00	22.11	179.95	1.09	1.05	1.05
50.00	3.55	3.54	0.00	21.98	179.53	1.08	1.04	1.05
100.00	3.57	3.57	0.00	22.10	179.01	1.09	1.04	1.06
150.00	3.60	3.60	0.01	22.20	178.54	1.11	1.05	1.09
200.00	3.60	3.60	0.00	22.35	178.04	1.13	1.06	1.12
300.00	3.65	3.66	0.01	22.70	177.08	1.18	1.09	1.19
375.00	3.68	3.75	0.07	23.18	176.60	1.22	1.13	1.25
400.00	3.73	3.73	0.01	23.26	176.18	1.23	1.14	1.28
500.00	3.87	3.88	0.01	24.27	175.75	1.29	1.21	1.38
550.00	3.84	3.95	0.11	24.90	175.68	1.32	1.25	1.44
600.00	3.96	4.03	0.07	25.74	175.59	1.35	1.30	1.50
700.00	4.03	4.17	0.14	27.76	175.20	1.41	1.41	1.64
750.00	4.15	4.42	0.27	29.19	175.46	1.44	1.46	1.72

1. Total Loss = Insertion Loss + 3dB splitter loss.

SBTCJ-1W+
TOTAL LOSS

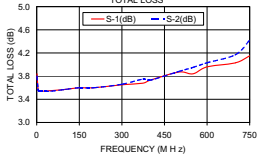

SBTCJ-1W+
ISOLATION

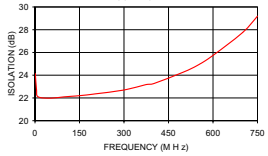

SBTCJ-1W+
VSWR

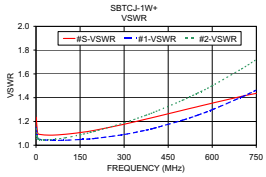

Demo Board MCL P/N: TB-227
Suggested PCB Layout (PL-117)

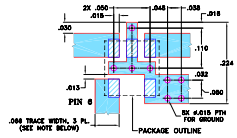

NOTES: 1. TRACE WIDTH IS SHOWN FOR ROGERS RO4350B WITH DIELECTRIC THICKNESS .030" ± .002", COPPER: 1/2 OZ. EACH SIDE. FOR OTHER MATERIALS TRACE WIDTH MAY NEED TO BE MODIFIED.
2. BOTTOM SIDE OF THE PCB IS CONTINUOUS GROUND PLANE.
DENOTES PCB COPPER LAYOUT WITH SMOBC (SOLDER MASK OVER BARE COPPER)
DENOTES COPPER LAND PATTERN FREE OF SOLDER MASK

electrical schematic

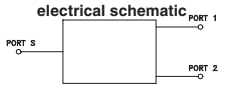

For detailed performance specs & shopping online see web site

Notes: 1. Performance and quality attributes and conditions not expressly stated in this specification sheet are intended to be excluded and do not form a part of this specification sheet. **2.** Electrical specifications and performance data contained herein are based on Mini-Circuit's applicable established test performance criteria and measurement instructions. **3.** The parts covered by this specification sheet are subject to Mini-Circuits standard limited warranty and terms and conditions (collectively, "Standard Terms"); Purchasers of this part are entitled to the rights and benefits contained therein. For a full statement of the Standard Terms and the exclusive rights and remedies thereunder, please visit Mini-Circuits' website at www.minicircuits.com/MCLStore/terms.jsp.

REV. H
M127604
ED-8081A/1
SBTCJ-1W+
DJ/TD/CP/AM
100621

Surface Mount

Power Splitter/Combiner

SCPJ-2-9+
SCPJ-2-9

2 Way-180° 50Ω 200 to 900 MHz

CASE STYLE: YY161
PRICE: $30.95 ea. QTY (1-9)

+ RoHS compliant in accordance with EU Directive (2002/95/EC)

The +Suffix identifies RoHS Compliance. See our web site for RoHS Compliance methodologies and qualifications.

Maximum Ratings

Operating Temperature	-40°C to 85°C
Storage Temperature	-55°C to 100°C
Power Input (as a splitter)	1W max.
Internal Dissipation	0.125W max.

Permanent damage may occur if any of these limits are exceeded.

Pin Connections

SUM PORT	1
PORT 1	5
PORT 2	6
GROUND	2,3,4,7,8

Features

- wideband, 200 to 900 MHz
- good isolation, 24 dB typ.
- excellent amplitude unbalance, 0.4 dB typ.

Applications

- VHF/UHF
- cellular
- communication systems

Outline Drawing

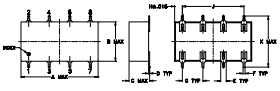

PCB Land Pattern

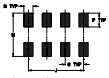

Suggested Layout,
Tolerance to be within ±.002

Outline Dimensions (inch/mm)

A	B	C	D	E	F	G
0.75	0.38	0.28	0.01	0.05	0.02	0.2
19.05	9.65	7.11	0.25	1.27	0.51	5.08

H	J	K	M	N	P	wt
0.075	0.6	0.45	0.47	0.1	0.15	grams
1.91	15.24	11.43	11.94	2.54	3.81	1.60

Demo Board MCL P/N: TB-50+
Suggested PCB Layout (PL-060)

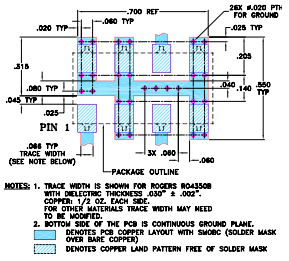

NOTES: 1. TRACE WIDTH IS SHOWN FOR ROGERS RO4350B WITH DIELECTRIC THICKNESS .030" ± .002", COPPER: 1/2 OZ. EACH SIDE. FOR OTHER MATERIALS TRACE WIDTH MAY NEED TO BE MODIFIED.
2. BOTTOM SIDE OF THE PCB IS CONTINUOUS GROUND PLANE.
DENOTES PCB COPPER LAYOUT WITH SMOBC (SOLDER MASK OVER BARE COPPER)
DENOTES COPPER LAND PATTERN FREE OF SOLDER MASK

Electrical Specifications

FREQ. RANGE (MHz)	ISOLATION (dB)	INSERTION LOSS (dB) ABOVE 3 dB	PHASE UNBALANCE (Degrees)	AMPLITUDE UNBALANCE (dB)
f_L-f_U	Typ. Min.	Typ. Max.	Max.	Max.
200-900	24 17	1.0 1.8	6	0.7

Typical Performance Data

Frequency (MHz)	Total Loss[1] (dB) S-1	Total Loss[1] (dB) S-2	Amplitude Unbalance (dB)	Isolation (dB)	Phase Unbalance (deg.)	VSWR S	VSWR 1	VSWR 2
201.54	4.06	3.65	0.41	22.58	183.33	1.42	1.27	1.13
265.38	3.90	3.60	0.29	22.25	181.67	1.37	1.21	1.14
297.31	4.03	3.71	0.33	22.26	180.97	1.36	1.19	1.14
361.15	3.91	3.68	0.23	22.27	179.90	1.33	1.17	1.15
393.08	3.96	3.73	0.23	22.30	179.67	1.29	1.17	1.14
463.64	4.01	3.83	0.18	22.66	178.81	1.28	1.18	1.15
502.27	3.91	3.79	0.13	23.00	178.58	1.23	1.19	1.14
540.91	3.98	3.84	0.14	23.36	178.37	1.24	1.20	1.15
618.18	4.03	3.96	0.07	24.25	181.90	1.20	1.20	1.15
695.45	4.05	4.06	0.00	25.27	181.65	1.10	1.20	1.17
734.09	4.08	4.05	0.04	25.64	181.51	1.11	1.20	1.20
811.36	4.15	4.23	0.08	24.90	181.15	1.08	1.17	1.25
850.00	4.26	4.24	0.02	23.66	179.95	1.05	1.16	1.31
913.64	4.34	4.46	0.12	21.20	180.00	1.16	1.13	1.37

1. Total Loss = Insertion Loss + 3dB splitter loss.

SCPJ-2-9
TOTAL LOSS

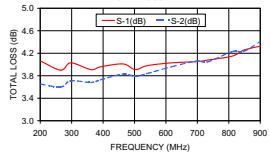

SCPJ-2-9
ISOLATION

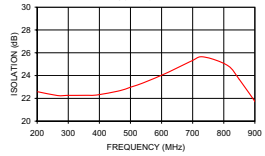

SCPJ-2-9
VSWR

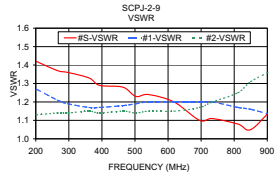

electrical schematic

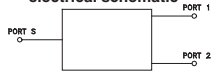

For detailed performance specs & shopping online see web site

Mini-Circuits®
ISO 9001 ISO 14001 AS 9100 CERTIFIED

P.O. Box 350166, Brooklyn, New York 11235-0003 (718) 934-4500 Fax (718) 332-4661 *The Design Engineers Search Engine* Provides ACTUAL Data Instantly at minicircuits.com

IF/RF MICROWAVE COMPONENTS

Notes: 1. Performance and quality attributes and conditions not expressly stated in this specification sheet are intended to be excluded and do not form a part of this specification sheet. **2.** Electrical specifications and performance data contained herein are based on Mini-Circuit's applicable established test performance criteria and measurement instructions. **3.** The parts covered by this specification sheet are subject to Mini-Circuits standard limited warranty and terms and conditions (collectively, "Standard Terms"); Purchasers of this part are entitled to the rights and benefits contained therein. For a full statement of the Standard Terms and the exclusive rights and remedies thereunder, please visit Mini-Circuits' website at www.minicircuits.com/MCLStore/terms.jsp.

REV. C
M127604
SCPJ-2-9
HY/TD/CP/AM
100621

Surface Mount

RF Transformer

ADT1-1WT+
ADT1-1WT

75Ω 0.4 to 800 MHz

CASE STYLE: CD542
PRICE: $2.95 ea. QTY (10-49)

+ RoHS compliant in accordance with EU Directive (2002/95/EC)

The + Suffix identifies RoHS Compliance. See our web site for RoHS Compliance methodologies and qualifications.

Maximum Ratings

Operating Temperature	-20°C to 85°C
Storage Temperature	-55°C to 100°C
RF Power	0.5W
DC Current	30mA

Permanent damage may occur if any of these limits are exceeded.

Pin Connections

PRIMARY DOT	3
PRIMARY	1
SECONDARY DOT	6
SECONDARY	4
SECONARY CT	2
NOT USED	5

Features

- excellent amplitude unbalance, 0.1 dB typ. and phase unbalance, 1 deg. typ. in 1dB bandwidth
- aqueous washable
- protected under US patent 6,133,525

Applications

- impedance matching
- balanced amplifier

Outline Drawing

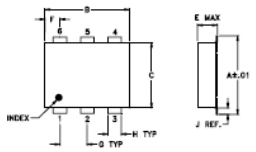

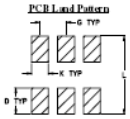

Suggested Layout,
Tolerance to be within ±.002

Outline Dimensions (inch / mm)

A	B	C	D	E	F	G
.272	.310	.220	.100	.112	.055	.100
6.91	7.87	5.59	2.54	2.84	1.40	2.54

H	J	K	L	wt
.030	.026	.065	.300	grams
0.76	0.66	1.65	7.62	0.20

Demo Board MCL P/N: TB-430

Config. A

Transformer Electrical Specifications

RATIO Ω	FREQUENCY (MHz)	INSERTION LOSS* 3 dB MHz	2 dB MHz	1 dB MHz	PHASE UNBALANCE (Deg.) Typ. 1 dB bandwidth	2 dB bandwidth	AMPLITUDE UNBALANCE (dB) Typ. 1 dB bandwidth	2 dB bandwidth
1	0.4-800	0.4-800	0.5-700	1-400	1	4	0.1	0.5

* Insertion Loss is referenced to mid-band loss, 0.3 dB typ.

Typical Performance Data

FREQUENCY (MHz)	INSERTION LOSS (dB)	INPUT R. LOSS (dB)	AMPLITUDE UNBALANCE (dB)	PHASE UNBALANCE (Deg.)
0.30	0.68	12.11	0.15	0.25
1.00	0.57	14.38	0.07	0.36
5.00	0.42	15.29	0.03	0.41
10.00	0.38	15.54	0.00	0.40
25.00	0.38	15.73	0.02	0.37
50.00	0.38	15.91	0.03	0.49
200.00	0.48	17.38	0.03	1.48
400.00	0.64	19.64	0.26	2.02
600.00	1.18	15.20	0.79	1.45
800.00	2.44	9.75	1.72	0.40

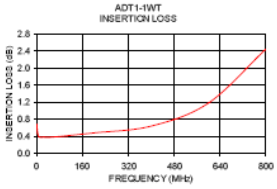

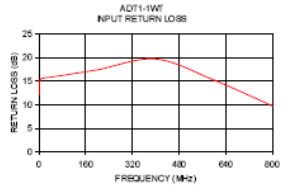

Mini-Circuits®
ISO 9001 ISO 14001 AS 9100 CERTIFIED
For detailed performance specs & shopping online see web site
P.O. Box 350166, Brooklyn, New York 11235-0003 (718) 934-4500 Fax (718) 332-4661 The Design Engineers Search Engine Provides ACTUAL Data Instantly at minicircuits.com
IF/RF MICROWAVE COMPONENTS
Notes 1. Performance and quality attributes and conditions not expressly stated in this specification sheet are intended to be excluded and do not form a part of this specification sheet. 2. Electrical specifications and performance data contained herein are based on Mini-Circuits applicable established test performance criteria and measurement instructions. 3. The parts covered by this specification sheet are subject to Mini-Circuits standard limited warranty and terms and conditions (collectively, "Standard Terms"); Purchasers of this part are entitled to the rights and benefits contained therein. For a full statement of the Standard Terms and the exclusive rights and remedies therunder, please visit Mini-Circuits' website at www.minicircuits.com/MCLStore/terms.jsp.

REV. D
M112648
ADT1-1WT
ED-7157/2
DJT/TD/CP/AM
071101

Microchip Transformer (Balun)

Wire Wound Type

● DXW21BN Series

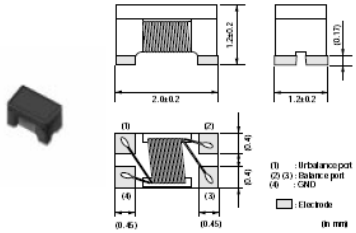

Equivalent Circuit

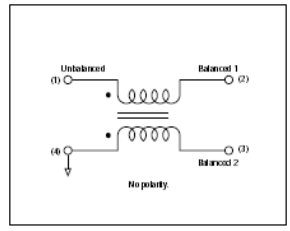

Part Number	Frequency Range	Port Impedance	Insertion Loss at Freq. Range (max.) (dB)	CMRR at Freq. Range (min.) (dB)	Rated Power (dBm)
DXW21BN7511S	1 to 1.5GHz	75 ohm - 75 ohm	1.4	20	27
DXW21BN7511T	50 to 870MHz	75 ohm - 75 ohm	1.0	20	27

Operating Temperature Range: -40°C to +85°C
Only for reflow soldering.

⚠Note • This PDF catalog is downloaded from the website of Murata Manufacturing co., ltd. Therefore, it's specifications are subject to change or our products in it may be discontinued without advance notice. Please check with our sales representatives or product engineers before ordering.
• This PDF catalog has only typical specifications because there is no space for detailed specifications. Therefore, please approve our product specifications or transact the approval sheet for product specifications before ordering.

The subsequent pages contains (regular) datasheets for inductors and capacitors from Johanson Technology. After that follows additional datasheets for mechanical and environmental specifications which contains more information than the regular datasheet about this topic.

MULTI-LAYER HIGH-Q CAPACITORS

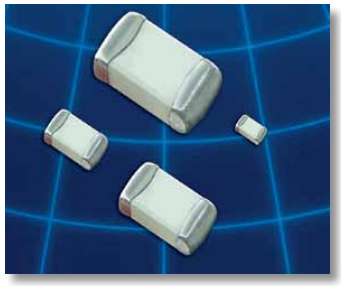

These lines of multilayer capacitors have been developed for High-Q and microwave applications.

• The **S-Series** (R03S, R07S, R14S, R15S) capacitors give an ultra-high Q performance, and exhibit NP0 temperature characteristics.

• The **L-Series** (R05L) capacitors give mid-high Q performance, and exhibit NP0 temperature characteristics.

• The **E-Series** (S42E, S48E, S58E) capacitors give excellent high-Q performance from HF to Microwave frequencies. Typical uses are high voltage, high current applications. They are offered in chip (Ni barrier or Non-Magnetic Pt.-Ag) or in Non-Magnetic leaded form.

• The **W-Series** (R05W) capacitors offer a large capacitance value in an ultra-small 0201 package size. These exhibit a X7R temperature characteristic.

• RoHS compliance is standard for all unleaded parts (see termination options box).

HOW TO ORDER

252	S48	E	470	K	V	4	E

VOLTAGE (DC)
6R3 = 6.3 V
101 = 100 V
160 = 16 V
250 = 25 V
500 = 50 V
201 = 200 V
251 = 250 V
301 = 300 V
501 = 500 V
102 = 1000 V
152 = 1500 V
202 = 2000 V
252 = 2500 V
362 = 3600 V
502 = 5000 V
722 = 7200 V

CASE SIZE
R03 (01005)
R05 (0201)
R07 (0402)
R14 (0603)
R15 (0805)
S42 (1111)
S48 (2525)
S58 (3838)

DIELECTRIC
S = Ultra High Q NPO
L = High Q NPO
E = Ultra High Q NPO, High Voltage, High Power,
*T = High Temp (175C) Ultra High Q NPO
W= X7R

CAPACITANCE (pF)
1st two digits are significant; third digit denotes number of zeros, R = decimal.
100 = 10 pF
101 = 100 pF

TOLERANCE
A = ± 0.05 pF
B = ± 0.10 pF
C = ± 0.25 pF
D = ± 0.50 pF
F = ±1 %
G = ±2%
J = ±5%
K = ± 10%

For tolerance availability, see chart.

TERMINATION
Nickel Barrier
V = Ni/Sn (Green)
T = Ni/SnPb
G = Ni/Au (Green)
Non-Mag*
U = Cu/Sn (Green)
C = Cu/SnPb
Leaded (All Non-Mag)*
1 = Microstrip
2 = Axial Ribbon
3 = Axial Wire
4 = Radial Ribbon
5 = Radial Wire

Part Number written: **252S48E470KV4E**

MARKING
3 = Cap Code & Tolerance
4 = No Marking
6 = EIA Code
(Marking on 0805 and larger only)

PACKAGING
S = Bulk
W = Waffle Pack
<u>01005 - 0603</u>
Y = Paper 5" Reel
T = Paper 7" Reel
*R = Paper 13" Reel
*J = Paper 5" Reel - Horizontally Oriented Electrodes
*N = Paper 5" Reel - Vertically Oriented Electrodes
*L = Paper 7" Reel - Horizontally Oriented Electrodes
*V = Paper 7" Reel - Vertically Oriented Electrodes
<u>0805 - 3838</u>
Z = Embossed 5" Reel
E = Embossed 7" Reel
*U = Embossed 13" Reel
*M = Embossed 5" Reel - Horizontally Oriented Electrodes
*Q = Embossed 5" Reel - Vertically Oriented Electrodes
*G = Embossed 7" Reel - Horizontally Oriented Electrodes
*P = Embossed 7" Reel - Vertically Oriented Electrodes
Tape specifications conform to EIA RS481

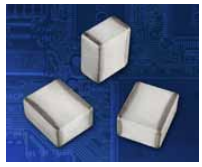

"*" - Not available for all MLCC - Call factory for info.

Low ESR / High-Q Capacitor Selection Chart

Cap. Value \ EIA Size			Miniature Size - Portable Electronics				RF Power Applications						
			01005	0201 (R05)		0402	0603	0805	1111	2525	3838		
			(R03S)	NPO (R05L)	X7R* (R05W)	(R07S)	(R14S)	(R15S)	(S42E)	(S48E)	(S58E)		
Capacitance pF	Code		Voltage										
0.1	0R1												
0.2	0R2		16 V	25 V		50/200 V	250 V		500V	1000V			
0.3	0R3		16 V	25 V		50/200 V	250 V	250 V	500V	1000V			
0.4	0R4		16 V	25 V		50/200 V	250 V	250 V	500V	1000V			
0.5	0R5		16 V	25 V		50/200 V	250 V	250 V	500V	1000V	2500V		
0.6	0R6		16 V	25 V		50/200 V	250 V	250 V	500V	1000V	2500V	3600V	7200V
0.7	0R7		16 V	25 V		50/200 V	250 V	250 V	500V	1000V	2500V	3600V	7200V
0.8	0R8		16 V	25 V		50/200 V	250 V	250 V	500V	1000V	2500V	3600V	7200V
0.9	0R9		16 V	25 V		50/200 V	250 V	250 V	500V	1000V	2500V	3600V	7200V
1.0	1R0		16 V	25 V		50/200 V	250 V	250 V	500V	1000V	2500V	3600V	7200V
1.1	1R1		16 V	25 V		50/200 V	250 V	250 V	500V	1000V	2500V	3600V	7200V
1.2	1R2	A	16 V	25 V		50/200 V	250 V	250 V	500V	1000V	2500V	3600V	7200V
1.3	1R3		16 V	25 V		50/200 V	250 V	250 V	500V	1000V	2500V	3600V	7200V
1.4	1R4	B	16 V	25 V		50/200 V	250 V	250 V	500V	1000V	2500V	3600V	7200V
1.5	1R5		16 V	25 V		50/200 V	250 V	250 V	500V	1000V	2500V	3600V	7200V
1.6	1R6	C	16 V	25 V		50/200 V	250 V	250 V	500V	1000V	2500V	3600V	7200V
1.7	1R7		16 V	25 V		50/200 V	250 V	250 V	500V	1000V	2500V	3600V	7200V
1.8	1R8	D	16 V	25 V		50/200 V	250 V	250 V	500V	1000V	2500V	3600V	7200V
1.9	1R9		16 V	25 V		50/200 V	250 V	250 V	500V	1000V	2500V	3600V	7200V
2.0	2R0		16 V	25 V		50/200 V	250 V	250 V	500V	1000V	2500V	3600V	7200V
2.1	2R1		16 V	25 V		50/200 V	250 V	250 V	500V	1000V	2500V	3600V	7200V
2.2	2R2		16 V	25 V		50/200 V	250 V	250 V	500V	1000V	2500V	3600V	7200V
2.4	2R4		16 V	25 V		50/200 V	250 V	250 V	500V	1000V	2500V	3600V	7200V
2.7	2R7		16 V	25 V		50 V	250 V	250 V	500V	1000V	2500V	3600V	7200V
3.0	3R0		16 V	25 V		50 V	250 V	250 V	500V	1000V	2500V	3600V	7200V
3.3	3R3		16 V	25 V		50 V	250 V	250 V	500V	1000V	2500V	3600V	7200V
3.6	3R6		16 V	25 V		50 V	250 V	250 V	500V	1000V	2500V	3600V	7200V
3.9	3R9		16 V	25 V		50 V	250 V	250 V	500V	1000V	2500V	3600V	7200V
4.3	4R3		16 V	25 V		50 V	250 V	250 V	500V	1000V	2500V	3600V	7200V
4.7	4R7		16 V	25 V		50 V	250 V	250 V	500V	1000V	2500V	3600V	7200V
5.1	5R1		16 V	25 V		50 V	250 V	250 V	500V	1000V	2500V	3600V	7200V
5.6	5R6	A**	16 V	25 V		50 V	250 V	250 V	500V	1000V	2500V	3600V	7200V
6.2	6R2	B	16 V	25 V		50 V	250 V	250 V	500V	1000V	2500V	3600V	7200V
6.8	6R8	C	16 V	25 V		50 V	250 V	250 V	500V	1000V	2500V	3600V	7200V
7.5	7R5	D	16 V	25 V		50 V	250 V	250 V	500V	1000V	2500V	3600V	7200V
8.2	8R2		16 V	25 V		50 V	250 V	250 V	500V	1000V	2500V	3600V	7200V
9.1	9R1		16 V	25 V		50 V	250 V	250 V	500V	1000V	2500V	3600V	7200V
10	100		16 V	25 V		50 V	250 V	250 V	500V	1000V	2500V	3600V	7200V
11	110		16 V	25 V		50 V	250 V	250 V	500V	1000V	2500V	3600V	7200V
12	120	F	16 V	25 V		50 V	250 V	250 V	500V	1000V	2500V	3600V	7200V
13	130		16 V	25 V		50 V	250 V	250 V	500V	1000V	2500V	3600V	7200V
15	150	G	16 V	25 V		50 V	250 V	250 V	500V	1000V	2500V	3600V	7200V
16	160		16 V	25 V		50 V	250 V	250 V	500V	1000V	2500V	3600V	7200V
18	180	J		25 V		50 V	250 V	250 V	500V	1000V	2500V	3600V	7200V
20	200			25 V		50 V	250 V	250 V	500V	1000V	2500V	3600V	7200V
22	220			25 V		50 V	250 V	250 V	500V	1000V	2500V	3600V	7200V
24	240	K		25 V		50 V	250 V	250 V	500V	1000V	2500V	3600V	7200V
27	270			25 V		50 V	250 V	250 V	500V	1000V	2500V	3600V	7200V
30	300			25 V		50 V	250 V	250 V	500V	1000V	2500V	3600V	7200V
33	330			25 V		50 V	250 V	250 V	500V	1000V	2500V	3600V	7200V

*** The R05W parts, which are X7R, can only be provided with "K" or "M" tolerance.** **Consult factory for Non-Standard values.**

****A tolerance only available for R07S (0402) and R14S(0603) caps**

Low ESR / High-Q Capacitor Selection Chart

Cap. Value \ EIA Size			Miniature Size - Portable Electronics				RF Power Applications						
			01005	0201 (R05)		0402	0603	0805	1111		2525	3838	
			(R03S)	NPO (R05L)	X7R* (R05W)	(R07S)	(R14S)	(R15S)	(S42E)		(S48E)	(S58E)	
Capacitance pF	Capacitance Code	Tolerance	Voltage										
36	360	F G J K		25 V			250 V	250 V	500V	1000V	2500V	3600V	7200V
39	390			25 V			250 V	250 V	500V	1000V	2500V	3600V	7200V
43	430			25 V			250 V	250 V	500V	1000V	2500V	3600V	7200V
47	470			25 V			250 V	250 V	500V	1000V	2500V	3600V	7200V
51	510			25 V			250 V	250 V	500V	1000V	2500V	3600V	7200V
56	560			25 V			250 V	250 V	500V	1000V	2500V	3600V	7200V
62	620			25 V			250 V	250 V	500V	1000V	2500V	3600V	7200V
68	680			25 V			250 V	250 V	500V	1000V	2500V	3600V	7200V
75	750			25 V			250 V	250 V	500V	1000V	2500V	3600V	7200V
82	820			25 V			250 V	250 V	500V	1000V	2500V	3600V	7200V
91	910			25 V			250 V	250 V	500V	1000V	2500V	3600V	7200V
100	101			25 V			250 V	250 V	500V	1000V	2500V	3600V	7200V
110	111				16 V			250 V	300V	500V	2500V	3600V	7200V
120	121							250 V	300V	500V	2500V	3600V	7200V
130	131							250 V	300V	500V	2500V	3600V	7200V
150	151							250 V	300V	500V	2500V	3600V	7200V
160	161							250 V	300V	500V	2500V	3600V	7200V
180	181							250 V	300V	500V	2500V	3600V	7200V
200	201							250 V	300V	500V	2500V	3600V	
220	221				16 V			250 V	200V	500V	2500V	3600V	
240	241								200V	500V	2500V	3600V	
270	271								200V	500V	2500V	3600V	
300	301								200V	500V	1500V	2500V	
330	331								200V	500V	1500V	2500V	
360	361								200V	500V	1500V	2500V	
390	391								200V	500V	1500V	2500V	
430	431	G J K							200V	500V	1500V	2500V	
470	471				16 V				200V	500V	1500V	2500V	
510	511								100V	500V	1000V	2500V	
560	561								100V	500V	1000V	2500V	
620	621								100V	500V	1000V	2500V	
680	681				16 V				50V		1000V	2500V	
750	751								50V		1000V	2500V	
820	821				16 V				50V		1000V	2500V	
910	911								50V		1000V	1000V	
1000	102				10 V				50V		1000V	1000V	
1200	122										1000V	1000V	
1500	152										500V	1000V	
1800	182										500V	1000V	
2200	222				10 V						300V	1000V	
2700	272										300V	500V	
3300	332											500V	
3900	392											500V	
4700	472				10 V							500V	
5100	512											500V	
10000	103				6.3 V								

*** The R05W parts, which are X7R, can only be provided with "K" and "M" tolerance.**
Consult factory for Non-Standard values.

Dielectric Characteristics

	NPO	X7R
TEMPERATURE COEFFICIENT:	0 ± 30ppm /°C, -55 to 125°C	± 15%, -55 to 125°C
QUALITY FACTOR / DF:	Q >1,000 @ 1 MHz, Typical 10,000	16VDC DF≤ 3.5% @ 1 KHz, 25°C 10VDC DF≤ 5.0% @ 1 KHz, 25°C
INSULATION RESISTANCE:	>10 GΩ @ 25°C,WVDC; 125°C IR is 10% of 25°C rating	>500 ΩF* or 10 GΩ* @ 25°C,WVDC; 125°C IR is 10% of 25°C rating * whichever is less
DIELECTRIC STRENGTH:	2.5 X WVDC Min., 25°C, 50 mA max	2.5 X WVDC Min., 25°C, 50 mA max
TEST PARAMETERS:	1MHz ±50kHz, 1.0±0.2 VRMS, 25°C	1KHz ±50Hz, 1.0±0.2 VRMS, 25°C
AVAILABLE CAPACITANCE:	Size 01005: 0.2 - 10 pF Size 0201: 0.2 - 100 pF Size 0402: 0.2 - 33 pF Size 0603: 0.2 - 100 pF Size 0805: 0.3 - 220 pF Size 1111: 0.2 - 1000 pF Size 2525: 1.0 - 2700 pF Size 3838: 1.0 - 5100 pF	100 - 10,000 pF

Mechanical & Environmental Characteristics

	SPECIFICATION	TEST PARAMETERS
SOLDERABILITY:	Solder coverage ≥ 90% of metalized areas No termination degradation	Preheat chip to 120°-150°C for 60 sec., dip terminals in rosin flux then dip in Sn62 solder @ 240°±5°C for 5±1 sec
RESISTANCE TO SOLDERING HEAT:	No mechanical damage Capacitance change: ±2.5% or 0.25pF Q>500 I.R. >10 G Ohms Breakdown voltage: 2.5 x WVDC	Preheat device to 80°-100°C for 60 sec. followed by 150°-180°C for 60 sec. Dip in 260°±5°C solder for 10±1 sec. Measure after 24±2 hour cooling period
TERMINAL ADHESION:	Termination should not pull off. Ceramic should remain undamaged.	Linear pull force* exerted on axial leads soldered to each terminal. *0402 ≥ 2.0lbs, 0603 ≥ 2.0lbs (min.)
PCB DEFLECTION:	No mechanical damage. Capacitance change: 2% or 0.5pF Max	Glass epoxy PCB: 0.5 mm deflection
LIFE TEST:	No mechanical damage Capacitance change: ±3.0% or 0.3 pF Q>500 I.R. >1 G Ohms Breakdown voltage: 2.5 x WVDC	Applied voltage: 200% rated voltage, 50 mA max. Temperature: 125°±3°C Test time: 1000+48-0 hours
THERMAL CYCLE:	No mechanical damage. Capacitance change: ±2.5% or 0.25pF Q>2000 I.R. >10 G Ohms Breakdown voltage: 2.5 x WVDC	5 cycles of: 30±3 minutes @ -55°+0/-3°C, 2-3 min. @ 25°C, 30±3 min. @ +125°+3/-0°C, 2-3 min. @ 25°C Measure after 24±2 hour cooling period
HUMIDITY, STEADY STATE:	No mechanical damage. Capacitance change: ±5.0% or 0.50pF max. Q>300 I.R. ≥ 1 G-Ohm Breakdown voltage: 2.5 x WVDC	Relative humidity: 90-95% Temperature: 40°±2°C Test time: 500 +12/-0 Hours Measure after 24±2 hour cooling period
HUMIDITY, LOW VOLTAGE:	No mechanical damage. Capacitance change: ±5.0% or 0.50pF max. Q>300 I.R. = 1 G-Ohm min. Breakdown voltage: 2.5 x WVDC	Applied voltage: 1.5 VDC, 50 mA max. Relative humidity: 85±2% Temperature: 40°±2°C Test time: 240 +12/-0 Hours Measure after 24±2 hour cooling period
VIBRATION:	No mechanical damage. Capacitance change: ±2.5% or 0.25pF Q>1000 I.R. ≥ 10 G-Ohm Breakdown voltage: 2.5 x WVDC	Cycle performed for 2 hours in each of three perpendicular directions Frequency range 10Hz to 55 Hz to 10 Hz traversed in 1 minute. Harmonic motion amplitude: 1.5mm

MECHANICAL CHARACTERISTICS

Size	Units	Length	Width	Thickness	End Band
01005	In	.016 ±.001	.008 ±.001	.008 ±.001	.006 Max.
(0402)	mm	(0.40 ±0.03)	(0.20 ±0.03)	(0.20 ±0.03)	(0.15 Max.)
0201	In	.024 ±.001	.012 ±.001	.012 ±.001	.008 Max.
(0603)	mm	(0.60 ±0.03)	(0.30 ±0.03)	(0.30 ±0.03)	(0.20 Max.)
0402	In	.040 ±.004	.020 ±.004	.020 ±.004	.010 ±.006
(1005)	mm	(1.02 ±0.1)	(0.51 ±0.1)	(0.51 ±0.1)	(0.25 ±.15)
0603	In	.062 ±.006	.032 ±.006	.030 +.005/-.003	.014 ±.006
(1608)	mm	(1.57 ±0.15)	(0.81 ±0.15)	(0.76 +.13-.08)	(0.35 ±.15)
0805	In	.080 ±.008	.050 ±.008	.040 ±.006	.020 ±.010
(2012)	mm	(2.03 ±0.20)	(1.27 ±0.20)	(1.02 ±.15)	(0.50 ±.25)

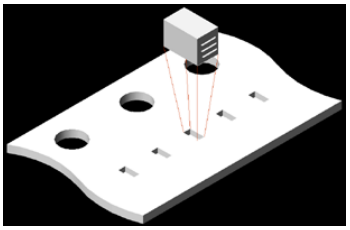

Horizontal Electrode Orientation

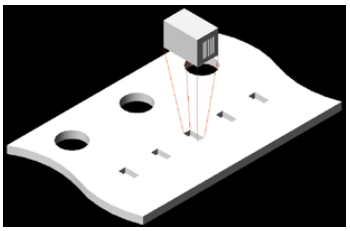

Vertical Electrode Orientation

E-Series Terminations and Leads

Termination	Size	Units	L	Tol	W	Tol	T	E / B	Tol
V,T U,C	S42E	In	0.110	+.020 -.010	0.110	+/- .015	0.102 Max.	0.015 Typ.	+/- 0.008
		mm	2.79	+0.51 -0.25	2.79	+/- 0.38	2.59 Max.	0.38 Typ.	+/- 0.20
	S48E	In	0.230	+.025 -.010	0.250	+/- .015	0.150 Max.	0.025 Typ.	
		mm	5.84	+0.63 -0.25	6.35	+/- 0.38	3.81 Max.	0.63 Typ.	
	S58E	In	0.380	+.015 -.010	0.380	+/- .010	0.170 Max.	0.025 Typ.	
		mm	9.65	+0.38 -0.25	9.65	+/- 0.25	4.32 Max.	0.63 Typ.	

For all E-Series Models:

OPERATING TEMP. :	-55 to +125°C
INSULATION RESISTANCE:	>1000 ΩF or >10 GΩ, whichever is less @ 25°C WVDC
TEMPERATURE COEFFICIENT:	0 ± 30ppm /°C, -55 to 125°C
DISSIPATION FACTOR (TYP.):	< 0.05% @ 1 MHz

Unleaded Termination Codes "V" (Ni/Sn), "T" (Ni/SnPb), "U" (Cu/Sn non-mag), "C" (Cu/SnPb non-mag)

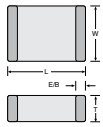

Microstrip Ribbon Leads (Non-Magnetic), Termination Code "1"

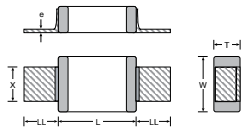

Axial Ribbon Leads (Non-Magnetic), Termination Code "2"

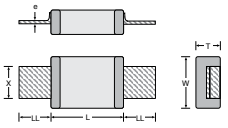

Axial Wire Leads (Non-Magnetic), Termination Code "3"

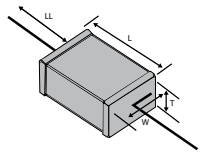

Radial Ribbon Leads (Non-Magnetic), Termination Code "4"

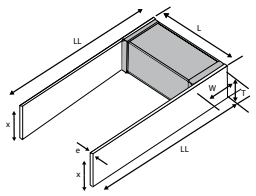

Radial Wire Leads (Non-Magnetic), Termination Code "5"

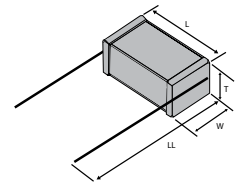

Lead	Size	Units	L	Tol	W	Tol	T (max)	E/B (typ)	LL(min)	X	Tol	e	Tol
1	S42E	In	0.135	+/- .015	0.110	+/- .020	0.120	0.015	0.25	0.093	+/-0.005	0.004	+/- 0.001
		mm	3.43	+/- 0.38	2.79	+/- 0.51	3.05	0.38	6.35	2.36	+/- 0.13	0.102	+/- 0.025
	S48E	In	0.245	+/- 0.025	0.250	+/- 0.015	0.160	0.025	0.50	0.240	+/- 0.005	0.004	+/- 0.001
		mm	6.22	+/- 0.64	6.35	+/-0.38	3.81	0.63	12.7	6.10	+/- 0.13	0.102	+/- 0.025
	S58E	In	0.38	+0.035 / - 0.010	0.38	+/- 0.010	0.170	0.04 MAX.	0.750	0.35	+/- 0.010	0.010	+/- 0.005
		mm	9.65	+0.89 / -0.25	9.65	+/- 0.25	4.32	1.02 MAX.	19.05	8.89	+/- 0.25	0.25	+/- 0.13
2	S42E	In	0.135	+/- .015	0.110	+/- .020	0.102	0.015	0.25	0.093	+/-0.005	0.004	+/- 0.001
		mm	3.43	+/- 0.38	2.79	+/- 0.51	2.59	0.38	6.35	2.36	+/- 0.13	0.102	+/- 0.025
	S48E	In	0.245	+/- 0.025	0.250	+/- 0.015	0.160	0.025	0.50	0.240	+/- 0.005	0.004	+/- 0.001
		mm	6.22	+/- 0.64	6.35	+/-0.38	3.81	0.63	12.7	6.10	+/- 0.13	0.102	+/- 0.025
	S58E	In	0.38	+0.035 / - 0.010	0.38	+/- 0.010	0.170	0.04 MAX.	0.750	0.35	+/- 0.010	0.010	+/- 0.005
		mm	9.65	+0.89 / -0.25	9.65	+/- 0.25	4.32	1.02 MAX.	19.05	8.89	+/- 0.25	0.25	+/- 0.13
3	S42E S48E S58E	In	0.145	+/- .020	0.110	+/- .015	0.102		0.50	#26 AWG, .016 (.406) dia. nominal			
		mm	3.68	+/- 0.51	2.79	+/- 0.38	2.59		12.70				
4	S42E S48E S58E	In	0.135	+/- .015	0.110	+/- .015	0.102		0.25	0.093	+/-0.005	0.004	+/- 0.001
		mm	3.43	+/- 0.38	2.79	+/- 0.38	2.59		6.35	2.36	+/- 0.13	0.102	+/- 0.025
5	S42E S48E S58E	In	0.145	+/- .020	0.110	+/- .015	0.102		0.50	#26 AWG, .016 (.406) dia. nominal			
		mm	3.68	+/- 0.51	2.79	+/- 0.38	2.59		12.70				

SERIES RESONANCE CHART

Typical Series Resonant Frequency (Series Mounted)

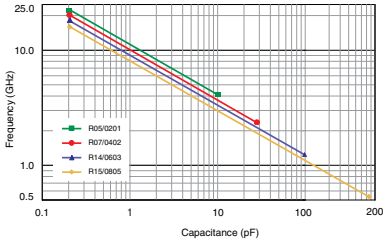

RF CHARACTERISTICS - L-SERIES

ESR vs Frequency: 0201/R05L

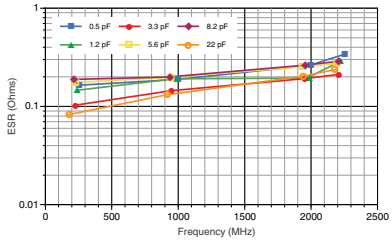

Q vs Frequency: 0201/R05L

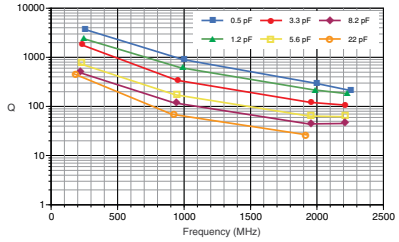

ESR vs Capacitance: 0201/R05L

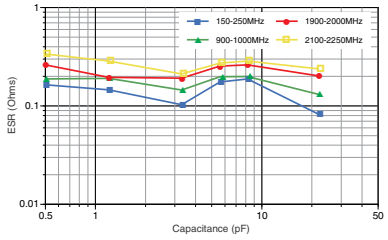

Q vs Capacitance: 0201/R05L

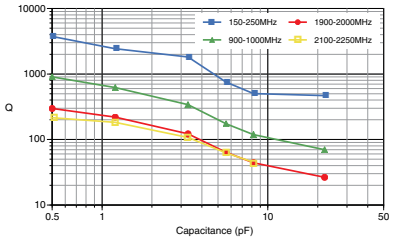

S-Series RF Characteristics versus Frequency

Equivalent Series Resistance: 0402/R07S

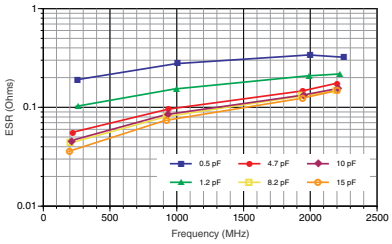

Q Factor: 0402/R07S

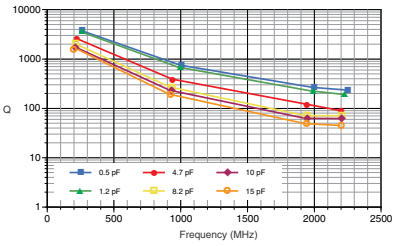

Equivalent Series Resistance: 0603/R14S

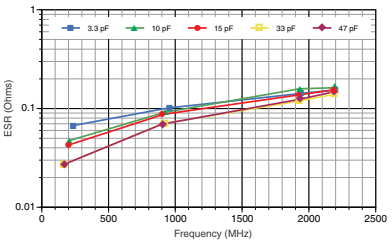

Q Factor: 0603/R14S

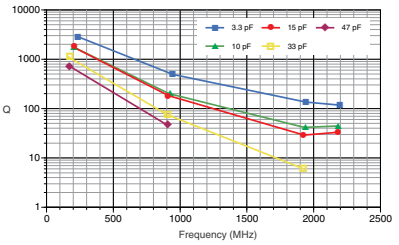

Equivalent Series Resistance: 0805/R15S

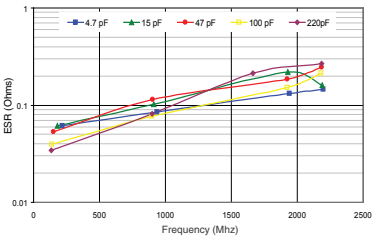

Q Factor: 0805/R15S

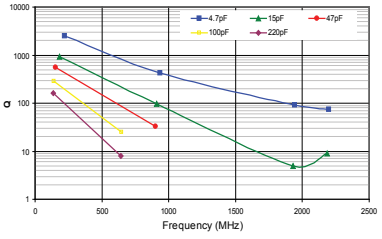

Measurements performed on a Boonton 34A Resonant Coaxial Line and represent typical capacitor performance.

S-Series RF Characterisitcs versus Capacitance

Equivalent Series Resistance: 0402/R07S

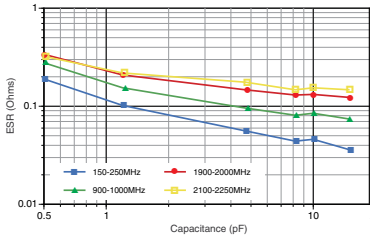

Q Factor: 0402/R07S

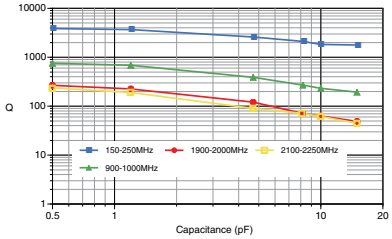

Equivalent Series Resistance: 0603/R14S

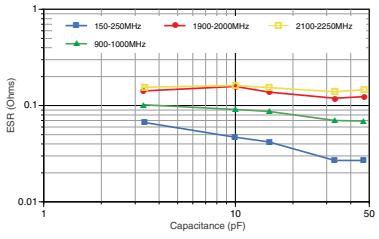

Q Factor: 0603/R14S

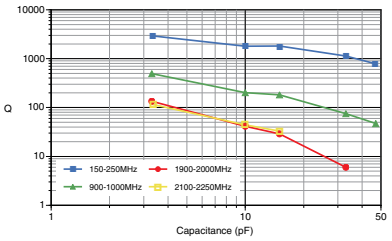

Equivalent Series Resistance: 0805/R15S

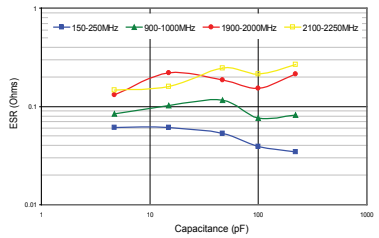

Q Factor: 0805/R15S

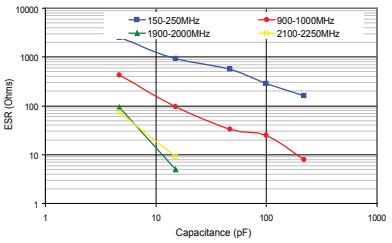

Measurements performed on a Boonton 34A Resonant Coaxial Line and represent typical capacitor performance.

S42E Series RF Characteristics versus Frequency

Equivalent Series Resistance: 1111/S42E

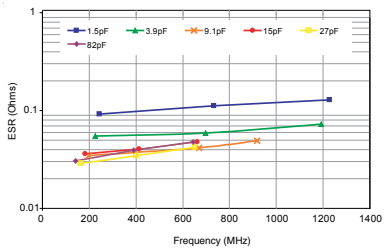

Q Factor: 1111/S42E

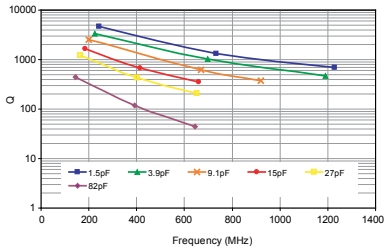

S42E Series RF Characteristics versus Capacitance

S42E Equivalent Series Resistance vs Capacitance, Typical

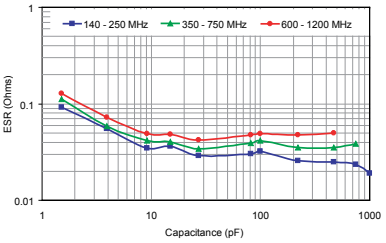

S42E Q vs. Capacitance, Typical

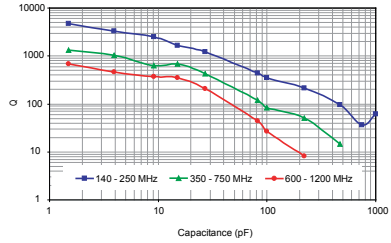

S42E SRF (Series Mount), Typical

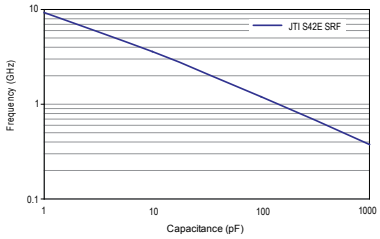

JTI S48E GRAPHICAL DATA

SRF (Shunt Mount), S48E, Typical (Preliminary)

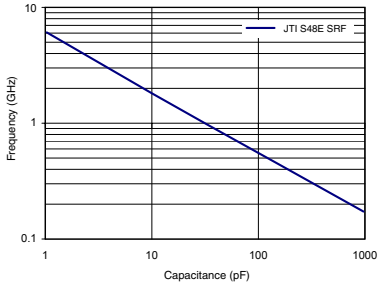

As measured on a 8720C VNA, using a Shunt-Through fixture, and using the S11 magnitude dip to determine the SRF

Current Rating vs. Capacitance, S48E, Typical (Preliminary)

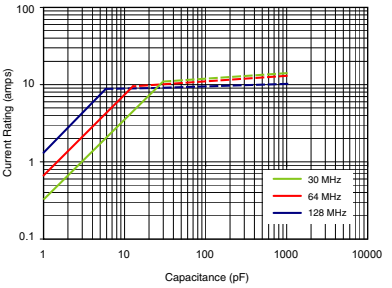

Solid traces show voltage limited current (Vrms)

Dotted traces show power dissipation limited current (Based on 4 Watts Power Dissipation, and 125 degrees C case temp.)

S48E Q vs. Capacitance, Typical (Preliminary)

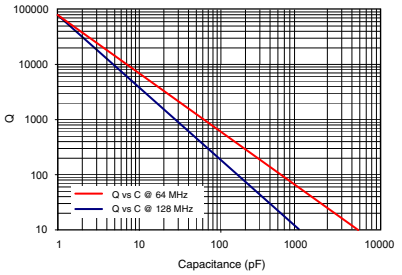

As measured on a 4287A LCR meter, using a 16092A fixture

S48E ESR vs. Capacitance, Typical (Preliminary)

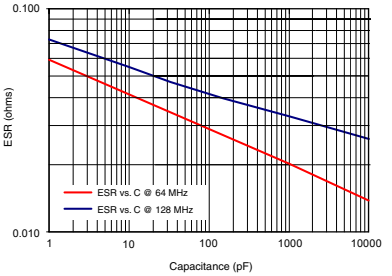

As measured on a 4287A LCR meter, using a 16092A fixture

RF Ceramic Chip Inductors

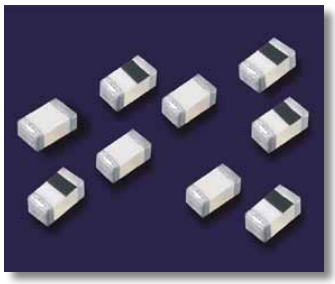

Polarity Half-Marked Inductors (0201 only)

High frequency multi-layer chip inductors feature a monolithic body made of low loss ceramic and high conductivity metal electrodes to achieve optimal high frequency performance.

These RF chip inductors are compact in size and feature lead-free tin plated nickel barrier terminations and tape and reel packaging which makes them ideal for small size/high volume wireless applications.

Applications & Features

- CELL/PCS Modules
- Broadband Components
- RF Tranceivers
- Wireless LAN
- RFID
- RoHS Compliant (Standard, "V" Code)
- Sn/Pb Terminations Optional ("T" Code)

Product Range Summary

EIA SIZE (mm)	SIZE CODE	L RANGE	Q FACTOR (Min.)	SRF (Typ.)	TEMPERATURE
0201 (0603)	L-05	0.6 - 39 nH	4 (100 MHz)	>21 GHz (1.0 nH)	-40°C to +100°C
0402 (1005)	L-07	1.0 - 120 nH	8 (100 MHz)	>21 GHz (1.0 nH)	-40°C to +100°C
0603 (1608)	L-14	1.0 - 220 nH	12 (100 MHz)	>23 GHz (1.0 nH)	-40°C to +100°C

Mechanical Characteristics

	0201 (0603)		0402 (1005)		0603 (1608)	
	Inches	mm	Inches	mm	Inches	mm
Length	.024 ±.001"	(0.6 ±0.03)	.039 ±.004"	(1.00 ±.10)	.063 ±.006"	(1.60 ±.15)
Width	.012 ±.001"	(0.3 ±0.03)	.020 ±.004"	(0.50 ±.10)	.031 ±.006"	(0.80 ±.15)
Thickness	.012 ±.001"	(0.3 ±0.03)	.020 ±.004"	(0.50 ±.10)	.031 ±.006"	(0.80 ±.15)
End Band	.006 ±.002"	(0.15 ±0.05)	.009 ±.004"	(0.23 ±.10)	.012 ±.008"	(0.30 ±.20)

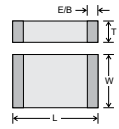

How to Order

L-	07	C	10N	J	V	6	T

DEVICE
Inductor

SIZE
05 = 0201
07 = 0402
14 = 0603

TYPE
B = Polarity Half-Marked (all 0201)
C = 0402 and 0603 (see "Marking")

VALUE
See Table

TOLERANCE

C = ± 0.2 nH	≤ 1.0 nH
S = ± 0.3 nH	1.0 to 5.6 nH
J = ± 5%	6.8 nH and above
K = ± 10%	3.3 nH and above

TERMINATION
V = Ni/Sn
T = Ni / SnPb

MARKING
4 = No Marking (all 0603)
6 = Orientation Mark (all 0201 and 0402*)

PACKAGING
Tape and Reel

Size	Code	Tape	Reel	Qty
0201	T	Paper	7"	15,000
0402	T	Paper	7"	10,000
0603	T	Paper	7"	4,000

Bulk (Loose Pcs.)

Size	Code
All	S

Part number written: L-07C10NJV6T

Orientation Full Marking (all 0402)

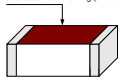

*Please note that all 0402 inductors (L-07C) have orientation full marking only.

RF Chip Inductor Selection Chart

Inductor Value / EIA Size			0201 (L-05)	0402 (L-07)	0603 (L-14)
Inductance nH	Code	Tolerance			
0.6	0N6	C S	300 mA		
0.7	0N7		300 mA		
0.8	0N8		300 mA		
0.9	0N9		300 mA		
1.0	1N0		300 mA	300 mA	300 mA (S only)
1.2	1N2		300 mA	300 mA (S only)	300 mA (S only)
1.3	1N3		300 mA		
1.5	1N5		300 mA	300 mA (S only)	300 mA (S only)
1.8	1N8	S	300 mA	300 mA	300 mA
1.9	1N9		300 mA	300 mA	
2.0	2N0		300 mA	300 mA	
2.2	2N2		300 mA	300 mA	300 mA
2.3	2N3		300 mA		
2.4	2N4		300 mA	300 mA	
2.5	2N5		300 mA		
2.7	2N7		300 mA	300 mA	300 mA
3.0	3N0	K S	300 mA	300 mA	
3.3	3N3		300 mA	300 mA	300 mA
3.6	3N6		300 mA	300 mA	
3.7	3N7		300 mA		
3.9	3N9		300 mA	300 mA	300 mA
4.3	4N3			300 mA	
4.7	4N7		300 mA	300 mA	300 mA
5.1	5N1		300 mA	300 mA	
5.6	5N6		300 mA	300 mA	300 mA
6.2	6N2			300 mA	
6.8	6N8	J K	250 mA	250 mA	300 mA
7.5	7N5			250 mA	
8.2	8N2		250 mA	250 mA	300 mA
10	10N		250 mA	250 mA	300 mA
12	12N		250 mA	250 mA	300 mA
13	13N		250 mA	250 mA	
15	15N		250 mA	250 mA	300 mA
18	18N		200 mA	200 mA	300 mA
20	20N		200 mA	200 mA	
22	22N		200 mA	200 mA	300 mA
23	23N			200 mA	
27	27N		200 mA	200 mA	300 mA
33	33N		200 mA	200 mA	300 mA
39	39N		200 mA	150 mA	300 mA
43	43N			150 mA	
47	47N			150 mA	300 mA
56	56N			150 mA	300 mA
68	68N			100 mA	300 mA
82	82N			100 mA	300 mA
100	R10			100 mA	300 mA
120	R12			100 mA	300 mA
150	R15				300 mA
180	R18				300 mA
220	R22				300 mA
270	R27				
330	R33				
390	R39				
420	R42				
560	R56				
680	R68				

Consult factory for Non-Standard values.
See web page for Chip Inductor Product Detail Summary by part number

RF Characteristics Characteristics (Typical)

INDUCTANCE VS FREQUENCY: SIZE 0201

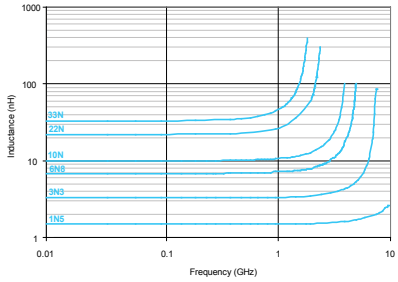

Q VS FREQUENCY: SIZE 0201

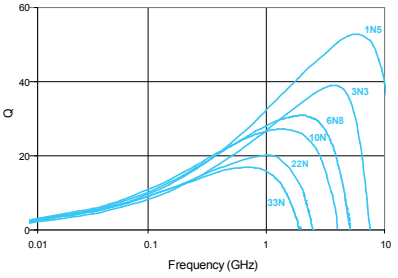

INDUCTANCE VS FREQUENCY: SIZE 0402

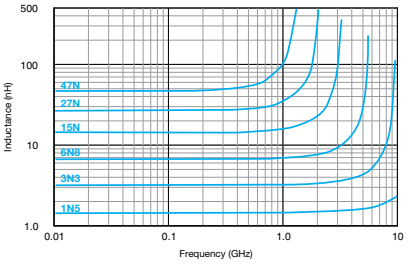

Q VS FREQUENCY: SIZE 0402

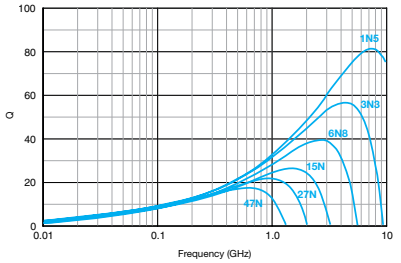

INDUCTANCE VS FREQUENCY: SIZE 0603

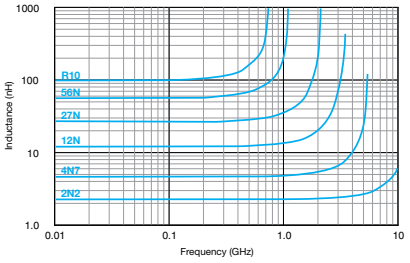

Q VS FREQUENCY: SIZE 0603

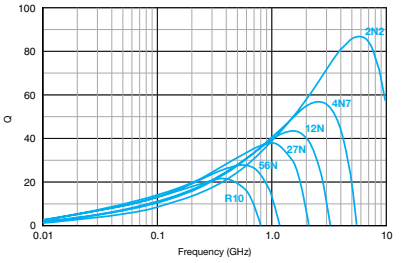

RF Wirewound Chip Inductors

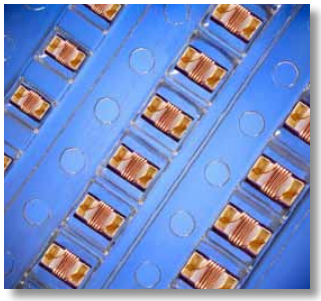

These high frequency High-Q chip inductors feature a monolithic body made of low loss ceramic wound with wire to achieve optimal high frequency performance.

These RF chip inductors are compact in size and are provided on tape and reel packaging which makes them ideal for high volume RF applications. They feature a nickel barrier with a top plating of gold for the ceramic core types (all 0402, all 0603, and most 0805 types), and with a top plating of 100% tin for the ferrite core types (0805 size, 470 nH and higher). Most inductance values between those listed are available on request.

Applications

- CELL/PCS Modules
- Broadband Components
- RF Tranceivers
- Cable Modem
- Bluetooth
- Wireless LAN
- RFID
- Cordless Phone
- Computer Peripherals
- ASDL

Product Range Summary

EIA SIZE (mm)	SIZE CODE	L RANGE	Q FACTOR (Typ.)	SRF (Typ.)	TEMPERATURE
0402 (1005)	L-07	1.0 - 120 nH	55 (900 MHz)	>11 GHz (1.0 nH)	-40°C to + 125°C
0603 (1608)	L-14	2.0 - 470 nH	60 (900 MHz)	>13 GHz (2.0 nH)	-40°C to + 125°C
0805 (2012)	L-15	2.2 - 10,000 nH	60 (500 MHz)	>11 GHz (2.2 nH)	-40°C to + 125°C*

*-40 deg. C to +85 deg. C for ferrite core types

Mechanical Characteristics

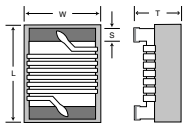

	0402 (1005)		0603 (1608)		0805 (2012)	
	Inches	mm	Inches	mm	Inches	mm
Length	.039 ±.004"	(1.00 ±.10)	.063 ±.008"	(1.60 ±.20)	.079 ±.008"	(2.00 ±.20)
Width	.022 ±.004"	(0.55 ±.10)	.041 ±.008"	(1.05 ±.20)	.049 ±.008"	(1.25 ±.20)
Thickness	.020 ±.004"	(0.50 ±.10)	.041 ±.008"	(1.05 ±.20)	.047 ±.008"	(1.20 ±.20)
End Band	.008 ±.004"	(0.20 ±.10)	.014 ±.004"	(0.35 ±.10)	.016 ±.004"	(0.40 ±.10)

How to Order

L-	07	W	4N3	S	V	4	T

DEVICE
Inductor

SIZE
07 = 0402
14 = 0603
15 = 0805

TYPE
W = Wirewound on Ceramic Core
F = Wirewound on Ferrite Core

VALUE
See Table

TOLERANCE*
C = ± 0.2 nH
S = ± 0.3 nH
G = ± 2%
J = ± 5%
K = ± 10%

TERMINATION
V = Ni / Au for "W"types, and V = Ni / 100% Sn for "F" types

MARKING
4 = No Marking

PACKAGING
Tape and Reel

Size	Code	Tape	Reel	Qty
0402	T	Paper	7"	10,000
0603	E	Embossed	7"	3,000
0805	E	Embossed	7"	2,000

Bulk (Loose Pcs.)

Size	Code
All	S

Example Part Number:
L-07W4N3SV4T is: 0402 Wirewound, 4.3 nanohenry, +/- 0.3 nH tolerance, Ni / Au termination, No Marking, Paper tape on a 7" reel.

RF WIREWOUND CHIP INDUCTOR SELECTION CHART

EIA Size / Inductor Value		0402 (L-07)		0603 (L-14)		0805 (L-15)		Core Type
Inductance nH	Code	Tolerance	Rated Current	Tolerance	Rated Current	Tolerance	Rated Current	
1.0	1N0	C, S	1360 mA					CERAMIC CORE ("VV" Type)
1.2	1N2	C, S	1300 mA					
1.6	1N6			C, S	700 mA			
1.8	1N8	C, S	1040 mA	C, S	700 mA			
1.9	1N9	C, S	1040 mA					
2.0	2N0	C, S	1040 mA	C, S	700 mA			
2.2	2N2	C, S	960 mA			C, S	800 mA	
2.4	2N4	C, S	790 mA					
2.6	2N6	C, S	640 mA					
2.7	2N7	C, S	640 mA			C, S	800 mA	
3.3	3N3	C, J, K	840 mA	C, S	700 mA	C, S	800 mA	
3.6	3N6	C, J, K	840 mA	C, S	700 mA			
3.9	3N9	C, J, K	840 mA	C, S	700 mA	C, S	600 mA	
4.3	4N3	C, J, K	700 mA	C, S	700 mA			
4.7	4N7	C, J, K	640 mA	C, S	700 mA	C, S	600 mA	
5.1	5N1	C, J, K	800 mA	C, J, K	700 mA			
5.6	5N6	C, J, K	760 mA	C, J, K	700 mA	C, J, K	600 mA	
6.2	6N2	C, J, K	760 mA					
6.8	6N8	C, J, K	680 mA	C, G J, K	700 mA	C, G J, K	600 mA	
7.5	7N5	C, J, K	680 mA	C, J, K	700 mA	J, K	600 mA	
8.2	8N2	C, J, K	680 mA	C, G J, K	700 mA	C, G, J, K	600 mA	
8.7	8N7	C, J, K	480 mA	G, J, K	700 mA			
9.0	9N0	C, J, K	680 mA					
9.5	9N5	C, J, K	680 mA	G, J, K	700 mA			
10	10N	G, J, K	480 mA	G, J, K	700 mA	G, J, K	600 mA	
11	11N	G, J, K	640 mA	G, J, K	700 mA			
12	12N	G, J, K	640 mA	G, J, K	700 mA	G, J, K	600 mA	
13	13N	G, J, K	560 mA			J, K	600 mA	
15	15N	G, J, K	560 mA	G, J, K	700 mA	G, J, K	600 mA	
16	16N	G, J, K	560 mA	G, J, K	700 mA	G, J, K	600 mA	
18	18N	G, J, K	420 mA	G, J, K	700 mA	G, J, K	600 mA	
19	19N	G, J, K	480 mA					
20	20N	G, J, K	420 mA	G, J, K	700 mA	G, J, K	600 mA	
22	22N	G, J, K	400 mA	G, J, K	700 mA	G, J, K	600 mA	
23	23N	G, J, K	400 mA	G, J, K	700 mA			
24	24N	G, J, K	400 mA	G, J, K	700 mA	J, K	600 mA	
27	27N	G, J, K	400 mA	G, J, K	600 mA	G, J, K	600 mA	
30	30N	G, J, K	400 mA	G, J, K	700 mA			
33	33N	G, J, K	400 mA	G, J, K	600 mA	G, J, K	500 mA	
36	36N	G, J, K	320 mA			J, K	600 mA	
39	39N	G, J, K	320 mA	G, J, K	600 mA	G, J, K	500 mA	
40	40N	G, J, K	320 mA					
43	43N	G, J, K	100 mA	G, J, K	700 mA	J, K	600 mA	
47	47N	G, J, K	100 mA	G, J, K	600 mA	G, J, K	500 mA	
51	51N	J, K	100 mA	G, J, K	600 mA	J, K	600 mA	
56	56N	J, K	100 mA	G, J, K	600 mA	G, J, K	500 mA	
68	68N	J, K	100 mA	G, J, K	600 mA	G, J, K	500 mA	
72	72N			G, J, K	400 mA			
82	82N	J, K	100 mA	G, J, K	400 mA	G, J, K	500 mA	
100	R10	J, K	100 mA	G, J, K	400 mA	G, J, K	500 mA	
110	R11	J, K	100 mA					
120	R12	J, K	100 mA	G, J, K	300 mA	G, J, K	500 mA	
150	R15			G, J, K	280 mA	G, J, K	400 mA	
180	R18			G, J, K	240 mA	G, J, K	400 mA	
220	R22			G, J, K	200 mA	G, J, K	400 mA	
270	R27			G, J, K	170 mA	G, J, K	350 mA	

See web page for WireWound Inductor Product Detail Summary by part number

EIA Size / Inductor Value		0402 (L-07)		0603 (L-14)		0805 (L-15)		Core Type
Inductance nH	Code	Tolerance	Rated Current	Tolerance	Rated Current	Tolerance	Rated Current	
330	R33			J, K	150 mA	G, J, K	300 mA	Ceramic
390	R39			J, K	100 mA	G, J, K	210 mA	
470	R47			J, K	100 mA	J, K	500 mA	FERRITE CORE ("F" Type)
560	R56					J, K	450 mA	
680	R68					J, K	400 mA	
820	R82					J, K	300 mA	
1000	1R0					J, K	180 mA	
1200	1R2					J, K	150 mA	
1500	1R5					J, K	130 mA	
1800	1R8					J, K	120 mA	
2200	2R2					J, K	110 mA	
2700	2R7					J, K	100 mA	
3300	3R3					J, K	210 mA	
3900	3R9					J, K	200 mA	
4700	4R7					J, K	180 mA	
5600	5R6					J, K	160 mA	
6800	6R8					J, K	130 mA	
8200	8R2					J, K	120 mA	
10000	10R					J, K	80 mA	

Consult factory for Non-Standard values.

RF Characteristics Characteristics (Typical)

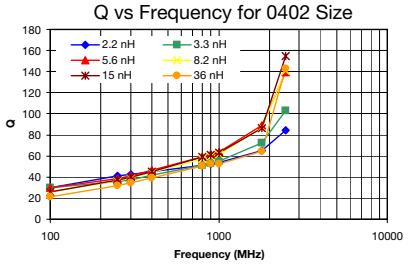

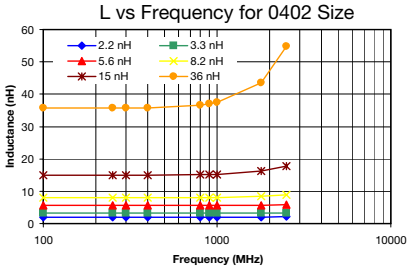

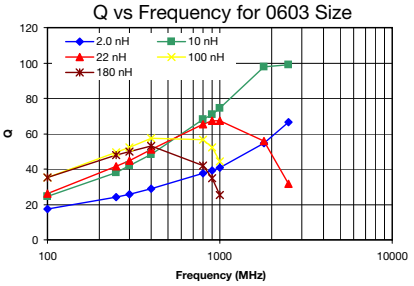

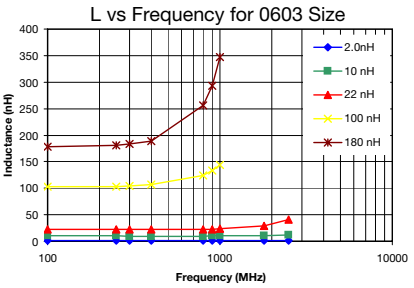

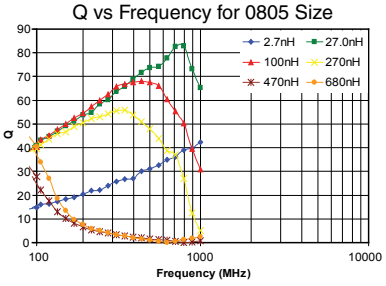

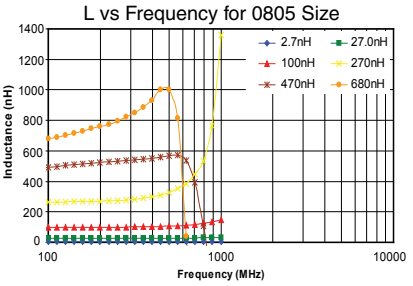

Mechanical & Environmental Characteristics

	Specification	Test Parameters
Solderability:	Solder coverage ≥ 75% of electrodes L = ± 10% Q = ±20%	Preheat 120±20°C for 1 min. Dip 230±10°C for 3±1 sec.
Resistance to soldering:	No apparent damage Solder coverage ≥ 75% L = ± 10% Q = ± 20%	Preheat 120±20°C for 1 min. Dip 260±10°C for 10±1 sec.
Thermal Shock:	No apparent damage L = ± 10% Q = ± 20%	100 cycles: 30±3 minutes @+100°C then 30±3 min. @ -40°C
Life Test:	No apparent damage L = ± 10% Q = ± 20%	1000 ±48 Hours @ +85±2°C, rated current (1-2 hour recovery)
Humidity Resistance:	Inductance change 2% or .5pF Max	1000 ±48 Hours @ +40±2°C, 90 - 95% relative humidity. Rated current (1-2 hour recovery)
Terminal Adhesion::	Termination should not pull off. Ceramic should remain undamaged.	Lateral pull force. 0201 ≥ 1.0Lbs 0402 ≥ 1.6Lbs For 0603 ≥ 2.2Lbs For 0805 ≥ 4.4Lbs
PCD Deflection:	No mechanical damage.	Glass Epoxy PCB: 1mm deflections

Figure H.1: Mechanical and Environmental characteristics for Johanson Technology RF Ceramic Inductors

	SPECIFICATION	TEST PARAMETERS
OPERATING TEMPERATURE RANGE	Ceramic core: -40°C to +125°C Ferrite core: -40°C to +85°C	
COEFFICIENT OF EXPANSION	Ceramic Core: 7.2 x 10^{-6} / deg. C (typ.) Ferrite Core: 10 x 10^{-6} / deg. C (typ.)	
INDUCTANCE AND TOLERANCE	Within Specified Tolerance	Measuring Frequency : As shown in Product Table Measuring Temperature : + 25 °C
QUALITY FACTOR	Within Specified Tolerance	Measuring Frequency : As shown in Product Table Measuring Temperature : + 25 °C
INSULATION RESISTANCE	1000 mega ohms minimum	Measured at 100V DC between inductor terminals and center of case.
DIELECTRIC WITHSTANDING VOLTAGE	No damage occurs when the test voltage is applied.	Measured at 500V AC between inductor terminals and center of case for a maximum of 1 minute.
TEMPERATURE COEFFICIENT OF INDUCTANCE (TCL)	Ceramic Core: +25 to +125 ppm / °C Ferrite Core: +25 to +500 ppm / °C $TCL = \frac{L1 - L2}{L1(T1-T2)} \times 10^6$ (ppm /°C)	Over - 40 °C to + 85°C at frequency specified in Product Table.
COMPONENT ADHESION (PUSH TEST)	0402 series - 350g 0603 series - 1.0Kg 0805 series - Minimum 2Kg for ceramic core parts and 1 Kg for ferrite core parts.	The component shall be reflow soldered onto a P. C. Board (230 °C ± 5°C for 20 seconds). Then a dynometer force gauge shall be applied to any side of the component.
DROP TEST	Change In Inductance: No more than 5% Change In Q: No more than 10% Change In Appearance: Without distinct damage	The inductor shall be dropped two times on a concrete floor or a vinyl tile from a 1 meter height.
THERMAL SHOCK TEST	Change In Inductance: No more than 5% Change In Q: No more than 10% Change In Appearance: Without distinct damage	Each cycle shall consist of 30 minutes at -40 °C followed by 30 minutes at +85 °C with a 20-second maximum transition time between temperature extremes. Test duration is 10 cycles.

Figure H.2: Mechanical and Environmental characteristics for Johanson Technology RF Wirewound Inductors

The subsequent pages contains datasheets for resistors from Multicomp, Panasonic and Vishay, as well as the SMA connector used.

General Purpose Chip Resistors

Anti-Sulfuration

Features:

- High reliability and stability ±1%
- Sulfuration resistant
- Automotive grade AEC Q-200 compliant
- 100% CCD inspection
- Lead-free

Applications:

Automotive application
Consumer electrical equipment
EDP, computer application
Telecom application

RoHS Compliant

Description

The resistors are constructed in a high grade ceramic body (aluminium oxide). Internal metal electrodes are added at each end and connected by a resistive paste that is applied to the top surface of the substrate. The composition of the paste is adjusted to give the approximate resistance required and the value is trimmed to within tolerance by laser cutting of this resistive layer

The resistive layer is covered with a protective coat. Finally, the two external end terminations are added. For ease of soldering the outer layer of these end terminations is a Tin (lead free) alloy

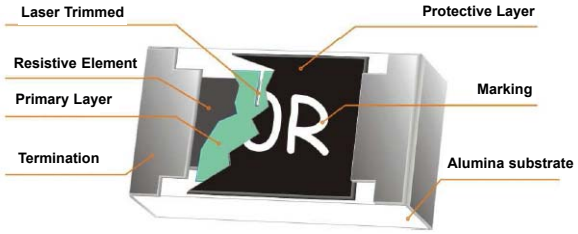

Fig 1. Construction of a Chip-R

Quick Reference Data

Item	General Specification							
Series no.	MCMR12		MCMR08		MCMR06		MCMR04	
Size code	1206 (3216)		0805 (2012)		0603 (1608)		0402 (1005)	
Resistance range	1 Ω to 10 MΩ (±5% tolerance), jumper 1 Ω to 10 MΩ (±1% tolerance)							
Resistance tolerance	±1% E96 / E24	±5% E24	±1% E96 / E24	±5% E24	1% E96 / E24	±5% E24	±1% E96 / E24	±5% E24
TCR (ppm/°C) R > 1MΩ 10Ω < R ≤ 1MΩ R ≤ 10Ω	≤ +200 ≤ +100 -200 to +400		≤ +200 ≤ +100 -200 to +400		≤ +200 ≤ +100 -200 to +400		≤ +200 ≤ +100 -200 to +400	
Maximum dissipation at T_{amb} = 70°C	1/4 W		1/8 W		1/10 W		1/16 W	
Maximum operation voltage (DC or RMS)	200 V		150 V		75 V		50 V	
Maximum overload voltage (DC or RMS)	400 V		300 V		150 V		100 V	
Climatic category (IEC 60068)	55/155/56							

General Purpose Chip Resistors

Anti-Sulfuration

Note:

1. This is the maximum voltage that may be continuously supplied to the resistor element, see “IEC publication 60115-8”
2. Maximum operation voltage : So called RCWV (rated continuous working voltage) is determined by

$$RCWV = \sqrt{\text{Rated Power} \times \text{Resistance Value}}$$ or maximum RCWV listed above, whichever is lower

3. The resistance of jumper is defined < 0.05 Ω

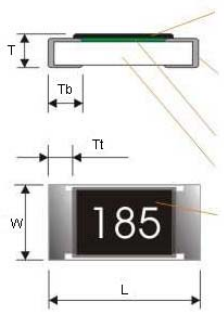

Protective Coat

End Termination

Resistive Layer

Ceramic Substrate

Protective Coat

Dimensions (unit : mm)

	MCMR12	MCMR08	MCMR06	MCMR04
L	3.1 ± 0.1	2 ± 0.1	1.6 ± 0.1	1 ± 0.05
W	1.6 ± 0.1	1.25 ± 0.1	0.8 ± 0.1	0.5 ± 0.05
T	0.6 ± 0.15	0.5 ± 0.15	0.45 ± 0.15	0.35 ± 0.05
Tb	0.45 ± 0.2	0.4 ± 0.2	0.3 ± 0.15	0.25 ± 0.1
Tt	0.5 ± 0.2	0.4 ± 0.2	0.3 ± 0.1	0.2 ± 0.1

Marking

Size \ No. of Digit of Code \ Tolerance	±5%	±1%
1206 / 0805	3-digits marking	4-digits marking
0603 (1608)	3-digits marking	3-digits marking
0402 (1005)	No marking	

3-digits marking (±5% : 1206, 0805 and 0603)

Each resistor is marked with a three digits code on the protective coating to designate the nominal resistance value

General Purpose Chip Resistors

Anti-Sulfuration

3-Digits Marking (1% : 0603)

Nominal Resistance	Description
1. E-24 series	As 0603 WR06X ±5%
2. E-96 series	The 1st two digit codes are referring to the CODE on the table, the 3rd code is the index of resistance value: Y = 10^{-2}, X = 10^{-1}, A = 10^{0}, B = 10^{1}, C = 10^{2}, D = 10^{3}, E = 10^{4}, F = 10^{5} EX : 17.8 Ω = 25 X, 178 Ω = 25 A, 1K78 = 25 B 17K8 = 25 C, 178 K = 25 D, 1M78 = 25 E
3. Remark	There is no marking for the items are not under E-24 and E-96 series

Code	R_value	Code	R_value	Code	R_value	Code	R_value	Code	R_value	Code	R_value	Code	R_value	Code	R_value
1	100	13	133	25	178	37	237	49	316	61	422	73	562	85	750
2	102	14	137	26	182	38	243	50	324	62	432	74	576	86	768
3	105	15	140	27	187	39	249	51	332	63	442	75	590	87	787
4	107	16	143	28	191	40	255	52	340	64	453	76	604	88	806
5	110	17	147	29	196	41	261	53	348	65	464	77	619	89	825
6	113	18	150	30	200	42	267	54	357	66	475	78	634	90	845
7	115	19	154	31	205	43	274	55	365	67	487	79	649	91	866
8	118	20	158	32	210	44	280	56	374	68	499	80	665	92	887
9	121	21	162	33	215	45	287	57	383	69	511	81	681	93	909
10	124	22	165	34	221	46	294	58	392	70	523	82	698	94	931
11	127	23	169	35	226	47	301	59	402	71	536	83	715	95	953
12	130	24	174	36	232	48	309	60	412	72	549	84	732	96	976

4-digits marking (±1% : 1206 / 0805)

Each resistor is marked with a three digits code on the protective coating to designate the nominal resistance value

Example

Resistance	10 Ω	12 Ω	100 Ω	6,800 Ω	47,000 Ω
3-digits marking(1206, 0805, 0603 ±5%)	100	120	101	682	473
4-digits marking	10R0	12R0	1000	6801	4702

Functional Description

Product characterization

Standard values of nominal resistance are taken from the E24 series for resistors with a tolerance of ±5%, and E24+E96 series for resistors with a tolerance of ±1%. The values of the E24 / E96 series are in accordance with “IEC publication 60063”

Derating

The power that the resistor can dissipate depends on the operating temperature; see Fig. 2.1

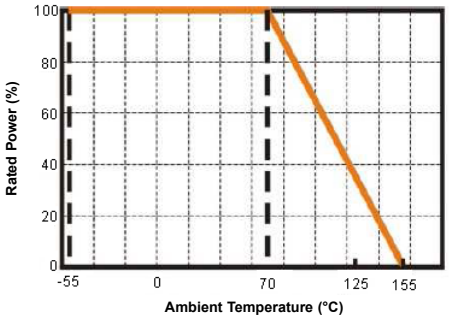

Fig 2.1 Maximum dissipation in percentage of rated power as a function of the ambient temperature

Mounting:

Due to their rectangular shapes and small tolerances, surface mountable resistors are suitable for handling by automatic placement systems
Chip placement can be on ceramic substrates and printed-circuit boards (PCBs)
Electrical connection to the circuit is by individual soldering condition
The end terminations guarantee a reliable contact

Soldering Condition

The robust construction of chip resistors allows them to be completely immersed in a solder bath of 260°C for 10 seconds. Therefore, it is possible to mount surface mount resistors on one side of a PCB and other discrete components on the reverse (mixed PCBs)

Surface mount resistors are tested for solderability at 235°C during 2 seconds. The test condition for no leaching is 260°C for 30 seconds. Typical examples of soldering processes that provide reliable joints without any damage are given in Fig 3

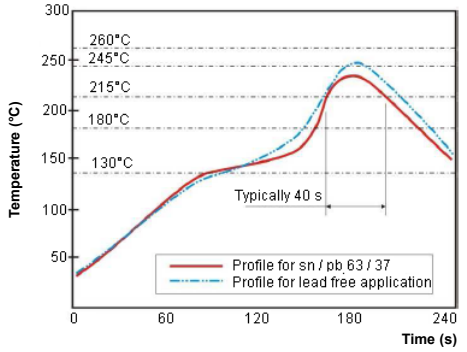

Fig 3. Infrared soldering profile for Chip Resistors

General Purpose Chip Resistors

Anti-Sulfuration

Test and Requirements

Essentially all tests are carried out according to the schedule of IEC publication 115-8, category **LCT/UCT**/56(rated temperature range : Lower Category Temperature, Upper Category Temperature; damp heat, long term, 56 days). The testing also meets the requirements specified by EIA, EIAJ and JIS
The tests are carried out in accordance with IEC publication 68, "Recommended basic climatic and mechanical robustness testing procedure for electronic components" and under standard atmospheric conditions according to IEC 60068-1, sub-clause 5.3. Unless otherwise specified, the following value supplied :
Temperature : 15 to 35°C
Relative humidity : 45 to 75%
Air pressure : 86 kPa to 106 kPa (860 mbar to 1,060 mbar)
All soldering tests are performed with midly activated flux

Test	Procedure / Test Method	Requirement	
		Resistance ±5%, ±1%	**0 Ω**
Electrical Characteristics JISC5201-1: 1998 Clause 4.8	- DC resistance values measurement - Temperature Coefficient of Resistance (T.C.R) Natural resistance change per change in degree centigrade $\frac{R2 - R1}{R_1 (t_2 - t_1)} \times 10^6$ (ppm/°C) t_1 : 20°C+5°C-1°C R_1 : Resistance at reference temperature R_2 : Resistance at test temperature	Within the specified tolerance Refer to "Quick Reference Data"	
Resistance to soldering heat (R.S.H) MIL-STD-202 method 210	Un-mounted chips completely immersed for 10 ±1 second in a SAC solder bath at 270°C ±5°C	ΔR/R maximum ± (0.5%+0.05 Ω) No visible damage	< 50 mΩ
Solderability J-STD-002	a) Bake the sample for 155°C dwell time 4 hours / solder dipping 235°C / 5 s b) Steam the sample dwell time 1 hour/ solder dipping 215°C/ 5 s c) Steam the sample dwell time 1 hour/ solder dipping 260°C / 7 s	95% coverage minimum, good tinning No visible damage	
Temperature cycling JESD22 method JA-104	1,000 cycles, -55°C to +155°C, dwell time 5 to 10 mins	ΔR/R maximum ± (0.5%+0.05 Ω) No visible damage	< 50 mΩ
Moisture Resistance MIL-STD-202 method 106	65 ±2°C, 80 to 100% RH, 10 cycles, 24 hours / cycle	ΔR/R maximum ± (0.5%+0.05 Ω) No visible damage	< 50 mΩ
Bias Humidity MIL-STD-202 method 103	1,000 +48/-0 hours; 85°C, 85% RH, 10% of operation Power	ΔR/R maximum ± (1%+0.05 Ω) No visible damage	< 50 mΩ
Operational Life MIL-STD-202 method 108	1,000 +48/-0 hours; 35% of operation power, 125 ±2°C	ΔR/R maximum ± (1%+0.05 Ω) No visible damage	< 50 mΩ
High Temperature Exposure MIL-STD-202 method 108	1,000+48/-0 hours; without load in a temperature chamber controlled 155±3°C	ΔR/R maximum ± (1%+0.05 Ω) No visible damage	< 50 mΩ

General Purpose Chip Resistors

Anti-Sulfuration

Test	Procedure / Test Method	Requirements	
		Resistance ±5%, ±1%	0 Ω
Mechanical Shock MIL-STD-202 method 213	1/2 sine pulse / 1,500 g peak / Velocity 15.4 ft/s	Within the specified tolerance No visible damage	< 50 mΩ
Board Flex AEC-Q200-005	Resistors mounted on a 90 mm glass epoxy resin PCB(FR4), bending once 2 mm for 10 s	ΔR/R maximum ± (1%+0.05 Ω) No visible damage	< 50 mΩ
Terminal strength AEC-Q200-006	Pressurizing force: 1 Kg, Test time: 60±1 s	No remarkable damage or removal of the terminations	
Vibration MIL-STD-202 method 204	Test 5 g's for 20 minimum, 12 cycles each of 3 orientations	ΔR/R maximum ± (1%+0.05 Ω) No visible damage	< 50 mΩ
Thermal shock MIL-STD-202 method 107	Test –55 to 155 / dwell time 15 minimum / maximum transfer time 20 seconds 300 cycles	ΔR/R maximum ± (0.5%+0.05 Ω) No visible damage	< 50 mΩ
ESD AEC-Q200-002	Test contact 1 KV (0.5 KV for 0402 only)	ΔR/R maximum ± (1%+0.05 Ω) No visible damage	< 50 mΩ

Test Condition for Jumper (0 Ω)

Item	MCMR12	MCMR08	MCMR06	MCMR04
Power rating at 70°C	1/4 W	1/8 W	1/10 W	1/16 W
Resistance	Maximum 50 mΩ			
Rated current	2 A	1.5 A	1 A	1 A
Peak current	5 A	3.5 A	3 A	2 A
Operating temperature	-55 to +155°C			

Part Number Explanation:

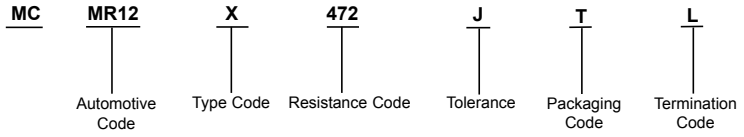

General Purpose Chip Resistors

Anti-Sulfuration

Automotive Code	**:** MCMR12 : 1206, MCMR08 : 0805, MCMR06 : 0603 and MCMR04 : 0402
Type Code	**: X :** ±5%, 1 Ω to 10 MΩ, ±1%, < 10 Ω; > 1 MΩ **W :** ±1%, < 10 Ω; > 1 MΩ
Resistance Code	**: ±5%,** E24 : 2 significant digits followed by no. of zeros and a blank 200 Ω = 221_ ("_" means a blank) **: ±1%,** E24+E96 : 3 significant digits followed by no. of zeros E96 : 37.4 KΩ = 3,742 E24 : 200 Ω = 2,200
Tolerance	**: F :** ±1%, **J :** ±5% and **P :** Jumper
Packaging Code	**: T :** 7" Reeled taping
Termination Code	**: L :** Sn base (lead free)

* Anti-Sulfur test conditions : H2S 3 ppm, 40°C, RH 90%, 1,000 hours, criteria : +/-1%

MCMR12, MCMR08, MCMR06:

1. Reeled tape packaging : 8 mm width paper taping 5,000 pieces per 7" reel, 10 k pieces per 10" reel, 20 k pieces per 13" reel
2. Bulk packaging : 5,000 pieces per poly-bag

MCMR04:

1. Reeled tape packaging : 8 mm width paper taping 10,000 pieces per reel
2. Bulk packaging : 10,000 pieces per poly-bag

Important Notice : This data sheet and its contents (the "Information") belong to the members of the Premier Farnell group of companies (the "Group") or are licensed to it. No licence is granted for the use of it other than for information purposes in connection with the products to which it relates. No licence of any intellectual property rights is granted. The Information is subject to change without notice and replaces all data sheets previously supplied. The Information supplied is believed to be accurate but the Group assumes no responsibility for its accuracy or completeness, any error in or omission from it or for any use made of it. Users of this data sheet should check for themselves the Information and the suitability of the products for their purpose and not make any assumptions based on information included or omitted. Liability for loss or damage resulting from any reliance on the Information or use of it (including liability resulting from negligence or where the Group was aware of the possibility of such loss or damage arising) is excluded. This will not operate to limit or restrict the Group's liability for death or personal injury resulting from its negligence. Multicomp is the registered trademark of the Group. © Premier Farnell plc 2011.

Anti-Surge Thick Film Chip Resistors
0603, 0805, 1206, 1210, 0805

Type: **ERJ P03, P06, P08, P14**
ERJ P6W

■ Features

- ESD surge characteristics superior to standard metal film resistors
- High reliability
  Metal glaze thick film resistive element and three layers of electrodes
- Suitable for both reflow and flow soldering
- High power···0.2 W : 1608(0603) size(ERJP03)
  0.25 W : 2012(0805) size(ERJP06)
  0.33 W : 3216(1206) size(ERJP08)
  0.5 W : 3225(1210) size(ERJP14), double-sided resistive elements structure 2012(0805) size(ERJP6W)
- Reference Standards···IEC 60115-8, JIS C 5201-8, EIAJ RC-2134B
- RoHS compliant

■ Explanation of Part Numbers

- ERJP03, P06, P08, P14

1	2	3	4	5	6	7	8	9	10	11	12
E	R	J	P	0	6	D	1	0	0	2	V

Product Code

Thick Film Chip Resistors

Size, Power Rating

Type: inch	Power R.
P03 : 0603	0.2 W
P06 : 0805	0.25 W
P08 : 1206	0.33 W
P14 : 1210	0.5 W

Resistance Tolerance

Code	Tolerance
D	± 0.5 %
F	± 1 %
J	± 5 %

Resistance Value

The first two or three digits are significant figures of resistance and the third or 4th one denotes number of zeros following.
Three digit type (±5%),
four digit type (±1%, ±0.5%)
Example: 222→2.2 kΩ, 1002→10 kΩ

Packaging Methods

Code	Packaging	Type
V	Punched Carrier Taping 4 mm pitch, 5,000 pcs.	ERJP03 ERJP06 ERJP08
U	Embossed Carrier Taping 4 mm pitch, 5,000 pcs.	ERJP14

- ERJP6W(double-sided resistive elements structure)

1	2	3	4	5	6	7	8	9	10	11	12
E	R	J	P	6	W	F	1	0	0	2	V

Product Code

Thick Film Chip Resistors

Size, Power Rating

Type: inch	Power R.
P6W : 0805	0.5 W

Resistance Tolerance

Code	Tolerance
F	± 1 %
J	± 5 %

Resistance Value

The first two or three digits are significant figures of resistance and the third or 4th one denotes number of zeros following.
Three digit type (±5%), four digit type (±1%)
Example: 222→2.2 kΩ, 1002→10 kΩ

Packaging Methods

Code	Packaging
V	Punched Carrier Taping 4 mm pitch, 5,000 pcs.

■ Construction

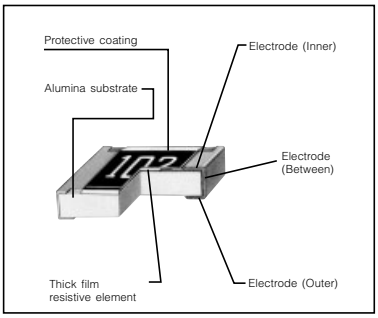

■ Dimensions in mm (not to scale)

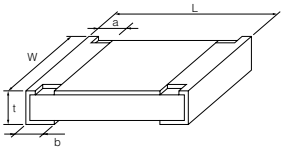

Type (inch size)	Dimensions (mm) L	W	a	b	t	Mass (Weight) [g/1000pcs.]
ERJP03 (0603)	$1.60^{\pm0.15}$	$0.80^{+0.15}_{-0.05}$	$0.15^{+0.15}_{-0.10}$	$0.30^{\pm0.15}$	$0.45^{\pm0.10}$	2
ERJP06 (0805)	$2.00^{\pm0.20}$	$1.25^{\pm0.10}$	$0.25^{\pm0.20}$	$0.40^{\pm0.20}$	$0.60^{\pm0.10}$	4
ERJP6W (0805)	$2.00^{\pm0.20}$	$1.25^{\pm0.20}$	$0.35^{\pm0.20}$	$0.35^{\pm0.20}$	$0.65^{\pm0.10}$	6
ERJP08 (1206)	$3.20^{+0.05}_{-0.20}$	$1.60^{+0.05}_{-0.15}$	$0.40^{\pm0.20}$	$0.50^{\pm0.20}$	$0.60^{\pm0.10}$	10
ERJP14 (1210)	$3.20^{\pm0.20}$	$2.50^{\pm0.20}$	$0.35^{\pm0.20}$	$0.50^{\pm0.20}$	$0.60^{\pm0.10}$	16

Design and specifications are each subject to change without notice. Ask factory for the current technical specifications before purchase and/or use.
Should a safety concern arise regarding this product, please be sure to contact us immediately.

■ Ratings

Type (inch size)	Power Rating at 70 °C (W)	Limiting Element Voltage[1] (V)	Maximum Overload Voltage[2] (V)	Resistance Tolerance (%)	Resistance Range (Ω)	T.C.R. (×10⁻⁶/°C)	Category Temperature Range (°C)
ERJP03 (0603)	0.2	150	200	±0.5	10 to 1 M (E24, E96)	±150	−55 to +155
				±1	10 to 1 M (E24, E96)	±200	
				±5	1 to 1 M (E24)	R < 10 Ω : −150 to +400 10 Ω ≤ R : ±200	
ERJP06 (0805)	0.25	150 (400)[3]	200 (600)[3]	±0.5, ±1	10 to 1 M (E24, E96)	R < 33 Ω : ±300 33 Ω ≤ R : ±100	−55 to +155
				±5	1 to 3.3 M (E24)	R < 10 Ω : −100 to +600 10 Ω ≤ R < 33 Ω : ±300 33 Ω ≤ R : ±200	
ERJP6W (0805)	0.5	150	200	±1	10 to 1 M (E24, E96)	±200	−55 to +155
				±5	1 to 1 M (E24)	R < 10 Ω : −100 to +600 10 Ω ≤ R : ±200	
ERJP08 (1206)	0.33	200 (500)[3]	400 (1000)[3]	±0.5, ±1	10 to 1 M (E24, E96)	±100	−55 to +155
				±5	1 to 10 M (E24)	R < 10 Ω : −100 to +600 10 Ω ≤ R : ±200	
ERJP14 (1210)	0.5	200	400	±0.5, ±1	10 to 1 M (E24, E96)	±100	−55 to +155
				±5	1 to 1 M (E24)	R < 10 Ω : −100 to +600 10 Ω ≤ R : ±200	

(1) Rated Continuous Working Voltage (RCWV) shall be determined from RCWV=$\sqrt{\text{Power Rating} \times \text{Resistance Values}}$, or Limiting Element Voltage listed above, whichever less.
(2) Overload (Short-time Overload) Test Voltage (SOTV) shall be determined from SOTV=2.5 × Power Rating or max. Overload Voltage listed above whichever less.
(3) Please contact us when resistors with guaranteed high voltage are need.

Power Derating Curve

For resistors operated in ambient temperatures above 70 °C, power rating shall be derated in accordance with the figure on the right.

✻ When the temperature of ERJP06/08/14 is 155 °C or less, the derating start temperature can be changed to 125 °C. (See the dotted line)

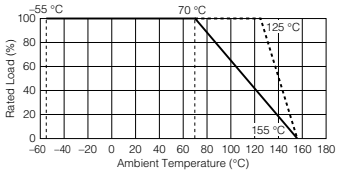

■ ESD Characteristic

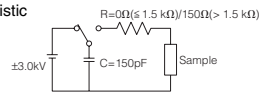

Anti-Surge Thick Film Chip Resistors(ERJP Type)
Thick Film Chip Resistors(ERJ Type)

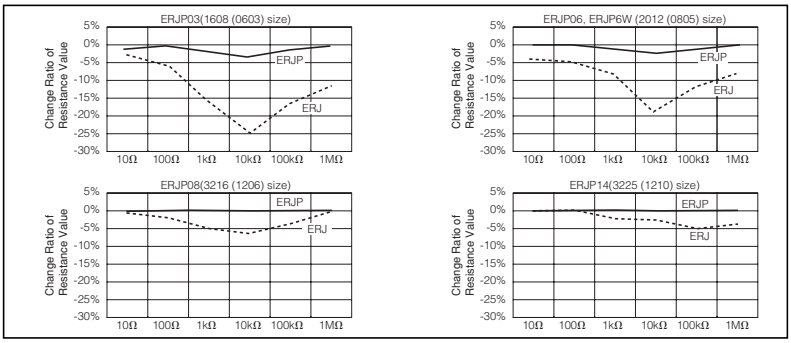

Anti-Pulse Thick Film Chip Resistors
0805, 1206, 1210

Type: **ERJ T06, T08, T14**

■ Features

- Anti-Pulse characteristics
  High pulse characteristics achieved by the optimized trimming specifications
- High reliability
  Metal glaze thick film resistive element and three layers of electrodes
- Suitable for both reflow and flow soldering
- High power···0.25 W : 2012(0805) size
  0.33 W : 3216(1206) size
  0.5 W : 3225(1210) size
- Reference Standards···IEC 60115-8, JIS C 5201-8, EIAJ RC-2134B
- RoHS compliant

■ Explanation of Part Numbers

1	2	3	4	5	6	7	8	9	10	11
E	R	J	T	0	6	J	1	0	0	V

Product Code
Thick Film Chip Resistors

Size, Power Rating	
Type: inch	Power R.
T06 : 0805	0.25 W
T08 : 1206	0.33 W
T14 : 1210	0.5 W

Resistance Tolerance	
Code	Tolerance
J	± 5 %

Packaging Methods		
Code	Packaging	Type
V	Punched Carrier Taping 4 mm pitch, 5,000 pcs.	ERJT06 ERJT08
U	Embossed Carrier Taping 4 mm pitch, 5,000 pcs.	ERJT14

Resistance Value
The first two digits are significant figures of resistance and the third one denotes number of zeros following. Example: 222→2.2 kΩ

■ Construction

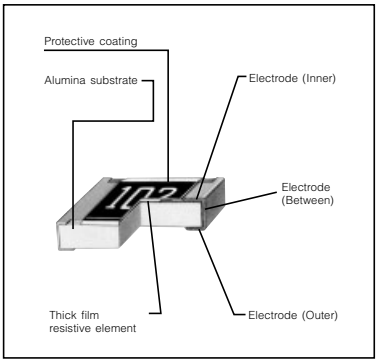

■ Dimensions in mm (not to scale)

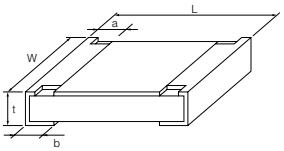

Type (inch size)	Dimensions (mm) L	W	a	b	t	Mass (Weight) [g/1000pcs.]
ERJT06 (0805)	$2.00^{\pm0.20}$	$1.25^{\pm0.10}$	$0.25^{\pm0.20}$	$0.40^{\pm0.20}$	$0.60^{\pm0.10}$	4
ERJT08 (1206)	$3.20^{+0.05}_{-0.20}$	$1.60^{+0.05}_{-0.15}$	$0.40^{\pm0.20}$	$0.50^{\pm0.20}$	$0.60^{\pm0.10}$	10
ERJT14 (1210)	$3.20^{\pm0.20}$	$2.50^{\pm0.20}$	$0.35^{\pm0.20}$	$0.50^{\pm0.20}$	$0.60^{\pm0.10}$	16

Design and specifications are each subject to change without notice. Ask factory for the current technical specifications before purchase and/or use.
Should a safety concern arise regarding this product, please be sure to contact us immediately.

■ Ratings

Type (inch size)	Power Rating at 70 °C (W)	Limiting Element Voltage[1] (V)	Maximum Overload Voltage[2] (V)	Resistance Tolerance (%)	Resistance Range (Ω)	T.C.R. ($\times 10^{-6}$/°C)	Category Temperature Range (°C)
ERJT06 (0805)	0.25	150	200	±5	1 to 1 M (E24)	Less than 10 Ω : -100 to +600 Less than 33 Ω : ±300 More than 33 Ω : ±200	−55 to +155
ERJT08 (1206)	0.33	200	400	±5	1 to 1 M (E24)	Less than 10 Ω : -100 to +600 More than 10 Ω : ±200	−55 to +155
ERJT14 (1210)	0.5	200	400	±5	1 to 1 M (E24)	Less than 10 Ω : -100 to +600 More than 10 Ω : ±200	−55 to +155

(1) Rated Continuous Working Voltage (RCWV) shall be determined from RCWV=$\sqrt{\text{Power Rating} \times \text{Resistance Values}}$, or Limiting Element Voltage listed above, whichever less.
(2) Overload (Short-time Overload) Test Voltage (SOTV) shall be determined from SOTV=2.5 × Power Rating or max. Overload Voltage listed above whichever less.

Power Derating Curve

For resistors operated in ambient temperatures above 70 °C, power rating shall be derated in accordance with the figure on the right.

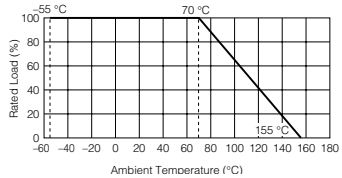

■ Limiting Power Curve

● In rush pulse Characteristic

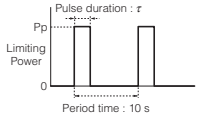

Test cycle : 1000 cycles
Spec : Resistance value = within ±5%

● : Anti-Pulse Thick Film Chip Resistors (ERJT Type)
○ : Thick Film Chip Resistors (ERJ Type)

● **ERJT06** (2012 (0805) size)

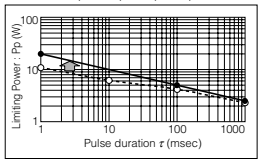

● **ERJT08** (3216 (1206) size)

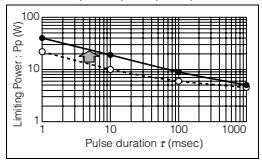

● **ERJT14** (3225 (1210) size)

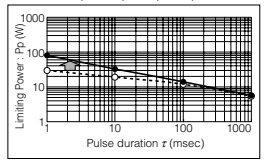

Design and specifications are each subject to change without notice. Ask factory for the current technical specifications before purchase and/or use.
Should a safety concern arise regarding this product, please be sure to contact us immediately.

CRCW....-HP e3

Vishay

Pulse Proof, High Power Thick Film Chip Resistors

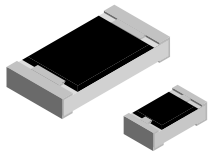

FEATURES

- Excellent pulse load capability
- Enhanced power rating
- Double side printed resistor element
- Protective overglaze
- Lead (Pb)-free solder contacts on Ni barrier layer
- Pure tin plating provides compatibility with lead (Pb)-free and lead containing soldering processes
- Compliant to RoHS directive 2002/95/EC
- AEC-Q200, rev. C compliant

STANDARD ELECTRICAL SPECIFICATIONS

MODEL	SIZE		POWER RATING P_{70} W	LIMITING ELEMENT VOLTAGE MAX. V	TEMPERATURE COEFFICIENT ppm/K	TOLERANCE %	RESISTANCE RANGE Ω	E-SERIES
	INCH	METRIC						
CRCW0402-HP e3	0402	1005	0.125 (1)	50	± 100	± 1	1R to 1M	E24 + E96
					± 200	± 5		E24
			Zero-Ohm-Resistor: $R_{max.}$ = 0.010 Ω, $I_{max.}$ = 2.5 A					
CRCW0603-HP e3	0603	1608	0.25	75	± 100	± 1	1R to 1M	E24 + E96
					± 200	± 5		E24
			Zero-Ohm-Resistor: $R_{max.}$ = 0.010 Ω, $I_{max.}$ = 4 A					
CRCW0805-HP e3	0805	2012	0.33	150	± 100	± 1	1R to 1M	E24 + E96
					± 200	± 5		E24
			Zero-Ohm-Resistor: $R_{max.}$ = 0.010 Ω, $I_{max.}$ = 5 A					
CRCW1206-HP e3	1206	3216	0.5	200	± 100	± 1	1R to 1M	E24 + E96
					± 200	± 5		E24
			Zero-Ohm-Resistor: $R_{max.}$ = 0.010 Ω, $I_{max.}$ = 6 A					
CRCW2010-HP e3	2010	5025	1.0	400	± 100	± 1	1R to 1M	E24 + E96
					± 200	± 5		E24
			Zero-Ohm-Resistor: $R_{max.}$ = 0.010 Ω, $I_{max.}$ = 10 A					
CRCW2512-HP e3	2512	6332	1.5	500	± 100	± 1	1R to 1M	E24 + E96
					± 200	± 5		E24
			Zero-Ohm-Resistor: $R_{max.}$ = 0.010 Ω, $I_{max.}$ = 14 A					

Notes

(1) CRCW0402-HP resistors feature a single side printed resistive layer only

- These resistors do not feature a limited lifetime when operated within the permissible limits. However, resistance value drift increasing over operating time may result in exceeding a limit acceptable to the specific application, thereby establishing a functional lifetime
- Marking and packaging: see appropriate catalog or web page
- Power rating depends on the max. temperature at the solder point, the component placement density and the substrate material

TECHNICAL SPECIFICATIONS

PARAMETER	UNIT	CRCW0402-HP	CRCW0603-HP	CRCW0805-HP	CRCW1206-HP	CRCW2010-HP	CRCW2512-HP
Rated Dissipation P_{70} (1)	W	0.125	0.25	0.33	0.5	1.0	1.5
Limiting Element Voltage $U_{max.}$ AC/DC	V	50	75	150	200	400	500
Insulation Voltage $U_{ins.}$ (1 min)	V	> 75	> 100	> 200	> 300		
Insulation Resistance	Ω	> 10^9					
Category Temperature Range	°C	- 55 to + 155					
Weight	mg	0.65	2	5.5	10	25.5	42

Note

(1) The power dissipation on the resistors generates a temperature rise against the local ambient, depending on the heat flow support of the printed-circuit board (thermal resistance). The rated dissipation applies only if the permitted film temperature of 155 °C is not exceeded.

For technical questions, contact: thickfilmchip@vishay.com

Document Number: 20043
Revision: 07-May-09

PART NUMBER AND PRODUCT DESCRIPTION

PART NUMBER: CRCW0603562RFKEAHP (1)

C	R	C	W	0	6	0	3	5	6	2	R	F	K	E	A	H	P

MODEL/SIZE	VALUE	TOLERANCE	TCR	PACKAGING (2)	SPECIAL
CRCW0402 **CRCW0603** **CRCW0805** **CRCW1206** **CRCW2010** **CRCW2512**	**R** = Decimal **K** = Thousand **M** = Million **0000** = Jumper	**F** = ± 1 % **J** = ± 5 % **Z** = Jumper	**K** = ± 100 ppm/K **N** = ± 200 ppm/K **0** = Jumper	**EA** **EB** **EC** **ED** **EE** **EI** **EL** **EF** **EG** **EH**	Up to 2 digits **HP** = Pulse proof, High Power

PRODUCT DESCRIPTION: CRCW0603-HP 100 562R 1 % ET1 e3

CRCW0603-HP	100	562R	1 %	ET1	e3
MODEL	TCR	RESISTANCE VALUE	TOLERANCE	PACKAGING (2)	LEAD (Pb)-FREE
CRCW0402-HP CRCW0603-HP CRCW0805-HP CRCW1206-HP CRCW2010-HP CRCW2512-HP	± 100 ppm/K ± 200 ppm/K	10R = 10 Ω 562R = 562 Ω 10K = 10 kΩ 1M = 1 MΩ 0R0 = Jumper	± 1 % ± 5 %	ET1 ET5 ET6 ET7 EF4 EG1 E20 E02 E67 E82	e3 = Pure tin termination finish

Notes

(1) Preferred way for ordering products is by use of the PART NUMBER

(2) Please refer to table PACKAGING, see below

PACKAGING

MODEL	REEL							
	TAPE WIDTH	DIAMETER	PITCH	PIECES/ REEL	PACKAGING CODE			
					PART NUMBER		PRODUCT DESC.	
					PAPER	BLISTER	PAPER	BLISTER
CRCW0402-HP	8 mm	180 mm/7" 330 mm/13"	2 mm 2 mm	10 000 50 000	ED EE		ET7 EF4	
CRCW0603-HP	8 mm	180 mm/7" 285 mm/11.25" 330 mm/13"	4 mm 4 mm 4 mm	5000 10 000 20 000	EA EB EC	EI EL	ET1 ET5 ET6	EG1 E20
CRCW0805-HP	8 mm	180 mm/7" 285 mm/11.25" 330 mm/13"	4 mm 4 mm 4 mm	5000 10 000 20 000	EA EB EC	EI EL	ET1 ET5 ET6	EG1 E20
CRCW1206-HP	8 mm	180 mm/7" 285 mm/11.25" 330 mm/13"	4 mm 4 mm 4 mm	5000 10 000 20 000	EA EB EC	EI EL	ET1 ET5 ET6	EG1 E20
CRCW2010-HP	12 mm	180 mm/7"	4 mm	4000		EF		E02
CRCW2512-HP	12 mm	180 mm/7"	8 mm 4 mm	2000 4000		EG EH		E67 E82

DIMENSIONS in millimeters

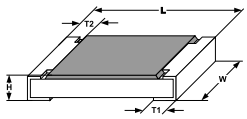

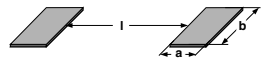

SIZE		RESISTANCE RANGE Ω	DIMENSIONS					SOLDER PAD DIMENSIONS					
								REFLOW SOLDERING			WAVE SOLDERING		
INCH	METRIC		L	W	H	T1	T2	a	b	l	a	b	l
0402	1005	1R - 1M	1.0 ± 0.05	0.5 ± 0.05	0.3 ± 0.1	0.25 ± 0.1	0.2 ± 0.1	0.4	0.6	0.5			
0603	1608	1R - 1M	1.6 ± 0.1	0.85 ± 0.1	0.45 ± 0.1	0.3 ± 0.2	0.3 ± 0.2	0.5	0.9	1.0	0.9	0.9	1.0
0805	2012	1R - 1M	2.0 ± 0.15	1.25 ± 0.15	0.50 ± 0.1	0.4 ± 0.2	0.35 ± 0.2	0.7	1.3	1.2	0.9	1.3	1.3
1206	3216	1R - 1M	3.1 ± 0.2	1.6 ± 0.15	0.50 ± 0.15	0.5 ± 0.2	0.45 ± 0.2	0.9	1.7	2.0	1.1	1.7	2.3
2010	5025	1R - 1M	5.0 ± 0.15	2.5 ± 0.15	0.6 ± 0.1	0.6 ± 0.2	0.6 ± 0.2	1.0	2.5	3.9	1.2	2.5	3.9
2512	6332	1R - 1M	6.3 ± 0.2	3.15 ± 0.15	0.6 ± 0.1	0.6 ± 0.2	0.6 ± 0.2	1.0	3.2	5.2	1.2	3.2	5.2

FUNCTIONAL PERFORMANCE

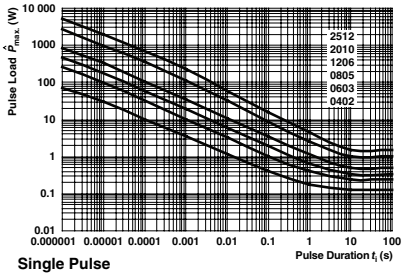

Single Pulse

Maximum pulse dissipation as a function of the pulse duration, single pulse for CRCW...-HP

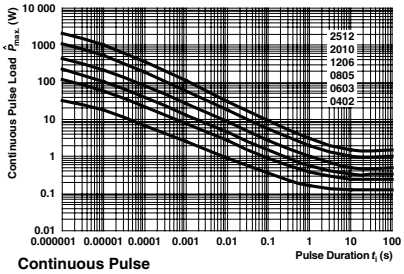

Continuous Pulse

Maximum pulse dissipation as a function of the pulse duration, continuous pulse for CRCW...-HP

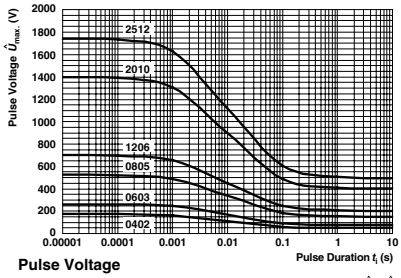

Pulse Voltage

Maximum pulse voltage, single and continuous pulses; applicable if $\hat{P} \leq \hat{P}_{max.}$; for permissible resistance change equivalent to 8000 h operation

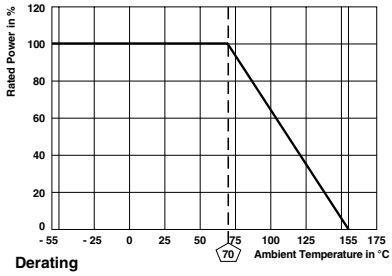

Derating

TEST PROCEDURES AND REQUIREMENTS

EN 60115-1

TEST (clause)	CONDITIONS OF TEST	REQUIREMENTS PERMISSIBLE CHANGE (ΔR)
		STABILITY CLASS 2 OR BETTER
	Stability for product types:	1 Ω - 1 MΩ
	CRCW....-HP e3	
Resistance (4.5)	-	± 1 %, ± 5 %
Temperature coefficient (4.8.4.2)	20/- 55/20 °C and 20/125/20 °C	± 100 ppm/K, ± 200 ppm/K
Overload (4.13)	$U = 2.5 \times \sqrt{P_{70} \times R}$ ≤ 2 × $U_{max.}$; Duration: according the style	± (0.5 % R + 0.05 Ω)
Solderability (4.17.5)	Aging 4 h at 155 °C, dryheat Solder bath method; 235 °C; 2 s Visual examination	Good tinning (≥ 95 % covered) no visible damage
Resistance to soldering heat (4.18.2)	Solder bath method; (260 ± 5) °C; (10 ± 1) s	± (1 % R + 0.05 Ω)
Rapid change of temperature (4.19)	30 min at LCT = - 55 °C; 30 min at UCT = 125 °C; 5 cycles	± (1 % R + 0.05 Ω)
Damp heat, steady state (4.24)	(40 ± 2) °C; 56 days; (93 ± 3) % RH	± (2 % R + 0.05 Ω)
Climatic sequence (4.23)	16 h at UCT = 125 °C; 1 cycle at 55 °C; 2 h at LCT = - 55 °C; 1 h/1 kPa at 15 °C to 35 °C; 5 cycles at 55 °C $U = \sqrt{P_{70} \times R}$ $U = U_{max.}$; whichever is less severe	± (2 % R + 0.05 Ω)
Endurance at 70 °C (4.25.1)	$U = \sqrt{P_{70} \times R}$ $U = U_{max.}$; whichever is less severe 1.5 h ON; 0.5 h OFF; 70 °C; 1000 h	± (2 % R + 0.05 Ω)
Endurance at upper category temperature (4.25.3)	UCT = 155 °C; 1000 h	± (2 % R + 0.05 Ω)

APPLICABLE SPECIFICATIONS

- EN 60115-1 Generic specification
- AEC-Q200 Generic specification
- EN 140400 Sectional specification
- EN 140401-802 Detail specification
- IEC 60068-2-X Variety of environmental test procedures
- IEC 60286-3 Packaging of SMD components

Disclaimer

All product specifications and data are subject to change without notice.

Vishay Intertechnology, Inc., its affiliates, agents, and employees, and all persons acting on its or their behalf (collectively, “Vishay”), disclaim any and all liability for any errors, inaccuracies or incompleteness contained herein or in any other disclosure relating to any product.

Vishay disclaims any and all liability arising out of the use or application of any product described herein or of any information provided herein to the maximum extent permitted by law. The product specifications do not expand or otherwise modify Vishay’s terms and conditions of purchase, including but not limited to the warranty expressed therein, which apply to these products.

No license, express or implied, by estoppel or otherwise, to any intellectual property rights is granted by this document or by any conduct of Vishay.

The products shown herein are not designed for use in medical, life-saving, or life-sustaining applications unless otherwise expressly indicated. Customers using or selling Vishay products not expressly indicated for use in such applications do so entirely at their own risk and agree to fully indemnify Vishay for any damages arising or resulting from such use or sale. Please contact authorized Vishay personnel to obtain written terms and conditions regarding products designed for such applications.

Product names and markings noted herein may be trademarks of their respective owners.

THIS DRAWING IS UNPUBLISHED. RELEASED FOR PUBLICATION JULY ,2006.
© COPYRIGHT 2006 BY TYCO ELECTRONICS CORPORATION. ALL RIGHTS RESERVED.

LOC	DIST
E	B

REVISIONS

P	LTR	DESCRIPTION	DATE	DWN	APVD
	A	FIRST ISSUE	31JUL06	JMS	FWK

NOTES

1. SINGLE PACK IN ACCORDANCE WITH AMP SPEC 107-3275
2. 100 TRAY PACK IN ACCORDANCE WITH AMP SPEC 107-3275
3. Au PLATING
4. ELECTRICAL CHARACTERISTICS

FREQUENCY RANGE:	DC-3GHz
NOMINAL IMPEDANCE:	50 OHMS
INSULATION RESISTANCE:	5000 MOHMS
DIELECTRIC WITHSTAND VOLTAGE:	500V RMS
CONTACT RESISTANCE:	CENTRE CONTACT 3 mOHMS OUTER CONTACT 2 mOHMS

5. MECHANICAL CHARACTERISTICS

DURABILITY:	50 CYCLES
TORQUE SETTING	0.15-0.20 NM

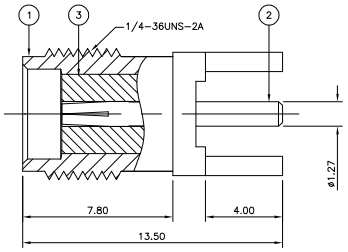

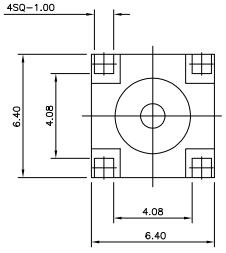

RECOMMENDED PCB LAYOUT
WITH MOUNTING POSTS

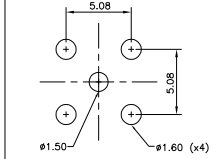

1	1	PTFE	INSULATOR	3
1	1	PHOSPHER BRONZE [2]	SOCKET	2
1	1	ZINC ALLOY [3]	BODY	1
5--15--0		MATERIAL	DESCRIPTION	ITEM
[1]	[2]	QUANTITY PER ASSY	PARTS LIST	

THIS DRAWING IS A CONTROLLED DOCUMENT.

DIMENSIONS: mm

TOLERANCES UNLESS OTHERWISE SPECIFIED:
0 PLC ± –
1 PLC ± –
2 PLC ± –
3 PLC ± –
4 PLC ± –
ANGLES ± –

MATERIAL: SEE TABLE
FINISH: –

DWN	31JUL06 J.SANDWELL
CHK	31JUL06 S.PARLOW
APVD	31JUL06 F.WHEELER-KING
PRODUCT SPEC	–
APPLICATION SPEC	–
WEIGHT	–

tyco Electronics
Tyco Electronics Corporation
Bideford EX39 4HE

NAME: SMA STRAIGHT PCB SOCKET DIE CAST
–
–

SIZE	CAGE CODE	DRAWING NO	RESTRICTED TO
A3	00779	C-1814832	–

CUSTOMER DRAWING | SCALE NTS | SHEET 1 OF 1 | REV A

AMP 1470-19 REV 31MAR2000